UNIVERSITY OF SOUTHAMPTON

FACULTY OF ENGINEERING, SCIENCE AND MATHEMATICS

School of Civil Engineering and the Environment

Oscillating Water Column Wave Pump: A Wave Energy Converter for Water Delivery

by

Davide Magagna

Thesis for the degree of Doctor of Philosophy

April 2011

UNIVERSITY OF SOUTHAMPTON

ABSTRACT

FACULTY OF ENGINEERING, SCIENCE AND MATHEMATICS

School of Civil Engineering and the Environment

Doctor of Philosphy

Oscillating Water Column Wave Pump: A Wave Energy Converter for Water Delivery

by Davide Magagna

The research presented in this dissertation investigates the development and the performances of a new type of Wave Energy Converter (WEC) aimed to provide water delivery and energy storage in the form of potential energy. The Oscillating Water Column Wave Pump (OWCP) concept was proposed and tested through a series of experimental investigations supported by scientific theory.

The OWCP was developed after an extensive study of the existing wave energy technology available, from which it emerged that the Oscillating Water Column (OWC) device could be further implemented for water delivery purposes. The existing theory of the OWC was employed to develop a mathematical theory able to describe the system wave response and water removal of the OWCP.

In order to understand and validate the mathematical models of the OWCP, experimental investigations were carried out under the influence of incident linear waves in a two-dimensional (2D) and three-dimensional (3D) wave flume. The experimental equipment and methodology are outlined, including the description of wave flumes, models and data acquisition equipment.

Experimental tests were used to verify the concept of the OWCP and assess its performances, investigating both the response of the device to the waves with and without water removal. In order to increase the efficiencies of delivery, array configurations of multiple OWCPs were adopted.

The research demonstrated that up to 14% of the energy carried by the incoming waves can be converted into useful potential energy for a single device. Moreover a further increase of the efficiencies can be obtained with the array configuration improving the overall capability of the OWCP, for optimal separation distance between the array components.

Further model tests are required to extended this research to validate the developed mathematical models as an effective prediction tool of the performances of the OWCP and further increase the efficiency of water removal that can be achieved.

Contents

List of Figures

List of Tables

Nomenclature

ABBREVIATIONS

$2D$	Two dimensioal
$3D$	Three dimensional
BEM	Boundary Element Model
FFT	Fast Fourier Transform
JONSWAP	Joint North Sea Wave Project
KC	Keulegan-Carpenter Number
MWL	Mean Water Level
OB	Oscillating Bodies
OT	Overotopping Devices
OWC	Oscillating Water Column
OWCP	Oscillating Water Column Wave Pump
PM	Pierson-Moskowitz
PTO	Power Take Off
RAO	Response Amplitude Operator
SSG	Seawave Slot-cone Generator
TAPCHAN	Tapered Channel Wave Power Device
WEC	Wave Energy Converters

d.o.f	Degress of freedom

CAPITAL SYMBOLS

A_0	Amplitude of the exciting force
A_d	Area device
B	Radiation Damping
B_{77}	Radiation Damping OWC 7th mode
C	Wave Celeirty [m/s]
C_d	Drag Coefficient
C_f	Spring Coefficient
C_g	Wave Group Celerity [m/s]
E	Efficiency in Power Absorption
E_s	Specific Energy for Unit Area
$F(t)$	Hydrodynamic Pressure Force
F_0	Wave Force
F_{PTO}	Force Power Take Off
F_{WS}	Force due to Wave Structure Interaction
F_{d7}	Diffraction Force 7th mode
F_{drag}	Drag Force
F_e	Excitating Force
$F_{friction}$	Friction Forces
$F_{gravity}$	Gravity restoring force
F_{others}	Other Forces acting on OWCP
F_{r7}	Radiation Force 7th mode

H	Wave Height [m]
H_s	Significant Wave Height [m]
K_r	Reflection Coefficient
K_t	Transmission Coefficient
L	Wave Length [m]
L_m	Main Length parameter model [m]
L_p	Main Length dimension prototype [m]
M	Magnification Factor
N_i	Surf Similarity Parameter or Iribarren number
N_p	Number of panels for BEM
P_a	Power Output of Array [kW]
P_s	Power of a single autonomous device [kW]
P_{crest}	Power in the overtopping
P_{res}	Power in the reservoir
P_w	Wave Power [kW/m]
Q	Overtopping Flowrate
Re	Reynold Number
R_C	Freeboard [m]
S	Surface water subject to pressure
T	Wave Period [s]
T_P	Peak Wave Period [s]
T_d	Natural period of oscillation affected by damping [s]
T_n	Natural period of oscillation [s]

T_s	Significant Wave Period [s]
W	Quality factor for the decay of force oscillation tests

LOWER CAP SIMBOLS

$2b$	Width between two closely spaced walls
a	Wave Amplitude [m]
a_s	Submersion depth of walls [m]
d	Damping coefficient
d_s	Submersion depth of OWCP [m]
f	Wave Frequency [Hz]
g	Gravitational Constant [m/s^2]
h	Water Depth [m]
h_w	Height of the wall [m]
h_f	Continuos Friction Losses [m]
h_l	Local losses [m]
h_{res}	Water level in reservoir [m]
h_r	Height of removal [m]
k	Wave Number
k_E	Discharge coefficient at the exit of the OWCP
k_I	Discharge Coefficient at the entrance of OWCP
k_s	Pipe Roughness [m]
l_a	Added Length of Water [m]
l_t	Total Length of Water moved [m]
n	Indicator - Degrees of Freedom

p	Water Pressure [Pa]
p_0	Atmospheric Pressure [Pa]
q	Array quality factor
q_e	q factor in terms of efficiency
s_d	Separation distance [m]
t	Time [s]
u	Horizontal Particle Velocity [m/s] - Velocity component on the x axis
w	Vertical Particle Velocity [m/s] - Velocity component on the z axis
x	Horizontal Position [m]
y_p	length of water removed
y_r	Removal Height
z	Vertical Position [m]

GREEK SYMBOLS

$\boldsymbol{\Omega}$	Normalised driving frequency
$\boldsymbol{\Upsilon}$	Wave Surface Elevation [m]
$\boldsymbol{\alpha}$	angle of inclination of Output Duct
$\boldsymbol{\beta}$	angle of inclination of slope
$\boldsymbol{\delta}$	Spring Coefficient
$\boldsymbol{\eta}_{max}$	Maximum Efficiency
$\boldsymbol{\eta}_{res}$	Efficiency in reservoir
$\boldsymbol{\eta}$	Efficiency of the OWCP
$\boldsymbol{\gamma}$	Damping Coefficient

$\boldsymbol{\lambda}$	Scaling Factor
$\boldsymbol{\lambda}_{max}$	Maximum Capture Width [m]
$\boldsymbol{\mu}$	Added mass coefficient
$\boldsymbol{\mu}_{77}$	Addedd Mass OWC 7th mode
$\boldsymbol{\nu}$	Viscosity
$\boldsymbol{\omega}$	Wave Angular Frequency [rad/s]
$\boldsymbol{\omega}_0$	Natural Frequency of Oscillation of OWC
$\boldsymbol{\omega}_n$	Natural Frequency of Oscillation of OWCP [rad/s]
$\boldsymbol{\phi}$	Velocity Potential
$\boldsymbol{\phi}_7$	Radiataion potential due to 7th mode of motion
$\boldsymbol{\phi}_d$	Diffraction potential
$\boldsymbol{\phi}_r$	Radiation potential
$\boldsymbol{\rho}$	Water Density [kg/m^3]
$\boldsymbol{\xi}_E$	Damping coefficient at the exit of the OWCP
$\boldsymbol{\xi}_I$	Damping coefficient at the entrance of the OWCP
$\boldsymbol{\xi}_r$	Damping coefficient due to radiation
$\boldsymbol{\zeta}$	Displacement float

Form of declaration

I, Davide Magagna, declare that the thesis entitled *Oscillating Water Column Wave Pump: a Wave Energy Converter for Water Delivery* , and the work presented in the thesis are both my own, and have been generated by me as the result of my own original research.

I confirm that:

- This work was done wholly while in candidature for a research degree at this University.
- Where any part of this thesis has previously been submitted for a degree or any other qualification at this university or any other institution, this has been clearly stated.
- Where I have consulted the published work of others, this is always clearly attributed.
- Where I have quoted from the work of others, the source is always given. With the exception of such quotations, this thesis is entirely my own work.
- I have acknowledged all main sources of help.
- Where the thesis is based on work done by myself jointly with others, I have made clear exactly what was done by others and what I have contributed myself.
- Part of this work has been published as Magagna and Muller 2009
- Part of this work has been published as Magagna et al. 2009
- Part of this work has been published as Magagna et al. 2010a
- Part of this work has been published as Magagna et al. 2010b

Signed:.....

Date:.....

Acknowledgments

I would like to thank the following who played important parts for the completion of this doctorate:

My supervisor, Gerald Müller, for the opportunity to carry out this research projects, for the continuous supervision and valuable suggestions along the way. I'd like to thank him for the many positive conversations we had, the useful insights and the teaching possibilities he gave me.

My second supervisor, AbuBakr Bahaj, for the positive feed backs and hints, and for pushing me when times were tough. And everyone within the Sustainable Energy Research Group, who listened to me and gave me useful suggestions with regards to programming, writing or carrying out experiments.

Dr. Dimitris Stagonas, with whom I collaborated over the years. His experience helped me gain a better understanding of the physical processes investigated in this research. Thanks also for helping in the longs hours setting up the lab equipment.

My parents Roberto and Teresa and my sister Simona, for their support from far away. For the hours spent on the phone listening and encouraging me towards the completion of this work.

My colleagues Tasos, Matt, Pascal, Nick, Mark, Jack, with whom I shared time in the office; for the continuous and mutual help both at academic a personal level.

My flatmates Francesco, Stefano, Alessia, Iain, Elena and Candida, they all helped in their own way. Barbara for proof-reading and calming me down in the last few weeks of writing. Marco, Mauro, Stefano, Tommaso, Catia, Carlo, Riccardo that have supported me over the years. Marta for the smile. The guys at Romsey Rugby and London Italian Rugby for providing a stress-relieve valve from the academic work.

To those people who unfortunately are no longer here, but whose presence is still alive in my thoughts.

Chapter 1

Introduction and Overview

1.1 Background

Over the past 40 years the interests in exploiting the energy contained within the oceans have increased. As a result of the extensive amount of research carried out, over 50 different types of wave energy converters (WECs) have been developed. Few of these devices have already been deployed at full scale, while others are awaiting prototype testing in real sea conditions (Falcao, 2008).

Whilst work is constantly carried in order to identify an economically-feasible device for the generation of electricity from wave power, researchers have widened their interests to identify alternative or complimentary applications for wave energy devices.

With "alternative or complimentary applications" for wave energy converters it is intended the use of WECs not directly aimed to the generation and the commercialisation of electricity. Examples of these applications can be found in the rising interests towards wave powered desalination, wave driven flushing and the combination of coastal defence strategies with wave power harnessing.

Among many devices, the Oscillating Water Column (OWC) has received the most attention from the scientific community. The OWC exploits the sea-level rises in an enclosed chamber due to the incoming waves to compress air. The compressed air is then used to drive a purposely designed turbine for the generation of electricity

The OWC has already been employed in conjunction with caisson breakwaters for coastal defence purposes (Dhinakaran et al., 2002) or installed near-shore to drive sea-water desalination (Sharmila et al., 2004).

1.1.1 Case for evaluation of alternative applications of wave energy converters

The case for the evaluation of different applications for WECs is stated by the need to address specific issues that arise during the development of a device such as structural stability and environmental impact to mention a few. Mutual benefits can be obtained while implementing alternative applications for wave energy, making it advantageous to install wave energy converters in the near-shore area.

As a matter of fact, due to ease of installation and operational management, installations of onshore Wave Energy Converters are strongly favoured. The integration of WEC with other coastal activities, from flooding prevention to near-shore desalination and water augmentation, provides the possibility of using well established tools for the wave-structure analysis of the converter. The combination ultimately allows for the availability of energy in different form as a surplus to standard structures.

Whilst the implementation of a WEC for electricity purposes can be limited by the efficiency of generation; developing a WEC for alternative use presents the researcher with a fully developed and conversion system. This allows for the determination of the power supply required from the beginning and defines the design project from start to end.

The advantages of WECs for alternative applications also lie in the possibility of storing energy, mostly in the form of pressure or potential energy. This will allow for the use of the energy when required.

1.1.2 Investigating the problem

The application of wave energy converters and in particular OWC systems has, so far, been aimed to generate electricity. Whilst it is understandable that most efforts and time are spent in the implementation of devices with higher efficiency, the exploitation of the energy contained in waves can be of use for alternative applications. Furthermore this can lead to the implementation of the device through a series of tests and processes that were initially neglected.

Through a review of the current state of the art technology developed for Wave Energy Conversion, it is possible to identify a suitable device that could be implemented for alternative applications, such as water delivery and energy storage in the near-shore.

By assessing the limitations presented by the chosen technology it is possible to investigate its use for different purposes. A modified version of the standard OWC technology is proposed in this thesis. The proposed Oscillating Water Column Wave Pump is designed for water delivery and storage of potential energy. The modified OWC does not present a variable air-water interface, allowing for experimental tests to be employed without scaling issues related to compressibility of the two fluids.

For devices such as the OWC, the use of physical tests has always been controversial due to the presence of a water-air interface requiring different scaling approaches. It follows that evaluating an OWC type of device for water delivery through physical investigations requires a simplification of the problem, focusing on the hydraulic issues surrounding the device.

Whilst implementing the Oscillating Water Column Wave Pump, it is therefore possible to provide a feedback to the development of standard OWC technology through the assessment of alternative application of the device itself. The assessment an of alternative applications for WECs can then be seen not only as a development problem, but as a promising path to evaluate and improve the functioning of the current wave energy technology.

1.2 Research Needs

The existing work is focused on the production of electricity and existing devices have been modelled and tested for such applications. The methodologies chosen in the modelling comprise either highly mathematical works or simplified experimental tests. Both approaches on their own have so far achieved limited success.

There is a clear need of developing the physical experimental part of research to investigate the real performances of the systems and the work done(Brito-Melo et al., 1999).

In order to take the knowledege forwards an overtopping device aimed to the delivery of water is proposed and investigated. In this thesis a combination of experimental tests and mathematical models to produce further fundamental understanding with the dynamics of the response of the

OWC, has been studied.

1.3 Research Aims

The research here presented aims to develop a wave pump that exploits the energy contained within waves to lift water from the mean water level to 2-5 meters of hydraulic head from wave with height ranging between 0.5-1.5 m.

The hydraulic head generated could be employed for storage of energy, or to generate the necessary pressure require for reverse osmosis desalination systems.

1.4 Research Objectives

The aim presented in 1.3 will be achieved through the following objectives:

To	investigate the existing technology for wave energy conversion and their limitations
Identify	a suitable device to work as a wave pump for the delivery of water and evaluate the possibility of its development
Support	with scientific theory the development of any concept presented in this work
Verify	by the means of hydraulic modelling the proposed scientific theory
Implement	a numerical model to predict the performance of the device
Indicate	the potential full scale performance on any concept developed and studied
Identify	and discuss the possible applications for which any device may be employed for.

1.5 Research Limitations

Much of the research and development on resonating wave energy converters is aimed to determine the ideal external damping coefficients, in order to apply a control strategy to the WEC. This is normally carried through the use of Boundary Element Models (BEM) and Computational Fluids Dynamics (CFD). Damping coefficients are important since they affect the response of a WEC for a given wave frequency; however at this stage it was chosen to use physical tests for their evaluation.

The research will involve the following:

- Use of experimental tests to evaluate the damping coefficients required for mathematical models
- Wave flume and basin studies will only consider normal wave directions, with sinusoidal and monochromatic waves generated.
- The removal mass will be averaged over the number of waves used for the tests. Flowrate measurements systems cannot be implemented through the use of load cells given the small amounts of mass removed for each passing wave.
- Only one design of the proposed device is evaluated. Considerations on how the shape of the device could improve performances will be presented further along.
- No specific applications of the collected water will be considered in full. The development of a high pressure pump for water desalination was considered as a side development of this research, however the main focus of this research is the interaction between the device and incident waves.

1.6 Contributions

Part of the results presented in this research were published as:

- Magagna D. and Muller G.,(2009). A wave energy driven RO stand-alone desalination system: initial design and testing, Desalination and Water Treatment. 7(09), 47-52. Appendix D

The author also presented results obtained in this research at the following conferences as follows:

- Magagna, D., Stagonas, D., Warbrick, D., Muller, G., (2009). Resonating wave energy converter for delivery of water for desalination and energy generation. Proceedings of the 7th European Wave and Tidal Energy Conference (EWTEC2009), 7-10 September 2009, Uppsala, Sweden. Appendix E
- Magagna, D., Stagonas, D., Muller, G., (2010). Using small-scale hydraulic models for the preliminary development and investigation of near-shore wave energy converters. Proceedings on the Third International Conference on the Application of Physical Modelling to Port and Coastal Protection (CoastLab2010), 28-30 September 2010 and 1st October 2010, Barcelona, Spain. Appendix F

- Magagna, D., Stagonas, D., Warbrick, D., Muller, G., (2010). Physical investigations into the capture width of an array of OWC Wave Pumps for maximum efficiency. Proceeding of the 3rd International Conference on Ocean Energy (ICOE2010), 6 October, Bilbao, Spain. Appendix G

1.7 Thesis Structure

This thesis is organised in 9 chapters, structured as follows:

Chapter 1. Introduction and Overview. An introduction to research issue, study aims,objective and limitations of the research.

Chapter 2 Glossary of Terms. Presentation of the terminology used in this work and wave theory.

Chapter 3 Literature Review. Presentation of the state of the art of wave energy conversion, and in-depth review of the chosen technology the OWC.

Chapter 4 Theory of the Oscillating Water Column Wave Pump. Presentation of the concept analysed in this research and development of a suitable theory.

Chapter 5 Physical Modelling: Methodology and Plan. Overview of laboratory facilities and of layout of experimental plan.

Chapter 6 Response and Efficiency of the OWCP: Results. In depth analysis of the performance of the device working independently in terms of response to incident waves and efficiency of water removal.

Chapter 7 Evaluation of the Performances of Multiple OWCPs Installed in an Array Configuration. In depth analysis of the performances of multiple devices working in array configurations.

Chapter 8 Full Scale Performances of the OWCP. Presentation of a case study evaluating the performances of the OWCPs at full scale under the influence of irregular sea states.

Chapter 9 Discussion and Conclusions. Overall conclusion, identification of possible application for the device and future work.

Chapter 2

Glossary of Terms

This chapter aims to outline and clarify the concepts and terminology that will be used during this study. This is followed by a background chapter on wave energy applications, describing the state of art of the current wave energy technology exploiting the power contained in ocean waves.

The following chapter is divided in two main sections, the first section of this chapter aims to provide a description of wave characteristics and their characterisation; while the second is focused on at defining the wave energy conversion technology and the mechanisms of response of the different type of devices.

2.1 Wave Characteristics

Understanding the physics of ocean waves is crucial when working on Wave Energy Conversion. It is not purpose of this work to present the reader with a full derivation of the wave theory, but to highlight the most important characteristics of ocean waves related to the work that is presented. There is a wide range of work available in literature where further information can be found, such as the work carried by Dean and Dalrymple (1990); Young (1999); Svendsen (2006) on which the following is based.

To facilitate the explanation Figure 2.1 is used as reference to define the basic wave characteristics. As indicated in Figure 2.1 two physical properties can be directly identified in a wave: wave height H and the wave period T. From the knowledge of these two properties any other characteristic of wave can be derived.

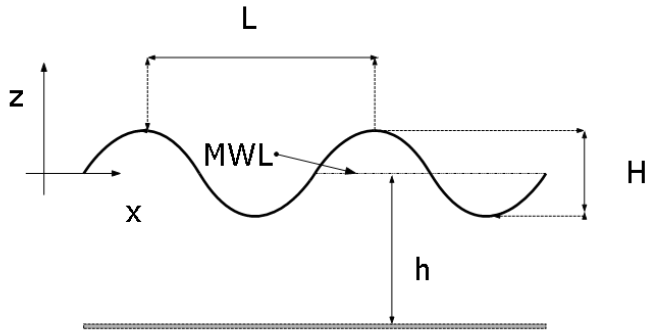

Figure 2.1: Representation of waves characteristics, where L is the wavelength, H is the wave height, h is the water depth and MWL indicates the Mean Water Level in absence of waves.

2.1.1 Wave height, wave period, wave length and water Depth

The magnitude of a wave may be represented by four components: height, period, frequency and length.

The **wave height**, H , is the measure of the vertical distance from a wave trough to a wave crest.

The **wave period**, T , is the time interval between three consecutive up or down zero crossing point of a wave. The **wave frequency** f is defined as the inverse of T. $f = 1/T$

The **wave Length** L (see Figure 2.1) is the horizontal distance between two consecutive up and down zero crossing point of a wave measured orthogonally to the wave crest.

The mathematical simplification of the wave length is dependent on the **water depth** h .

2.1.2 Linear wave theory

The simplest mathematical theory to describe ocean wave behaviour is the Airy's theory which is often termed linear wave theory. The theory, which is based on the assumption formulated by Airy (1845), describes the propagation of waves above a horizontal bottom. At the base of Airy's assumptions is the existence of a velocity potential ϕ that satisfies Laplace's equation.

The surface elevation of the waves is described by a sinusoidal curve (see Figure 2.1) and is a function of the horizontal position x and of the time t . The **surface elevation** is normally regarded as Υ and it is expressed as follows:

$$\Upsilon = (x, t) = a\cos(kx - \omega t) \tag{2.1}$$

where:

a is the wave amplitude , corresponding to half of the wave height $a = H/2$;

k is the wave number;

ω is the angular frequency.

The measurements of repeating units of a propagating wave is defined as the **wave number** k. k is determined by its relation with the wave length L, expressed as $k = 2\pi/L$.

The **angular frequency** ω is related to the wave frequency by the following relation $\omega = 2\pi f$.

There is a unique relation between k and ω, which is represented by equation 2.2. This relation is known as the **dispersion coefficient.** The dispersion coefficient defines a particular wave travelling with determined T and L.

$$\omega^2 = gk \tanh(kh) \tag{2.2}$$

The **celerity** C of a travelling wave is represented by the ratio between L and T, $C = L/T = k/\omega$

2.1.3 Effects of water depth

As seen in equation 2.2, the water depth plays a key role in the relation between k and ω. Waves can also be classified on the h/L criterion, also known as wave steepness, which allows for the identification of three possible scenarios: deep water, intermediate and shallow water waves Young (1999).

Shallow water conditions are defined when $h/L \leq 1/20$

Intermediate water conditions are defined when $1/20 \leq h/L \leq 1/2$

Deep water conditions are defined when $h/L > 1/2$

The trajectories of water particles vary with water depth, since the vertical and horizontal component of the particle velocity depend on the water depth. The motion of water particles is circular in deep water conditions and tends to be horizontal in shallow waters (Figure 2.2).

The water depth affects the group velocity of travelling waves, as well as influencing the energy content of the wave and their height while approaching the shore. The **group velocity** (or celerity) C_g is the velocity of a train of waves travelling in a group. The group velocity is used to represent the movement of energy in waves, and tends to be slower than that of the

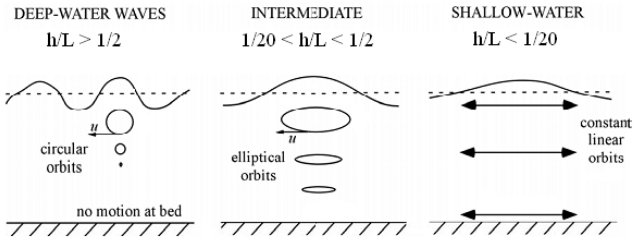

Figure 2.2: Water particle motion patterns at different water depths (Dean and Dalrymple, 1990)

waves (Dean and Dalrymple, 1990).

The **specific energy per unit area** E_s contained in a wave is expressed as

$$E_s = \frac{1}{8}\rho g H^2 \tag{2.3}$$

The **wave power** P_w represents the combined potential and kinetic energy of waves travelling with a speed equal to the group velocity normal to a unit width of wave crest in deep water. For linear waves, the wave power per unit crest is also expressed by the rate at which wave energy is advected , as stated in equation 2.4.

$$P_w = E_s C_g = \frac{\rho g^2}{32\pi} T H^2 \tag{2.4}$$

A summary of linear waves properties is presented in Table 2.1

It has to be noticed that the linear wave theory is broadly used as a primary tool to identify and describe ocean waves. Linear wave theory provides a good approximation for the description of many coastal processes, however the non-linear wave theory is used when the results obtained are thought to be too approximative.

2.1.4 Monochromatic and panchromatic waves and Sea States

The Airy's wave theory describes with good accuracy single frequency waves. A sinusoidal single frequency single wave train is defined normally as a **monochromatic wave**.

Real waves however, are the combination of multiple monochromatic wave trains. **Panchromatic waves** represent a sea state comprising the superposition of multiple single frequency sinusoidal components, the distribution of which is dictated by the spectral shape.

The spectral shape of sea states is obtained through the use of a Fast Fourier Transform

Wave Property	Shallow Water h/L < 1/20	Intermediate Water 1/20< h/L <1/2	Deep Water h/L >1/2
Wave Profile	$\Upsilon(x,t) = a\cos(kx - \omega t)$	$\Upsilon(x,t) = a\cos(kx - \omega t)$	$\Upsilon(x,t) = a\cos(kx{-}\omega t)$
Wave Length	$L = T\sqrt{gh}$	$L = \frac{g}{2\pi}T^2\tanh(kh)$	$L = \frac{g}{2\pi}T^2 \simeq 1.56T^2$
Dispersion relation	$\omega^2 = gk^2h$	$\omega^2 = gk\tanh(kh)$	$\omega^2 = gk^2$
Velocity Potential	$\phi = \frac{ag}{\omega}\frac{\cosh k(h+\Upsilon)}{\cosh(kh)}\cos(kx - \omega t)$		$\phi = \frac{ag}{\omega}e^{kx}\cos(kx{-}\omega t)$
Horizontal Particle Velocity	$u = \frac{\omega a}{kh}\cos(kx - \omega t)$	$u = \frac{\omega a\cosh k(h+\Upsilon)}{kh}\cos(kx{-}\omega t)$	$u = \omega a e^{kx}\cos(kx{-}\omega t)$
Vertical Particle Velocity	$w = \omega a\frac{\Upsilon + h}{h}\cos(kx - \omega t)$	$w = \frac{\omega a\cosh k(h+\Upsilon)}{kh}\sin(kx{-}\omega t)$	$w = \omega a e^{kx}\sin kx{-}\omega t)$
Group Celerity	$C_g = C$	$C_g = \frac{1}{2}C(1 + \frac{2kh}{\sinh 2kh})$	$C_g = \frac{1}{2}C$

Table 2.1: Classification of linear waves properties according to relative depth kh (Young, 1999)

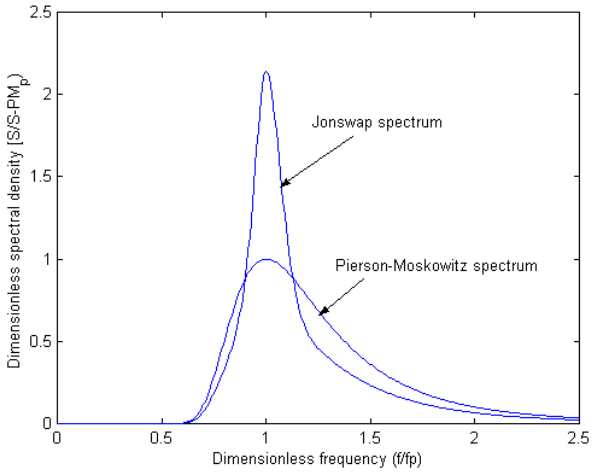

Figure 2.3: Comparison between Pierson-Moskowitz and JONSWAP spectra (Young, 1999)

(FFT), which converts the time series of a data set and identifies frequency domain of a panchromatic wave train (Young, 1999).

Statistical analysis are employed in the determination of the sea states for a given location.

The **significant wave height** , H_s, is defined as is the average wave height of the one-third largest waves. The **significant wave period** , T_s, is consequently defined as the average period of the one-third highest waves in a wave record. Alternatively the peak wave period , T_P, is defined as the period with the maximum wave energy.

In the case of random sea, statistically significant values for the wave period and wave height are needed to generate a wave spectrum. A **wave spectrum** is a method of representing the distribution of wave energy as a function of frequency.

Three wave spectra are commonly used for the description of random seas: the Pierson-Moskowitz spectrum (PM), the Joint North Sea Wave Project spectrum (JONSWAP) and the Bretscheneider spectrum. Both the JONSWAP and the Bretscheneider spectra represent special cases of the PM spectrum. The PM spectrum defines a one dimensional shape based on the assumptions of fully developed wind generated waves (Young, 1999). The JONSWAP spectrum identifies the variance over a frequency range of waves status in the North Sea, while the Bretscheneider allows for the consideration of waves that are not fully developed (Figure 2.3) . Wave spectra are widely used to analyse the response of WECs under random seas excitation during numerical and physical testing.

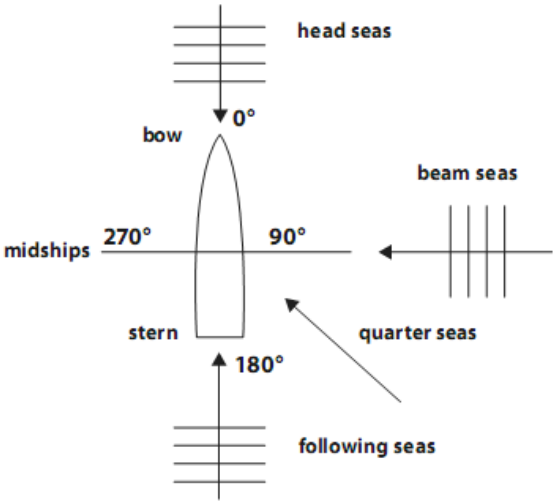

Figure 2.4: Seaways definitions (EMEC, 2009)

2.2 Seaway Definitions and Device Characteristics

2.2.1 Seaways

The interaction between WECs and waves is dependent on the sea state. Sea states are classified according to the way they approach a device (Figure 2.4).

Beam sea is defined as the seaway impacting on the side of a floating body at 90^{o} to the longitudinal axis.

A **following sea** is defined as the seaway impacting a floating body at the stern and the travelling from the stern to the bow of a body. A **head sea** is the seaway impacting a floating body at the bow and then travelling from the bow to the stern.

A **quarter sea** is the seaway that approaches floating at an angle between the beam and the following sea (EMEC, 2009).

2.2.2 Device response

The response of a device to wave excitation depends on its design and 6 different types of motion that can take place according to the device's characteristic: heave, pitch,roll, surge, sway and yaw.

The **yaw** motion is the oscillatory movement parallel to a vertical axis. The **pitch** movement is an oscillatory motion on the horizontal transverse axis. **Roll** is the oscillatory motion on the horizontal longitudinal axis. **Surge** is a translational movement parallel to the longitudinal

horizontal axis; while **sway** is a translational movement parallel to the horizontal transverse axis. Finally **heave** is defined as translational movement on the vertical axis.

Other important characteristics of devices are the draft and the freeboard. The **draft** of a device is the dimension of a body below the water surface due to a load on the body itself. The **freeboard** R_C is the dimension of a body above the mean water level.

The dimensioning of a device and its orientation defines the type of WEC. A **point absorber** WEC is a device very small compared to the typical wavelength. Devices comparable in length with the typical wavelength are either **attenuators** of **terminators**. An attenuator is aligned to the direction of the wave propagation, whilst attenuators are aligned perpendicularly to the waves direction of propagation (Previsic et al., 2004).

2.2.3 Power and efficiency

Final concepts that require prior understanding are those associated with the device power and efficiency. The **device power** is defined as the pneumatic or mechanical power produced by a device due to the a seaway excitation. The **efficiency** of a WEC (or overall efficiency) is expressed as the ratio of power output (electricity) to the power absorbed. The **hydrodynamic efficiency** of a device refers to the primary conversion from wave power to pneumatic or mechanical power. Efficiencies are two-dimensional estimation of the power absorbed and cannot be greater than 100%. Values above 100% can be reached for the **capture width** or **absorption length** of a device which are three dimensional ratios of the absorbed power compared to the specified geometry of the device. Both capture width and absorption length take into account three-dimensional absorption by the device, therefore considering a greater energy input than the frontal wave attack.

The **bandwidth curve** of a device consists of a plot of the efficiency against the wave frequency for fixed geometrical parameters. This allows to determine the **tuning frequency** of a device, which identifies the frequency at which maximum efficiency is obtained (Cruz, 2008b).

2.3 Summary

In this chapter a glossary of the terms used within this report has been presented. This will allow the reader to better understand the concepts and the hypothesis of what will be presented in this thesis.

Chapter 3

Literature Review

Chapter 2 presented an introduction to the terms and theory commonly used for the analysis of wave energy devices.

This chapter is divided in two main sections: Section 3.1 provides a background on the development of wave energy conversion research and presents the state of art of all of the relevant wave energy technologies already in existence. The purpose of this section is to identify, after a review of the existing technologies, a suitable technology that can be employed to harness wave energy for the delivery of water.

Section 3.2 presents a review of the Oscillating Water Column device. The OWC represents the design foundation of the OWCP presented in this work. Through a review of the working principles of the OWC it will be possible to derive a theory for the OWCP.

3.1 Introduction to Wave Energy Conversion

Wave energy conversion is the harnessing of the energy that is contained within ocean waves to generate electrical or mechanical power. Ocean waves are a form of solar energy. Winds, generated by unbalance in the solar energy irradiated on the earth, act as the energy transfer agent between solar radiation and waves. In this process solar energy is concentrated, making wave energy highly valuable due to the its energy flux which is of an order of magnitude higher than the one of sun and wind energy (Hagerman, 2002). The global annual average flux of wave energy is 8 kW/m of shoreline, compared to the 300 W/$m^2$of panel area for solar energy (Isaacs and Schimtt, 1980).

Interest in ocean wave energy has been widely increasing since the 1970s when the UK

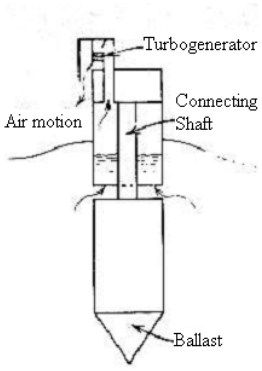

Figure 3.1: Schematic diagram illustrating the principle of operation of Masuda Buoy ocean wave energy converter (Masuda et al., 1986)

government boosted the funding for alternative energy research to overcome the petrol crisis of 1973 (Falcao, 2008). It was the wave-powered buoy designed by Masuda et al. in 1968 who demonstrated that it was possible to generate electricity from waves (Figure 3.1); meanwhile it was the work carried by Salter (1974) that augmented the optimism towards wave energy conversion development. In his paper Salter presented the concept of a pitching duck and showed that an efficiency of conversion of 90% of the incoming wave power could be achieved. This was confirmed later by the theoretical work carried by Budar and Falnes (1975) and Evans (1976).

From the early stage of mathematical works until now, worldwide, researchers have implemented over 100 different type of wave energy converters (Cruz, 2008b), although only few devices have reached prototype testing or full scale operation (Falcao, 2008). Problems with funding of the research and the experimental testing of devices are the reasons behind the slow development of a viable WEC. It is believed, however, that the development of wave energy technology has been slowed down by limiting the importance of physical modelling with numerical modelling being preferred at the initial stage of research. Physical model of WECs at an early stage is now envisaged as a fundamental step towards the successful development of a valid device (Holmes, 2003; Forestier et al., 2007; EMEC, 2009).

3.1.1 Device classification

As previously mentioned about 100 different types of WECs have been developed over the past 40 years. A full list of technologies developed can be found on the Marine and Hydrokinetic Technology Database of the U.S. Department of Energy website (U.S.D.E, 2009), which presents an up-to-date archive of marine energy converters. The wide variety of WECs developed, as a

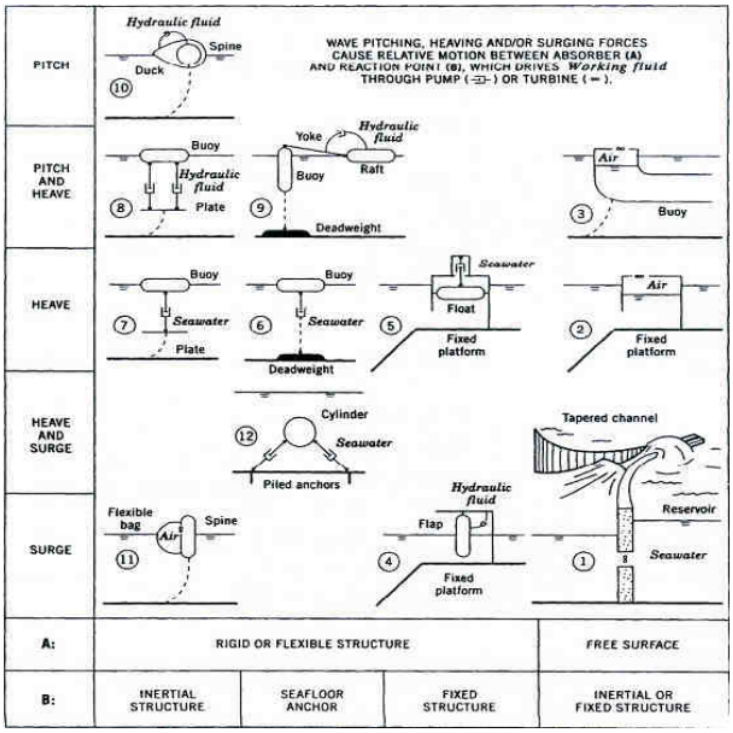

Figure 3.2: Classification of wave energy converters and their principles. Reaction points description is presented in the columns, while the rows show the type of energy absorption mechanisms (Hagerman, 2002)

result of the many ways in which wave energy can be absorbed, can be summarised through the use of a classification. Devices have been classified differently according to working principles, location and period of development. The classification presented by Hagerman (2002) provides a comprehensive review of the different technologies and is still employed in more recent reviews such as Brooke (2003); Previsic et al. (2004); Cruz (2008b).The Hagerman (2002) classification is presented in Figure 3.2.

Falcao (2008) presented an extension of Hagerman's classification of WECs, in which he evaluated devices that have reached prototype testings and categorized them on their working principle (Table 3.1).

From Table 3.1 three main categories of WECs can be identified: Oscillating Water Column (OWC) , Oscillating Bodies (OB) and Overtopping (OT) devices. It has to be noticed that the list presented in Table 3.1 consists of devices which are coupled with an electric Power Take Off system (PTO) designed for generation of electricity. Therefore devices like the DELBUOY (Hicks et al., 1989) and the SIBEO (Czitrom, 1997) which have reached the prototype stage but are not aimed directly to the generation of electricity have not been included in the table. The

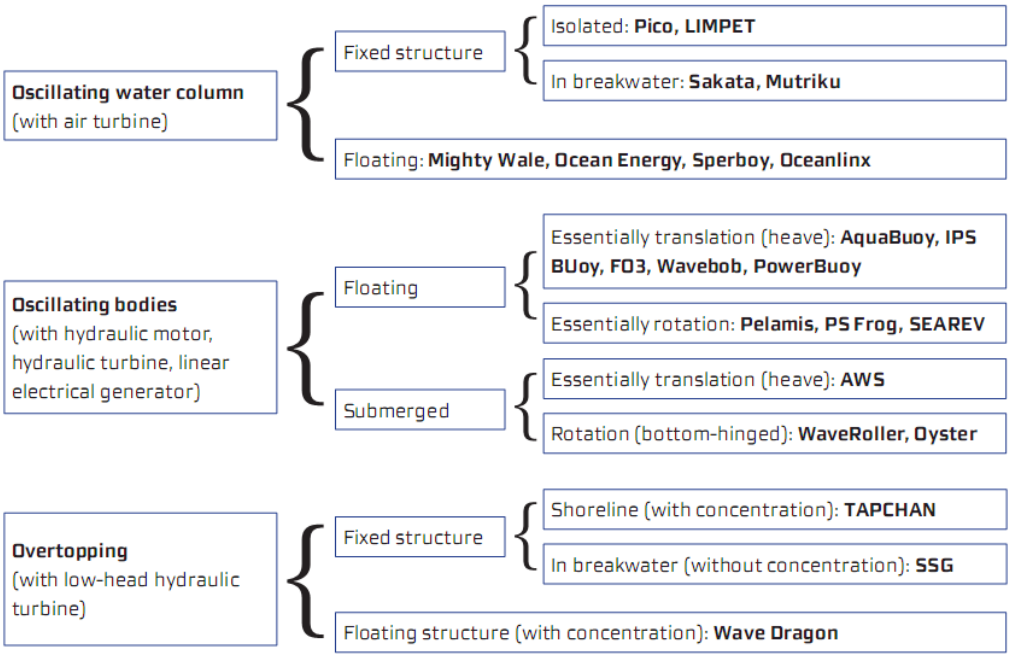

Table 3.1: Wave energy technologies that have reached prototype testing, classified on working principle. (Falcao, 2008)

development of WECs not aimed to produce electricity will be investigated later on in this work.

3.1.2 Oscillating water column

One of the first type of devices developed from the early stage of research is the Oscillating Water Column (OWC) (McCormick, 1981).

The main principle of the OWC is based on exploiting the rise in water level within a resonance chamber to compress air which is used to drive a turbine for the generation of electricity.

The OWC comprises a partly submerged duct or structure with an opening in contact with the sea, inside which air is trapped. A turbine for energy extraction is installed above the water-air interface. The incident waves generate an oscillatory motion of the internal free surface, which forces the air to flow through a turbine for the generation of electricity (Figure 3.3).

The concept of OWC was first developed by Newman (1974) while investigating the reflection of waves between two closely spaced vertical walls. Newman noticed that the motion of water between the two walls was oscillatory and that amplification of the incident wave height was observed. The full concept of OWC was presented later by Evans (1976), who simulated the coupling of a turbine by implementing in his mathematical model a single dash-pot system. By analysing the damping generated by the response of the turbine, Evans could determine the

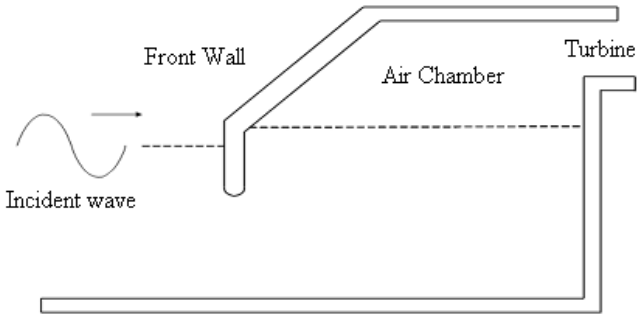

Figure 3.3: Schematic representation of a generic OWC device (Cruz, 2008a)

Country	Location	Site	Status
Australia	Port Kembla	Breakwater	Advance Stage Development
China	Dawanshan	Shoreline	Operational
China	Shanwei		Advance Stage Development
India	Vizhinjam	Harbor	Operational
Japan	Sanza	Shoreline Gully	Operational
Japan	Sakata Port	Breakwater	Operational
Japan	Kujukuri-Cho	Breakwater	Operational
Japan	Haramachi		Operational
Mexico		Marina	Operational - Pump
Norway	Toftoy	Cliff Wall	Operational
Spain*	Mutriku	Breakwater	Operational
Portugal	Pico	Rocky Gully	Operational
U.K.	Isle of Islay	Shoreline Gully	Operational
U.K.	Isle of Islay	Cliff Wall	Operational

Table 3.2: Fixed OWC devices installed worldwide (Brooke, 2003). *Mutriku Breakwater started operation in 2007.

efficiency of absorption of the incoming wave power. Two important results were obtained by the early work carried out by Evans: the amplification obtained within the walls of the OWC can reach 5 times the values of the incident wave height, and amplification is maximised when the natural frequency of oscillation of the OWC is tuned with the incoming wave frequency.

The development of OWC devices was favoured by the possibility of building the device in the near-shore zone, due to the advantages presented by ease of maintenance, installation and limited mooring of the device. Onshore OWC are regarded as first generation devices, as they were the first technology deployed and installed worldwide. Full scale prototypes were installed from 1985 onwards in Norway, India, Japan, United Kingdom and Portugal. The existing ones have been summarised in Table 3.2 by Brooke (2003)OWC technology according to the type of installation in the near shore area.

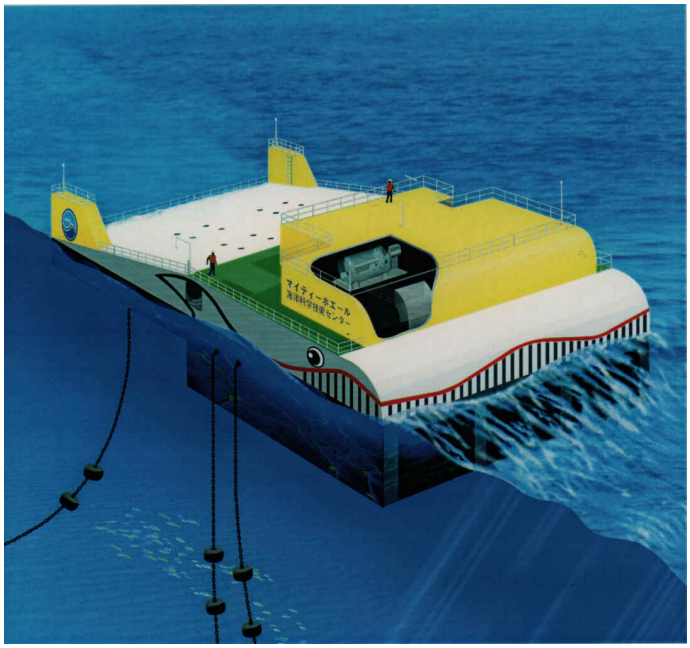

Figure 3.4: Prototype of the Mighty Whale floating OWC device.

From Table 3.2 one can notice how OWC devices have often been coupled with coastal defencive structures such as breakwaters and harbours. One of the best solutions found to reduce energy impact on a beach or structure is to use the structure to actively absorb the incoming energy. Over the past years defencive OWCs have been installed in Spain (Mutriku Breakwater, as presented by Torre-Enciso et al. (2009)) and are planned to be built in Portugal (Maciel, 2009).

One of the disadvantages of fixed OWCs is the reduced energy flux carried by shallow water waves, compared to deep water waves. The development of floating OWC devices allows the deployment of OWC systems in deep water waves, thus the harnessing of more powerful waves. Different floating OWCs were developed over the past 20 years including the Mighty Whale (Hotta et al., 1996) shown in Figure 3.4.

The major problem associated with OWC devices is represented by the resonance control system. Resonance control is needed to modify the type of damping that is imposed on the oscillatory mass of water from the wind turbine. In order to assure that the OWC is tuned with the incoming wave frequency, damping has to be modified to vary the natural frequency of oscillation of the device. To avoid the problems, OWCs are tuned with the significant wave conditions for a given location.

The use of floating OWCs allow the employment of a well developed technology in deep

water, hence in more powerful waves. Their deployment is however dependent on the results of prototype testing and those of other non-resonating devices.

3.1.3 Overtopping (OT) devices

Overtopping devices are designed to gather energy through a surging ramp that induces swelling of the incoming wave, in the same way that a sloping beach does. The focused waves are conveyed into a reservoir where overtopping water is collected. Energy in the reservoir is collected in the form of potential energy, and yielding a positive head difference with the energy of the water surrounding the reservoir. A low head turbine is used to convert the stored potential energy into electric energy whilst water is released back into the sea.

Installations of overtopping devices can be found onshore and offshore, predominantly in the north sea. Overtopping technologies have been mainly developed in the North Sea area, predominantly in Norway and Denmark.

The first overtopping device built at prototype scale was the TAPCHAN (Figure 3.5) installed off the coast of Noway in 1985 (Mehlum, 1986) with a nominal power of 350kW. The TAPCHAN concept was assessed a decade later for installation on the island of Java on the Pacific Ocean (Tjugen, 1995). The TAPCHAN consists of a tapered channel that gradually narrows down to allow the swelled waves to spill over the channel walls. The TAPCHAN was based on the same principles of the wave pumps presented by Bruun and Viggosson (1977), where the focused water was used for flushing of marinas and harbours. Other devices such as the Wave Dragon (Kofoed et al., 2006), shown in Figure 3.6, and the Wave Plane (WavePlane, retrieved on 15 May 2009) comprise a sloping ramp on which run-up effects take place and allow for water to overtop in a reservoir.

The Wave Dragon has reached prototype testing and is soon going to be installed off the western coast of Denmark under the supervision of Aalborg University Wave Energy Group. The efficiency of the Wave Dragon was determined to be 18% wave power to electricity generation (Tedd et al., 2006).

A recent development in the field of OT devices is the Seawave Slot-cone Generator (SSG) (Vicinanza and Frigaard, 2008) , designed as an onshore OT device.

The SSG (Figure 3.7) consists of a breakwater structure which integrates the run-up concept that was developed for the Wave Dragon. In particular the SSG is formed by multiple reservoirs placed on top of each other in which water spills driving multiple vertical axis turbines.

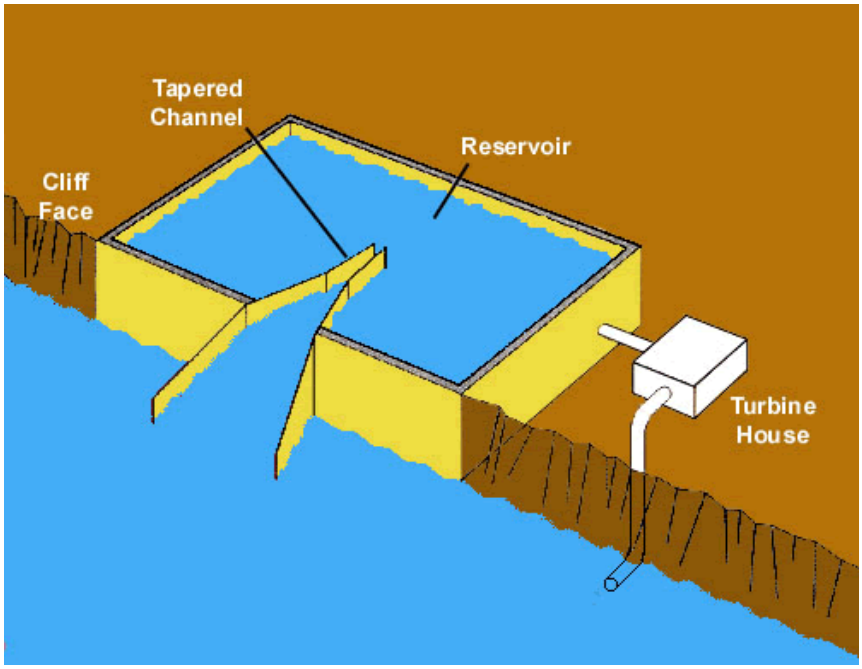

Figure 3.5: Schematic of the TAPCHAN overtopping WEC (Mehlum, 1986)

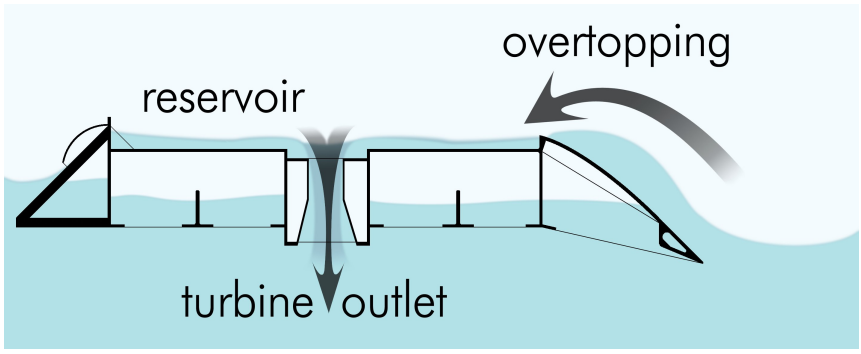

Figure 3.6: Side view of the Wave Dragon overtopping device (Kofoed et al., 2006)

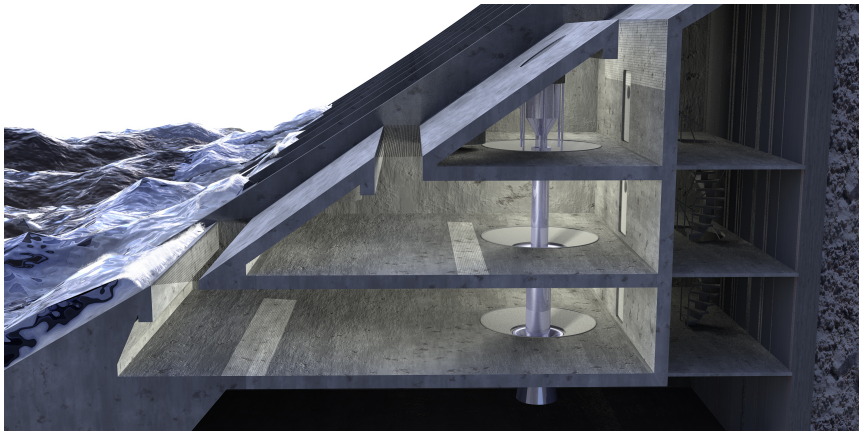

Figure 3.7: Seawave Slot-cone Generator multi-reservoir overtopping device (Vicinanza and Frigaard, 2008).

The main design arrangements for overtopping devices are dependent on the ramp and its inclination that generates the swelling and run-up of the waves. The inclination of each ramp is fundamental since, unlike coastal defence structures, overtopping devices have to maximise the spilling of water in the reservoir. The general tendency is to determine the best slope inclination for average wave conditions, as it is not possible to modify the slope once the device is operative. It was found that the best results are obtained when the inclination of the slope ranges between 30° to 40° Kofoed (2002).

The development of devices like the SSG integrates the need of assuring coastal protection with the possibility of recovering part of the energy contained in the impacting waves, in the same way the Mutriku Dragon was developed. The possibility of storing energy in the form of potential energy, and the higher efficiency attainable by low-head turbines makes onshore overtopping devices a viable solution for the generation of wave powered electricity.

3.1.4 Oscillating bodies (OB) devices

Different devices can be classified within the OB category, alternatively named as the Third Generation devices to represents the latest development in terms of WEC technologies. The OB classification presents a wider range of devices, with different working principles compared to OWC or OT devices.

Broadly speaking third generation devices are designed for offshore installation to exploit the more powerful wave regimes, and consist of more complex devices compared to OWC or OTs. The general OB device is partly or completely submerged, and designed to operate in an array of devices to maximise the generation of electricity. A wide range of OB devices has been developed. Figure 3.8 shows examples of heaving point absorbers such as the PowerBuoy (OPT, 2010), the AquaBuoy (Finavera, 2010) and the Wavebob. The Wavebob is the first wave energy device that has generated electricity off the coast of the Republic of Ireland (Webber et al., 2009).

A surging type of point absorbing WEC was developed by Aquamarine Power and Queen's University of Belfast. The Oyster is a bottom-hinged, near-shore surging paddle WEC mounted on the seabed (Whittaker and Folley, 2007). A full size prototype of the Oyster, rated at 350 kW of power, was installed in Orkney in November 2009, at the European Marine Energy Centre, for prototype testing. The design of the Oyster, shown in Figure 3.9, allows for the device to be employed for desalination applications. Folley (2008) evaluated the applicability of wave energy conversion for desalination and later analysed the use of the Oyster as an autonomous system for

Figure 3.8: From left to right schematic of the PowerBuoy (OPT, 2010), AquaBuoy (Finavera, 2010) and Wavebob (Webber et al., 2009).

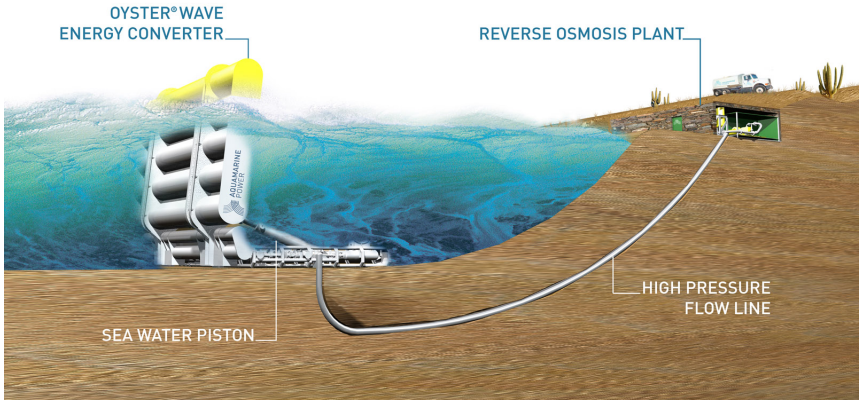

Figure 3.9: The Oyster wave energy conversion system for desalination application (Folley et al., 2008)

desalination (Folley et al., 2008). Further analysis, carried by Folley and Whittaker (2009), were aimed to the determination of the cost of desalted water if produced with an Oyster powered autonomous desalination device.

The Pelamis (Yemm et al., 2000) and the Anaconda (Chaplin et al., 2007) are two of wavelength absorbers WECs. The Pelamis (shown in Figure 3.10) was evaluated as the only mature technology for prototype testing in the U.S. due to its survivability and cost effectiveness (Previsic et al., 2004), however this technology has yet to reach full commercialisation. The Anaconda is reaching prototype testing at the current time and has drawn much attention in the media due to its simple design and manufacturing (www.guardian.co.uk, retrieved on May 6 2009), making it cost-effective and highly resistant in harsh conditions.

3.1.5 WECs for alternative applications

The generation of electricity is not always the final step of the process of wave energy conversion. Whilst much attention is paid to successfully generate electricity from wave power, it is possible

Figure 3.10: Installation of the Pelamis WEC in a wave farm (Yemm et al., 2000)

to exploit parts of it for other coastal applications.

Over the past 20 years, different applications have been associated with the conversion of Wave Energy. An overview of the possible combinations of WECs for near shore activities powered by wave energy can be seen in Table 3.3. The benefits that can be achieved by combining wave energy conversion with other activities, and presents existing scenarios of devices which were implemented and tested for such purpose, are summarised in Table 3.3.

Coastal protection strategies can be combined with electricity generation in order to reduce cost of installation and provide double functionality. Other applications such as marina flushing and seawater desalination can exploit wave power to further reduce operational costs. Few examples of devices which have reached prototype or full scale installation can be found in literature (Cruz, 2008b).

The Wave pump concept was introduced by Bruun and Viggosson (1977) who studied a system to increase the flushing of enclosed harbours. They employed a system that was similar to those installed in ancient Mediterranean harbours as reported by Franco (1996). The Wave pump consisted of a concrete channel where incoming waves were conveyed. The narrowing of the channel allowed for the waves to swell and overtop into the harbour, thus reducing the flushing time of the enclosed area. The same principle was then applied to the TAPCHAN as

Type of Application	Hypothesis	Benefits	Case	Problems
Wave Powered Desalination	Converting wave power into mechanical energy for the generation of the pressure required for Reverse Osmosis Membrane Process	Feed and Power available directly on site	DELBUOY and Oyster devices were developed and tested for RO.Vinjzialan Plant in India	DELBUOY halted by poor survivability of the device. Oyster is under development Vinjzialan Plant does not employ direct conversion system, low efficiency.
Coastal Protection	Implementing wave energy converters in the coastal structure, whilst reducing the impact generated on the structure	Part of the energy that is absorbed by the WEC is effectively removed from the system reducing wave loads and pressures.	Mutriku Dragon, OWC Cassion Breakwater, SSG	OWCs integrated Breakwaters presents same limitations and low efficiency like traditional OWC devices. SSG is under prototype testing
Flushing of Ports, Marina and Farms	Using the energy contained in wave to drive fresh water in confined area	Increased amount of water from wave action augments mixing of oxygen, reduces pollutants concentration and increase nutrients.	Wave Pumps (natural and artificial) SIBEO	Low flow rates have favoured installations of other flushing mechanisms. Little interests in development of such device due to economical return.

Table 3.3: Benefits and Case for alternative and complimentary application for Wave Energy Devices

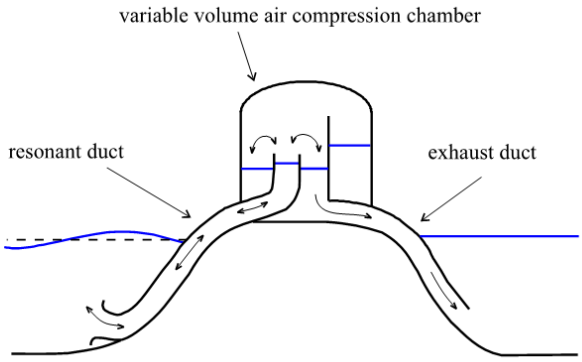

Figure 3.11: Schematic of the SIBEO Seawater Pump. The resonant duct is in contact with the incoming wave train. The exhaust duct is used to discharge water into the marina. The Compression chamber is used to control and maintain resonance conditions. (Czitrom, 1997)

seen in section 3.1.3. The Wave pump converted the momentum contained in the wave particles to potential energy. A full scale model of the Wave pump was installed in Panama, helping the flushing of the marina. Similar installation of natural examples of the Wave pump can be found on fishing atolls in the pacific ocean (Callaghan et al., 2006).

The Wave pump concept was later revisited by Czitrom (1997) who introduced the SIBEO seawater pump for the flushing of lagoons. The SIBEO (Figure 3.11) device presented only few features of the wave pump introduced by Bruun and Viggosson (1977). Whilst aimed to the deliver water for coastal management applications in the near shore, the SIBEO resembled in its operational system the OWC. The device comprised a resonant duct which was in contact with the incoming wave train, an exhaust duct employed to discharge water in the marina and a compression chamber which was used to control resonant conditions.

In Figure 3.11 it is possible to notice that the the Compression Chamber is divided into three sections. The chamber is controlled so that the volume and pressure of the air can be varied and adapted in response to changes in the sea conditions. Once water is spilled in the chamber by the resonance duct, changes in the pressure within the chamber allow for the water to be pushed through the exhaust duct. The SIBEO has found application in the port of Ensenada in South Mexico, as shown in Figure 3.12, where it was used for the flushing of fisheries (Czitrom et al., 2006).

The Wave pump and the SIBEO were developed to exploit wave energy for coastal management purposes. Hicks et al. (1989) developed a wave energy device aimed to direct sea-water desalination. The DELBUOY (Figure 3.13) consisted of a point absorbing device equipped with

Figure 3.12: Installation of the SIBEO on the shore of Ensenada in Mexico. It can be seen how the device represents a simple low cost WEC of easy installation .(Czitrom et al., 2006)

a floating buoy. The oscillatory movement of the waves caused the buoy to act on a piston-pump which pressurised seawater and forced it through a reverse osmosis membrane. The DELBUOY device reached prototype scale testing, however a full scale installation of device in Puerto Rico was interrupted due to a storm disrupting the foundations of the device and halting funding to the project (Davies, 2005). The disruption of the DELBUOY presented researchers with the issue of the structure survivability of the WECs, and prompted work on the mooring of devices.

The CETO WEC (SPPL, 2010) has been developed on the same principle of the DELBUOY, but its main purpose is the electricity generation. Both DELBUOY and CETO were designed to work in a farm of multiple devices.

Other devices were considered for application in the field of seawater desalination. Cruz and Salter (2006) presented a modified version of the Salter's Duck (Figure 3.14).

The modified Duck was designed to exploit the asymmetric pitching movement to generate pressure differences. The "desalinating ducks" convert wave energy into pressure changes that aid the collection of pure water as steam from seawater. By lowering air pressure, the system can draw steam from water at lower temperatures. Folley and Whittaker (2009) evaluated with the means of a mathematical model, a case for employing the Oyster device for seawater desalination. Sharmila et al. (2004) presented the case of an OWC device coupled with an RO osmosis membrane. The device is installed on the coast of India in Vizhinjam. The OWC is employed to generate electricity through a Wells turbine. The electricity generated is used to drive a Reverse Osmosis Membrane for the desalination of seawater. The OWC operates with an efficiency of

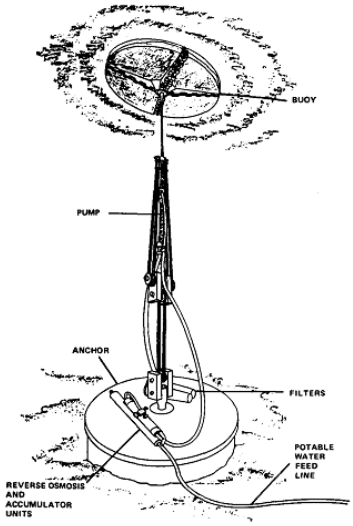

Figure 3.13: Schematic of the DELBUOY device (Hicks et al., 1989).

18% (wave power to electricity), however the plant is running to assure the supply of drinking water to an arid area.

Other applications such as coastal defense have been evaluated during the design of Caisson Breakwater coupled with OWC (Dhinakaran et al., 2002; Thiruvenkatasamy et al., 2005; Boccotti, 2007) and in the case of the SSG converter (Vicinanza and Frigaard, 2008).

3.1.6 Summary

Section 3.1 presented a review of the existing technology in the field of wave energy conversion. The objective of this section was to help identifying a WEC design that could be employed towards the development of a wave energy converter for water delivery. Two kinds of WEC can be used to exploit the energy carried by waves to generate potential energy: Overtopping devices and the OWC.

In particular the OWC can generates a resonant type of response lifting the incoming wave up to 5 time the initial value, whilst overtopping devices exploit the run-up of wave to deliver water into a reservoir. The possibilities of tuning the OWC to respond to the changes in the wave conditions, and the application of an OWC-type device like the SIBEO for water delivery, leads to the conclusion that it is possible to exploit the principle of the OWC to develop a resonant WEC aimed to deliver water.

For this reason the OWC and the SIBEO device were chosen as main references for the

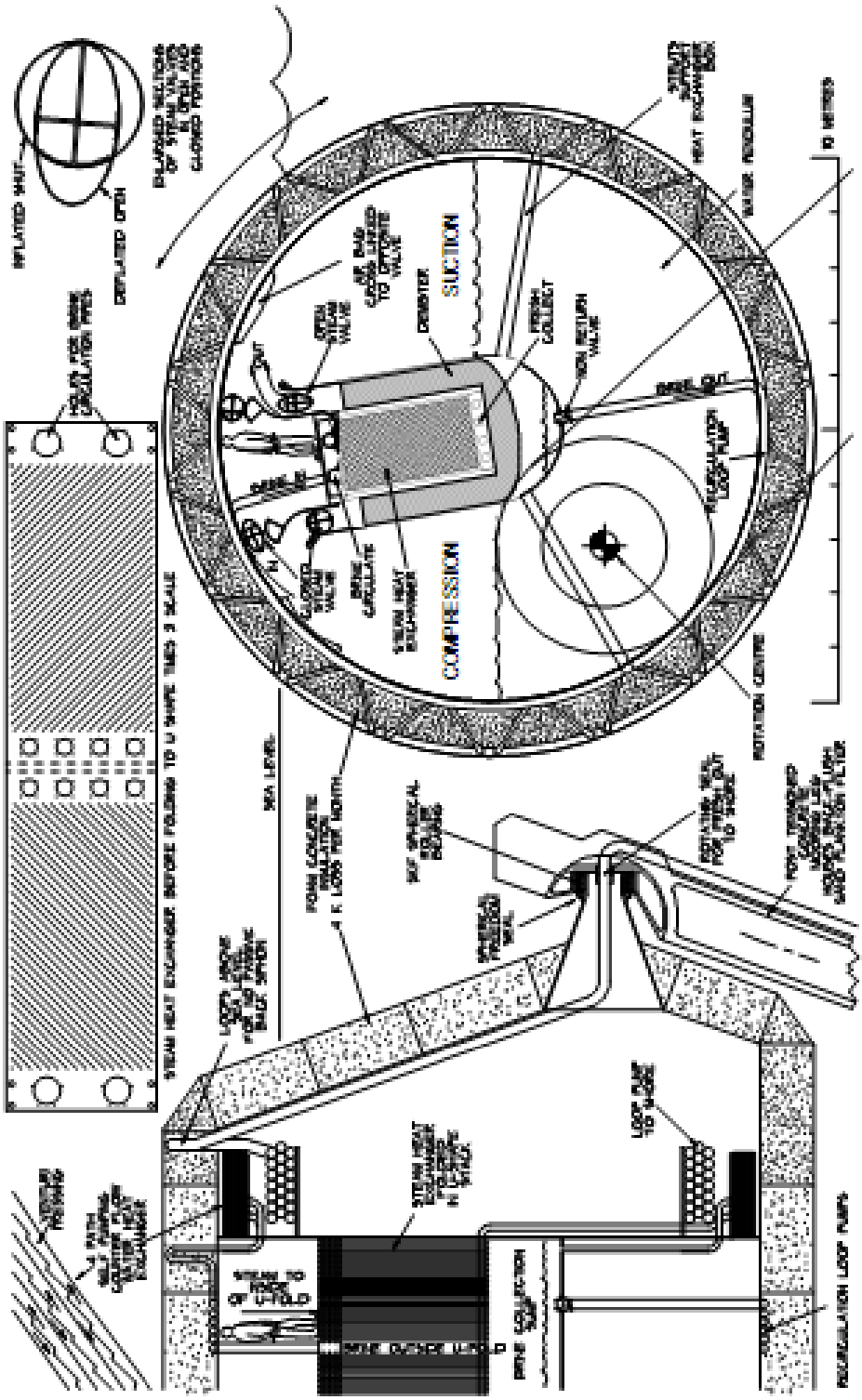

Figure 3.14: Schematic of the desalination Duck (Cruz and Salter, 2006)

development of the Oscillating Water Column Wave Pump (OWCP) presented in this work. An in depth review of the mechanism of the OWC is presented in Chapter 3.2.

3.2 Literature Review: Oscillating Water Column

OWC devices represent the class of WECs which has gained most of the attention from the scientific community, and they constitute the basics of wave energy conversion (Cruz, 2008b), by providing a cost-effective and reliable solution for the conversion of wave energy into useful power (Heath, 2008).

One of the aspects making the implementation of OWCs advantageous, compared to other WECs, is the fact that the functioning mechanisms of OWC are well defined and common to every installation. This similarity allowed for faster development and optimisation of the technology compared to the point absorber WECs, which are developed singularly. Numerous OWC installations have been built worldwide, as aforementioned in Table 3.2. Up to date, 13 OWCs are currently installed allowing for an important exchange of knowledge and expertise. Considering the amount of research dedicated to the OWC, the device is still far from reaching optimum efficiency. Many of the issues that the OWC presents are related to the development of such technology, which finds its root in mathematical analysis of wave phenomena.

The possibility of employing the OWC for pumping and water delivery provide the opportunity to further explain the dynamics of the device, allowing for the full evaluation of alternative uses of the device. The following section presents the development of the OWC and highlights areas of research needed, such as demonstrating the applicability of the OWC for overtopping purposes.

3.2.1 Initial Development of the OWC

The processes that led to the development of the OWC device started with theoretical investigation of the behaviour of waves propagating into a wave flume. The initial description of the OWC can be found in Newman (1974) who investigated the behaviour of a wave travelling towards two closely spaced vertical walls. Newman was interested in determining the changes in the wave field due to the presence of the two walls. He aimed to determine the amount of waves that got reflected by the interfering obstacles and the part of waves which got transmitted after the two walls. He defined the reflection coefficient (K_r) as the ratio between the reflected wave

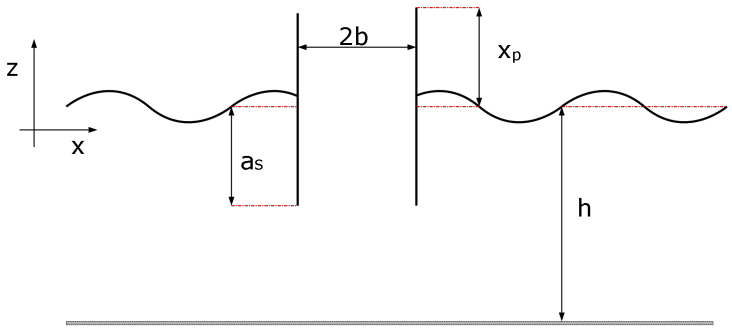

Figure 3.15: Formulation of Newman's investigation (Newman, 1974)

height to the incoming wave height; and the transmission coefficient (K_t) as the ratio between the transmitted wave height to the incoming wave height. Newman worked in a 2-dimensional wave tank and assumed that linear wave conditions could be employed in the description of the problem. The schematic of Newman's experiment can be seen in Figure 3.15.

In order to determine the reflection and transmission coefficients, Newman used a mathematical model and solved the problem by using the methods of matching asymptotic expansion. This method allows the decomposition of the problem in two domains, later solved with the use of asymptotic series (Verhulst, 2005). Newman separated the problem in inner (inside the walls) and outer (outside the walls) part. While solving for K_r and K_t, Newman noticed that the water level within the two walls increased at the passing of waves. Moreover, he noticed that the behaviour of the water column contained within the two walls was of a resonant type and dependent on the incoming wave frequency and on the characteristic dimensions of the two walls $2b$ and a_s .

The same method was later used by Evans (1978) when he re-assessed Newman's work. Evans, who earlier determined a theory for wave energy absorption by longitudinal oscillating bodies in Evans (1976), was the first to investigate the potential of Newman results and to consider the motion of the column of water within the two walls for wave energy application.

In order to develop the concept of the OWC, Evans combined the work of Newman with the design of a damped-oscillating heaving body studied by Budar and Falnes (1975). The damper on the heaving body allowed for the wave energy to be transferred from the wave to the load.

Evans therefore simulated the power take off system of the OWC by adding a single damper on the device. The addition of a float-spring-dash-pot system was not considered by Newman.

The damper allowed the oscillating water to compress air at the upper end of the tube. This air was then forced out through a small orifice and sent to a turbine (Evans, 1978).

Evans defined the problem in a 2-dimensional domain, considering regular waves acting on the two vertical walls with orthogonal angle of incidence. He, therefore, provided a mathematical explanation to the phenomena. Evans assumed linear wave conditions for describing the problem, and considered a wave travelling from $x = +\infty$ as shown in Figure 3.15. By considering the real part of the Velocity Potential ϕ (equation 3.1)

$$\phi(x, z, t) = Re\left\{\phi(x, z)e^{-i\omega t}\right\} \tag{3.1}$$

Evans proceeded then to assess the equation of the pressure field p of a traveling wave as follows:

$$p - \rho g z + \frac{\partial \phi}{\partial t} = p_0 \tag{3.2}$$

where p_0 represents the atmospheric pressure, z is the vertical displacement of the water within the two walls, g the gravitational acceleration and ρ the water density . Outside the water column $p = p_0$, whilst considering the changes in p within the two walls it is possible to determine the force per unit float acting on the water column (equation 3.3);. Considering as 1 the unit length and using ζ to represent the displacement of the damper, the force per unit float can be expressed as:

$$p \times 2b \times 1 = -m\ddot{\zeta} - C_d\dot{\zeta} - C_f\zeta \tag{3.3}$$

Where the coefficients C_d and C_f represents respectively the damping and the friction within the float.

A further assumption was then made by Evans, who considered that the water level within the water column is independent of the location x; hence $\Upsilon(x, t) = \Upsilon(t)$ assuming that water level within the column is uniform. By using this assumption, Evans generated what has been later referred to as the Rigid Piston Modelling of the OWC, when from a 2D formulation the problem is analysed in 3D. Evans stated that the movement of the water column contained within the walls is comparable to the one of a piston, and that the air received a uniform compression at the passing of waves.

Evans considered the kinematic boundary conditions of linear wave theory expressed in equation 3.4:

$$k\phi + \frac{\partial \phi}{\partial z} = 0 \tag{3.4}$$

and rewrote it for the water within the two walls as follow

$$k_1 + \frac{\partial \phi}{\partial z} = 0,\ y = 0,\ 0 \leq x \leq 2b \tag{3.5}$$

by considering $k_1 = k[1 + \delta + i\gamma]^{-1},\ \delta = (C_f - m\omega^2)/2b\rho g,\ \gamma = d\omega/2b\rho g$

with γ representing the damping coefficient and δ the spring coefficient. By applying the methods of matching asymptotic, Evans determined the value of the velocity potential away from the two thin walls.

$$\phi \sim \begin{cases} e^{-ikx} + K_r e^{ikx}, & x \to +\infty \\ K_t e^{ikx}, & x \to -\infty \end{cases} \tag{3.6}$$

From equation 3.6 it was possible to state that the velocity potential is affected at the point of origin of the wave by the reflected waves, while the velocity potential is only dependent on the transmission coefficient after the waves have passed the device. In both cases the wave amplitude is equal to ω/g.

Further derivations allowed for the determination of K_t and K_r, from which Evans defined the efficiency in power absorption of the walls E as follows:

$$E = 1 - |K_t|^2 - |K_r|^2 \tag{3.7}$$

From equation 3.7 Evans derived that the maximum efficiency in absorption that can be obtained is $E = \frac{1}{2}$ when $d = 0$ and γ is chosen to assure that resonant conditions are maintained within the chamber. Resonant conditions are obtained in the chamber when the natural frequency of oscillation of the device ω_0 matches the angular wave frequency ω, where ω_0 is given as:

$$\omega_0 = \sqrt{\frac{g}{a_s}} \tag{3.8}$$

Whilst the case where $d = \gamma = 0$ would generate the results obtained initially by Newman (1974), Evans noted that by adapting the value of γ it is possible to increase the level ζ within

the two walls, hence maximising the force that is transmitted to the float.

Evans defined the magnification factor M as the ratio of the maximum displacement of the water column to the incoming wave amplitude a . M is given by equation 3.9 as follows:

$$M \simeq e^{k_1 a}/8bk_1 \tag{3.9}$$

In his paper Evans (1978) showed how values of M up to values of 4.5 can be reached if the device is tuned with the wave frequency however the bandwidth of response is relatively small, indicating that is necessary to control damping to assure response of the device to different wave conditions.

One of the insights that gained from the earlier work carried out by Evans is the fact that the energy absorption can be increased if the transmission of the waves travelling after having hit the walls is reduced. The work carried out by Evans was still purely theoretical and did not take into account the effects of the air turbine, the dependency of ζ on x . Furthermore while the damping coefficient was proved to be fundamental for the functioning of the device, Evans did not present any assumption of how geometry and wave conditions affected it.

A first review of the initial model of the OWC was presented a few years later again by Evans (1981). Evans focused on the determination of the damping coefficient for an OWC and also analysed the motion of the device following excitation from incoming waves. Furthermore Evans integrated his work with that of Count (1978) to asses the effects of damping generated when the waves hit the walls, therefore evaluating the damping due to the radiation of waves away from the walls.

Count (1978) analysed the motion response of partially submerged structures to determine the dynamics of the object in n degrees of freedom, and determined the force acting on the structure. Count, by extending the existing methods to solve hydrodynamics problems, described the oscillatory motion of the system as follows:

$$\sum_{i=1}^{n}\{I_{ij}\ddot{X}L_j + B_{ij}Xj\} = F_i^w(t) + F_i^{ext}(X_j,\dot{X}_j,\ddot{X}_j)\; i = 1,2,n \tag{3.10}$$

where $X_j, \dot{X}_j, \ddot{X}_j$ represent respectively the displacement, velocity and acceleration matrix of the device in the j^{th} motion. I_{ij} is the inertia matrix while B_{ij} is the spring matrix due to buoyancy. F^{ext} represents the external force applied at the i^{th}mode; whilst F^w is the wave induced force acting on the walls at any time.

Evans (1981) reformulated equation 3.10 for a 1 degree of freedom problem, considering as the only coordinate the displacement of the water column within the two walls $\zeta(t)$ as a function of the time.

Equation 3.10 became then

$$m\ddot{\zeta}(t) + d\dot{\zeta}(t) + C_f\zeta(t) = F(t) \tag{3.11}$$

From equation 3.11 Evans proceeded to decompose the hydrodynamic pressure force $F(t)$ in two components: $F_s(t)$ the exciting force acting on the two walls, corresponding to F^{ext} in the work by Count (1978); and $F_r(t)$ representing the wave induced radiation force, corresponding to F^w of equation 3.10.

Equation 3.11 was then reformulated in the time domain to account for the separation of exciting force as follows

$$F(t) = F_s(t) + F_r(t) = Re(X_s e^{i\omega t}) - (m+\mu)\ddot{\zeta}(t) - B\dot{\zeta}(t) - C_f\zeta(t) \tag{3.12}$$

Where the complex term X_s represents the amplitude of the exciting force $F_s(t)$, $m + \mu$ represents the total mass including the added mass term μ,which in turn represents the increase in the inertia of the system due to the radiation of waves. B is the wave induced radiation damping. Both μ and B are function of the wave frequency ω.

Evans then proceeded to re-asses the efficiency E of absorption of the device as a function of ω from equation 3.12

$$E(\omega) = \frac{4\omega^2 dB\gamma_c}{\{C_f - (m+\mu)\omega^2\}^2 + \omega^2(d+B)^2} \tag{3.13}$$

In equation 3.13 Evans considered the role of physical damping and friction d, C_f and the effects of radiation damping and added mass B, μ. The coupling coefficient γ_c represents the effect of the wave amplitude away from the device, as reported in Evans (1976).

Therefore in order to maximise $E(\omega)$ it is necessary that the device is tuned to the incoming wave frequency. This is achieved when

$$\omega = \omega_0 \tag{3.14}$$

giving that resonance is obtained when

$$C_f = M\omega_0^2 = (m + \mu(\omega_0))\omega_0^2 \tag{3.15}$$

and

$$d = B(\omega_0) \tag{3.16}$$

It is clear from equations 3.15 and 3.16 that the ideal functioning of the OWC depends on the determination of the damping and added mass coefficients.

The determination of the hydrodynamic coefficients could be carried out both in the time and frequency domain, and they play a fundamental role in the assessing the performance of the OWC, and of any WEC. The possibility to implement a resonance control system, as presented by Bjarte-Larsson and Falnes (2006); Falnes (1993); Babarit and Clement (2006), aims to modify the radiation damping and added mass matrix in order to maximise power absorption and performance of the device.

3.2.1.1 Capture width of the OWC

Evans (1981) found another relationship between the geometrical device of the the OWC and the wave conditions in the form of the capture width of the device.

The capture width represents the ratio of total mean power absorbed by the device to the mean power per unit crest wave width of the incident wave train (Cruz, 2008b), where the term *mean* refers to the average value per energy period. In short the capture width represents the length of wave crest that contains the absorbed wave power (Mei, 1989).

The capture width is used to evaluate the performances of an isolated 3D device, and it considers the overall power absorbed by the OWC and not only the amount of incident wave power like in the case of efficiency. The relative capture width (width absorbed/width device) can posses values greater than one. Three dimensional effects permit the OWC to absorb power from a wave front which is bigger than the width of the device itself.

Evans (1981) determined the relationship between the capture width and the wave length of the incoming wave train, and subsequently went on to determine the maximum capture width for submerged devices. He found that the maximum capture width λ_{max} of the device is dependent on the motion of the device and relates to L as follows:

$$\lambda_{max} = \frac{\epsilon L}{2\pi} \tag{3.17}$$

with the coefficient ϵ depending on the motion of the device accordingly

$$\epsilon = \begin{cases} 1 & heave \\ 2 & sway, surge \end{cases}$$

For a 1 d.o.f. OWC model the only motion considered is heave, from which it follows that $\lambda_{max} = \frac{L}{2\pi}$.

3.2.1.2 Overtopping OWC

Knott and Flower (1979) considered the work carried by Evans (1978) and evaluated the possibilities of using the OWC device for overtopping purposes. They assessed the use of the device with two identical semi submerged walls in deep water waves, whilst achieving values of the magnification factor M up to 4 times the incoming wave amplitude, in the same order of magnitude of those obtained initially by Evans (1978).

Knott and Flower simulated the removal of water from the OWC by implementing a non linear mathematical model to describe the mechanism of the OWC. The results obtained showed that the removal of substantial amounts of water can be achieved only at low wave frequencies. Hence long waves carrying high energy were required in the system implemented by Knott and Flower.

The work of Knott and Flower was left unfinished with research of the OWC focused on the generation of electricity. It is possible to identify the limitations that affected the work carried by Knott and Flower. Their simulation was run with 2 identical semi submerged thin walls, hence allowed for a high transmission rate of the wave after having encountered the interference of the walls. Furthermore, whilst assessing the removal of water they have failed to suggest how the potential energy gained could be employed for the generation of electricity. However, they where the first to develop and consider non-linearities in the mathematical description of wave energy converters.

Czitrom (1997) reassessed the proposed OWC from Knott and Flower, and incorporated their work in the development of an OWC for seawater delivery. The work of Czitrom was made possible by the integration of the design of Knott and Flower (1979) with the progresses made in

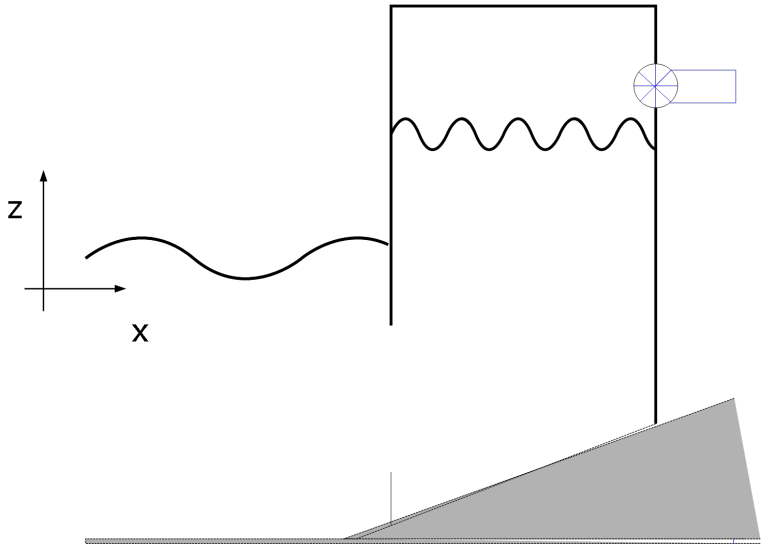

Figure 3.16: Oscillating pressure profile within the OWC profile (Evans, 1982). The profile of the free surface is affected by the presence of the turbine and varies along the chamber.

the description of the OWC mechanism over the past 20 years. In particular the mathematical description of the OWC was completed by Evans (1982) who considered the oscillations of air pressure within the two walls, as an integration to the rigid-piston model.

3.2.2 OWC Oscillating pressure mathematical model

The mathematical description of the OWC was further implemented by Evans (1982), when he introduced the concept of the oscillating pressure within the two walls.

The behaviour of the water column was assumed uniform within the resonant chamber and considered similar to the one of a rigid piston. Evans noted that if the distance $2b$ between the two walls was large enough, waves could develop within the two walls generating a non uniform pressure on the entrapped air (Figure 3.16).

The pressure term p of equation 3.2 was modified to include the variation given by the generated waves as follows:

$$p_c(t) = p_0 + p(t)\ p(t) = Re(\mathbf{P}e^{i\omega t}) \tag{3.18}$$

where $p_c(t)$ represents the pressure within the chamber, and $\mathbf{P}$ is a complex matrix that allows to relate the pressure generated by the incoming waves.

By considering the changes in pressure, Evans was then able to assess the turbine's effect on the water column. This led to a more complete and accurate determination of the damping coefficients for the OWC device.

Evans, however, was mostly focused on the determination of the hydrodynamic characteristics of the OWC and therefore the hydrodynamic efficiency of the device. The overall conversion efficiency from waves to electricity was not assessed in the work carried out by Evans, since the PTO mechanism was yet to be identified. The full wave to wire description of the OWC includes the investigation of up to 4 different domains, as presented by Weber and Thomas (2001). The four domains include the hydrodynamic domain,the aerodynamic domain relative to the air-flow within the OWC chamber, the PTO domain and finally the aerodynamic domain of the air-flow exiting the duct.

With a full mathematical description of the OWC ready, research was then focused on three main objectives:

- Identifying a valuable power take-off system for the generation of electricity
- Determining the hydrodynamic coefficients to maximise the output of the OWC
- Validating the mathematical results through the use of physical models of the OWC

Of particular relevance to the purpose of this review are the latter two paths. The work carried on the development of a counter-rotating Wells turbine presents a strong component of mechanical engineering. It has although little relevance with the work presented here. On the other hand, the determination of hydrodynamic coefficients of the OWC along with physical investigation into the mechanisms of conversion represent the part of research that was actually focused on the primary energy conversion from wave energy to potential energy.

3.2.3 Hydrodynamic analysis of the OWC

The hydrodynamic domain analysis focuses on the effects of the wave field on the performance of the device, by separating the wave field effects of radiated and diffracted problems. Hence it is possible to determine the damping coefficients and the added mass term for the device and derive the response of the device to the effects of the air turbine. The determination of the hydrodynamic coefficient can be carried out numerically in both frequency and time domain, and experimentally.

The initial work on the OWC was mostly aimed to provide a better understanding of wave making theory and energy absorption. The various models presented by Newman (1974); Evans (1978); Count (1978); Evans (1982) whilst describing the process of absorption of the OWC did not address the practicality of the development of the OWC from a theoretical concept to an actual WEC.

A first step in the direction of optimising the OWC device was undertaken by Reitan (1991) who presented a mathematical model for the description of the OWC based on the analysis of the velocity potential outside the water column and within the air chamber. By doing so Reitan avoided the issues of radiation damping and scattering forces due to the wave generated during impact with the OWC walls, and determined the relationship between the capture width of the device and the wave frequency. Reitan however admitted that although relationships between the geometry of the device and the absorption can be found, these were just good estimates and that they were no substitute of the detailed calculation one can determine accounting the actual configuration of the device.

Following the work carried by Reitan, the mathematical description of the OWC was implemented for the accurate determination of the hydrodynamic coefficients. The advances in the development of the wells turbine allowed to account for the turbine effects on the damping coefficients.

Evans and Porter (1995) suggested a mathematical model for the determination of the hydrodynamic coefficients of an OWC device coupled with a bi-directional Wells turbine. They considered the turbine to add a further mass-dash-pot to the model developed by Evans (1982). The OWC coupled with the turbine could be considered then equivalent to a mechanical system represented by a double-mass-damped oscillatory system (Figure 3.17)

Evans and Porter (1995) provided a mathematical description based on the mechanical equivalent of the system. They employed a 2×2 matrix which was directly related to B and μ, both considered as functions of the wave frequency. Evans and Porter, however, had to employ a linearised solution to the problem to determine the values of the coefficients. This proved to limit the description of a strongly non-linear system.

A further implementation to the model was presented by Evans and Porter (1997) where they considered the effects of scattering and radiation of differently shaped structures for the determination of damping and added mass. The model still employed a linearised solution to solve the system.

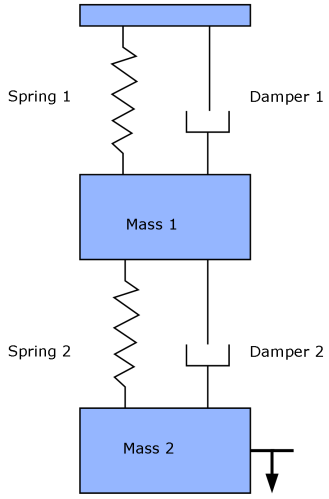

Figure 3.17: Mechanical equivalent of the OWC equipped with Wells Turbine (Evans, 1982)

Brendmo et al. (1996) used mechanical and electrical analogies of the OWC to describe the dynamics of the oscillating water column and to include viscous losses that until then were neglected in the linearization. In both cases they considered the viscous losses independent from the frequency of the excitation force, thus reducing the OWC description to a simpler dynamical system with easier solution. Moreover, they integrated the two mathematical models of the OWC with an experimental method employed to determine the hydrodynamic coefficients.

Brendmo et al. (1996) were among the first to employ a physical model to simulate the overall functioning of the OWC, even though they did not employ a Wells turbine, but simulated the pressure drop due to the conversion process. Until then, physical models of the OWC were used mainly to analyse losses at the entrance of the device and to assess structural stability in extreme case scenarios.

Perdigao and Sarmento (2003) later on suggested a mathematical model aimed to improve the overall efficiency of conversion of the OWC. They developed a model to assess conditions for which the maximum wave absorption could be obtained in order to maximise the generation of electricity.

Morris-Thomas et al. (2007) evaluated the use of different geometries for the determination of B and μ and improve the hydrodynamic efficiency of the OWC. By using different shapes of the OWC they achieved a reduction of the viscous losses and increased the performances of the device.

Recent work on assuring a quick response of the device to the changing conditions was carried

out by Olvera et al. (2007) . Olvera et al. evaluated the use of a parametric resonance control in the SIBEO device to maintain resonant conditions. They evaluated how a change in a single parameter (such as pressure within the chamber or the air volume) could shift the device towards resonance and how quickly would the system take to adapt.

3.2.3.1 Panel methods for the determination of the hydrodynamics coefficients

A widely used instrument for the determination of the wave induced motion and loads is represented by 3D panel methods (Delaure, 2001). 3D panel methods, or Boundary Element Methods (BEM) are based on the potential flow theory. Panel methods offer the advantage to be of minimal computational requirements (McCabe, 2004), and to provide a three dimensional solution to the hydrodynamic problem(Delaure, 2001).

The assumptions for the use of BEM are the same of linear wave theory presented in section 2.1, which consider the flow to be both frictionless and irrotationtal. These assumptions allow us to define the existence of the velocity potential ϕ as a function of x, y, z, t. The description of the application of the potential theory to the OWC is widely available in literature and can be found in Falnes (2003); Brito-Melo (2000); Delaure (2001); Lee et al. (1996) among others.

The principles of BEM methods rely on solving the unknown potential of the the boundary problem for discrete points (panels) of the wet surface. Once the body shape is defined and discretised, BEM methods determine the radiation and diffraction velocity potentials on the body wetted surface by using Green's theorem with the free-surface source-potential as the Green function (Wamit, 2006).

The method is based on the definition of ϕ and of the pressure p (equations 3.19 and 3.20) on the solid boundaries and on the separation of the velocity potential related to the hydrodynamic force in diffraction problems and radiation problems (equation 3.21). The diffraction problem relates to the body being fixed and exposed to the excitation of sea waves, while the radiation problem assesses the velocity potential caused by the body motions in otherwise calm waters.

$$\phi(x, y, z, t) = Re\left\{\phi(x, y, z)e^{-i\omega t}\right\} \tag{3.19}$$

$$p(x, y, z, t) = Re\left\{p(x, y, z)e^{-i\omega t}\right\} \tag{3.20}$$

and

$$\phi = \phi_d + \phi_r \tag{3.21}$$

Pressure and potential are related by the following relation:

$$p = \rho i \omega \phi \tag{3.22}$$

The application of BEM for the OWC, however, requires the definition of a further radiation term as explained by Brito-Melo (2000). The further radiation term ϕ_7, is related to the movement of the internal free surface of water, and it is considered as the 7th mode of motion of the body. Therefore the total potential becomes

$$\phi = \phi_d + \phi_r + \phi_7 \tag{3.23}$$

In the case of a fixed body OWC, the radiation term due to body movements is $\phi_r = 0$, and equation 3.23 becomes

$$\phi = \phi_d + \phi_7 \tag{3.24}$$

The hydrodynamic force is given by the surface integral of the pressure acting on the body. Brito-Melo (2000) defines the diffraction force causing the movement of the water column as follows:

$$F_{d7} = i\omega\rho \iint_{Si} (\phi_d) dS \tag{3.25}$$

and the radiation force as:

$$F_{r7} = i\rho\omega \iint_{Si} \phi_7 \left(\frac{i\omega}{\rho g} p\right) dS = -\rho Re \left[\iint_{Si} \phi_7 dS\right] \left(\frac{\omega^2}{\rho g} p\right) - \omega\rho Im \left[\iint_{Si} \phi_7 dS\right] \left(\frac{i\omega}{\rho g} p\right) \tag{3.26}$$

From equation 3.26 it is possible to define the hydrodynamic coefficient of the addedd mass μ_{77} and of the radiation damping B_{77} given by

$$A_{77} = \rho Re \left[\iint_{Si} \phi_7 dS\right] \tag{3.27}$$

$$B_{77} = \omega\rho Im \left[\iint_{Si} \phi_7 dS\right] \tag{3.28}$$

Boundary Element Methods exploit the Green Function to solve the integrals presented in

equations 3.25 and 3.26. The integration is carried over the total number of panels N_p, generating a equal number of equations to be solved (Newman, 1992).

The application of BEMs code for the OWC was firstly implemented by Lee et al. (1996), who adapted the panel code WAMIT to account the movement of the internal surface of the water column. Lee et al. (1996) also identified two possible problems in the description of the OWC with the BEM methods due to issues related with the thin walls of the structure and to the resonating character of the OWC.

Brito-Melo et al. (1999) converted the 3D BEM code AQUADIN, normally employed for the analysis of floating structures, to solve the radiation-diffraction problem of the OWC. By modifying the boundary condition of the internal water surface they could consider the variation of the imposed pressure due to the turbine. The formulation still considered acceptable the employment of linear wave conditions (Figure 3.18). The AQUADYN model of the Pico Power Plant was implemented by Brito-Melo et al. (2003) to account for the diffraction of the waves due to the bathymetry at the mouth of the OWC (Figure 3.19). The model however could be employed only for the analysis of the efficiency of the Pico OWC, and has been recently employed to assess maintenance work that needed to be undertaken to implement the performances of the power plant (Neumann et al., 2007).

The WAMIT code was used by Delaure (2001) to describe an onshore OWC. Delaure developed a panel structure for a general OWC, and included the free surface mode to determine the movement of the water column. Delaure carried parametric studies in order to improve the hydrodynamics of the device (Figure 3.20). Following this work, Delaure and Lewis (2003) addressed the modelling of the OWC device with BEM and showed good agreements between the simulation and experimental results in the case of no external damping being applied.

The WAMIT code was employed by Sykes et al. (2007) to investigate the hydrodynamics of a floating OWC. In this case all the 7th modes of motion of the device were accounted in the determination of the radiation and diffraction terms. Sykes et al. (2007) concluded that predicted results from the BEM code agreed well with the experimental results for small amplitude waves, and that the discrepancies were related to the viscous effects. Payne (2006), however, noted that possible discrepancies between experimental test and simulation are due to the discretisation process of the panel within the WAMIT code.

Lopes et al. (2009) instead assessed how to employ a resonant control system following BEM

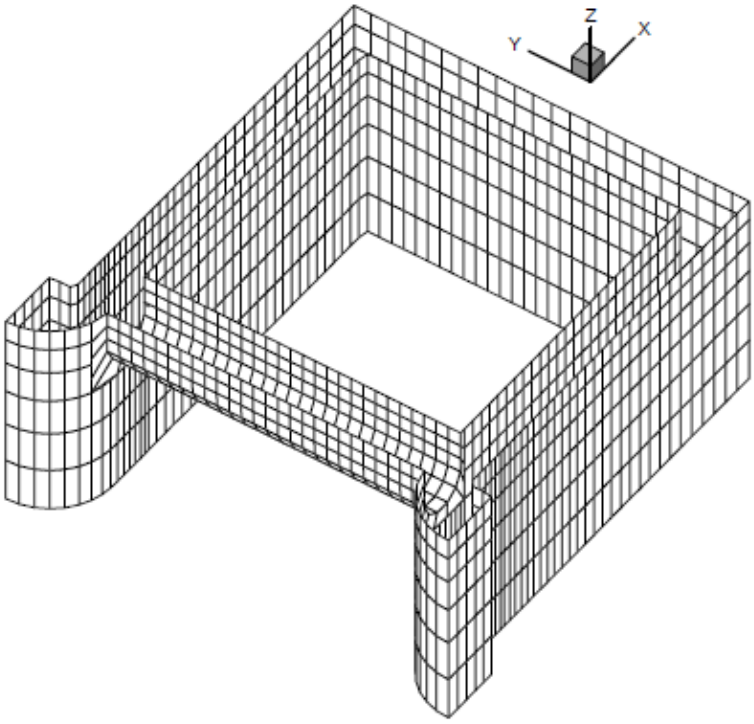

Figure 3.18: Overview and schematic of the BEM panalleing of the OWC Pico Power Plant installed on the Azores,Portugal, Brito-Melo et al. (1999).

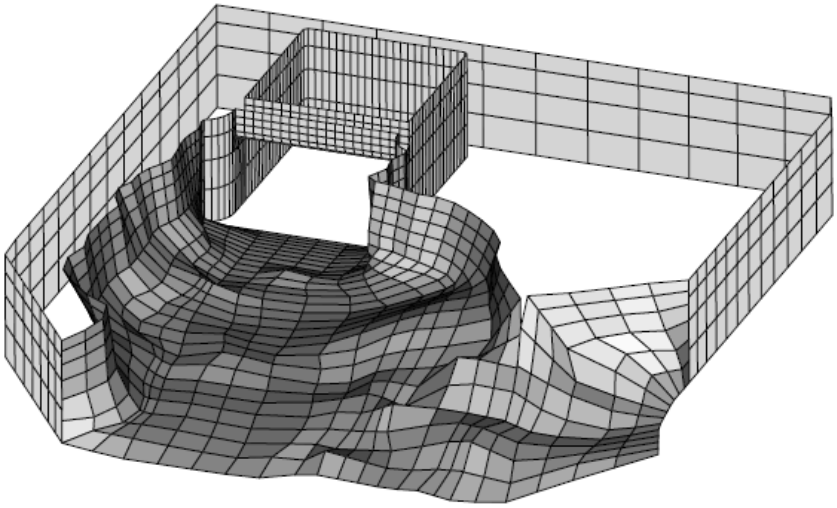

Figure 3.19: BEM discretization the OWC Pico Power Plant including shore profile, Brito-Melo et al. (2003).

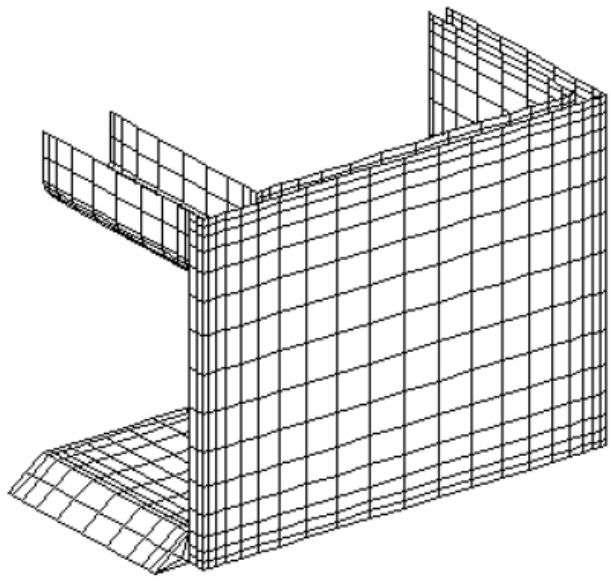

Figure 3.20: Discretization od the OWC for analysis with WAMIT presented by Delaure (2001).

and physical modelling of the device. They tried to use a non-predictive system to allow the OWC system to shift towards resonant conditions.

3.2.3.2 Non-linear modelling of the OWC

Panel methods provide a quick way to assess the hydrodynamics coefficients of the OWC and the forces and pressure acting upon it. However, as highlighted in the previous section, limitations and discrepancies were noted between numerical simulations and experiments at the increase of the wave amplitude and when the external damping applied from the wells turbine. In order to increase the accuracy of the mathematical simulation, non-linear models of the OWC have been implemented. These could be developed either using time domain software such as ACHIL3D, as done by Josset and Clement (2007), or by transforming the frequency domain hydrodynamic coefficients to time domain retardation function as showed by Josset et al. (2006).

In particular Josset and Clement (2007) used an in-house developed software, ACHIL3D, which is based on the time domain to implement the non-linear terms within the fluid domain. Josset and Clement (2007) adpted their model to the Pico wave power plant in the Azores. They separated the domain into an inner problem, within the OWC walls, and an outer problem outside the OWC walls. This separation led to a reduction of the computational time of the outer problem, whilst it allowed to implement fully the non-linearities due to the PTO system (Figure 3.21). Furthemore this showed to increase the performance of the power plant by 15% .

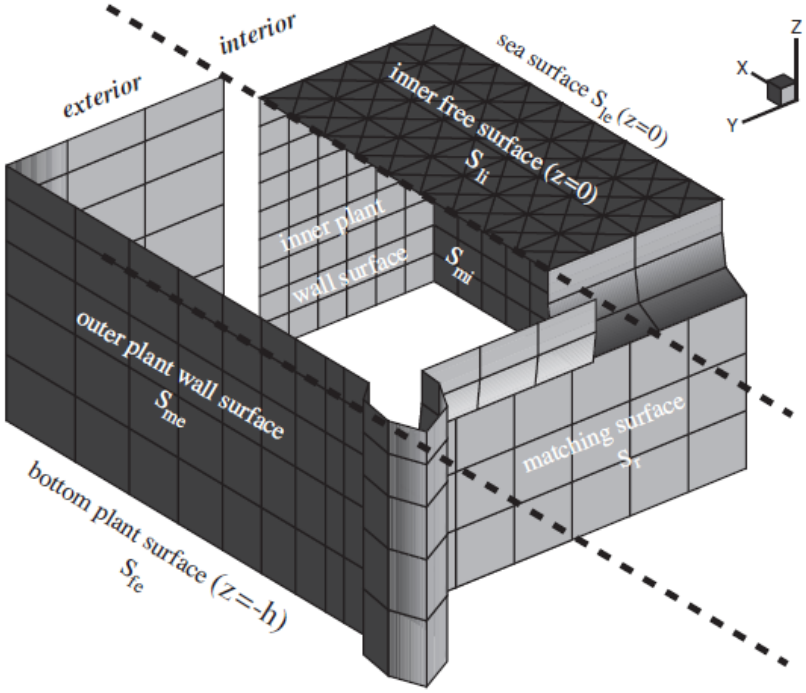

Figure 3.21: Inner and outer problem meshes and surface definition for the dime domain model of the OWC presented by Josset and Clement (2007).

Koo and Kim (2010) have recently developed a non-linear model of the OWC using a Non-Linear numerical wave tank and compared their result with BEM and CFD simulations. Their approach allowed to reduce the computational time of the simulations. They noted that accounting non-linear effects increased the accuracy of the determination of the energy efficiency of the OWC. However their results showed that linear theory results approximate the overall efficiency of the device reasonably well.

3.2.3.3 Summary of the mathematical approaches

What emerges from the analysis of the work carried on the mathematical studies of the OWC is the predominant application of this technique to determine the hydrodynamic coefficients in order to improve the performances of the device. Recent developments have assured more accurate models to determine these coefficients.

Mathematical models are now being employed to evaluate the employability of an active resonance control system. This however can not be achieved unless predictive models of wave state achieve higher accuracy.

From a design point of view of the OWC, the use of mathematical models has been prominent. Mathematical models allow for a quick overview of the problem and for a fast evaluation of the governing principles of the energy conversion: from wave to pressure, from pressure to electricity. However, the degree of complexity that surrounds the mathematical description of wave energy conversion is such that the simplification and linearisation of the problem have to be employed to solve the problem. This led to an underestimation of power capacity that can be obtained from OWC plants and a miscalculation of the hydrodynamic parameters affecting the power output of the device. It is therefore necessary to provide results from physical testing of the OWC to accompany the mathematical work for validation.

3.2.4 Physical modeling of the OWC

One of the main issues of the initial development of the OWC was the lack of physical modelling to support the theoretical work carried out. This was due to the difficulties in simulating the power take-off system for the device, and therefore the use of a physical model was limited to assess the force acting on the structure rather than predict the functioning of the device.

Sykes et al. (2007) described the issue of simulating the PTO for an OWC equipped with a bi-directional Wells. They concluded that the water-air interface required the use of different scaling factors, hence it was impossible to simulate the performance of the turbine accurately. Sykes et al. resorted to use a linearised mathematical model to determine the efficiency of conversion for an OWC due to the impossibility of using an accurate scaling factor. The work carried by Sykes et al. summarised the main issues of the modelling of the OWC, and proved that a change in the physical modeling of the OWC is necessary. Until the work carried out by Sykes et al. most of the physical testing of the OWC was focused on the determination of the loss factor at the mouth of the device, pressure force acting on the walls and assessing the changes in the waves which were assumed linear in the theoretical models.

Recently, due to the installation of a few prototypes of the OWC it has been possible to assess the performances of the device directly, and consider the overall performance of the device. Following the performance data obtained by the Pico Power Pant in the Azores, where an overall efficiency of 15-20% was achieved at favourable wave conditions, Neumann et al. (2007) monitored and designed a recovery project for the power plant to increase the performances.

The evaluation of the performance of a fully functional OWC was carried by Boccoti (Boccotti, 2007; Boccotti et al., 2007) on a benign experimental facilities installed on the Tirrean Sea

in the south of Italy. The favourable site allowed for installation and testing of an OWC on a breakwater. The test were completed with a method presented earlier by Boccotti (2004) where he tried to derive a wave spectrum for the site and apply it to control resonance conditions. Results of the work carried out were then used by Filianoti and Camporeale (2008) to derive a full mathematical model for the estimation of the overall performance of the OWC.

Lopes et al. (2009) employed experimental testing to evaluate the performance of a OWC with latching control. Due to the restriction imposed by determining the performance of the Wells Turbine, they assessed the effects of the control system on the changes generated on the magnification factor within the chamber. The testing procedure also allowed for the estimation of the viscous losses at the entrance of the device ranging between 35-60% depending on the external damping applied on the device.

Whilst allowing for the assessment of the full operational efficiency of the device, employing full scale testing does not allow the evaluation of different configurations of the device and limit the implementation of the device after installation. On the other hand, there is a limited amount of work in literature that considers the employment of the physical tests of the OWC.

In particular physical testing of the OWC were aimed to assess loss and damping coefficients and design improvement. Brendmo et al. (1996) carried out wave tank testing of an OWC device to determine the losses due to viscosity for validation of their mathematical model. They used small amplitude waves to limit non-linearities and vortex formation at the mouth of the OWC. They determined the damping coefficients for the OWC regardless of conversion efficiency of the device.

The effects of the seabed on the performance of an OWC were analysed by Wang et al. (2002) who used a 1:12 scale model of the device. They tested different configurations of the seabed, by changing the slope of the bed profile leading to the OWC mouth. They employed the results obtained to implement a mathematical model to simulate changes to the waves in the near-shore.

The assessment of different configurations of the OWC was carried by Morris-Thomas et al. (2007). They employed different shapes and thicknesses of the wall to determine the ideal hydrodynamic configuration of the OWC, and assess implications to the PTO system.

The assessment of the forces acting over the front wall of the OWC was presented by Thiruvenkatasamy et al. (2005) who evaluated the impact of non-breaking waves on the device. The work of Thiruvenkatasamy et al. (2005) is also one of the few case studies presented on the

evaluation of the OWC installed on a breakwater. Similar work was carried out about a decade earlier by Koola et al. (1995); Graw (1996). They both evaluated the role of the OWC as an active coastal defence structure if installed onshore. They assessed different configurations of the OWC installed in Madras and assessed the absorption of the energy carried by the incoming wave train. They obtained efficiency in absorption of 75% compared to the one obtained through mathematical studies.

A different case is the one presented by Czitrom et al., (2000; 2000, b). Czitrom et al.,tested the SIBEO device in a wave flume. The design of the device allowed for the testing of the control system, since no turbine was installed but a compression chamber that acted as resonance control system. It was therefore possible to test the device in order to validate the mathematical theory. The SIBEO was tested with both monochromatic and polychromatic wave trains. Monochromatic wave tank tests were used to perfection the geometry of the input duct in order to diminish vortex formation at the entrance. Random sea tests were employed to assess the functioning of the resonance control system.

The importance of physical testing for the OWC and WECs has been highlighted over the past decades. Physical tests allow for the evaluation of the full conversion process and can provide an insight on the conversion processes that might have been overlooked during a mathematical description of the device. Forestier et al. (2007) assessed the use of physical testing in the early stages of the development of a WEC. They concluded that whilst overlooked initially physical tests are now fundamental to assess the functioning and survivability of the device. The conclusion of the work of Forestier et al. (2007) was in contrast with the way OWCs were initially developed. The path of development has often proceeded as follows (Cruz, 2008b):

- Hydrodynamic description of the OWC and analytical modelling of the device
- Numerical analysis of the device, determination of capture width and coupling with Wells turbine
- Experimental test to determine and correct damping and friction coefficients. Tests of survivability
- Time domain analysis to test for irregular waves conditions and non-linear PTO

- 3D BEM modelling to improve the design.

The process of implementation of the OWC has not followed a logical order, leading to a series of difficulties and poor performance as highlighted by (Neumann et al., 2007).

It has become clear that physical tests are a necessary tool to assess and validate the development of an OWC type of device.

3.3 Summary

This chapter presented a review of the state of the art of wave energy development. Through this review, the OWC device was chosen as the on technology that could be implemented for water delivery. An in-depth review of the OWC device was presented to allow the development of an overtopping type of OWC.

It was shown that most of the work on the OWC was carried out through the use of mathematical modelling. In order to solve the formulation of the mathematical problem different assumptions were made. In most of the cases the problem was solved by linearising the behaviour of the system. This allowed to determine approximate solutions regarding the efficiency in absorption of the device, and the efficiency in conversion of the Wells turbine.

The use of linearised system allowed to develop a resonance control system for the tuning of the device to different wave conditions. This is achieved through the modification of the external damping imposed over the system by the turbine. The modification of the damping coefficients allows for the device bandwidth to be increased but can reduce the efficiency of absorption of the device as assessed by Lopes et al. (2009).

The vast amount of theoretical work carried out on the OWC has not been supported effectively by physical tests for validation. Difficulties are experienced in the modelling of the water air interface and reproducing the effect generated by the turbine over the free surface of water within the OWC chamber Sykes et al. (2007). This led to the overestimation of the Power output that can be generated by the device at full scale, and to a low efficiency in the full scale operation of the device like in the case of the Pico Power Plant (Neumann et al., 2007).

Knott and Flower (1979) proposed a version of the OWC for overtopping and water collection, their ealy work was left unfinished and partially reassessed by Czitrom (1997), who developed a modified OWC device aimed to assess water delivery. The SIBEO device comprises a resonant

input duct with an outflow duct to allow for water delivery towards a marina or lagoon. The two ducts are jointed in a variable volume compression chamber, which acts as a control system for tuning. The volume and pressure of the air contained within the chamber are adapt to allow for the system to change to different wave conditions. Full physical and mathematical investigations were carried out on the SIBEO (Czitrom et al., 2000; 2000, b), thus making the device the first OWC type of device to obtain such an in depth analysis. A full scale SIBEO device was later installed and is still operational in Ensenada (Mexico) (Czitrom et al., 2006).

The work carried on the SIBEO can be seen as complimentary towards the development of OWC device for electricity generation. However the success obtained by the SIBEO states the case that it is possible to employ the OWC principles for water delivery.

From the work of Knott and Flower (1979) and Czitrom (1997) it emerged that it is feasible to develop an OWC device for the delivery of water and the generation of potential energy. Investigations on the performances of a simple overtopping OWC type are still limited. The possibility of investigating the use of the OWC for overtopping purposes allows for further research into the mechanics of the device and of its applications.

In order to take the knowledge forwards an overtopping OWC device is hereby presented and investigated. The Oscillating Water Column Wave Pump is therefore developed.

Chapter 4

Theory of the Oscillating Water Column Wave Pump

Section 3.2 showed how an OWC device can be developed not only for the production of electricity but also for the the delivery of water in marinas for flushing and coastal management purposes.

This chapter presents the reader with the details of the proposed Oscillating Water Column Wave Pump device and the theoretical description of the functioning.

4.1 Proposed OWCP

On the basis of the work available in literature the possibility of developing an Oscillating Water Column device for water delivery was investigated. The Oscillating Water Column Wave Pump (OWCP) devices presents a simpler system compared to the SIBEO device developed by Czitrom (1997). The working principles of the device are similar to the ones of the OWC and so are its interaction with the incident waves, as highlighted by Knott and Flower, 1979.

The novelty of the device consists in the way energy is removed from the system, with a fixed power take off system affecting the restoring force during the oscillatory motion of the water column.

The OWCP is composed of a two part resonant duct: a horizontal underwater section (inflow) and an inclined pumping section (outflow), which extends above mean water level (MWL). The two ducts are connected at an angle, which influences the natural frequency of oscillations of the device.

The OWCP works as an energy converter, changing the kinetic energy of the incoming wave

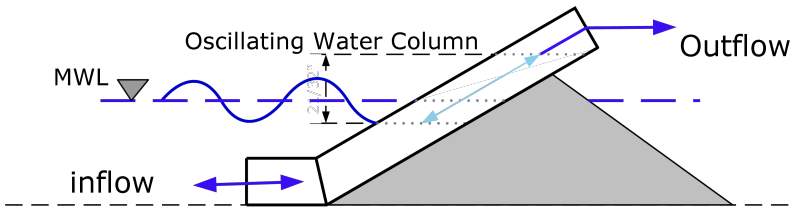

Figure 4.1: Schematic of the proposed OWCP installed onshore.

into potential energy to lift the water inside the tube. The device is effectively a resonator, and in order to maximise water delivery, it must be tuned to the incident wave period. A schematic of the proposed OWCP can be found in Figure 4.1.

The OWCP is designed to deliver water. Compared with the classical OWC, no turbine is installed at the end of the outflow duct. Atmospheric pressure is therefore acting on the free water surface within the OWCP pipe. The absence of a water/air interface at variable pressure simplified the mechanical equivalent of the OWCP from a double-mass damped oscillator (like the OWC) to a single mass damped oscillator.

The main differences between the proposed OWCP investigated in this work and the SIBEO device presented by Czitrom (1997) are to be found in the absence of the water/air interface and in the way that resonance control is achieved. Resonant conditions for the SIBEO were maintained through control of the air compression chamber and by adjustment of the volume of air contained in the chamber to modify the stiffness of the air spring (Czitrom et al.,2000). In order to modify the air spring and the volume of air contained within the chamber, the SIBEO was equipped with a microchip that sampled the wave conditions and varied the volume of air in the chamber accordingly (Godoy-Diana and Czitrom, 2007).

The proposed OWCP can therefore be considered as a simplified version of the OWC; thus allowing for the non-linearities of the behaviour to be taken into account in the description of the device and providing the possibilities to validate a theoretical model of the OWCP with an extensive set of physical tests.

Physical and mathematical investigations will be employed to validate the aims of this project of developing a simple wave energy converter for water delivery to generate a hydraulic head of 2-5 m.

4.2 Theoretical Formulation of the OWCP response

The response of the OWCP to incident waves is assumed to be similar to the OWC one. In order to formulate a theory to assess the behaviour of the device it is important to define its main characteristics.

The OWCP is designed to work in the near-shore environment, installed on an existing breakwater or another bottom-mounted structure. The main body of the device is fixed, with only the internal water column subject to movement under the action of the incoming waves. The OWCP structure therefore does not affect the hydrodynamic response of the water column, but interferes with the incoming wave field generating a destructive diffraction wave.

The response of the OWCP is therefore related only to the movement of the internal free surface of water. In the case of a vertical device, the main response would correspond to an oscillatory motion in the heave direction.

4.2.1 Mechanics of the OWCP

The OWCP response to the incoming wave force can be represented physically by a damped oscillator, as shown by Evans (1981) and Falnes (2003). The general equation of motion for an oscillator can be expressed in the time domain as follows:

$$m\ddot{\zeta} = F - C_d\dot{\zeta} - C_f\zeta \tag{4.1}$$

where m represents the mass of water subject to the oscillation, F represents the exciting force, C_d is the damping coefficient, C_f is the spring coefficient and ζ represent the vector of displacement. Equation 4.1 represents the general behaviour for an oscillating body under the influences of regular waves.

Therefore in the case of sinusoidal waves that validate the assumptions of linear wave theory, the response of the OWCP can be described in the frequency domain as follows:

$$m\zeta(\ddot{\omega}) = F(\omega) - C_d\zeta(\dot{\omega}) - C_f\zeta(\omega) \tag{4.2}$$

By expressing the equation of motion in the time domain, equation 4.2 does not account for any non-linearities that can affect the movement of the water column. In this case ζ and F are a function of the angular frequency ω.

Following the decomposition of the forces acting on a body presented by Falnes (2003), the total hydrodynamic forces acting on the bodies can be separated in the exciting force $F_e(\omega)$ dependent on the incoming wave force $F_0(\omega)$, the diffraction force $F_d(\omega)$, and a radiation force $F_r(\omega)$ related to the response of the device.

It follows that

$$F_e(\omega) = F_0(\omega) + F_d(\omega) \tag{4.3}$$

whilst an analysis of the radiation force, as shown by Newman (1977), could see F_r being decomposed in two terms: the added mass term μ and a radiation damping term B.

μ refers to the mass of water that is moved by the device oscillating in absence of incoming wave, hence the loss of energy that is lost by forcing the water to move; whilst the damping term B is related to the decay of motion if movement is forced in absence of incoming waves. Both μ and B are represented by a 6×6 matrix, in the general case of 6 d.o.f of the device. Thus the radiation force can be considered as follows:

$$F_r(\omega) = \mu(\omega)\ddot{\zeta(\omega)} + B(\omega)\dot{\zeta(\omega)} \tag{4.4}$$

By considering the decomposition of the forces as presented in equation 4.3 and equation 4.4, equation 4.2 can be rewritten as follows:

$$(m + \mu(\omega))\ddot{\zeta(\omega)} \;=\; F_e(\omega) - B(\omega)\dot{\zeta(\omega)} - C_f\zeta(\omega) \tag{4.5}$$

Since the response of the OWCP to wave excitation is in 1 degree of freedom (heave), equation 4.5 can be expressed as:

$$(m + \mu_{33}(\omega))\ddot{\zeta(\omega)} \;=\; F_{e3}(\omega) - B_{33}(\omega)\dot{\zeta(\omega)} - C_f\zeta(\omega) \tag{4.6}$$

with the subscript 3 denoting the heaving motion. Therefore the force term F_{e3} and the position vector $\zeta(\omega)$ become a 1×1 vector.

However as noted by Brito-Melo (2000) and by Delaure (2001), for an OWC type of device the correct terminology of the heaving motion of the water column is denoted with the subscript 7. This identifies the motion of the internal free surface compared to the the heaving motion (subscript 3) of the whole device. Therefore equation 4.6 can be rewritten as

$$(m + \mu_{77}(\omega))\ddot{\zeta(\omega)} = F_{e7}(\omega) - B_{77}(\omega)\dot{\zeta(\omega)} - C_f\zeta(\omega) \tag{4.7}$$

By expressing $\zeta(\omega)$ as a complex harmonic function of the time t

$$\zeta(\omega) = \hat{\zeta(\omega)}e^{-i\omega t} \tag{4.8}$$

the velocity and acceleration components can be derived as follows:

$$\dot{\zeta(\omega)} = -i\omega\hat{\zeta(\omega)}e^{-i\omega t} = -i\omega\zeta(\omega) \tag{4.9}$$

$$\ddot{\zeta(\omega)} = \omega^2\hat{\zeta(\omega)}e^{-i\omega t} = \omega^2\zeta(\omega) \tag{4.10}$$

The force $F_{e7}(\omega)$ can be expressed as:

$$F_{e7}(\omega) = A_0\hat{F_{e7}(\omega)}e^{-i\omega t} = A_0\hat{F_{e7}} \tag{4.11}$$

with A_0 representing the amplitude of the exciting force. .

Equation 4.7 can be rearranged by substituting the terms from equations 4.9, 4.10 and 4.11, giving the following relation:

$$(m + \mu_{77}(\omega))(\omega^2\zeta(\omega)) = A_0\hat{F_{e7}} - B_{77}(\omega)(-i\omega\zeta(\omega)) - C_f\zeta(\omega) \tag{4.12}$$

From equation 4.12 the response amplitude operator (RAO) for the OWCP, can be determine. The RAO is given by:

$$RAO = \frac{\zeta(\omega)}{A_0} = \frac{\hat{F_{e7}(\omega)}}{-(m + \mu_{77})\omega^2 + i\omega B_{77}(\omega) + C_f} \tag{4.13}$$

The RAO expressed in equation 4.13 represents the amplitude response of the OWCP per unit of input of a linear system, and it is independent of the incoming wave amplitude. In case of a non-linear system the RAO is dependent on the incoming wave amplitude.

With reference to Figure 4.2 it is possible to rearrange equation 4.6 to describe the specific response of the OWCP, as:

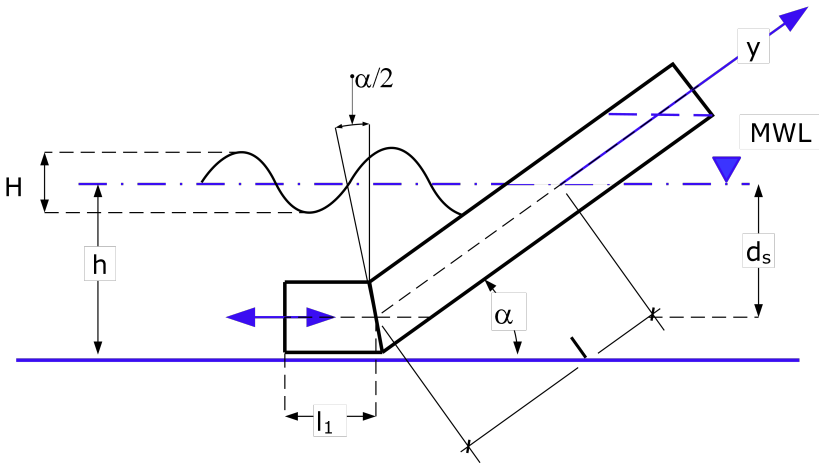

Figure 4.2: Schematic of the proposed OWCP with related variables: l_1 length of input duct; l length of output duct; d_s submersion depth of the OWCP; α inclination angle of output duct; y_p delivery height; h water depth at MWL; H wave height.

$$(m + \mu_{77}(\omega))\ddot{y(\omega)} = F_{e7}(\omega) - B_{77}(\omega)\dot{y(\omega)} - C_f y(\omega) \tag{4.14}$$

Equation 4.14 can be converted in the time domain (equation 4.15) and expanded to include non linearities. Equation 4.15 presents only the response of the OWCP due to fluid-structure interactions. The non-linear terms affecting the response of the device will be assessed later.

$$(m + \mu_{77})\ddot{y(t)} = F_e(t) - B\dot{y(t)} - C_f y(t) \tag{4.15}$$

It has to be noted that the derivation of equation 4.14 and of the hydrodynamics terms μ_{77} and B are obtained from the derivation of the potential theory as presented in Newman (1977) and in Falnes (2003). μ_{77} and B can be converted from the frequency domain to time domain operators by the use of an Inverse Fourier Transform.

4.2.1.1 Resonant behaviour of the OWCP

The OWCP is a resonant type of device, the response of the device is dependent on the incoming wave frequency. When the device is tuned with the wave frequency, strong amplifications take places within the OWCP chamber. In the absence of damping this would result in an infinite motion of the water column. Radiation damping, wall effects and flow separation effects all contribute to limit the motion of the water column.

The natural frequency of oscillation of the OWCP is dependent on the the mass of wa-

ter m contained within the wall of the OWCP, the submergence depth d_s of the device, and the angle of inclination of the device α, as shown in equation 4.16:

$$\omega_n = \sqrt{\frac{g}{l_1 + l}} = \sqrt{\frac{g}{l_1 + \frac{d_s}{sin\alpha}}} \tag{4.16}$$

The natural period of oscillation of the OWCP can be derived from equation 4.16 and it is given by:

$$T_n = \frac{2\pi}{\omega_n} \tag{4.17}$$

External factors such as damping and added mass acts on the value of ω_n by shifting it towards lower values.

4.3 Assessment of the Non-Linearities

A factor that seems to strongly influence the behaviour of OWC devices and consequently their performances is related to the non-linear losses at the entry of the device (Czitrom et al.,2000). Non-linear effects are due to different simultaneous effects such as wave reflection off the structure, vortex formation and viscous losses. For the OWCP device, given the dimension of the pipes, end effects have to be accounted as additional non-linear friction losses. These are dependent on the mass of water exiting the OWCP from the input pipe during downward restoring motions of the column of water.

Non-linear effects were firstly assessed by Knott and Flower (1979) who considered the energy losses at the entrance and of a ducted energy converter.

The overall equation of motion can be considered as follows:

$$m\ddot{\zeta} = F_{WS} + F_{PTO} + F_{drag} + F_{gravity} + F_{friction} + F_{others} \tag{4.18}$$

where the term F_{WS} indicates the forces due to wave/structure interaction, including the components of excitation force and diffraction force as seen in equation 4.3. The radiation force F_r, is included in the wave/structure type of force:

$$F_{WS} = F_0 + F_d + F_r \tag{4.19}$$

The term F_{PTO} refers to the force generated by the power take off system. The term F_{drag} refers

to drag forces due to flow separation and vortexes forming in proximity of the OWCP, due to sharp edges. The term $F_{gravity}$ refers to the buoyancy and restoring force. The term $F_{friction}$ refers to friction forces within the OWCP wall which causes a reduction of the motion of the water column. The term F_{others} refers to other type of internal losses due to the angle bend of the device.

In the determination of the response so far presented the gravity force term and the wave/structure force term have been all considered. Non-linearities are due to drag effects, friction effects and depend on the role of the PTO.

A rule of thumb for addressing the role of non-linear forces is provided by the Keulegan-Carpenter number, KC, as shown by Faltinsen (1990). KC indicates the validity of linear theory for a given wave structure interaction and, according to its non-linear forces could be neglected or taken into consideration. KC is given by:

$$KC = \frac{2\pi d}{L} \tag{4.20}$$

with d representing the characteristic dimension of the diameter of the device and L the wave length of the incoming wave. When $KC < 2$ non linear forces have a lower effect on the device compared to wave structure interaction forces; however in the case of $KC > 10$ the dominant effects are those of flow separation with drag forces dominating over radiation and diffraction forces.

4.3.1 Drag forces

Drag forces for ducted Wave Energy Converters are due to flow separation, eddy and vortex formation at the water interface with the mouth of the duct. The work of Lighthill (1979) and Knott and Flower (1980) aimed to address the issue of flow separation at a pipe exit during oscillating flows. Knott and Flower (1980) indicated how these losses are dependent on the geometry of the pipe and the amplitude of the water motion and the Reynolds number.

Generally the drag force is given by:

$$F_{drag} = -\frac{1}{2}\rho C_d A_d \left|\dot{\zeta}\right| \dot{\zeta} \tag{4.21}$$

with A_d representing the reference area, of cross-section of the OWCP and C_d represents

the drag coefficient, which is a function of the Reynolds number:

$$C_d = f(Re) = f\left(\frac{\rho V D}{\nu}\right) \tag{4.22}$$

where ρ represents the water density, V the velocity of the water flow, D the diameter of the pipe and ν the viscosity of the liquid.

Knott and Flower (1980) noted that the losses due to vortex formation can be accounted only when a certain amplitude of motion is achieved and are also frequency dependent. They noted that with a frequency-control system eddy formation could be limited, through a reduction of the Reynolds number. However, as in the case of the OWCP, when the restoring force is given by the gravity acting upon the water column, this cannot be achieved at full scale.

4.3.1.1 Entrance and Exit losses

Entrance and Exit losses are due to flow separation and eddy formation at the mouth of the OWCP. They are usually neglected in long pipe systems (Chadwick and Morfett, 1998), however in the case of the OWCP they need to be accounted. As reported in Chadwick and Morfett (1998), no general treatment for local head losses, h_l, is available. Entrance and exit losses are normally associated with turbulence losses and can be determined as follows:

$$h_{l,OWCP} = \frac{k_{I,E}\dot{\zeta}^2}{2g} \tag{4.23}$$

with $k_{I,E}$ representing a discharge coefficient that can be related to the damping coefficients $\xi_{I,E}$ used for the development of the mathematical model of the OWCP presented in section 4.2. Values of the discharge coefficients can be found in literature (Chadwick and Morfett, 1998; Hamill, 2001), and can be applied in the present context.

Values for the entrance loss coefficient k_I can be found in literature, by assuming that the entrance of water in the OWCP is similar to the localised losses of water leaving a reservoir and entering a pipe, as shown in Figure 4.3. For the OWCP a value of $k_I = 0.5$ has been assumed.

In the same way, the values of the exit friction coefficient k_E can be compared to a sudden exit loss from a pipe to a reservoir. In this case the value of $k_E = 1.0$ can be assumed as illustrated in Figure 4.4.

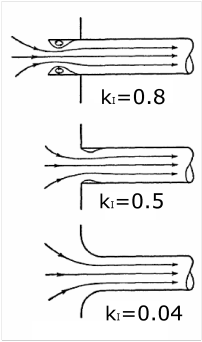

Figure 4.3: Entrance Losses Coefficients for differently shaped pipes (Vennard, 1940).

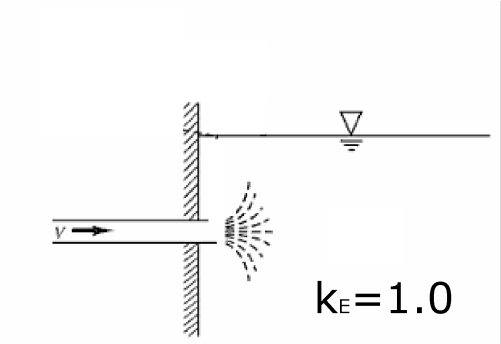

Figure 4.4: Exit Losses Coefficient (Houghtalen et al., 1996)

In general F_{drag} will be given by equation 4.24

$$F_{drag} = \frac{1}{2}\rho A_d k_{I,E} \dot{y(t)} \left|\dot{y(t)}\right| \tag{4.24}$$

in particular the value of $k_{I,E}$ will change according to the type of motion within the OWCP as follows:

$$\begin{aligned} F_{drag} &= \tfrac{1}{2}\rho A_d k_I \dot{y(t)} \left|\dot{y(t)}\right| \quad when \quad \dot{y(t)} > 0 \\ F_{drag} &= \tfrac{1}{2}\rho A_d k_E \dot{y(t)} \left|\dot{y(t)}\right| \quad when \quad \dot{y(t)} < 0 \end{aligned} \tag{4.25}$$

Delaure (2001) reported values of the drag coefficients depending on the natural frequency of oscillation of a ducted cylindrical OWC after the work of Liu and Bergdahl (1999).

The coefficients are given as follows:

$$k_I = -1.9003(\omega/\omega_n)^3 + 6.7679(\omega/\omega_n)^2 - 8.7851(\omega/\omega_n) + 4.2731 \tag{4.26}$$

$$k_E = 3.8772(\omega/\omega_n)^3 - 13.808(\omega/\omega_n)^2 + 17.921(\omega/\omega_n) - 5.5023 \tag{4.27}$$

The different coefficients determined by Liu and Bergdahl (1999), showed an higher influence of the downwards motion drag coefficient for ducted OWC devices.

4.3.2 Friction losses

Continuous losses are assessed through the use of the Darcy-Weisbach equation. The Darcy-Weisbach equation can be rearranged to describe the friction losses h_f as presented in equation 4.28, reported below

$$h_f = \frac{J(l+l_1)\dot{y(t)}^2}{2gd_{OWCP}} \tag{4.28}$$

where J represents the friction factor determined by the Coolebrook-White equation (4.29); $l+l_1$ represents the length of water in the OWCP; $\dot{y(t)}$ is the velocity of the water moving withing the OWCP and d_{OWCP} is the diameter of the OWCP.

J can be determined by solving the equation4.29 (Hamill, 2001), shown below:

$$\frac{1}{\sqrt{J}} = -2log\left(\frac{k_s}{3.7d_{OWCP}} + \frac{2.51}{Re\sqrt{J}}\right) \tag{4.29}$$

with k_s representing the roughness of the OWCP and Re being the Reynolds number.

Values of k_s for perspex can be found in literature, with $k_s = 3{\cdot}10^{-6}m$, as suggested in Hamill (2001).

For the specific case of the OWCP, $h_{f,OWCP}$ is mainly affected by $l+l_1$, $\dot{y(t)}$ and by d_{OWCP}. Given the dimension of the OWCP and the relatively small velocities within the OWCP, it is possible to assume that the effects of $h_{f,OWCP}$ are negligible compared to $h_{l,OWCP}$.

The overall force acting on the motion of the water column is therefore given by:

$$F_{friction} = h_f\rho g A_c = \frac{J(l+l_1)\dot{y(t)}^2}{2d_{owcp}}\rho A_d = \rho\frac{J(l+l_1)\dot{y(t)}^2}{2d_{owcp}}\left((l+l_1)\frac{\pi d_{OWCP}^2}{4}\right) \tag{4.30}$$

where A_d is to the section of the pump causing the friction losses.

4.3.3 Other forces

The design of the OWCP is such that it includes an angle bend between the input duct and the output duct. Whilst the presence of the angle bend could eventually be used to control the resonance by varying the overall angle, it causes a further dissipation of energy and losses to the water column motion.

The losses are dependent on the angle α, the Reynolds number and on the scale at which the device is operating. It is expected that steeper the angle of inclination of the pipe and higher will the losses in the system be.

The angle bend loss coefficient K_b is related to the energy losses as follows:

$$K_b = \frac{h_{l,b}}{V^2/2g} \tag{4.31}$$

where $h_{l,b}$ refers to the head losses due the the angle bend and V^2 refers to the velocity of the water column.

Standard values of K_b for different angles are provided in the "Charts for the Hydraulic Design of Channels and Pipes" edited by the American Society of Civil engineering (ASCE, 1990); as shown in Figure 4.5.

F_{others} is therefore given by:

$$F_{others} = \frac{1}{2} K_b(\alpha) A y(\dot{t})^2 \tag{4.32}$$

It has to be noted that in the contrary to what happens for the drag force, F_{others} is not dependent on the type of motion within the OWCP, but it is only affected by potential changes in the angle of inclination α.

4.3.4 Remarks on Non-linear forces

The motion of the water column within the OWCP cannot be represented only by considering the wave structure interaction, and therefore by using a linearised model to describe the response of the OWCP. Non-linear forces have a strong effect on the response of the device and therefore need to be accounted in the mathematical description of the OWCP.

As a consequence Boundary Element Methods and Frequency Domain models cannot be directly used in assessing the performances of the OWCP. Time domain models have to be employed in the determination of the response of the OWCP, as they present the only way to

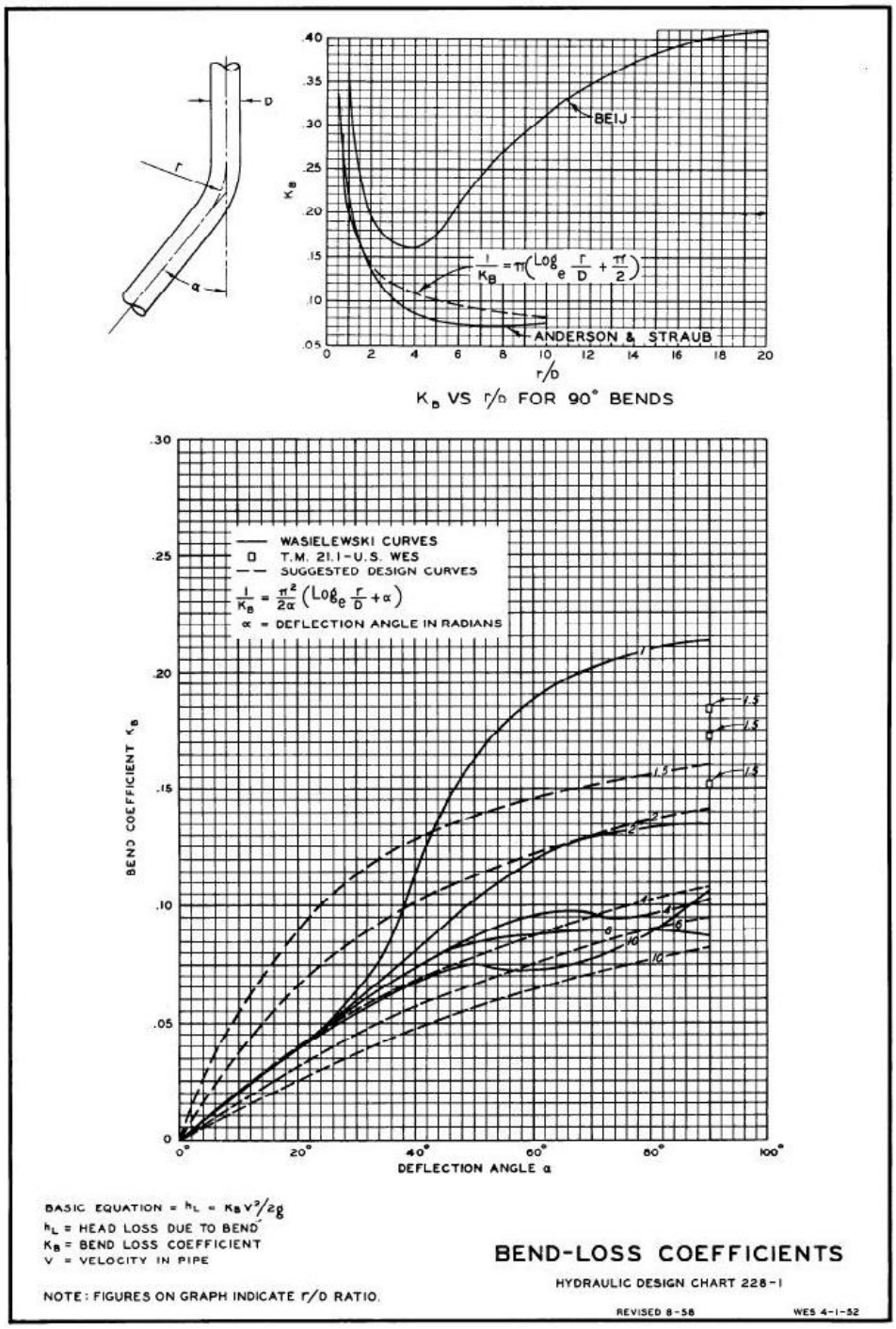

Figure 4.5: Values of the loss coefficient K_b for different values of the Reynolds number and of the angle of inclination α (ASCE, 1990)

address non-linear effects (McCabe, 2004). A time domain model was therefore developed by using the Matlab/Simulink code to analyse the response of the OWCP.

4.4 Water removal and Power Take Off

A separate discussion is needed for the response of the OWCP when water is removed from the device. The removal of water consists effectively in the Power Take Off system of the OWCP, affecting the response of the device to the incoming wave.

The PTO is often represented as an additional damper in an oscillatory system, as shown by Falnes (2003), El Marjani et al. (2008), which removes part of the energy from the system and converts it into useful energy. In the case of the OWC Mei (1976) and Evans (1981) considered the role of the air turbine to provide a further damping to the OWC and assessed the power production of a generic OWC device. Curran and Folley (2008) related the role of the air pressure and air velocity to define the damping caused by the turbine to the OWC.

For the OWCP the PTO system cannot be defined as a continuous damper, since the removal of water occurs only if the water level within the column rises to the water cut off point y_r , as shown in Figure 4.6. Furthermore, the removal of water affects the hydrostatic resorting force, reducing its influence when water is removed from the system. y_r corresponds to a freeboard height of removal h_r given by:

$$h_r = y_r sin\alpha \tag{4.33}$$

Water is removed from the OWCP when the following condition is satisfied:

$$y(t) > y_r \tag{4.34}$$

For each time step that satisfies equation 4.34 the amount of water exiting the OWCP is given by

$$y_p(t) = y(t) - y_r \tag{4.35}$$

The instantaneous volume dV of water collected is given by:

$$dV(t) = y_p(t)A \tag{4.36}$$

where A is the cross-sectional area of the OWCP. The overall volume of water V collected

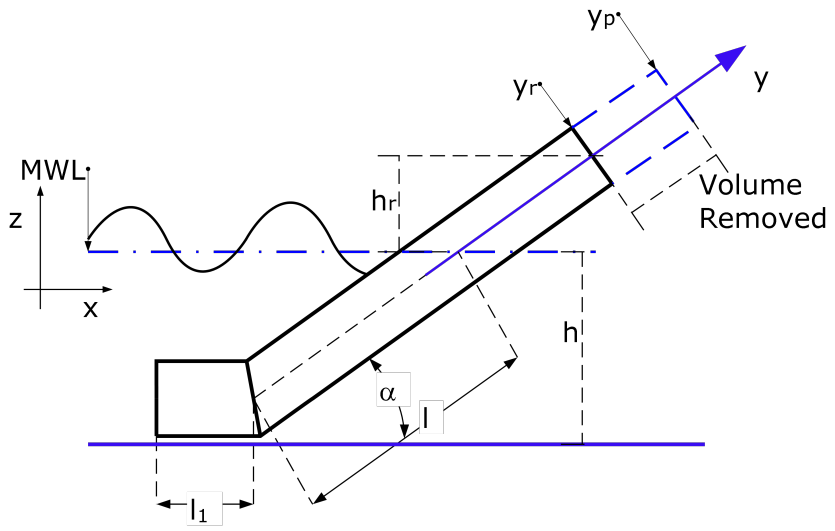

Figure 4.6: Schematic of the OWCP for water removal with y_p being the maximum delivery height if no water is removed and y_r being the removal height, l, l_1 respectively the output pipe and input pipe lengths; and α is the inclination of the pipe.

over a wave cycle is given by:

$$V = \int_0^{T_W} dV(t)dt \tag{4.37}$$

The total volume of water V_T collected over multiple wave cycles is given by the sum of each volume V collected for each wave cycle iw

$$V_T = \sum_{iw=1}^{n_{iw}} V_{iw} \tag{4.38}$$

4.4.1 PTO force and restoring force

The restoring force $F_{gravity}$ acting on the water column was so far defined as:

$$F_{gravity} = C_f y(t) \tag{4.39}$$

where the term C_f refers to the spring coefficient of a damped oscillator. For a WEC converter, this is associated with the volume of water displaced following a motion, or better the buoyancy force of the device. In the case of the OWCP, it refers to the mass of water displaced by the OWCP in both the upwards and downwards stroke of the oscillation.

This can be therefore rewritten as:

$$F_{gravity} = \rho g A_d y(t) \tag{4.40}$$

However, the role of $F_{gravity}$ is affected by the removal of water and its effects are reduced when mass is removed from the system.The freeboard height $h_r$is given by:

$$h_r = y_r - h \tag{4.41}$$

By considering the freeboard h_r, the amount of energy removed by the system in a cycle is given by:

$$E_r = \rho g h_r A_d y_p(t) \tag{4.42}$$

from which it is possible to determine the force F_{PTO} generated on the OWCP from the power take off system given by:

$$F_{PTO} = \rho g A_d y_p(t) \tag{4.43}$$

At this point it is possible to distinguish the role of $F_{gravity}$ and F_{PTO} according to the motion y of the water column. For the case when $y(t) < y_r$ only the restoring force will act on the OWCP. The equation of motion will be given by:

$$m\ddot{\xi} = F_{WS} + F_{drag} + F_{gravity} + F_{friction} + F_{others} \tag{4.44}$$

in the case of $y(t) > y_r$ the overall equation of motion will be given by equation 4.18. F_{PTO} will be included, whilst $F_{gravity}$ will be limited by the value y_r as follows:

$$\begin{aligned} F_{PTO} &= \rho g A_d y_p(t) \\ F_{gravity} &= \rho g A_d y_r \end{aligned} \tag{4.45}$$

Given the nature of the PTO systems, its role can only be implemented in the non-linear mathematical model.

4.5 Efficiency of the OWCP

In order to determine the efficiency of conversion of the OWCP it is necessary to assess the amount of water that can be removed from the device and stored in form of potential energy. Once water is collected from the OWCP it is possible to state that the behaviour of the device resembles the one of an overtopping device like the Wave Dragon or the SSG.

Margheritini et al. (2009) presented an analysis of the efficiency of the SSG based on the flux of water overtopped in the reservoir. They also identified five different efficiencies for the device on the base of the conversion processes from wave power to electricity. Of particular relevance for this project are the first two conversions:

- P_{crest} which identifies the power in the overtopping, and it is related to the freeboard R_c of the device. This dependency is translated with the value of y_r in this thesis as follows:

$$P_{crest} = Qy_r\rho g \tag{4.46}$$

where Q represents the flow rate of water removed from the OWCP at each passing wave, given by

$$Q = \frac{y_p A}{sin\alpha T} = \frac{(y - y_r)A}{sin\alpha T} \tag{4.47}$$

The efficiency in overtopping η is therefore given by

$$\eta = \frac{P_{crest}}{P_w} = \frac{Qh_r\rho g}{\frac{\rho g^2}{32\pi}TH^2} \tag{4.48}$$

when considering linear waves. For irregular waves η is given by equaation 4.49, as follows:

$$\eta = \frac{P_{crest}}{P_w} = \frac{Qh_r\rho g}{\frac{\rho g^2}{64\pi}TH_s^2} \tag{4.49}$$

- P_{res} which identifies the power in the reservoir. P_{res} is dependent on the level of water collected in the reservoir h_{res}, hence on the potential energy that can be stored.

$$P_{res} = \rho g h_{res} Q \tag{4.50}$$

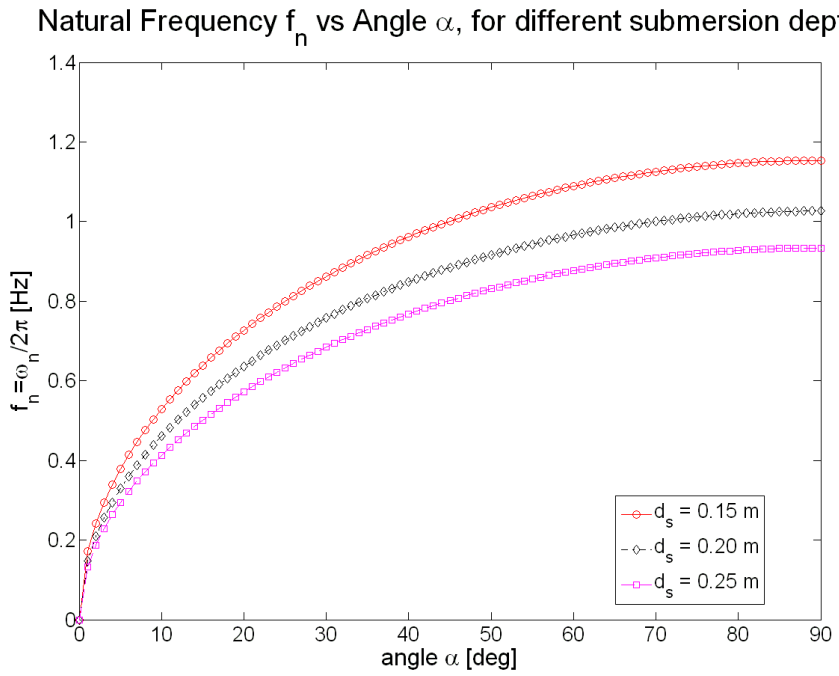

Figure 4.7: Natural frequency of oscillation of the OWCP at varying values of α for different values of the submersion depth d_s. The natural frequency of oscillation is expressed in terms of $f_n = \omega_n/2\pi$.

The efficiency of in the reservoir η_{res} is defined as:

$$\eta_{res} = \frac{P_{res}}{P_w} \tag{4.51}$$

In order to maximise the efficiency in overtopping and in the reservoir it is necessary to maximise the amount of water y_p that can be removed from the OWCP, therefore by assuring that y is maximised.

4.6 Initial Simulations

An initial analysis was conducted to investigate the response of the OWCP to the changes of natural frequency of oscillation ω_n by changing the angle of inclination of the output duct, the length of the input duct and the submersion depth d_s(Figure 4.7). By varying the angle of inclination, it is possible to modify the natural frequency of oscillation of the OWCP ω_n. This characteristic allows to implement a resonance control system to maximise the performance of the OWCP.

From Figure 4.7, one can observe that the angle α acts effectively as a resonance control

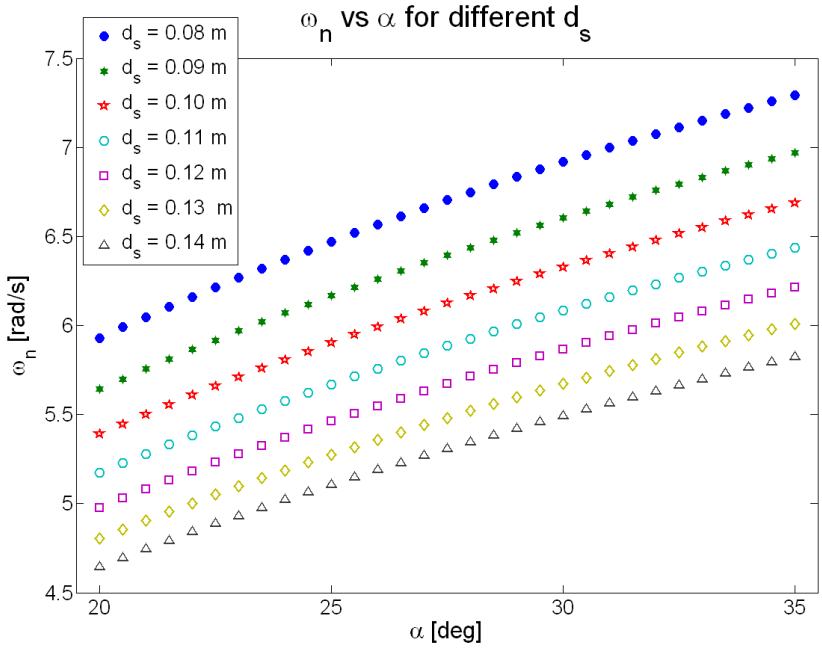

Figure 4.8: Natural frequency of oscillation of the OWCP for values of α between 20^{o} and 35^{o}, for different values of d_s.

parameter. Furthermore it can be seen from Figure 4.8 that the strongest variations in ω_n are obtained when α varies between 20^{o} and 35^{o}. ω_n is also affected by changes in d_s, shifting to lower values at the increase of the depth of submergence. These analyses confirm previous work carried out by Olvera et al. (2007) that showed that alterations of a single parameter of the system can cause changes in the resonance control of the OWC.

4.7 Mathematical Models of the OWCP response

A linear and a non-linear mathematical model were developed using the Matlab code. Both were aimed to determine the Response Amplitude Operator (RAO) for different configurations of the OWCP. A mono-chromatic sinusoidal wave input was considered. The radiation damping was considered independent from the driving wave frequency as presented by Knott and Flower (1979). They showed that for a pipe of 35mm of internal radius and 200 mm of length, the radiation damping ratio ξ_r, given by equation 4.52, is equal to 0.15. Knott and Flower (1979) tested their model using values of ξ_r varying between 0.09 and 0.35; the same conditions are

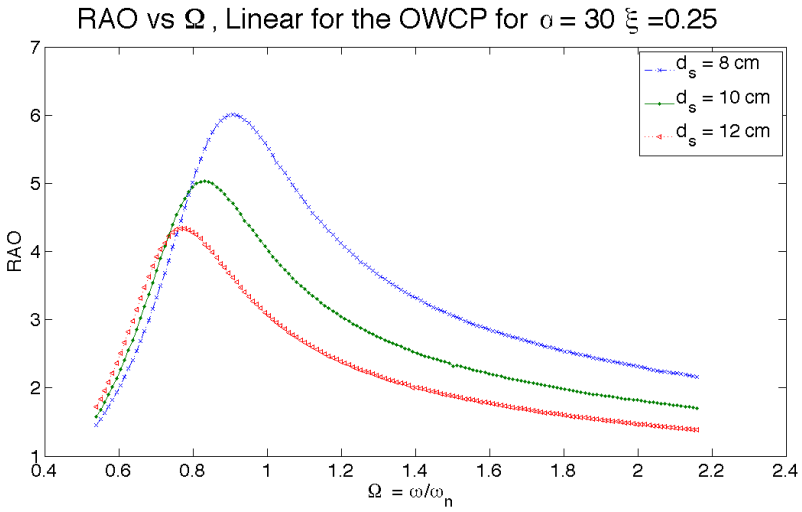

Figure 4.9: RAO of OWCP for linear conditions with $\alpha = 30$ and $\xi = 0.25$. Maximum RAOs are obtained for $0.8 \leq \Omega \leq 1$

applied in the following simulations.

$$\xi_r = \frac{B}{2\rho\sqrt{g(l+l_1)}} \tag{4.52}$$

Without considering the non-linear parameters, the equation of motion (equation 4.53) is written as a second order ordinary equation and solved with the Runge-Kutta 4 method for a range of driving frequency between $0.5\,Hz.$ to $2\,Hz.$

$$\rho psin(\omega t) = \rho(l+l_1)\ddot{y(t)} - B\dot{y(t)} - \rho g y(t) \tag{4.53}$$

Simulations were run over a range of different submersion depths and angles of inclinations. Results are shown over the normalised driving frequency Ω given by the ratio $\Omega = \omega/\omega_n$. Figures 4.9, 4.10, present the RAOs for different ξ and inclination configurations. It has to be noted that the RAO presents the response of the device in the particular degree of freedom considered, in this case heaiving of the internal water column; and that is not related with the overall power-output of the OWCP.

Equation 4.53 can be implemented to incorporate the non-linear forces presented in section 4.3. It is therefore possible to compare the linear simulations against the non-linear simulations as shown in Figure 4.11.

From Figure 4.11, it can be seen that the non-linear forces affect the response of the OWCP

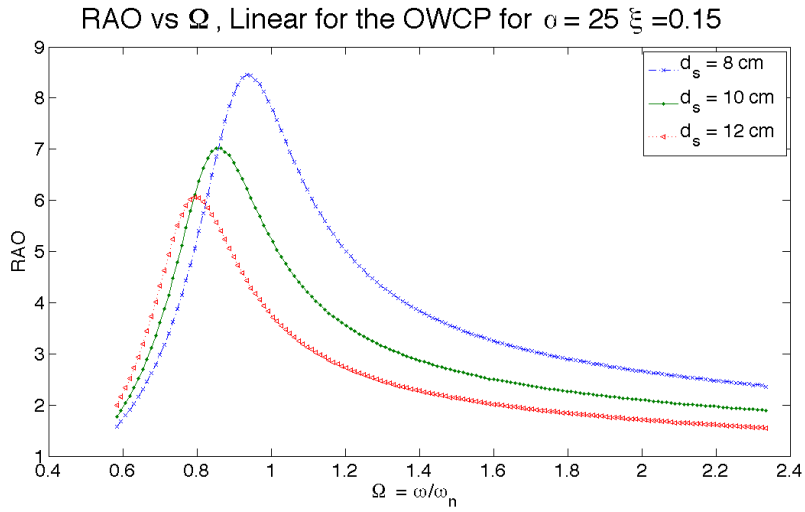

Figure 4.10: RAO of OWCP for linear conditions with $\alpha = 25$ and $\xi = 0.15$.

and shift its maximum value to a lower Ω, thus indicating that non-linearities add further damping to the system and that resonance conditions are reached for lower driving frequencies.

From the implementation of the non-linear model, it is possible to describe the motion of the water column under the excitation of an incoming wave and determine the mass of water that can be removed over a cycle, as presented in Figure 4.12. By assessing the response of the device and the removal of water over a range of ω it is possible to derive the bandwidth response of the OWCP and to determine the mass removed by the device over the cycle of operation. The efficiency in removal and the RAO for the OWCP in the case of $\alpha = 25$ and $d_s = 0.06\,m$ and $h_r = 0.05\,m$ can be seen in Figure 4.13.

The non-linear simulations allow to express the bandwidth response of the OWCP in terms of water removed from each OWCP configuration as shown in Figure 4.14 and in Figure 4.15. It can be seen that the total mass removed from the device is dependent on the removal height h_r. By reducing h_r from 0.07 m to 0.06 m the maximum amount of water removed from the OWCP increases four times, with a wider bandwidth response expected from the OWCP. Mathematical simulation can therefore be used to identify those values of h_r that either maximise the efficiency of the OWCP or the amount of water delivered by it; according to the type of application the OWCP is employed for.

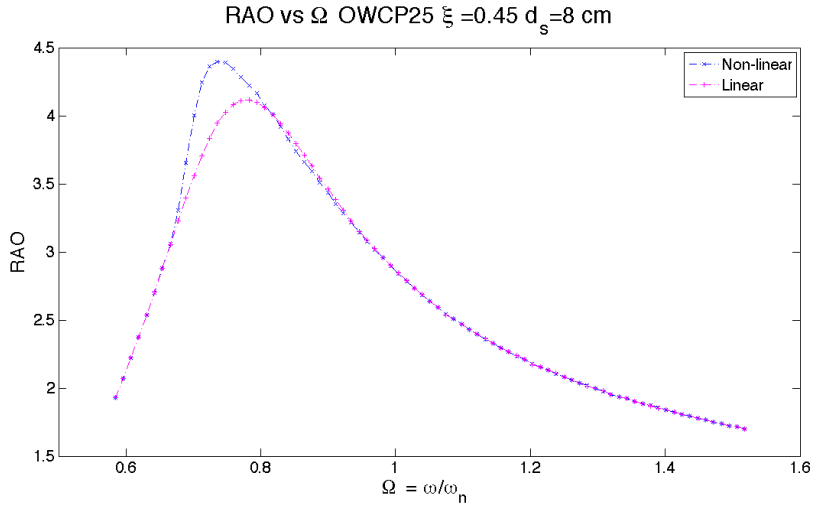

Figure 4.11: Linear and non-linear simulation for the OWCP25 with $\xi = 0.45$. It can be seen that the maximum RAO for the device is obtained at Ω =0.78 for the linear case, whilst in the non-linear case the maximum RAO is obtained for $\Omega = 0.73$, showing that the non linearities affect the theoretical performances of the device.

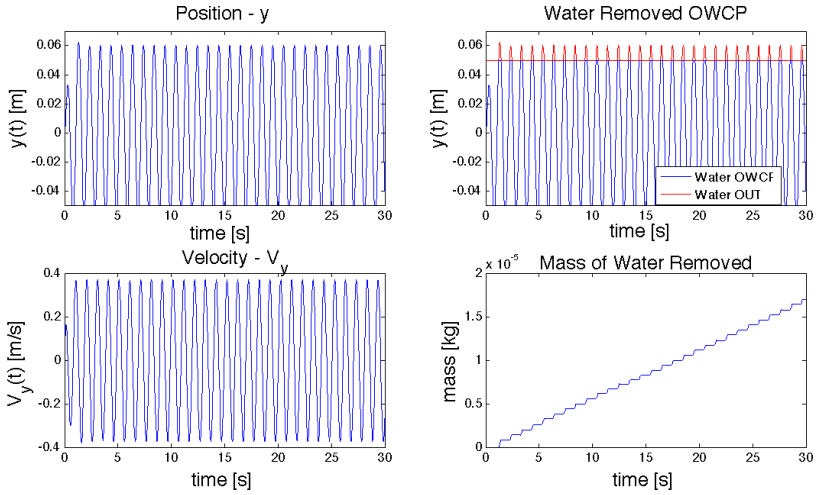

Figure 4.12: Response and mass of water removed from an OWCP with $\alpha = 25$ and $d_s = 0.08$m. The first quadrant show the position of the water column, whilst the velocity of the water column within the system is showed on the bottom left corner. The top right quadrant shows in red the amount of water that can be removed at the passing of wave, whilst the bottom right quadrant shows the cumulative mass removed over a cycle of 30 s, for $h_r = 0.0ym$.

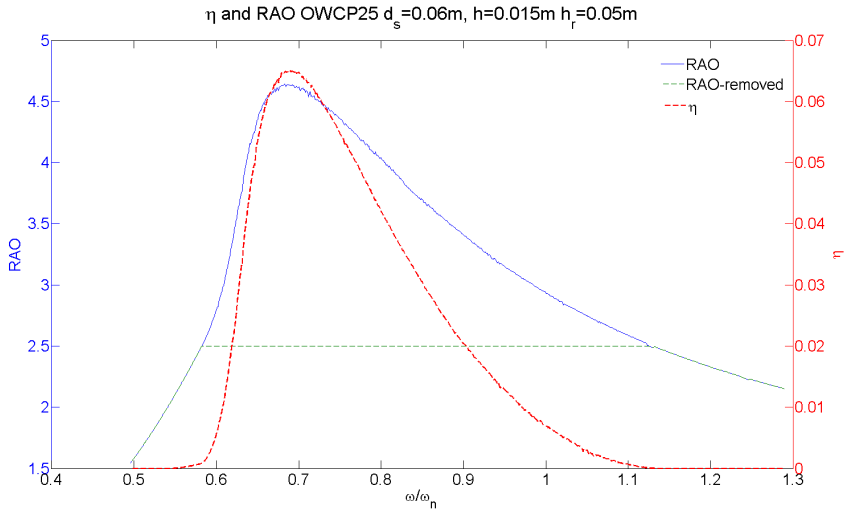

Figure 4.13: Efficiency of removal and RAO for OWCP with $\alpha = 25°$ and $d_s = 0.08$m with $h_r = 0.03m$. Efficiency of the OWCP up to 6.5% of the incoming wave energy is predicted.

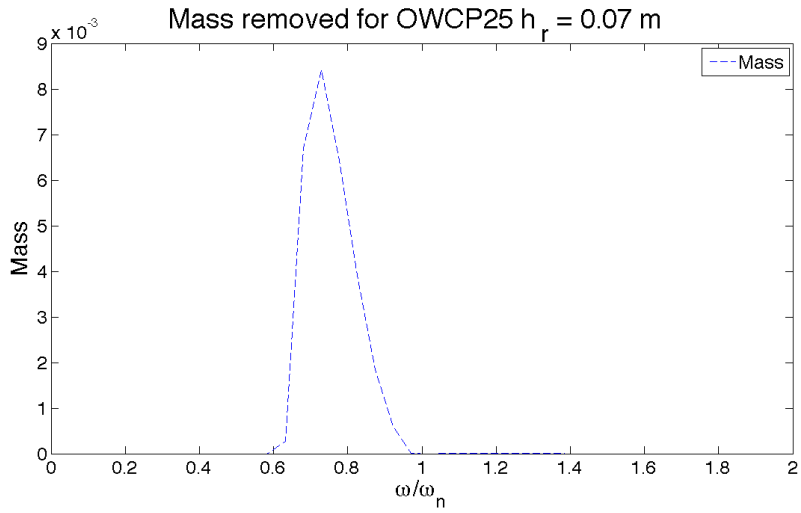

Figure 4.14: Mass removed for OWCP with $\alpha = 25°$ and $d_s = 0.08$m with $h_r = 0.07m$. The simulation was run for H=0.02 m with 30 incoming waves.

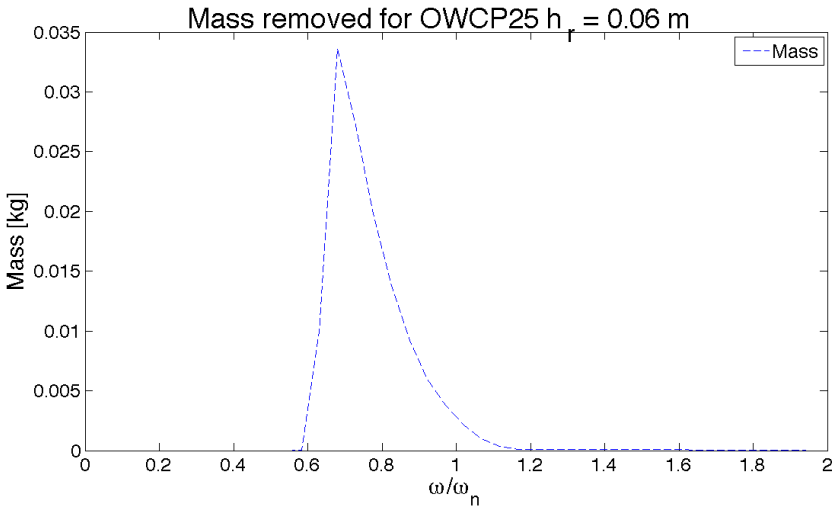

Figure 4.15: Mass removed for OWCP with $\alpha = 25°$ and $d_s = 0.08$m with $h_r = 0.06m$. The simulation was run for H=0.02 m with 30 incoming waves.

4.8 Summary

A scientific theory has been presented in order to model the response of the OWCP to incident waves. The theoretical description of the OWCP was based on the existing response theory developed for the OWC device. The response of the OWCP was considered similar to the one of a single-mass damped oscillator; a with non-linear power take off system implemented to account for the amount of water removed from the device.

A linear and a non-linear model were developed in order to assess the RAO of the OWCP for different installation configurations under the influence of monochromatic sinusoidal waves. The values of the radiation damping employed for the initial simulations were the one determined by Knott and Flower (1979). The values of RAO obtained from the numerical simulations were in the same order of magnitude of those available in the work of Evans (1978) and Lopes et al. (2009).

The non-linear model was implemented to account for the non-linear forcing terms presented in section 4.3. Simulations showed that the inclusion of non-linear terms shift the maximum RAO to lower value of the ω/ω_n ratio; thus responding to more powerful waves compared to those the device is tuned to. A further implementation of the non-linear model allowed to account for water removal from the OWCP. It was therefore possible to assess the efficiency of removal of the device and determine the amount of water that can be delivered by the device for given wave conditions. Under the influence of sinusoidal waves the maximum η is obtained at the same

driving frequency for which the maximum RAO is obtained, with predicted efficiency of up to 6.5% for the OWCP25 with $d_s = 0.06\,m$ and $h_r = 0.05\,m$. Overall, the efficiency in conversion achieved by the OWCP device are low compared to standard OWC technology achieving values of $\eta = 40\%$ (Perdigao and Sarmento, 2003); and compared to other overtopping devices such as the Wave Dragon for which an efficiency $\eta = 18\%$ was determined (Kofoed et al., 2006) and the SSG device achieving $\eta = 25\%$ under the influence of multidirectional 3D waves(Margheritini et al., 2008).

Mathematical simulation also showed that the removal height h_r play a signaifcant role in determining the amount of mass that can be removed and as a consequence the efficiency in power conversion of the device. A four time increased in mass delivered can be achieved by reducing the h_r from 0.07 to 0.06 m. h_r could be therefore used as an optimization paramater according to the application the OWCP is employed for.

In this chapter a scientific theory describing the response of the OWCP was developed. The theory included an analysis of the non-linear forces that could affect the performances of the device and led to the formulation of two numerical models describing the behaviour of the OWCP. These needs to be validated against experimental results of model OWCP devices. Once validated, the model can employed to determine the yearly delivery of water of a full scale device.

Chapter 5

Physical Modelling: Methodology and Plan

In Chapter 4 a theory for the OWCP was presented. A linear and a non-linear mathematical model were developed in order to describe the response of the device to the incoming waves and to assess the efficiency of the power output.

In this chapter an overview of the experimental equipment and tests carried out in order to assess the behaviour of the OWCP and to validate the mathematical models is presented.

5.1 Introduction

Physical tests are required to validate the model and assess the performances of the device, and the loss factors associated to it.

The importance of undergoing physical tests was discussed in section 3.2.4. Employing experimental methods plays a fundamental role in the correct evaluation of the response of a WEC. Moreover with a growing number of WECs being developed, the use of physical tests is essential to assess the validity of the devices and determine their performances. Over the past decade in order to assure uniformity in the evaluation of the devices a series of suggested guidelines for physical investigations into the performances of WECs were presented by Holmes (2003) and EMEC (2009). In both cases the evaluation and assessment process of devices performances is separated in 5 testing phases. These are summarised in Table 5.1.

The initial testing phase is aimed to verify of the concept of the proposed device. A second testing phase is carried out on a larger scale to determine the relationship with active damping

	Phase 1 *Validation model (lab.)*			Phase 2 *Design model (lab.)*	Phase 3 *Process model*	Phase 4 *Prototype*	Phase 5 *Demonstration*
	Concept	***Performance***	***Optimization***		***Sea trials***		
Primary scale (λ)	λ = 1 : 25 – 100 (∴ λ_t = 1 : 5–10)			λ = 1 : 10–25	λ = 1 : 3–10	λ = 1 : 1–2	λ = Full size
Tank	2D flume and 3D basin			3D basin	Benign site	Exposed site	Open location
Duration (inc. analysis)	1–3 weeks	1–3 months	1–3 months	6–12 months	6–18 months	12–36 months	1–5 years
Typical no. tests	50–500	250–500	100–250	100–250	50–250	Continuous	Statistical sample
Budget (€,000)	1–5	25–75	25–50	50–250	1,000–2,500	5,000–10,000	2,500–7,500
Excitation/Waves	Monochromatic linear waves (10–25 Δf) Panchromatic 5 reference	Panchromatic waves (20 min full scale) +15 classical spectra long crested head seas		Deployment: pilot site sea spectra Long & short crested classical seas Select mean wave approach angle	Extended test period to ensure all seaways included	Full scatter diagram for initial evaluation, continuous thereafter	

Table 5.1: Recommended phases of testing for WECs (EMEC, 2009)

and to establish the performances of the device in real sea conditions (Holmes, 2003). The third testing phase is carried on a benign site to evaluate the response of the device in different seaways (EMEC, 2009). The fourth and fifth testing phases are carried at prototype scale to assess full power output and survivability of the device (EMEC, 2009).

This thesis presents the development of a new type of WEC, the OWCP, hence the use of physical tests aimed to verify and validate the proposed design (phase 1) and to assess the power output of the device (phase 2).

In this chapter the experimental equipment used is presented, along with details regarding testing methodology and issues related with scaling of physical processes. Finally the experimental plan is outlined.

5.2 Experimental Equipment

Experiments were conducted in three different wave flumes: a narrow 2D wave tank, a longer 2D wave tank and a 3D wave basin. While the main aim is to assess the performances of the OWCP and provide data for the validation of the proposed OWCP theory, it is necessary to assure that the correct methodology for the simulations of waves are employed. A good reference in the determination of test parameters is described in Hughes (1993), indicating scaling and laboratory arrangements according to the type of investigation undertaken.

5.2.1 Narrow wave flume

The Narrow Wave Flume is a two-dimensional 7 m long, 0.3 m wide and 0.3 m deep wave channel used for simulation of small scale waves and wave structure interaction, shown in Figure 5.1. The narrow tank is used to represent a two-dimensional slice of the the wave spectrum. Waves are generated by the means of a piston-type linear wave generator. The wave generator is operated by an in-house software. Linear waves can be generated by inputting the frequency f of the required waves and the amplitude A of motion of the paddle. An absorbing beach is built at the back of the wave paddle to stop the formation of reflected waves that could alter the shape of the wave.

The Narrow Wave Flume is built in transparent acrylic allowing the user to employ visual investigations to monitor the use the wave development and the response of the device.

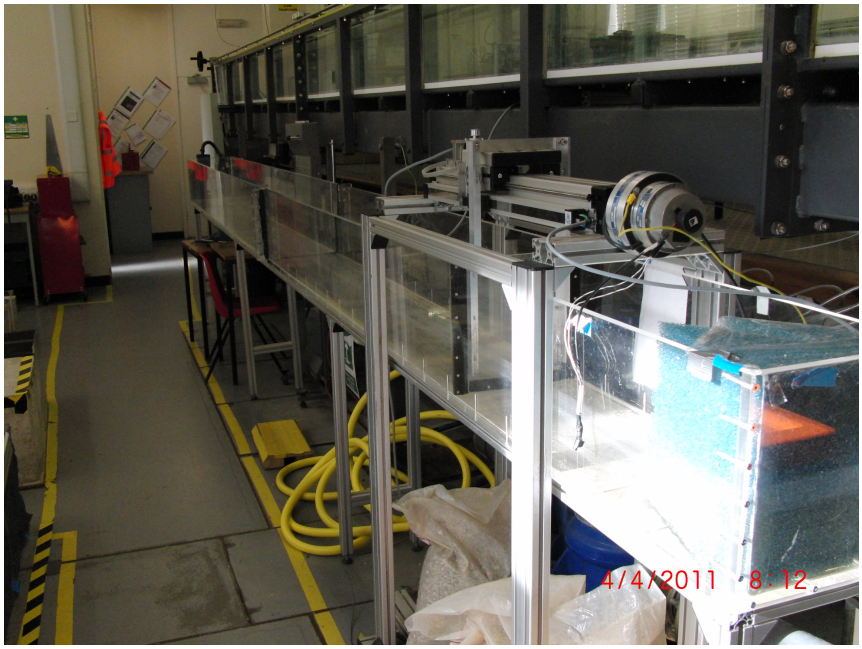

Figure 5.1: Narrow Wave Flume equipped with linear drive generator and piston type wave paddle.

5.2.2 Long wave flume

The Long Wave Flume is a two-dimensional 12 m long, 0.5 m long and 0.5 m deep wave channel. The flume employs a linear wave generator equipped with a piston-type wave paddle to generate sinusoidal wave with frequencies ranging between 0.3 to 3 Hz. Wave heights ranging between 1 and 11 cm can be generated in the flume. The long wave flume is employed to assess scale effects on the devices allowing to use a double scale compared to the Narrow Wave Flume.

5.2.3 Three Dimensional wave basin

The 3D Wave Basin consists of a 4 m long, 1.7 m wide and 0.4 m (Figure 5.2)deep wave basin equipped with a piston-type wave generator for the development of linear waves. Compared to wave tanks the wave basin allows investigation on multiples devices and to verify the angle of incidence of the waves. As for the previous flumes, the basin is equipped with a linear wave generator and a piston type wave paddle. Wave heights between 0.5 to 5 cm can be generated in the basin.

Figure 5.2: 3D Wave Basin equipped with linear wave generator and absorbing gravel beach.

5.2.4 Wave generation

The three flumes used for the simulation of waves are equipped with linear-drive, piston-type wave makers. These are considered ideal for the generation of shallow water waves for near-shore models Hughes (1993).

The paddle, presented in figure 5.3, is controlled by a PC equipped with a data acquisition card and a Test Point software control system. The software used generates sinusoidal waves once the frequency of the wave (Hz) and the amplitude A of motion of the paddle (V) are defined. A screen-shot of the Test Point interface is presented in Figure 5.4.

In order to monitor the real time wave amplitude resistance-type wave probes are employed. Recorded surface elevations for the 2D Narrow Wave Flume are presented in Figure 5.5, for two different values of the wave paddle amplitude A.

The Test-point control software is used to acquire the real-time data from the wave-probes for further analysis. The sampling frequency can be adjusted in order to match the required Nyquist frequency for the full wave representation, with a standard value of 256 samples per wave cycle automatically implemented.

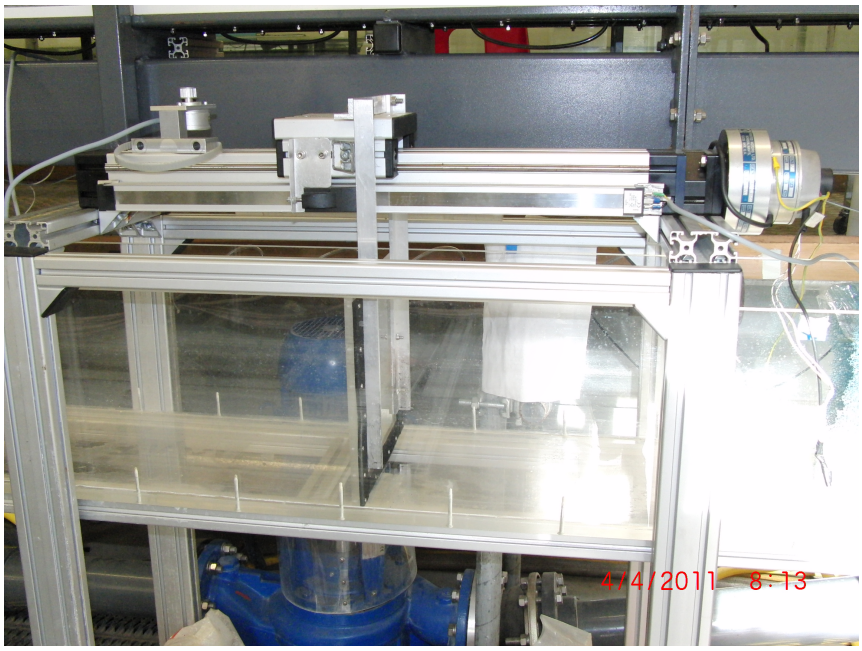

Figure 5.3: Linear Wave Generator and piston type wave paddle installed in the 2D Narrow Wave Flume.

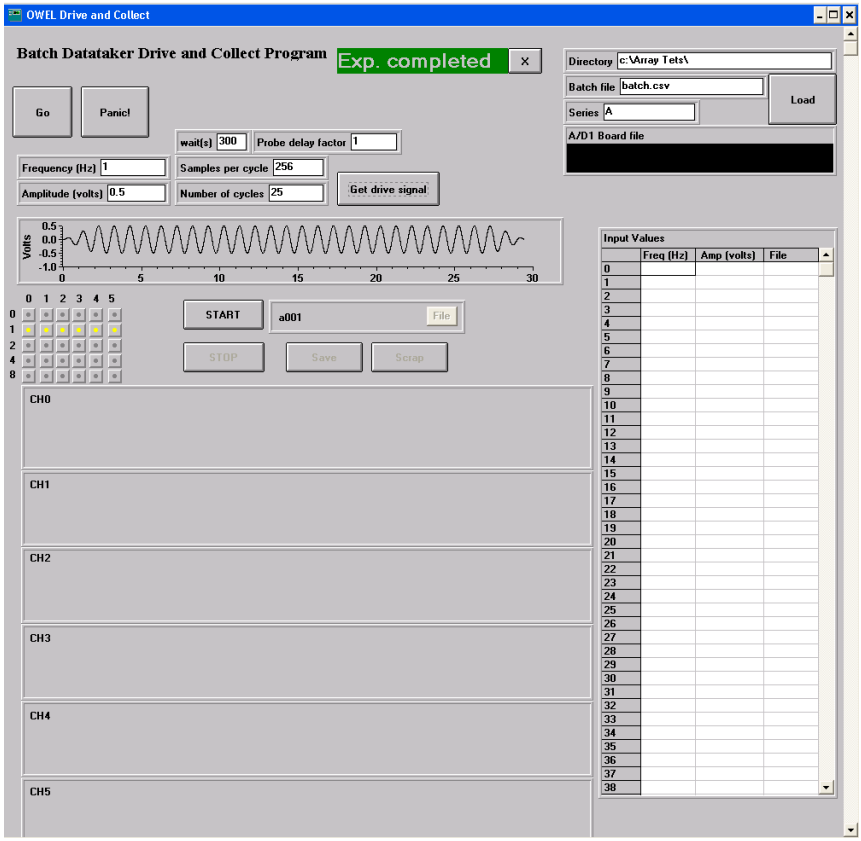

Figure 5.4: Screen-shot of the Test Point interface for control of wave paddle and data acquisition. The wave paddle amplitude A, the wave frequency f, the sampling frequency can be inputted in order to generate the required sinusoidal wave. The shape of the wave generated is shown below the inputs.

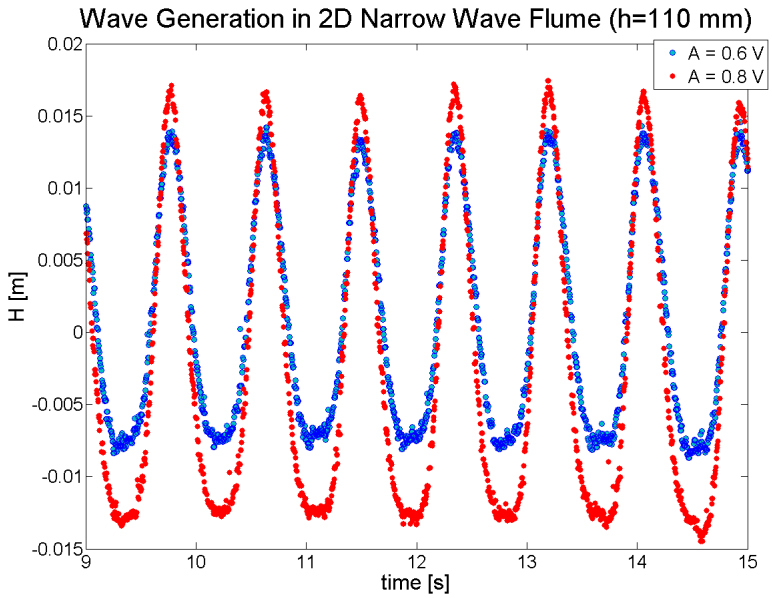

Figure 5.5: Recorded surface elevation for wave generated in the 2D Narrow Wave Flume, with $f = 1.16$Hz and $A = 0.6V$ (blue) and $A = 0.8V$ (red) for $h = 110mm$. It can be seen that an increase in A increases the wave height H. Due to small-water depth and higher wave frequency the waves present a larger trough than crest.

5.2.5 Wave measurements and analysis

Resistance-type wave probes are used to monitor the development and elevation of the waves in the wave tank. They consist of an intrusive and local instrument to determine the wave height. The behaviour of the wave probes is assumed to be linear with the water level, and probes are calibrated regularly to assure highest accuracy.

A minimum of two probes are required within the basin, this allows for reflection analysis and to separate the incoming wave towards the OWCP from the waves that are reflected by the device using the system presented by Frigaard and Brorsen (1995). (Appendix B.3). In most of the tests undertaken, three probes were installed within the flume, with the reflection analysis being carried out twice for improved results. In most of the tests undertaken, three probes were installed within the flume, allowing for increased accuracy whilst carrying out reflection analysis. For the validation phase of the numerical model the total incident wave height was used for comparison with experimental results. This allowed for higher accuracy due to short time series in the wave tank and for inclusion of the different effects, such as reflection and diffraction, in the mathematical model.

5.3 Scales and Scaling Issues

The use of experimental tests involves replicating with high accuracy the physical behaviour of waves and devices at a smaller scale. When working at laboratory scale it is therefore essential to assess the main force acting on the system and assure that the main physical process is correctly simulated. This requires that all the factors influencing a reaction are proportional between model and prototype (Hughes, 1993).

Different scaling laws can be adopted according to the type of investigation carried, in order to assure similarity between the model and the full scale device. Scaling laws are based on similitude criteria of the physical parameters: Kinematic, Gravity and Viscous laws, among others, have been developed in order to assure a reciprocality between scale test and prototype.

Hughes (1993) indicated that for most coastal processes either the Froude scaling law or the Reynolds law can be applied according to which force is predominant; gravity in the case of Froude's law and viscous forces for Reynold's scale.

Holmes (2003) stated that for most the studies involving WECs the main restoring force is provided by the gravity force. Hence, Froude's scale is normally employed for the physical modelling of wave energy converters, as can be seen in the work of Delaure (2001) and Payne (2006).

In the case of the OWCP, the restoring force acting on the water column is due to gravity. Froude's scaling law is therefore used to assure similarity between models and prototype.

5.3.1 Froude scaling law

The Froude number relates the influence of the inertial and gravitational force in an hydraulic flow (Hughes, 1993), and is given by:

$$\sqrt{\frac{inertial\,force}{gravity\,force}} = \frac{V}{\sqrt{gL}} \tag{5.1}$$

where V is the velocity of the flow, g the gravitational acceleration and L represents the wavelength of gravitational waves.

The Froude scaling law requires that the Froude number in the model and in the prototype should be the same

$$\left(\frac{V}{\sqrt{gL}}\right)_p = \left(\frac{V}{\sqrt{gL}}\right)_m \tag{5.2}$$

Physical Parameter	Unit	Multiplication factor
Length	[m]	λ
Structural mass:	[kg]	$\lambda^3 \cdot \rho_F / \rho_M$
Force:	[N]	$\lambda^3 \cdot \rho_F / \rho_M$
Moment:	[Nm]	$\lambda^4 \cdot \rho_F / \rho_M$
Acceleration:	[m/s^2]	$a_F = a_M$
Time:	[s]	$\sqrt{\lambda}$
Pressure:	[Pa=N/m^2]	$\lambda \cdot \rho_F / \rho_M$

Table 5.2: Main parameters of Froude similitude, where λ is the scale factor. (Hughes, 1993)

with the subscripts p and m indicating respectively the Froude number at prototype and model scale.

By defining λ the scale ratio between the wavelength of the prototype and the model, as shown in equation 5.3, it is possible to define the similitude parameters of the Froude Scaling law .

$$\lambda = \frac{L_p}{L_m} \tag{5.3}$$

The main parameters of the Froude similarities are reported in Table 5.2

Given the dimension of the test facilities available for carrying empirical tests and the guidelines presented by Holmes (2003) and EMEC (2009), it was chosen t to work with a factor $\lambda = 40$.

The maximum wave heights that can be generated in the narrow wave flume and in the 3D wave basin are of 5 cm, corresponding to real scale scenario of 2 m.

5.3.2 Scale effects

It is important to bear in mind that once chosen a scaling law, other forces considered secondary may not scale correctly. In particular, when considering the Froude scale, viscous forces and surface tension effects are neglected (Hughes, 1993). Neglecting these effects causes inaccuracies in determining the response of the devices.

The influence of secondary forces has been shown to be more prominent at model scale, and the smaller is the scale the stronger are these effects supposed to be.

In the case of the OWCP, the chosen scaling ratio is $\lambda = 40$. It is expected that strong friction forces will affect the response of the device at the input of the device and within the system. According to the dimension of the OWCP, secondary effects due to surface tension can take place and reduce the response of the device.

It is important to evaluate the role of secondary forces and to assess the scale effects in order to increase the accuracy in describing the OWCP.

In order to correctly validate the mathematical model, friction and scale generated effects were analysed by employing a different testing scale $\lambda = 20$ in the long wave flume.

5.4 OWCP Models Employed

Different configurations of the OWCP were built and tested in the three different testing facilities. The models were designed to investigate the RAO of the OWCP at different wave conditions and to provide data for the validation of the of the mathematical models presented in Chapter 4.

Following successful determination of the RAO, the models were employed to address the issues of water removal and pumping performances of the device.

All the models were built using transparent acrylic, with a wall thickness of 3mm. Different cross-sectional shapes were considered for the OWCP model: circular and square. For clarity, the OWCP model with a circular cross-section will be from now on referred as OWCP followed by the angle of inclination α of the output duct, whilst the models of the OWCP with a square cross-section will be referred as OWCPS followed by their significant dimension.

The OWCPS devices were built with the aim of comparing the capture width effects of similarly tuned device installed in array configuration. A diagram showing their design is presented in Figure 5.6

The characteristics of each configuration built can be found in Table 5.3 and Table 5.4.

In order to facilitate the determination of the motion of the water column within each model of the OWCP, a resistance gauge was installed within the model. The probe, consists of two 2 mm steel roads separated by 14 mm. The gauge operates in the same way of the wave probes used to monitor the real-time water surface elevation.

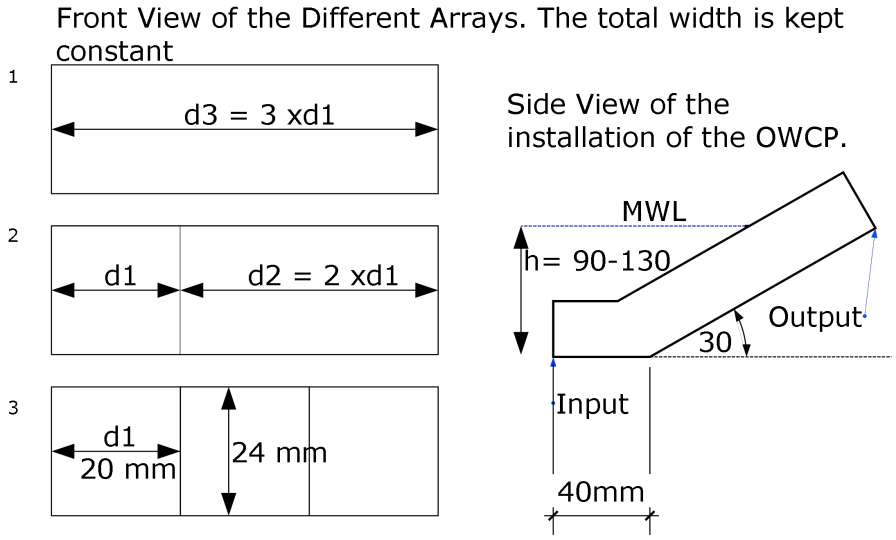

Figure 5.6: Design and proposed installation for the OWCPS models

Parameter/Configuration	OWCP35	OWCP30	OWCP25	OWCP20	OWCP15	OWCP25B
Inclination α	35°	30°	25°	20°	15°	25°
Input Duct l_1	0.035 m	0.04 m	0.05 m	0.05 m	0.06 m	0.08 m
Output Duct l	0.40 m	0.40 m	0.45 m	0.45 m	0.45 m	0.80 m
Diameter OWCP d_{OWCP}	0.024 m	0.024 m	0.024 m	0.024 m	0.024 m	0.048 m
Natural period of Oscillation T_P ($d_s = 0.11m$)	0.917. s	0.928 s	1.0646 s	1.1652 s	1.3176 s	2.12 s ($d_s = 0.2m$)

Table 5.3: Configurations of the OWCP models with circular cross-section. The configuration OWCP25B is employed for experimental tests with $\lambda = 20$

Parameter/Configuration	OWCPS1	OWCPS2	OWCPS3
Inclination α	30°	30°	30°
Input Duct l_1	0.04 m	0.04 m	0.04 m
Output Duct l	0.35 m	0.35 m	0.35 m
Heigth Cross-sectional Area	0.024 m	0.024 m	0.024 m
Cross-sectional length	d_1= 0.02 m	d_2= 0.04 m	d_3= 0.06 m
Natural period of Oscillation T_P ($d_s = 0.01m$)	0.928 s	0.928 s	0.928 s

Table 5.4: Configurations of the OWCP models with square cross-section

5.5 Experimental Plan

In order to validate the OWCP proposed in this thesis, and to evaluate its performances, a series of physical investigations were planned based on the guidelines presented by Holmes (2003); EMEC (2009).

A step by step experimental plan was determined in order to achieve the objectives presented in section 1.4; allowing for implementation of the OWCP after each single phase.

The experimental plan can be outlined as follows:

1. Validation of the OWCP concept: Different OWCP models are tested under the influence of monochromatic waves to verify and validate the proposed WEC. The main aim is to qualitatively assess the response of the device.

2. Damping and Inertia coefficients determination: Forced oscillation tests are used to determine the radiation damping and added mass term for validation of the mathematical models presented in Chapter 4.

3. Performance analysis of the OWCP: aimed to determine of the maximum lift height achievable for different configurations of the device and different wave conditions. The RAO is compared with the theoretical predictions from linear and non-linear mathematical models.

4. Assessment of the pumping ratio for a device working alone, and determination of the efficiency of the device expressed in terms of energy removed from the system compared to the energy contained in the incoming waves.

5. Evaluation of the response and efficiency of multiple OWCPs working in array configuration and assessment of the effects of the separation distance between the devices.

5.6 Summary

This chapter presented the reader with the experimental equipment and configurations of models built in order to verify the validity of the OWCP concept presented in Chapter 4. The chapter provided information on the best-practice for carrying physical tests on WEC.

An experimental plan was outlined and physical investigations were undertaken accordingly.

Chapter 6

Response and Efficiency of the OWCP: Results

6.1 Introduction

In the previous chapter the experimental equipment used to assess the performances and efficiencies of the various OWCP models built for testing was presented. This chapter deals with the results obtained from the physical testing of the OWCP models working autonomously. In particular the assessment of the RAO and η for each model are obtained and compared to the simulations from the numerical models presented in Chapter 4. More in detail this chapter deals with:

- Determiniation of the radiation damping and inertia masses in front of the OWCP through the use of forced oscillation tests
- Assessing the RAO of a single OWCP without PTO
- Assessing the RAO and η of a single OWCP when the PTO is active.

6.2 Hydrodynamic Coefficients

In section 3.2.3 it was shown how the mathematical description of a WEC is dependent on the correct determination of the hydrodynamic coefficients, added mass and radiation damping. They stand for respectively the added inertia or mass of water displaced and the generation of radiated waves due to the device motion. Their role with regards to the OWCP was presented

in section 4.2 as they affect the RAO of the water column and ultimately the removal of water from the device.

The determination of the hydrodynamic coefficients was conducted within the Narrow Wave Flume with forced oscillation (or decay) tests carried out to determine the damping ratio ξ_r, while visual investigations are employed to determine the added mass of water in front of the input pipe moved by the oscillatory motion of the water column.

6.2.1 Forced oscillation tests

Decay tests were designed in order to assess the shift in the natural frequency of oscillation ω_n and determine the damping ratio acting upon the OWCP models. The determination of the damping ratio is carried out by using forced oscillation tests. The movement of the water column is forced in the absence of exciting waves and the decay of the motion is controlled. It is then possible to relate the decay with the damping ratio of an harmonic oscillator. Flocard and Finnigan (2010) investigated decay tests to determine changes in ω_n due to damping, for a surging WEC by forcing its oscillation in the absence of waves. The device was pitched at an angle of 20^{o} and left to oscillate until rest position was reached.

In order to assess the damping of the OWCP, the model was placed in the 2D Narrow Wave Flume and motion of the water column was forced by the means of a water syringe. 50 ml of water were pushed in the OWCP generating an upward impulse of the water column. The impulse caused the water column within the OWCP to oscillate (Figure 6.1). The oscillatory motion of the water column was recorded until rest position was reached. The cycle time of the oscillation was determined and compared with the theoretical natural values of T_n.

The decay of the motion over time is represented by an exponential curve with a general equation given by equation 6.1 as shown by Clerc and Clerc (2003), as follows:

$$\delta = A_0 e^{-\frac{\omega_n t}{2W}} \tag{6.1}$$

where δ represents the decay function, A_0 a constant related to the initial conditions of the water column, ω_n is the natural frequency of oscillation of the OWCP given by equation 4.16, t is the time of decay and W is a quality factor related to the damping ratio ξ_r, presented in equation 4.52.

W is related to ξ_r by the following expression (Clerc and Clerc, 2003):

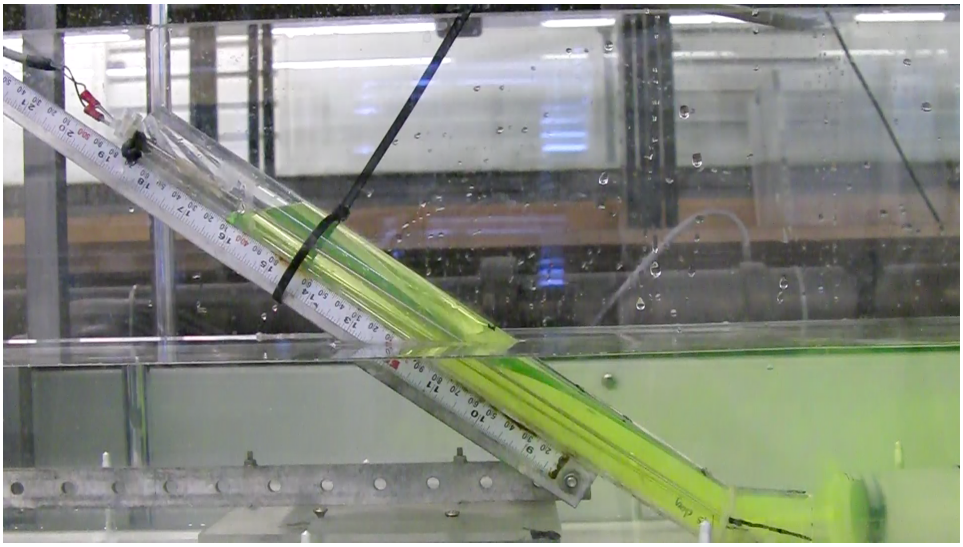

Figure 6.1: Setup of Forced Oscillation Tests, showing the input from the syringe on the right side of the OWCP.

$$W = \frac{1}{2\xi_r} \tag{6.2}$$

and it affects the natural period of oscillation of the device T_n by shifting it towards T_d as follows:

$$T_d = \frac{T_n}{\sqrt{1 - \frac{1}{4Q^2}}} = \frac{2\pi}{\omega_n \sqrt{1 - \frac{1}{4W^2}}} \tag{6.3}$$

T_d provides an indications of how damping effects the response of the device, indicating the actual tuning frequency of the device.

Forced oscillation tests were conducted at three different water depth conditions. A resistance-type wave gauge was used to record the displacement of the water in the OWCP. Each test condition was repeated five times to provide accuracy and reliability in the results. Sensitivity analysis was carried out to evaluate the effects of the added mass on the behaviour of the OWCP. Tests were complemented with video-imaging recording of the oscillatory motion. Full test set-up parameters are presented in Table 6.1.

The motion of the water column within the device was analysed to verify its behaviour. The movement was generated by an impulse force and the decay of the motion within the OWCP was recorded. The data recorded allowed the assessment of the displacement of the water in the device. Data series for three different tests conditions are presented in Figure 6.2, Figure 6.3 and

Parameter	Test 1	Test 2	Test 3
Inclination α	30°	25°	30°
Water depth h	0.065 m	0.080 m	0.100 m
Mass of water in OWCP l_t	0.105 m	0.130 m	0.177 m
Natural Period of Oscillation T_P	0.827 s	0.897 s	0.928 s
Repetitions	5	5	5
Recording time	20 s	20 s	20 s

Table 6.1: Test Parameters for Forced Oscillation investigations.

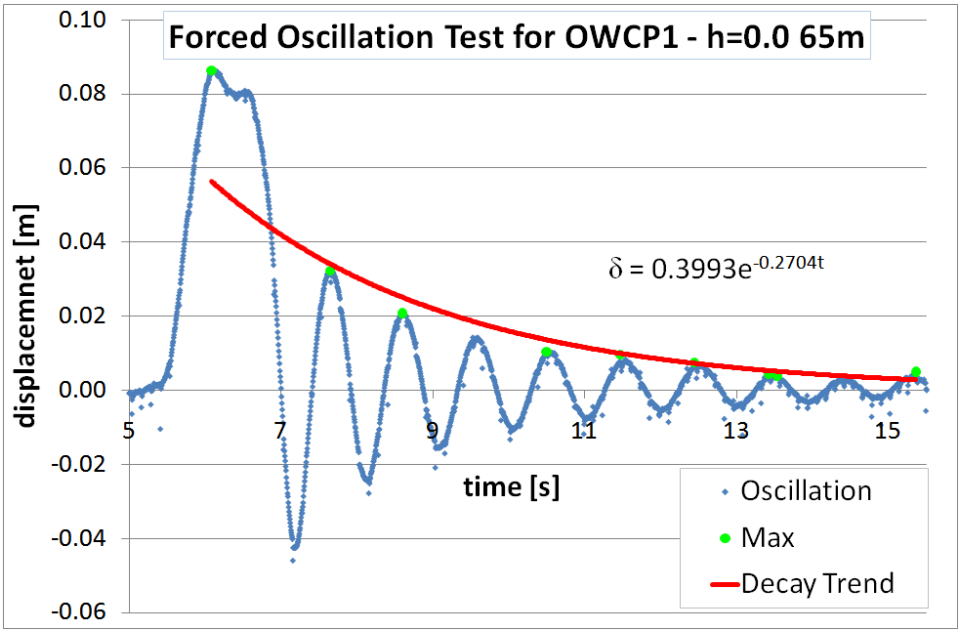

Figure 6.2: Oscillatory motion of water within the OWCP during the Forced Oscillation Test with h = 0.065 m.The peaks and the decay following the input force are showed.

Figure 6.4.

It can be seen from Figure 6.2, Figure 6.3 and Figure 6.4 that the decay of the oscillatory motion is different for the three cases examined.

Through the interpolation of the peaks for each oscillation presented in Figure 6.2, Figure 6.3 and Figure 6.4 it is possible to determine the period T_d of oscillation of the device. This was used to determine the value of the damping ratio ξ_r.

Values of T_d and of ξ_r are presented in Table 6.2, compared with the theoretical value of T_n.

From Table 6.2 it is possible to notice that for all the cases the values of T_d is higher than the theoretical value of T_n. Damping causes a significant shift in the values of T_d, with the an increase between 13.3 to 19% from the value of T_p. What can be noticed, however, is the role that the water depth plays on damping. It can be seen in Table 6.2 that lower is the value

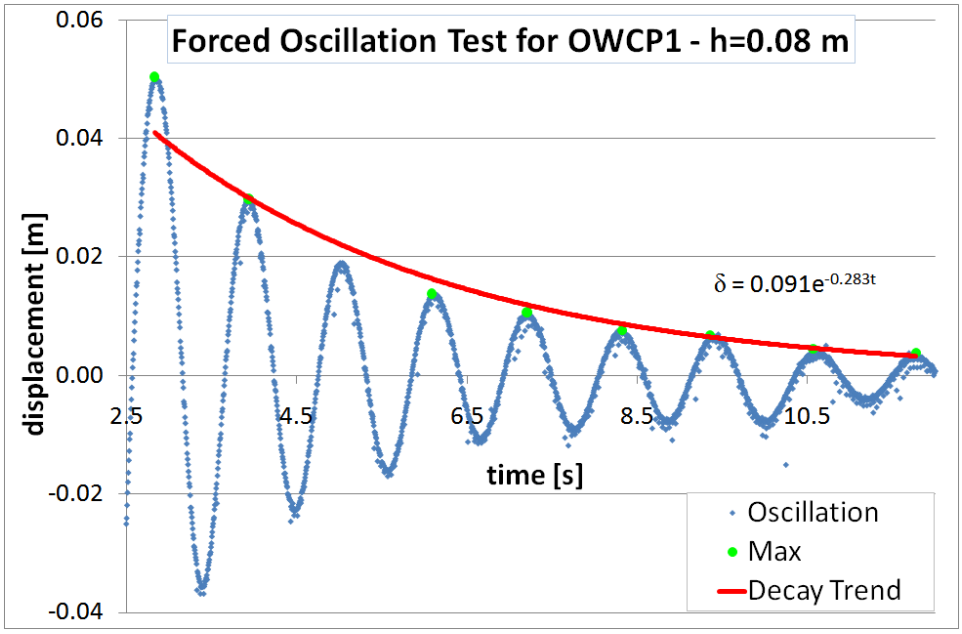

Figure 6.3: Oscillatory motion of water within the OWCP during the Forced Oscillation Test with h = 0.080 m.The peaks and the decay following the input force are showed.

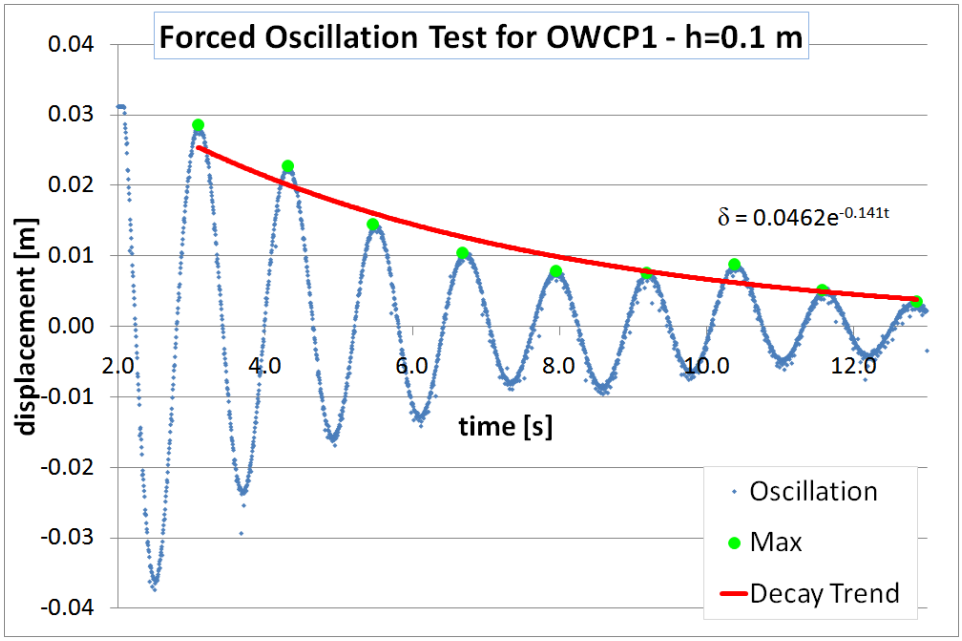

Figure 6.4: Oscillatory motion of water within the OWCP during the Forced Oscillation Test with h = 0.100 m.The peaks and the decay following the input force are showed.

Parameter	Test 1	Test 2	Test 3
Water Depth h	0.065 m	0.080 m	0.100 m
Natural Period of Oscillation T_n	0.827 s	0.897 s	0.928 s
Experimental Period of Oscillation T_d	0.954 s	1.107 s	1.195 s
Period Shift %	13.30 %	18.96 %	17.76 %
Quality Factor W	1.0034	0.8535	0.8788
Damping Ratio ξ_r	0.4983	0.5858	0.5689

Table 6.2: Comparison between theoretical and experimental results of the natural period of oscillation of the OWCP. The values of T_n, T_d, W and ξ_r are presented and compared. The shift be between T and T_d is determined.

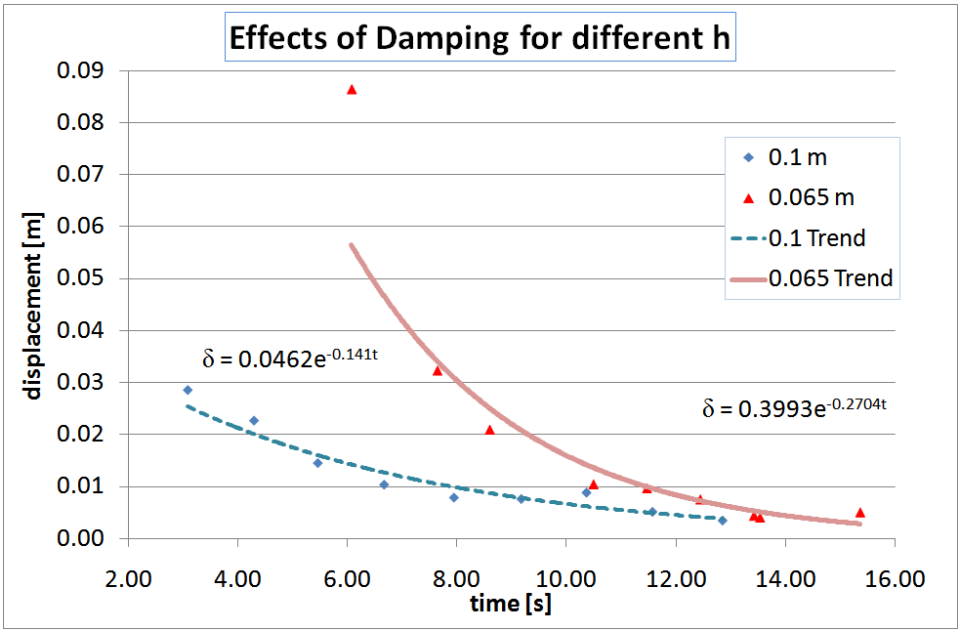

Figure 6.5: Effects of damping for different water depth conditions for Forced Oscillation Tests. It can be seen that the decay on the motion induced is stronger for the $h = 0.065\,m$condition.

of h and higher is ξ_r.

The values of ξ_r are higher than those previously used by Knott and Flower (1979) in their simulation of the overtopping OWC as a smaller device has been employed in the tests. These values can be applied to the mathematical models presented in Chapter 4 to increase the accuracy of the simulations.

In Figure 6.5 the decay of the motion of the water column for the conditions $h = 0.065\,m$ and $h = 0.100\,m$ is presented. It can be seen that the decay of the motion is stronger when the water depth is lower ($h = 0.065\,m$). Damping effects are proportional to the velocity of the water column. The lower inertia of the system with $h = 0.065\,m$ assures that the velocity is higher

Parameter	Test 1	Test 2	Test 3
Water Depth h	0.065 m	0.080 m	0.100 m
Experimental Period of Oscillation T_d	0.954 s	1.107 s	1.195 s
Length of Water at rest $l_1 + \frac{d_s}{sin\alpha}$	0.17 m	0.20 m	0.24 m
Added Length l_a	0.0562 m	0.105 m	0.115 m
Increase %	33.03	52.26	47.85
Total Lenght of water l_t	0.2262 m	0.3045 m	0.3548 m

Table 6.3: Determination of the added length coefficient, l_a, and total lenght of water moved, l_t. It can be seen that l_a could represent more than 50% of the water moved by oscillation of the water column.

(lower T_d); causing a faster decay of the motion.

6.2.2 Added mass - end of pipe effects

The added mass coefficient, μ, for the OWCP is related to what is normally considered the added increment length of fluid due to end of pipe effects (Knott and Flower, 1979), or length of end correction as presented by Chung (2008). This represents the mass of water in front of the input duct of the OWCP involved in the motion of the water column.

Chung (2008), who carried out visual investigation to assess the oscillatory motion of water in open pipes, expressed μ with the added lentgh term l_a and related it with the total length of water moved l_t. Following Chung's procedure it is possible to define l_t for the OWCP as follows:

$$l_t = l + l_a = l_1 + \frac{d_s}{sin\alpha} + l_a \tag{6.4}$$

and l_t can be related to T_d as follows:

$$T_d = 2\pi\sqrt{\frac{l_t}{g}} \tag{6.5}$$

By substituting equation 6.4 into equation 6.5 and rearranging the added length of water moved by the oscillatory motion of the water column, one can obtain :

$$l_a = g\left(\frac{T_d}{2\pi}\right)^2 - l_1 + \frac{d_s}{sin\alpha} \tag{6.6}$$

By considering the results obtained from the forced oscillation tests presented in Table 6.2, it is possible to derive the added length of water moved for the OWCP. The values of μ for the tests conducted are shown in Table 6.3.

Parameter	Range Value	Step Size
Wave Height H	0.01 - 0.05 m	0.02 m
Wave Paddle Amplitude A	0.6 - 1.2 V	0.2 V
Wave Period T	0.5 - 2 s	0.05 s
Water depth h	0.08 - 0.105 m	0.01 m
Submersion depth d_s	h - $h/2$	$h/2$
Beach Slope β	0, 1:8 , 1:20	

Table 6.4: Setup parameters for 2D Narrow Wave Flume testing of the OWCP.

The determination of the hydrodynamic coefficients presented in this section allows to improve the accuracy in the simulation and the results obtained from the mathematical model.

6.3 Response of OWCP Working Independetly

The mathematical description of the OWCP presented in Chapter 4, described a linear and a non-linear model for the evaluation of the response and performances of the OWCP (section 4.7). Both models need to be verified and validated with comparison to the experimental data.

This section deals with the determination of the RAO of the OWCP models with no active PTO installed for verification of the OWCP concept and validation of the mathematical models.

6.3.1 Experimental setup

The determination of the RAO for a stand-alone OWCP model through experimental test was carried out in the 2D Narrow Wave Flume presented in Chapter 5. The device was placed at the centre of the flume, with the input pipe positioned at a distance of 6 m from the the wave paddle, as shown in Figure 6.6.

The water depth in the flume was varied between 0.08 to 0.135 m. Monochromatic waves with a period varying between 0.75 s to 2 s were generated by the linear paddle with the wave heights varying between 0.01 and 0.05 m; thus we were able to replicate full scale waves with $H = 0.5 - 2\,m$ and $T = 4.75 - 12.65\,s$.

Three different slopes of the seabed were considered, with β varying between 0 (flat seabed), 1:20 and 1:8. A full description of the test parameters is presented in Table 6.4.

Figure 6.7 shows the OWCP30 model installed in the 2D Narrow Wave Flume under the influence of sinusoidal waves. The device is held in position by a purposely designed stand.

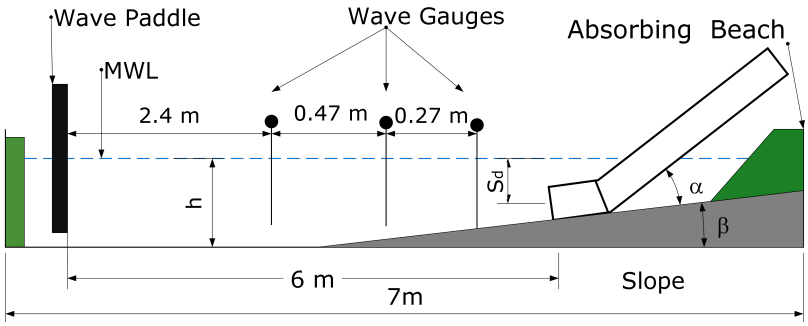

Figure 6.6: Setup of wave tank for narrow tank tests of the OWCP.

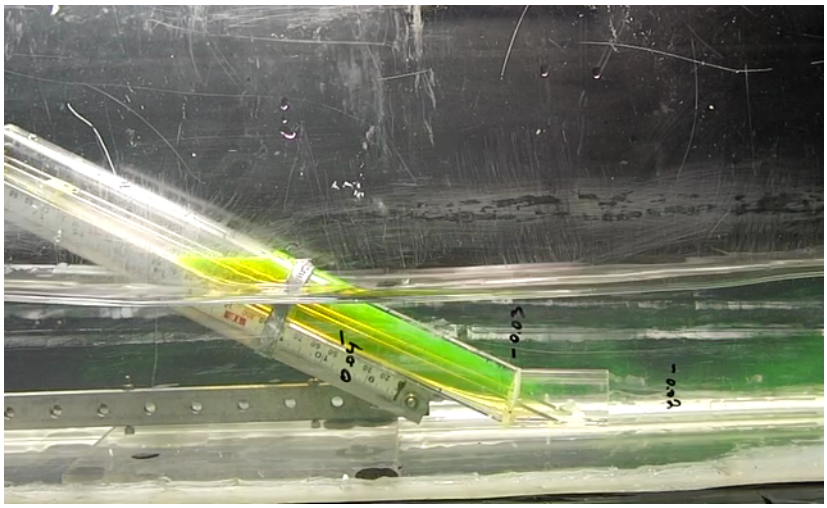

Figure 6.7: OWCP30 installaed in the 2D Narrow Wave Flume. The device is subject to the influence of sinusoidal wave. Dye is employed in order to monitor the displacement of the water column.

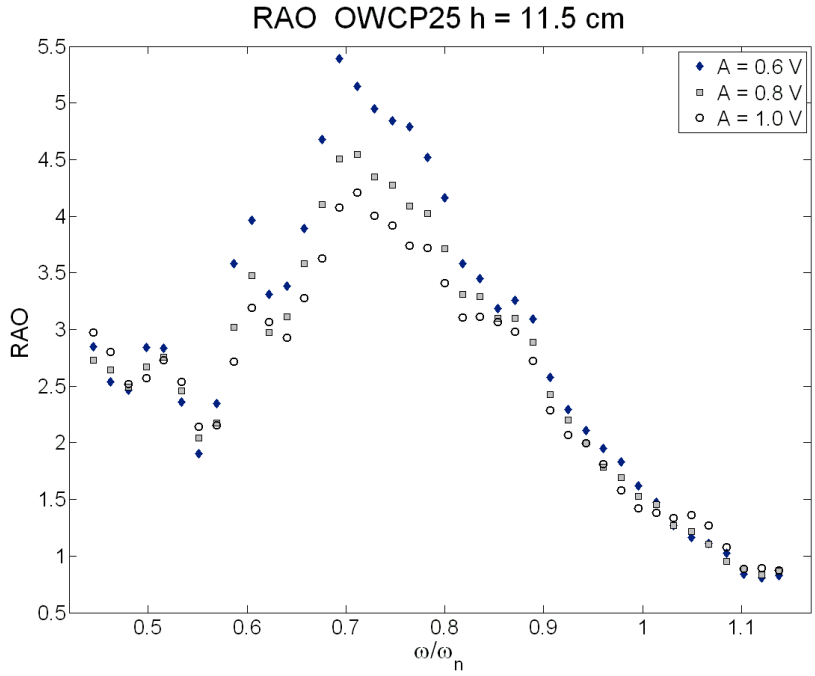

Figure 6.8: RAO for the OWCP25 model with $h = 0.115$m and $d_s = 0.06m$. The RAO is presented for different amplitudes A of the wave paddle. It is possible to notice that the highest RAO obtained is of 5.45.

6.3.2 RAO

The RAO of each model tested is determined by assessing for each wave condition, defined by H, T, the maximum displacement of the water column within the device y_{max} and comparing it with the incoming wave amplitude, as showed in Chapter 4. The RAO is therefore given by:

$$RAO = \frac{y_{max}}{H/2} \tag{6.7}$$

The RAO for each OWCP model presented in Table 5.3 was determined for each test run. From the RAO it is possible to assess the main frequency response at which the device operates best and the amplitude of the bandwidth response for which the RAO is maximised. This provides useful information for the selection of which configurations and devices could be employed for the removal of water.

Figures 6.8, 6.9 and 6.10 present the RAO response of the OWCP25, 30 and 35 obtained from experimental tests for similar conditions of h and d_s of installation in the 2D Narrow Wave Flume. It can be seen that the three RAOs present similar behaviours with the maximum obtained at a different Ω ratio. In particular, it can be seen that the higher RAO is achieved at $\Omega = 0.72$

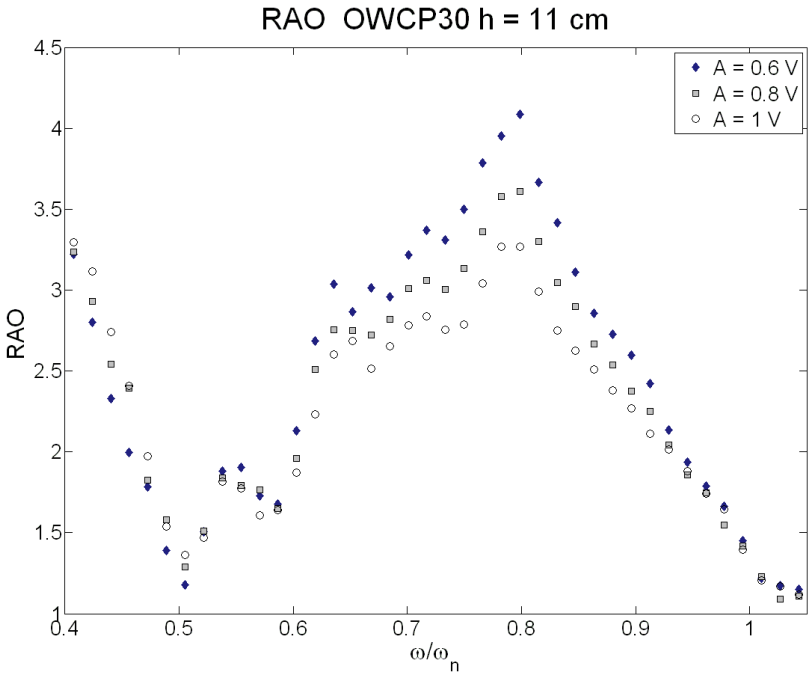

Figure 6.9: RAO for the OWCP30 model with $h = 0.11$m and $d_s = 0.065m$. The RAO is presented for different amplitudes A of the wave paddle. It is possible to notice that the highest RAO obtained is of 5.30.

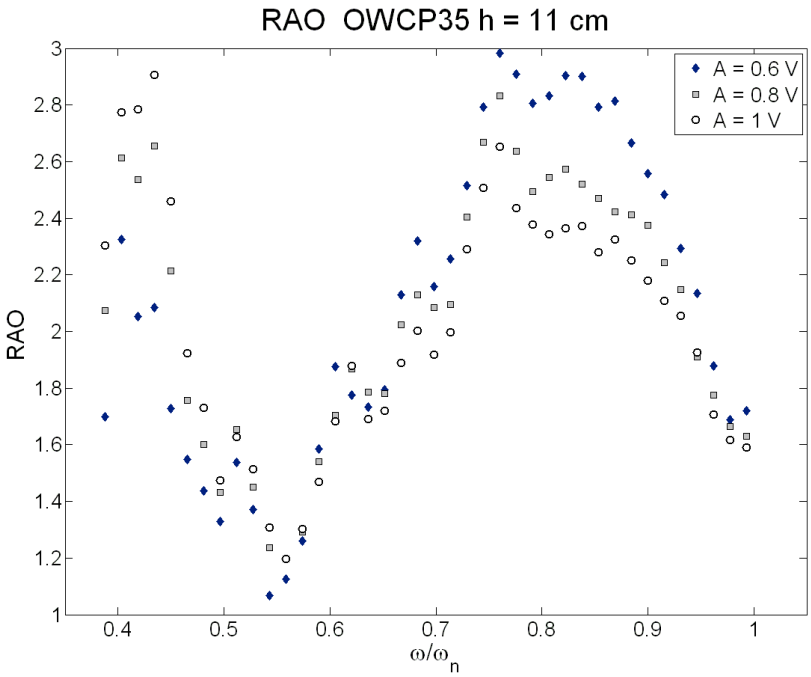

Figure 6.10: RAO for the OWCP35 model with $h = 0.11$m and $d_s = 0.065m$.

for the OWCP25, $\Omega = 0.82$ for the OWCP30 and $\Omega = 0.84$ for the OWCP35, with maximum RAOs of 5.45 for the OWCP25, 5.30 for OWCP30 model and 2.95 for the OWCP35. The RAO decreases with the increase of the angle of inclination α.

The results in Figures 6.8, 6.9 and 6.10 show that there is a clear non-linear effect influencing the responses of the devices. With the increase of A, and therefore of the wave height H, lower amplifications are obtained near resonance conditions, as indicated in section 4.2.1 where the RAO was defined.

From Figures 6.8, 6.9 and 6.10, it is possible to notice a double peak performance of the device with a minimum RAO in the three cases obtained for $0.5 \leq \Omega \leq 0.55$. Furthermore a sharp decrease in the RAO is noted for $\Omega > 0.9$ in the three cases presented. The response of each device tends towards a $RAO = 1$ for values of $\Omega > 1$, showing that the movement of the water column follows the one of the passing waves, with no amplification effect taking place within the output duct.

Through a spectral analysis of the waves generated in the flume and of the displacement of the water column, it is possible to see that strong non-linear effects take place. These are due to both shallow water effects and low-frequency waves not being fully developed within the wave flume. The effects of non-linearities effects are shown Figure 6.11 Non-linear effects are seen both in the waves and in the motion of the OWCP, hence affecting the RAO of the OWCP. By analysing the wave profile and the motion of the water column, it is possible to notice that for both low and high wave frequencies ($f < 0.65\,Hz$, $f > 1.15\,Hz$) the wave profile assumes cnoidal shape. This effect is due to the conditions of H/L and h for which the assumptions of linear wave theory are no longer applicable. The changes in the wave profile and the OWCP response for three different wave frequencies are presented in Figure 6.12. The frequency cases shown in Figure 6.12 refer to a low frequency scenario, a close to resonance scenario and to a high wave frequency case.

The wave and response profiles of Figure 6.12 show a double motion of the water column during a wave cycle for low frequencies. This occurs because of the non-linear wave shape, which generates a response of the OWCP due to what can be considered as a near pulsating excitation wave force. As a matter of fact, the frequency of oscillation of the OWCP is about two times the one of the wave, and the water column is able to respond to the impulse until the next wave impacts the device. This effect does not occur with higher wave frequencies, since $\omega > \omega_n$ and the excitation impulse generated by the wave does not allow the water column to oscillate freely.

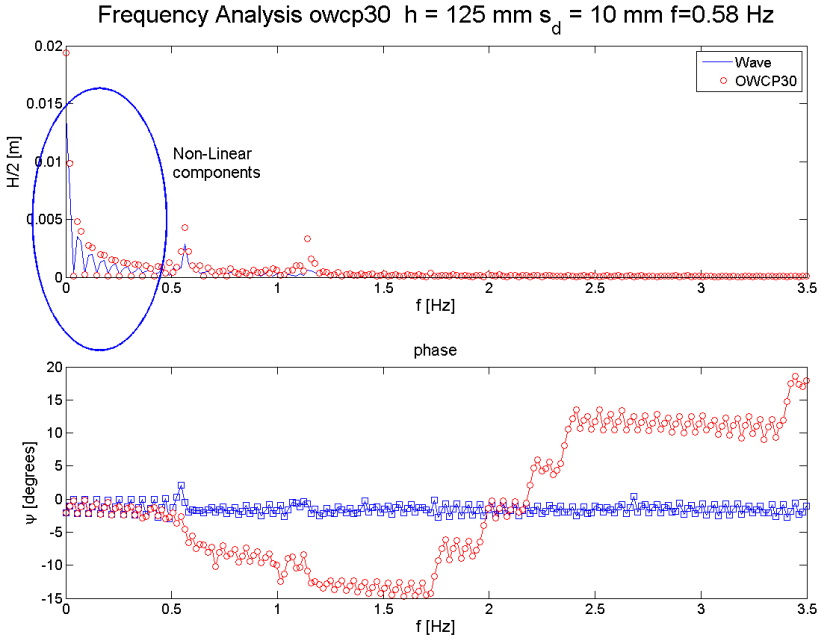

(a) Spectral analysis components for OWCP30 device with $h = 0.125\,m$ with driving wave frequency $f = 0.58\,Hz$

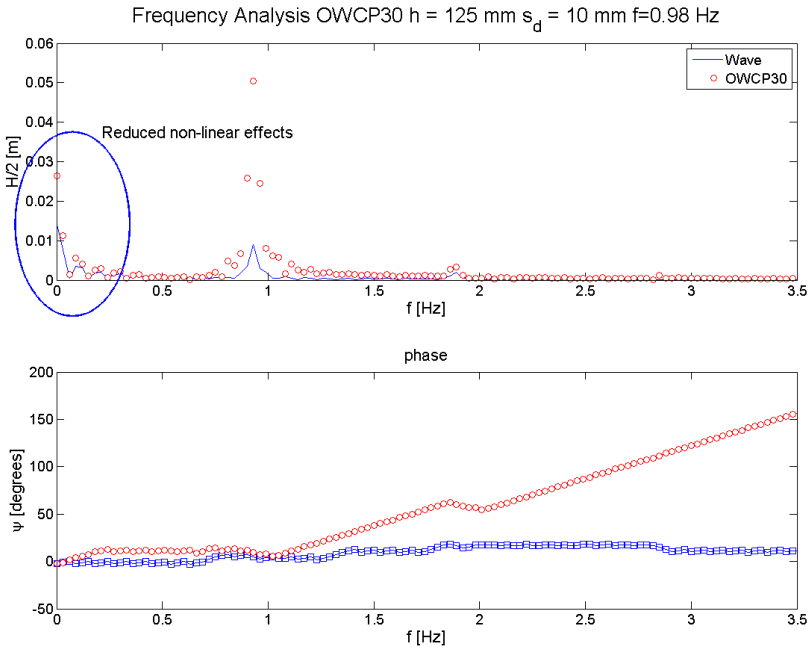

(b) Spectral analysis components for OWCP30 device with $h = 0.125\,m$ with driving wave frequency $f = 0.98\,Hz$

Figure 6.11: Spectral Analysis components for OWCP30 device with $h = 0.125\,m$ for $f = 0.58\,Hz$ and $f = 0.98\,Hz$. It can be seen that by increasing the wave frequency the non-linear components are reduced compared to the main frequency components..

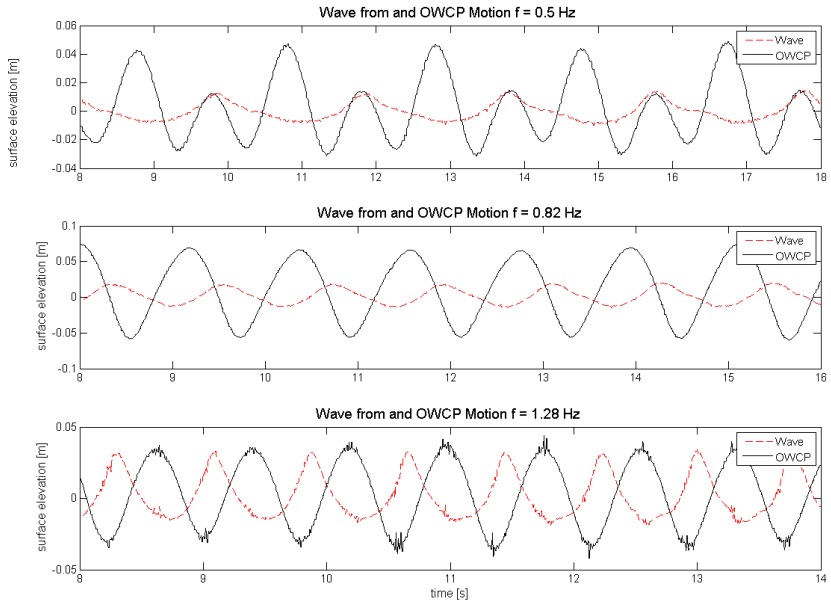

(a) Wave profile and water column profile of the OWCP30 for $f = 0.55Hz$, $f = 0.82Hz$ and $f = 1.28Hz$ when $h = 0.115\,m$.

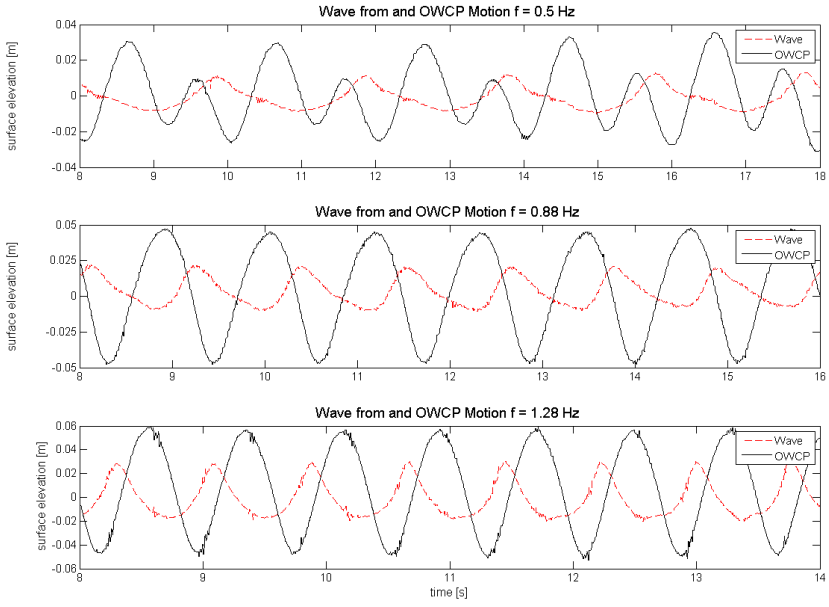

(b) Wave profile and water column profile of the OWCP35 for $f = 0.5Hz$, $f = 0.88Hz$ and $f = 1.28Hz$ when $h = 0.115\,m$.

Figure 6.12: Wave profile and water column profile of the OWCP30 and OWCP35 device for different frequencies when $h = 0.115\,m$. In the cases of low frequency and high frequency, the wave profile is no longer sinusoidal. This affects the response of the OWCPs, particularly at low wave frequencies, where it can be seen that the water column oscillates twice during a wave cycle.

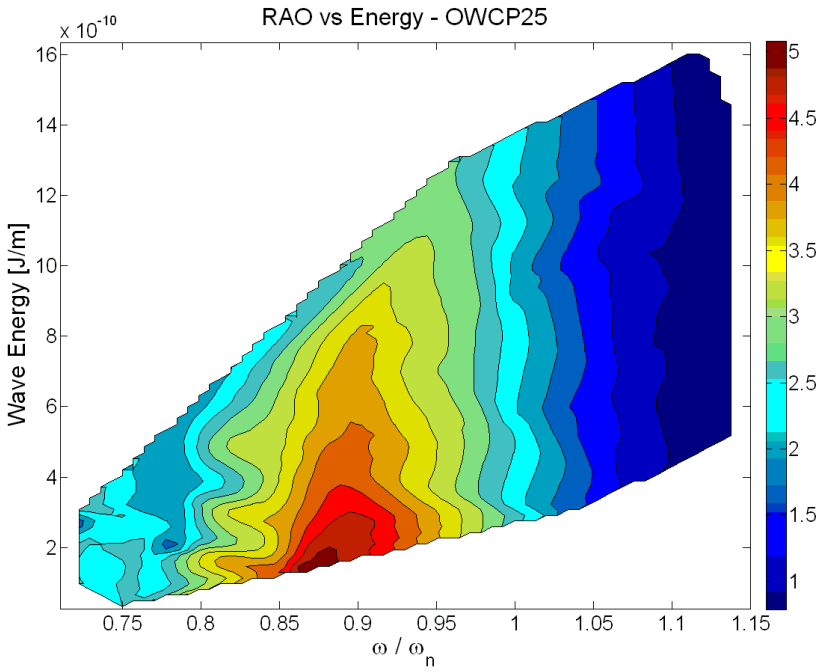

Figure 6.13: Response bandwitdh OWPC25. The maximum response of the device is obtained for $\Omega = 0.85$, with the higher response when $0.8 \leq \Omega \leq 0.9$. The highest RAOs are obtained for lower energy in the waves.

By analysing the wave energy content carried by the waves it is possible to assess the effects of the energy flux on the RAO, as shown in Figures 6.13, 6.14 and 6.15.

From Figures 6.13, 6.14 and 6.15 it is possible to see that the more energetic are the waves the lesser is the RAO obtained from the device, with a steady decrease in the values of the RAO and increase in E_s. Figure 6.13 shows that the OWCP25 can achieve $RAO > 3$ when $0.8 \leq \Omega \leq 1$ for the more energetic waves, whilst in Figure 6.14 it can be seen that the OWCP30 models achieves $RAO > 3$ for $0.80 \leq \Omega \leq 0.95$. The response of the OWCP35, shown in Figure 6.15, is limited to values of RAO between 2.5 to 3 for $0.85 \leq \Omega \leq 0.98$. The maximum RAO in the three cases presented is obtained for the lowest energy content for $E_s \simeq 2 \times 10^{-10}\, J/m$. This means that whilst the RAO obtained is high, the vertical displacement of the device is limited and water removal becomes unpractical.

The results of the RAO obtained for each device are presented in Table 6.5, summarising the maximum RAO obtained for each model tested and the value of Ω for which the response is maximised. From Table 6.5 it is possible to see that the highest RAOs are obtained for the OWCP25 and OWCP30 models, with the lowest RAOs obtained for the other models tested. The response curves for tests carried out are presented in Appendix A. From the analysis of the

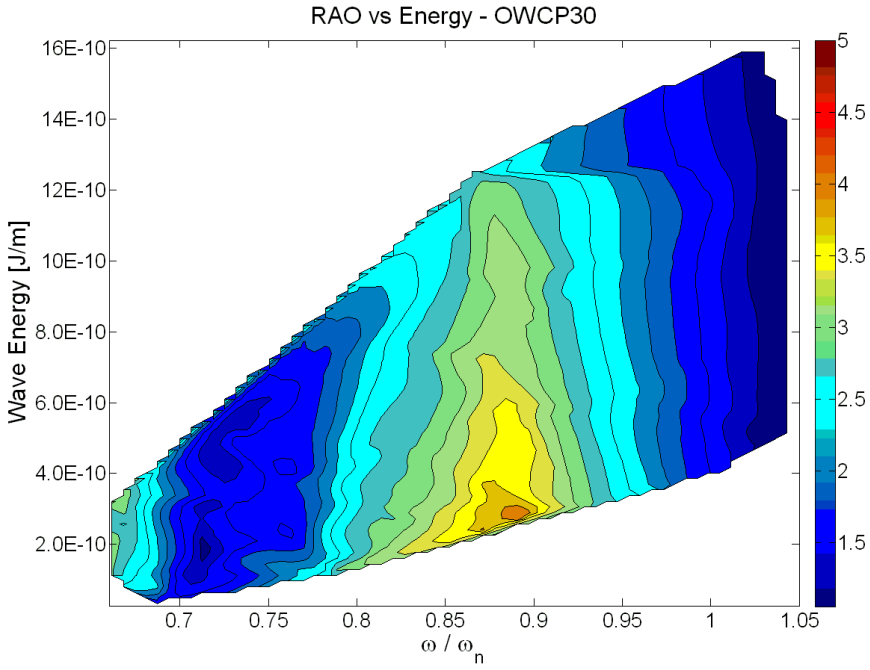

Figure 6.14: Response bandwitdh OWCP30. The maximum response of the device is obtained for $\Omega = 0.87$, with the highest responses when $0.8 \leq \Omega \leq 0.9$. The highest RAOs are obtained for lower energy in the waves.

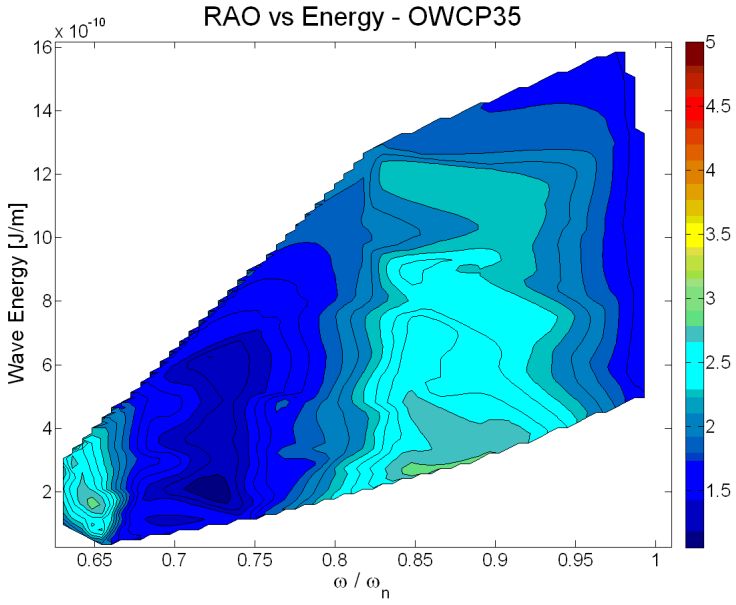

Figure 6.15: . Response bandwitdh OWCP35. The maximum response of the device is obtained for $\Omega = 0.88$, with the higher response when $0.8 \leq \Omega \leq 0.9$. The highest RAOs are obtained for lower energy in the waves.

Configuration	Maximum *RAO*	Ω	h, d_s	Vertical lift
OWCP15	11.57	0.666	$h = 0.13m$, $d_s = 0.065m$	$2.99 \times H/2$
OWCP20	9.52	0.546	$h = 0.10m$, $d_s = 0.065m$	$2.59 \times H/2$
OWCP25	14.11	0.733	$h = 0.13m$, $d_s = 0.065m$	$5.96 \times H/2$
OWCP30	10.31	0.693	$h = 0.13m$, $d_s = 0.065m$	$5.15 \times H/2$
OWCP35	2.97	0.84	$h = 0.115m$, $d_s = 0.065m$	$1.70 \times H/2$
OWCP25B	5.87	1	$h = 0.24m$, $d_s = 0.12m$	$2.49 \times H/2$

Table 6.5: RAOs for the different configurations of the OWCP under investigation. The maximum RAO for each model of the OWCP is presented along with the value of Ω for which the maximum RAO is reached. The wave flume configurations are expressed in terms of h and d_s at which maximuum response is obtained. The vertical RAO, considered in terms of $RAO \times sin\alpha$ is presented. It can be seen that the OWCP25 and OWCP30 provide the maximum response.

RAO tests of the different OWCP models it can be seen that the higher RAOs are obtained for deeper water depths h and for lower submersion depths. The conditions for which most of the models achieve higher response are for $h = 0.13\,m$ and $d_s = 0.065\,m$, corresponding to real-scale installations of $h = 5.2\,m$ and $d_s = 2.50\,m$.

By analysing the displacement of the water column in the model, it is possible to determine the vertical position achieved by the device and assess the possibility of removing water from the models.

In Figure 6.16 the vertical displacement of the water column for the OWCP25 and OWCP30 devices are presented for 3 different wave paddles amplitudes and frequencies. The values of f were chosen in order to match the values of Ω for which the RAO was maximised. As seen in Figure 6.8 and 6.9 respectively for the OWCP25 and OWCP30 devices, by increasing A, the RAO is decreased. However, by determining the vertical displacement of the water column it can be seen that the delivery of water can be obtained with a higher A, hence for lower RAOs.

The analysis of the vertical displacement of the water column, coupled with the results obtained by the RAOs test allows the selection of the devices to be investigated for water removal. The lower values of RAO obtained for the OWCP20 and OWCP15 models, coupled with a lower angle of inclination of the pipe means that the delivery of water above a certain height is unpractical.

It was chosen to evaluate the performances of the OWCP25, OWCP30 and OWCP35 for the

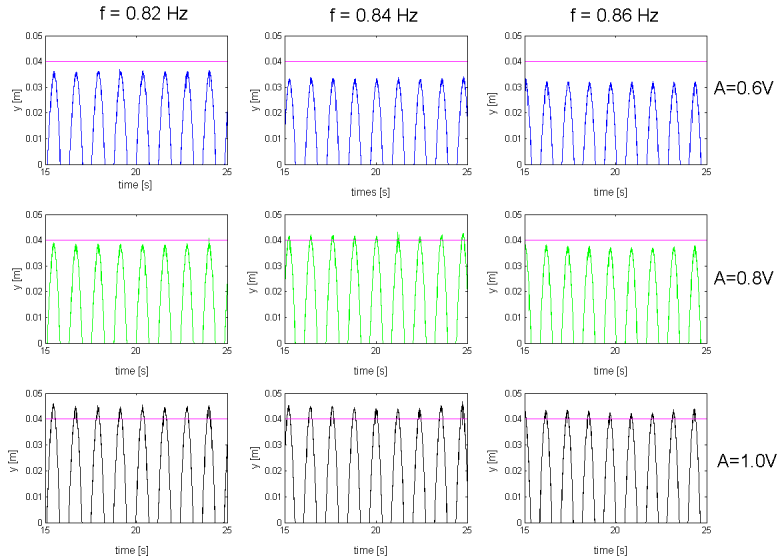

(a) Vertical discplacement for the OWCP25 model.

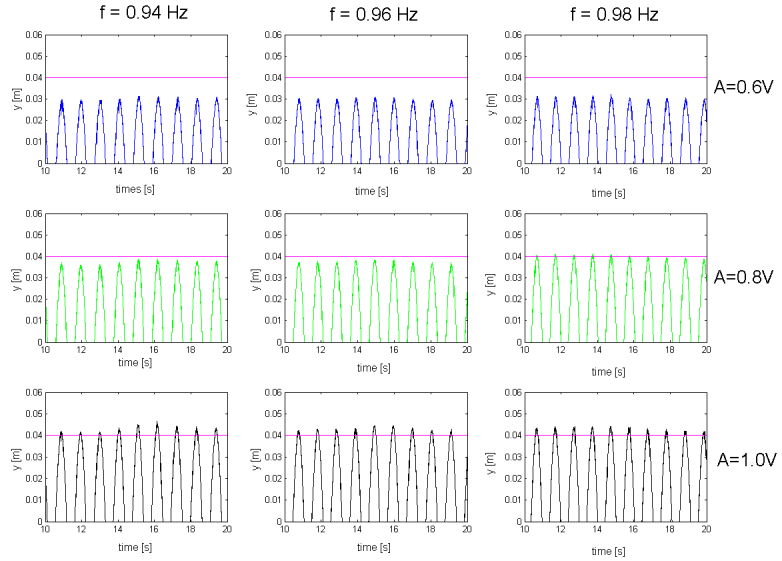

(b) Vertical discplacement for the OWCP30 model.

Figure 6.16: Vertical discplacement for the OWVP25 and OWCP30 models. The purple line indicates the water removal point set for $h_r = 0.04\,m$ above water level. The level $y = 0$ corresponds to the free surface of the water column being at M.W.L.

removal of water. The OWCP35 is considered due to a steeper inclination which would allow water delivery above a fixed height.

6.4 Removal of Water

The aim of this research is to investigate the use of the OWCP for the delivery of water. It is therefore necessary to test the models when PTO is active to determine the efficiency of removal and assess how the device responds to different wave conditions. For this reason the OWCP25, OWCP30 and OWCP35 models were tested in the 2D Narrow Wave Flume.

6.4.1 Experimental setup

Experimental tests of a single OWCP model were carried out in the 2D Narrow Tank. In order to determine the amount of water removal, the device was installed on a beach replicating a rubble mound breakwater. This allowed to install a reservoir behind the device for the collection of water free from the interference of the waves and from eventual overtopping of the waves on the structure.

To allow hydraulic similarity with coastal breakwaters, the rubble mound breakwater was built using gravel with a $d_{50} = 0.01m$ and with a slope of 1:2.5 as outlined by McConnel (1998), with a crest wall to limit overtopping into the reservoir.

The overall height of the wall was of 0.19 m from the bottom of the wave flume. The height of the structure h_w was determined by using Saniflou's method as outlined by Stagonas (2010) given by:

$$h_w = h + \frac{\pi H^2}{L} coth\left(\frac{2\pi h}{L}\right) + H \tag{6.8}$$

The OWCP was placed at the centre of the flume, with removal height y_r set at 0.175m (lower lift removal LL) and 0.185m (higher lift removal HL) from the bottom of the flume with $d_s = 0.06m$ for $h = 0.11m$ and $d_s = 0.075m$ for $h = 0.125m$. The procedure for the installation of the OWCP within the breakwater is shown in Figure 6.17.

The water depth in the flume was varied between 0.11 and 0.125. Sinusoidal waves were generated with wave heights varying between 0.02 and 0.05 m, and frequencies between 0.7 to 1 Hz.

(a) Assembly of the rubble mound breakwater with installation of OWCP at the centre of wave flume within the structure

(b) Complete installation of OWCP the within the rubble mound breakwater

Figure 6.17: Installation of the OWCP within a rubble mound breakwater for water removal tests

6.4.2 Efficiency of removal

In order to determine the efficiency of the OWCP, the mass of water m_w collected in the reservoir was weighed and averaged for the number n of incoming waves generated. It is therefore possible to determine the flowrate of water removed from the OWCP as follows:

$$Q = \frac{m_w}{nT} \tag{6.9}$$

The removal point the power removed from the OWCP, presented in equation 4.46, can be expressed as:

$$P_{crest} = Qh_r\rho g = \frac{m_w h_r \rho g}{nT}$$

Considering the power contained in each wave as presented in equation 2.4, given by:

$$P_w = E_s C_g = \frac{\rho g^2}{32\pi} T H^2$$

the efficiency of the OWCP can be expressed in terms of ratio between the potential energy generated over the specific energy:

$$\eta = \frac{P_{crest}}{P_w} = \frac{Qh_r\rho g}{\frac{\rho g^2}{32\pi} T H^2} = \frac{32\pi m_w h_r}{ngH^2T^2} \tag{6.10}$$

where d refers to the diameter of the OWCP.

Figure 6.18 shows the efficiency obtained for the OWCP25 model when the water depth was $h = 0.125\,m$, with the removal height set respectively at $y_r = 0.175\,m$ (a) and $y_r = 0.185m$ (b). It can be seen that in both cases the highest efficiencies obtained are above 10%, with maximum efficiency obtained of $\eta_{max} = 0.126$ for $h_r = 0.05\,m$, $\Omega = 0.615$ and $\eta_{max} = 0.102$ for $h_r = 0.06\,m$, $\Omega = 0.604$. A secondary peak in efficiency is obtained for $\Omega = 0.65$. It can be seen that the higher freeboard causes a shift towards lower values of the ω/ω_n ratio, indicating an effect of the PTO force on the frequency of operation of the OWCP. The RAO of the device is affected by the water removal, as for a higher η the RAO is minimised; however an overall higher shift in the RAO is noted compared to the tests presented in section 6.3, due to the influence of the rubble mound on the wave field. The influence of wave reflection on the performances of the OWCP will be discussed later.

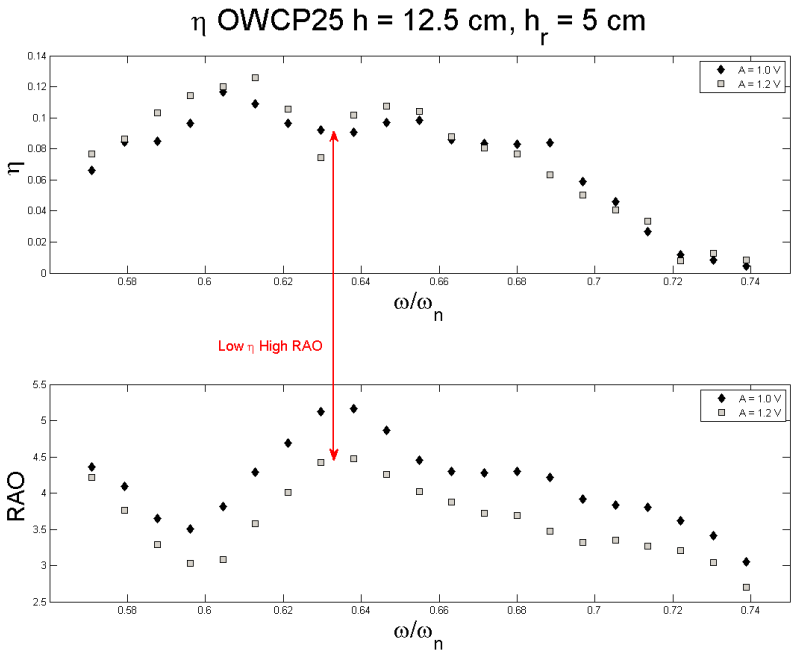

(a) η for the OWCP25 model tested with $h = 0.125\,m$ and $h_r = 0.05\,m$

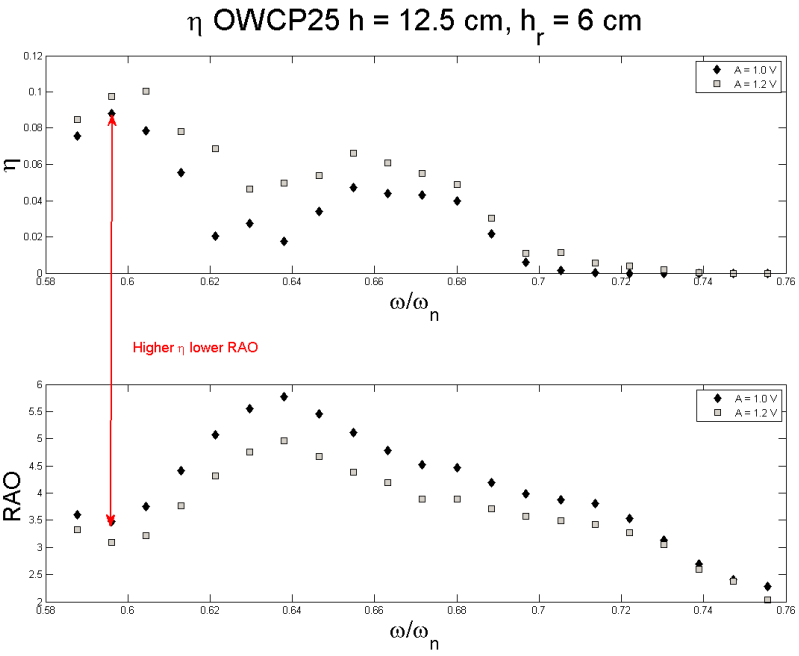

(b) η for the OWCP25 model tested with $h = 0.125\,m$ and $h_r = 0.06\,m$

Figure 6.18: η for the OWCP25 model tested with $h = 0.125\,m$ and $h_r = 0.05\,m$ (a) and $h_r = 0.06m$ (b).

Figure 6.19 shows the efficiencies obtained for the OWCP30 for $h = 0.125\,m$. The removal heights were set respectively at $y_r = 0.175\,m$ (a) and $y_r = 0.185m$ (b). The efficiency curves obtained show a significant reduction in the efficiency of the device when the freeboard is increased from $h_r = 0.05\,m$ to $h_r = 0.06\,m$. In case (a) $\eta_{max} = 0.104$ for $\Omega = 0.69$, whilst in case (b) $\eta_{max} = 0.037$ for $\Omega = 0.634$, with a reduction of 64% in terms of efficiency, compared to a reduction of 23% obtained for the OWCP when h_r was increased to $0.06\,m$. Furthermore, it can be seen that the double peak behaviour of the OWCP is emphasised when $h_r = 0.06\,m$, where the lower Ω peak becomes dominant.

Figure 6.20 shows the efficiencies obtained for the OWCP35 having $h = 0.125\,m$, with $h_r = 0.05\,m$ and $h_r = 0.06\,m$ respectively for case (a) and case (b). In case (a) the maximum efficiency was obtained for $\Omega = 0.76$ with $\eta_{max} = 0.065$, whilst in case (b) $\eta_{max} = 0.021$ for $\Omega = 0.69$; with a reduction in η_{max} from case (a) to case (b) of 67%. The effects of the increase in freeboard for the OWCP35 are comparable with those obtained from the test of the OWCP30 device shown in Figure 6.19, with an increase in h_r reflecting an overall lower efficiency, shifted towards lower ω/ω_n ratio. In both Figure 6.19 Figure 6.20, it is possible to see that by increasing h_r an increase of the wave height H, expressed in term of A, would generate a higher efficiency η.

A decrease in efficiency is noted for the devices with an increase of the angle α of inclination of the output duct, with the OWCP25 achieving higher efficiencies compared to the OWCP30 and the OWCP35.

The influence of the water depth on the performance of the OWCP models is showed in Figure 6.21 for the OWCP25 (a) and OWCP30 (b) device. It can be seen, in both cases presented, that η is maximised for deeper water depths, hence for higher d_s. Furthermore it can be seen that the increase in freeboard does not provide an increment in the efficiency of the device. In both cases, efficiencies above 10% in conversion and collection of the water are reached for $h_r = 0.05m$, corresponding to 2 m above MWL at full scale for $\lambda = 40$. It is important to show that up to the 14% of the energy carried by the waves is absorbed and converted by the OWCP reducing the energy impacting the breakwater structure.

The efficiencies of removal of the tested OWCPs for $h = 0.125\,m$ and $h_r = 0.05\,m$ are presented in Figure 6.22. Figure 6.22 shows that the OWCP25 and OWCP30 devices achieve significantly higher efficiencies compared to the OWCP35 model, suggesting that an the optimal angle of inclination of the output duct is obtained when $25° \leq \alpha \leq 30°$. This confirms the indications obtained from the RAO tests with the OWCP25 and OWCP30 models outperforming

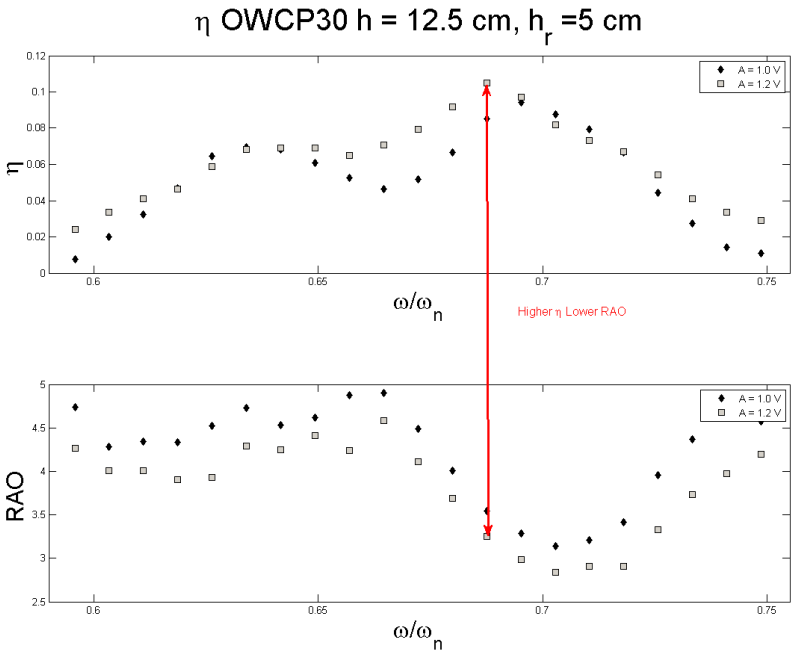

(a) η for the OWCP30 model tested with $h = 0.125\,m$ and $h_r = 0.05\,m$

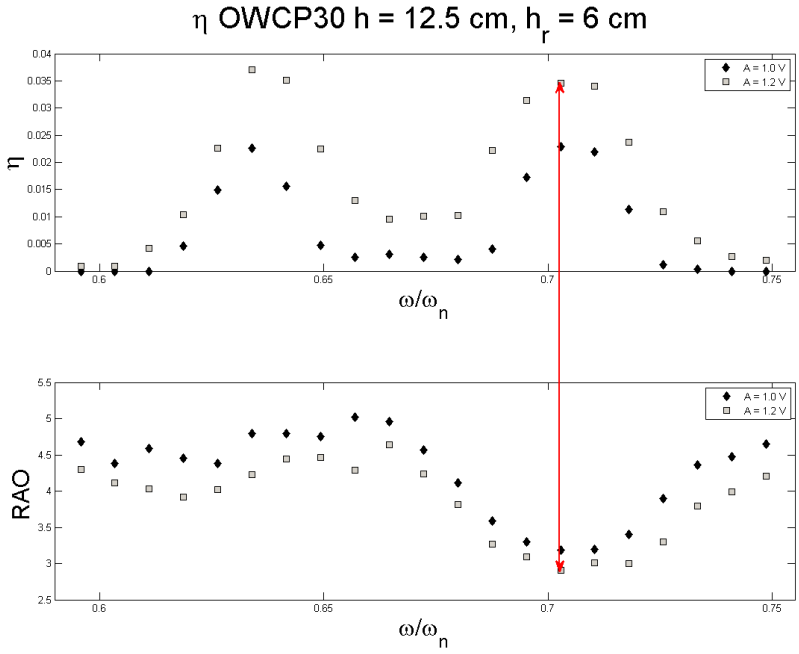

(b) η for the OWCP30 model tested with $h = 0.125\,m$ and $h_r = 0.06\,m$

Figure 6.19: η for the OWCP25 model tested with $h = 0.125\,m$ and $h_r = 0.05\,m$ (a) and $h_r = 0.06m$ (b).

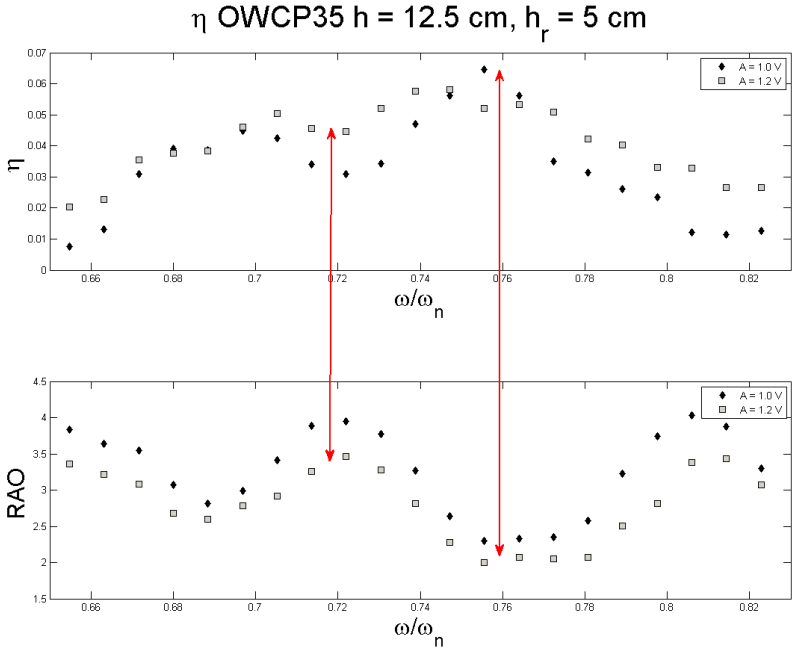

(a) η for the OWCP35 model tested with $h = 0.125\,m$ and $h_r = 0.05\,m$

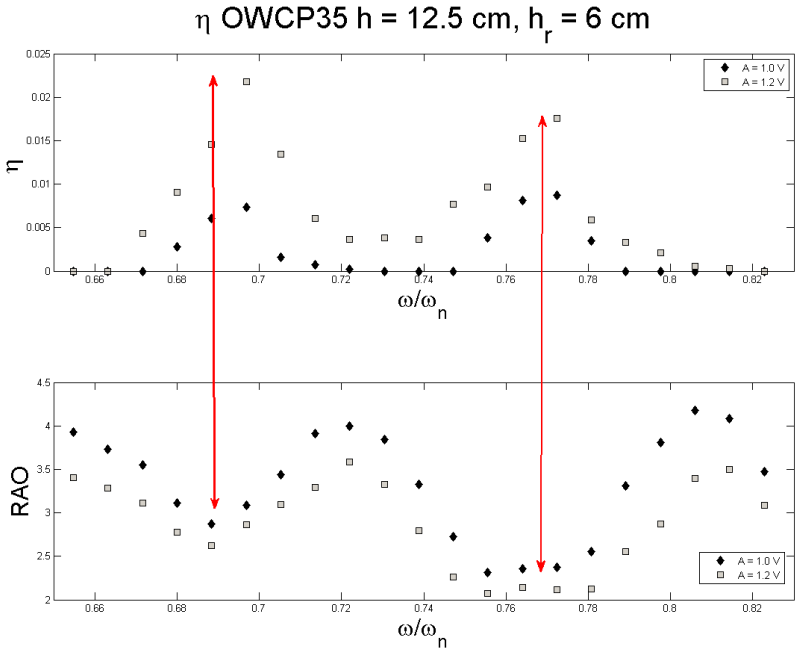

(b) η for the OWCP35 model tested with $h = 0.125\,m$ and $h_r = 0.06\,m$

Figure 6.20: η for the OWCP25 model tested with $h = 0.125\,m$ and $h_r = 0.05\,m$ (a) and $h_r = 0.06m$ (b).

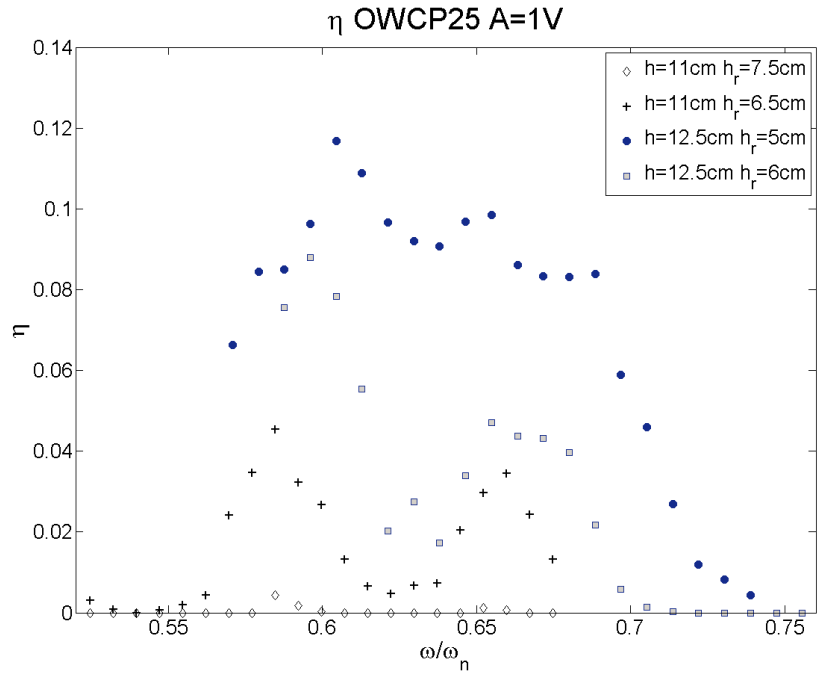

(a) η for the OWCP25 for $h = 0.11\,m$ and $h = 0.125\,m$.

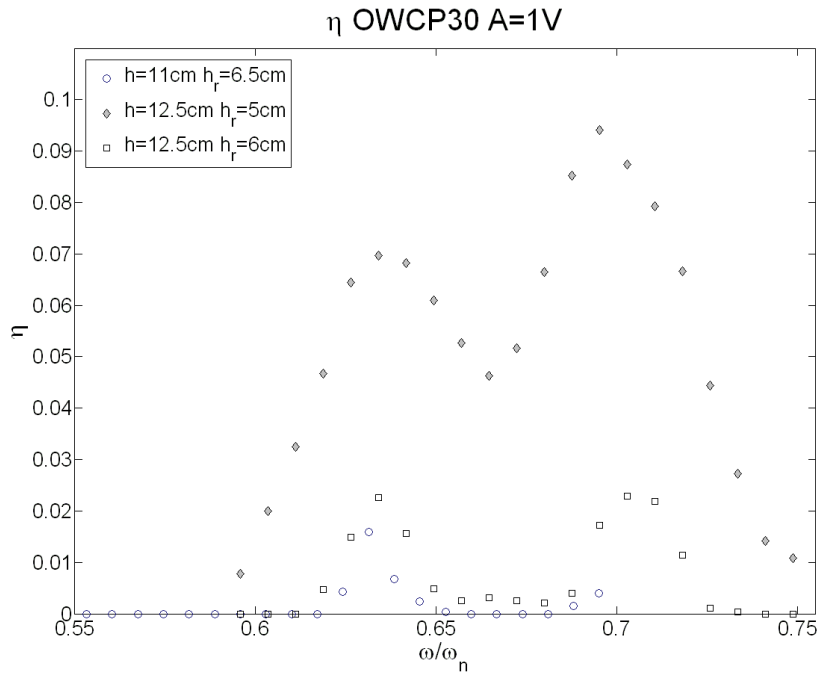

(b) η for the OWCP30 for $h = 0.11\,m$ and $h = 0.125\,m$. The case $h = 0.11\,m$ with $h_r = 0.075\,m$ is not presented since no water was removed for the tests considered.

Figure 6.21: η for the OWCP35 and OWCP30 for different water depths.

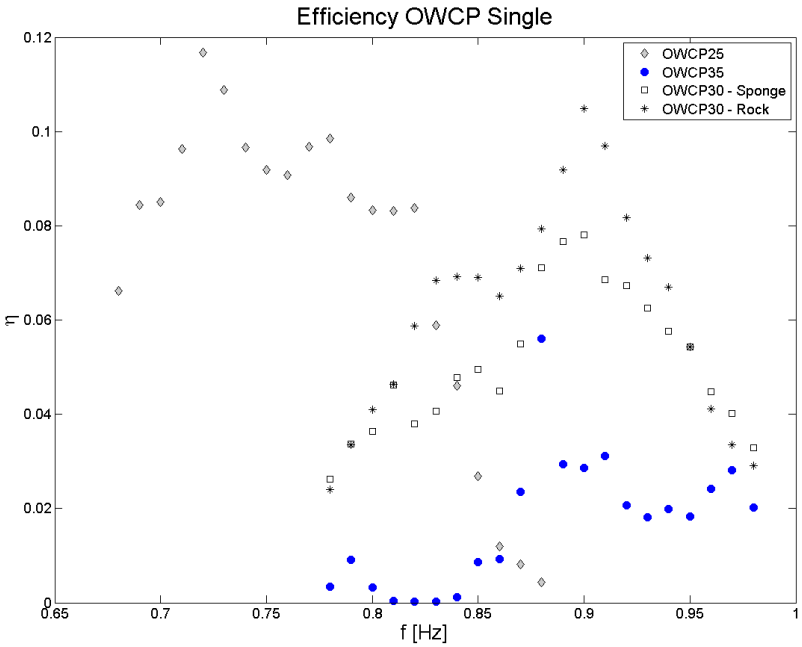

Figure 6.22: Efficiencies of removal of the tested OWCPs for $h = 0.125\,m$ and $h_r = 0.05\,m$.

the other tested models in terms of RAO. Furthermore, it can be seen that the maximum η for the OWCP25 and the OWCP30 are obtained for different values of the driving frequency f. The differences in f indicate the possibility of using multiple OWCP models installed simultaneously to allow continuous delivery at the changing of the incident wave conditions.

6.4.3 Reflection effects on water removal

The presence of the rubble mound within the flume generates reflected waves that modify the wave field and can affect delivery. To assess the role of the structure in affecting the wave field it is possible to determine the reflection coefficient, through the use of the surf similarity term presented by Battjes (1974):

$$N_i = \frac{tan\beta}{\sqrt{H/L}} \tag{6.11}$$

where N_i is the surf similarity parameter, or Iribarren number; β the inclination of the seabed (or in this case the breakwater), H, L are respectively the wave height and the wave length of the incoming wave at the toe of the slope.

The reflection coefficient K_r can be calculated once N_i is determined for rubble mound as follows (Hedges, 1989):

$$K_r = 0.6tanh\left(0.1N_i^2\right) \tag{6.12}$$

K_r provides an indication on the reflective quality of the structure and on the steepness of the incident waves.

In order to assess the effects of wave reflection from the breakwater structure, the OWCP30 device was tested installed on two different types of reflective beaches. One was built out of gravel, as presented in section 6.4.1, with a slope $\beta = 1 : 2.5$; an alternative beach was built by using absorbing foam. The absorbing sponge allows allows for a higher dissipation of energy, hence reducing K_r. The slope of the sponge beach was kept at $\beta = 1 : 2.5$ to assure similar Iribarren Number for the two beach profiles, and to allow the comparison of results.

Figure 6.9 presents the efficiency in delivery obtained for the OWCP30 model tested in the sponge beach, case (a), and on the rock beach, case (b). In both cases the water depth in the 2D wave flume was maintained at $h = 0.125\,m$ with $h_r = 0.05\,m$.

From Figure 6.9 it can be seen that $\eta_{max} = 0.78$ for case (a) and $\eta_{max} = 0.105$ in case (b). With a reduction in performances of 25.5% when moving from the rock to the sponge beach profile. In order to assess the influence of the beach profile on the performance of the OWCP it is necessary to determine K_r.

Figure 6.24 shows K_r and η for the two different beach profiles. It can be seen that for the two beaches considered, K_r presents a similar profile for changes in the wave frequency, with lower values of the reflection coefficient obtained for the sponge beach. In both cases the maximum efficiency obtained, for $f = 0.91\,Hz$, is achieved for the local minimum of K_r. When K_r is maximum, the efficiency drops, indicating that whilst the wave height in front of the OWCP is up to 50% higher, no positive effects are generated towards the performance of the device.

In Figure 6.25 the frequency analysis of the wave signal is shown for the $f = 0.83\,Hz$, $A = 1.2\,V$ for the two different types of beach. It can be seen that the response of the device (left side, black) is higher for the device installed on the gravel beach compared to the model installed on the sponge beach. The frequency analysis of the wave gauges (right side) shows the dominant wave in the flume generated for $f = 0.83\,Hz$. The amplitude of the wave recorded at gauge 2 is 30% higher than the one at gauge 1, showing stronger reflection effects for the rock beach profile.

Whilst for other overtopping wave energy devices, such as the WaveDragon, the structure

is designed in order to increase the delivery of water in the reservoir, Tedd et al. (2006), the performances of the OWCP show that for values of $K_r > 0.5$, the efficiency of the device drops.

Therefore the performances of the OWCP could be enhanced if the device is to be installed on a semi-reflective structure, such as a rubble mound breakwater. This identifies the possibility of coupling wave energy converters on defensive coastal structures, as discussed in section 3.1.5. In particular the coupling of the OWCP on a rubble mound resembles the concept of installation of the SIBEO (Czitrom, 1997) ,which aim was to deliver water into enclose marina for flushing; and the initial concept of the Wave Pump showed by Bruun and Viggosson (1977).

6.5 Comparison of Experimental Results with Mathematical Simulations

Two mathematical models were developed to predict the response and the efficiency in removal of the OWCP. The damping coefficients determined in section 6.2 were integrated in the formulation of the mathematical models in order to simulate the response of the OWCP under the influence of monochromatic sinusoidal waves and provide an estimation of the performances of the device. It is now possible to compare the results obtained from the simulations with those obtained from the experimental tests.

6.5.1 RAO

In section 6.3 the results of RAO tests for the OWCP models tested were presented, with Figures 6.8, 6.9 and 6.10 showing the RAO for three configurations tested.

Figure 6.26 and Figure 6.27 present the comparison between the numerical simulations and the experimental tests for the OWCP25 and OWCP35 respectively. In both cases it is possible to notice that the results obtained from the simulations present a bigger bandwidth compared to the experimental tests; with the non-linear simulations (NL) showing a closer agreement to the experimental results. In both cases, the non-linear simulation predictions indicate reasonably well the maximum RAO that can be achieved, although shifted towards lower values of the ω/ω_n ratio. In particular, the responses obtained from the numerical simulations show a lower decreasing trend compared to the experimental tests, after the maximum RAO is obtained; thus indicating that for wave frequencies higher than ω_n strong damping effects take place. In both Figure 6.26 and Figure 6.27, it can be seen that for $\omega/\omega_n < 0.6$ the mathematical simulations

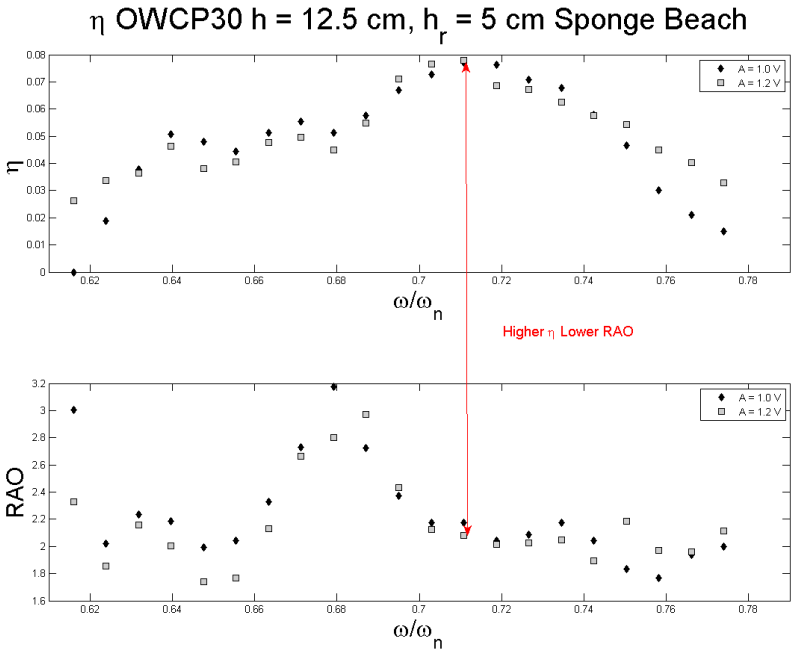

(a) η for the OWCP30 installed on a sponge beach, to investigate the effects of reflection of the waves from the breakwater on the performances of the device

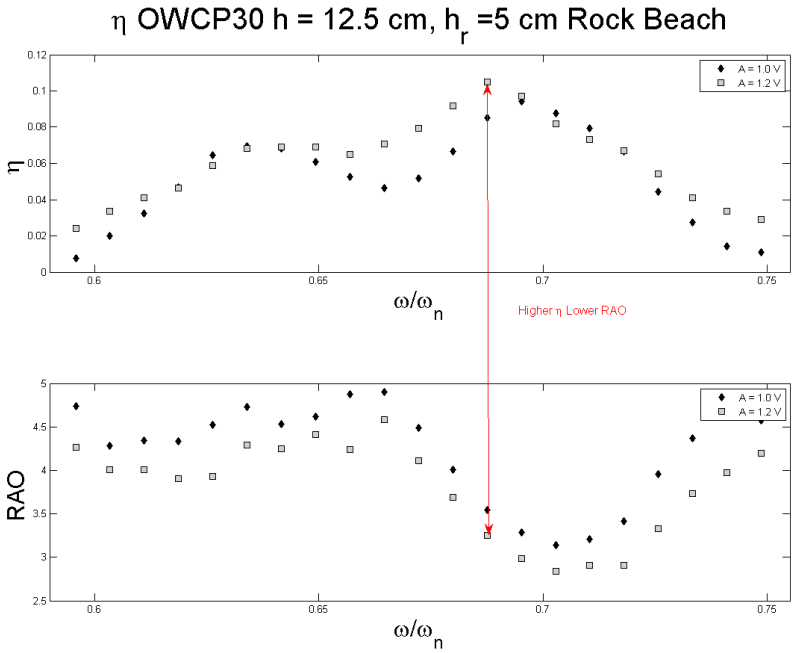

(b) η for the OWCP30 installed on the gravel breakwater.

Figure 6.23: η,RAO for the OWCP30 model tested on different reflective beaches with $h = 0.125\,m$ and $h_r = 0.175\,m$ for $1V \leq A \leq 1.2V$.

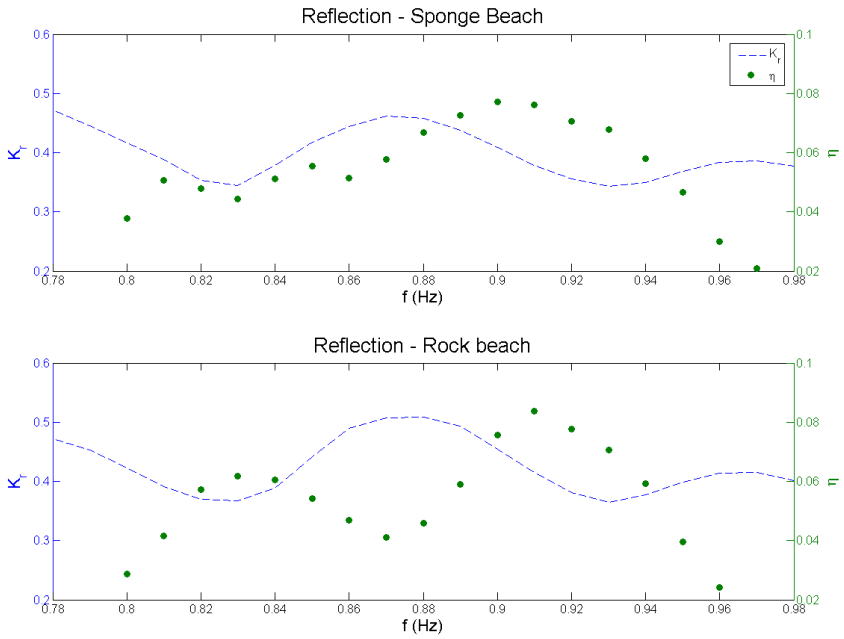

Figure 6.24: K_r,η for the OWCP30 model tested on different reflective beaches with $h = 0.125\,m$, $h_r = 5\,cm$ and $A = 1\,V$.

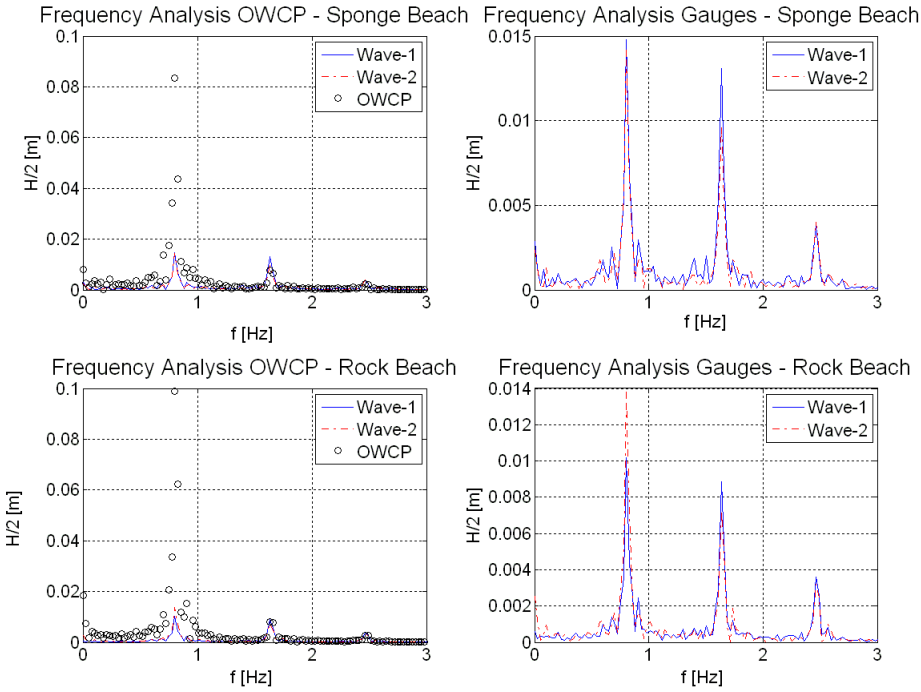

Figure 6.25: Frequency Analysis for the Wave Gauges and OWCP for the OWCP30 device installed on a rock and on a sponge beach with $f = 0.85\,Hz$, $A = 1V$, $h = 125\,mm$ in both cases.

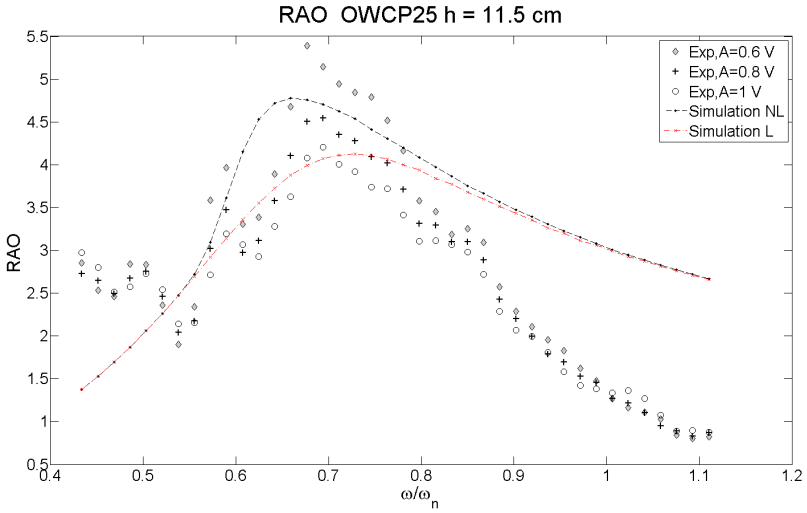

Figure 6.26: Comaprison of RAO Tests with mathematical simulation for the OWCP25 model. The dashed lines present the results obatined from the mathematical simulations, with the red line showing results obained from the linear model (L) and the black line showing non-linear model results (NL)

disagree with the experimental tests. As previously discussed, cnoidal wave forms are seen in the wave flume for $f < 0.65Hz$ and $f > 1.15Hz$, which disagrees with the linear wave theory for the values of frequencies considered. Both mathematical models, however, have been implemented with linear waves as exciting force, thus explaining the differences between the mathematical simulations and the experimental tests. When $0.65 < f < 1.15$ the agreement between the numerical models and the experimental results improves due to the validity of the linear wave assumption within the experimental wave flume.

By implementing the wave force in the mathematical models to include non-linear wave terms, it is possible to improve the agreement between models and experimental tests. Figure 6.28 shows the comparison between the mathematical model simulations and the RAO tests results for the OWCP30. It can be seen that the implementation of the non-linear wave effects in the wave, implemented at the lower frequency side of the graph, shows a decrease in the RAO resembling the one obtained from the experimental tests. The simulations provide an indication of the maximum RAO that can be obtained for a proposed configuration of the OWCP, however their accuracies need to be improved in order for the model to be used as an evaluation tool of the efficiency of the OWCP.

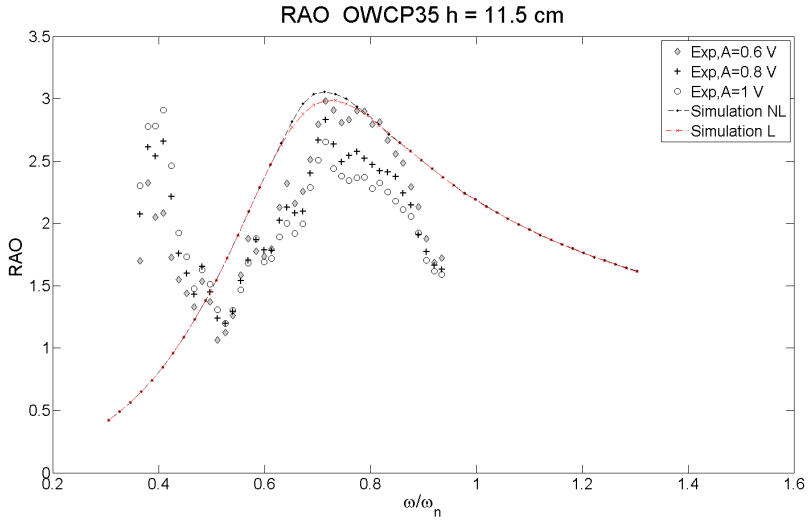

Figure 6.27: Comaprison of RAO Tests with mathematical simulation for the OWCP35 model. The dashed lines present the results obatined from the mathematical simulations, with the red line showing results obained from the linear model (L) and the black line showing non-linear model results (NL)

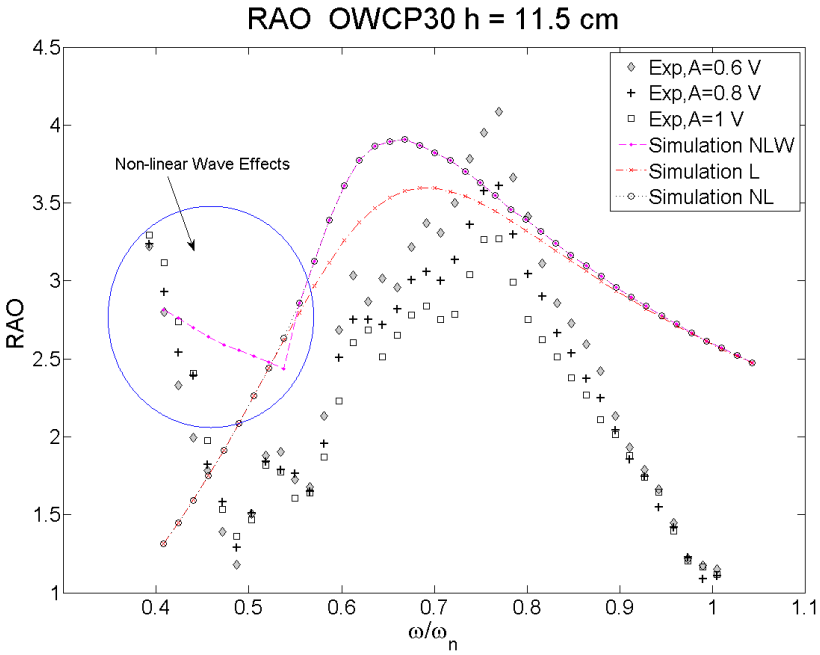

Figure 6.28: Comparison of RAO tests with mathematical simulation for the OWCP35 model. The dashed lines present the results obtained from the mathematical simulations, with the red line showing results obained from the linear model (L) and the black line showing non-linear model results (NL). The pink line (NLW) shows the simulations including the non-linear wave effects.

6.5.2 Water removal and efficiency prediction

The non-linear numerical model presented in section 4.4 was developed in order to estimate the performances of the OWCP device in terms of water removal and effinciency of power conversion. By comparing the results obtained from the experimental testing of the different OWCP configurations, it is possible to validate the non-linear model and to employ it for optimization purposes and real-scale performance predictions.

In Figure 6.29 results obtained from the experimental testing of the OWCP25 are compared with non-linear simulations for the same conditions: $h = 0.125$m, $h_r = 0.045m$ and $H = 0.02m$. Figure 6.30 and Figure 6.31 show the comparison of experimental results with numerical simulations for the OWCP35 device when $h = 0.125m$ and h_r respectively of 0.05 and $0.06m$. From Figures 6.29, 6.30 and 6.31, one can see that the mathematical models describe the response of the device in good agreement with the experimental results, providing indication of the value of ω/ω_n for which water delivery is maximised.

Whilst showing good agreements in terms of mass delivered and ω/ω_n, the bandwidth response obtained from the mathematical simulations is broader compared to the experimental results. A steep decrease in the amount of mass delivered is observed in the experimental results with no water delivered in the device for $\omega/\omega_n > 0.8$; contrasting with numerical simulations results. These discrepancies are similar to those obtained when validating the numerical model in terms of RAO, and they can be attributed to the non-linear effects taking place within the wave flume for higher frequency waves. Furthermore the bandwidth response obtained from the numerical simulations shows a single peak of delivery, whilst experimental results show a drop in water delivered for $\omega/\omega_n = 0.68$ and a secondary peak for $\omega/\omega_n = 0.72$. The presence of a secondary peak, previously highlighted in section 6.4.2, is related to experimental interferences and it is not accounted for in the mathematical description of the OWCP.

Comparison between mathematical simulations and experimental results can also be expressed in terms of efficiency of power converted. Figure 6.32 and Figure 6.33 present the efficiency curves obtained for the OWCP30 device with $h_r = 0.05\,m$ and for the OWCP25 device with $h_r = 0.07\,m$. It can be seen that in both cases the mathematical simulation provide a good indication of the maximum efficiency that can be achieved by the different configurations. The simulations show good accuracies with the experimental results until the maximum value of efficiency η is achieved, at the point experimental results show a steep decrease of the efficiency curves to values of $\eta = 0$ compared to a relatively smooth decrease in the mathematical

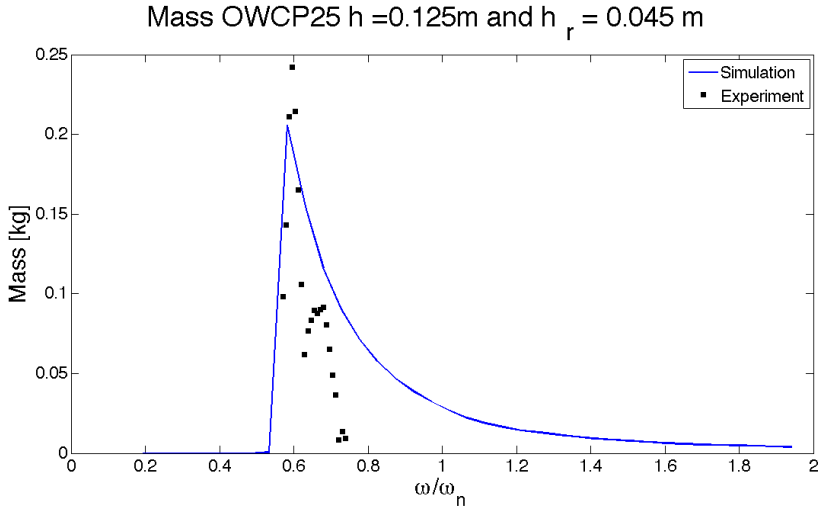

Figure 6.29: Comaprison of water remoaval tests with mathematical simulation for the OWCP25 model. The blue line presents the results obtained from the non-linear mathematical simulations.

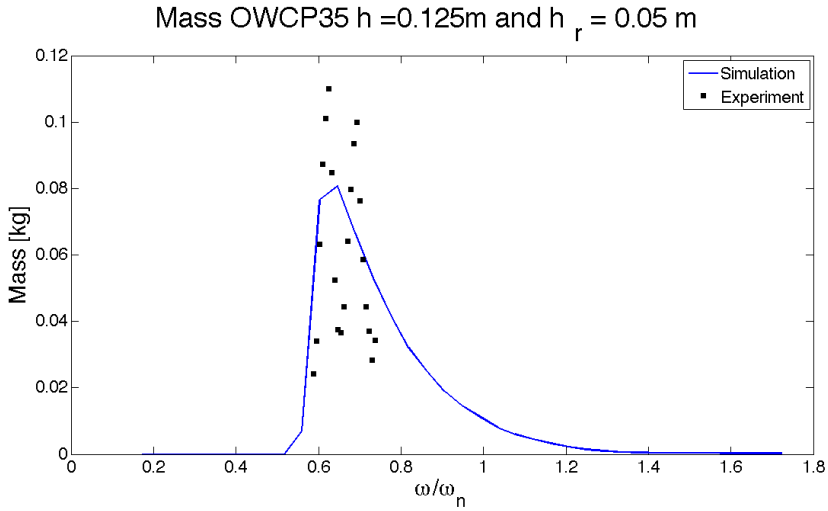

Figure 6.30: Comaprison of water remoaval tests with mathematical simulation for the OWCP35 model. The blue line presents the results obtained from the non-linear mathematical simulations.

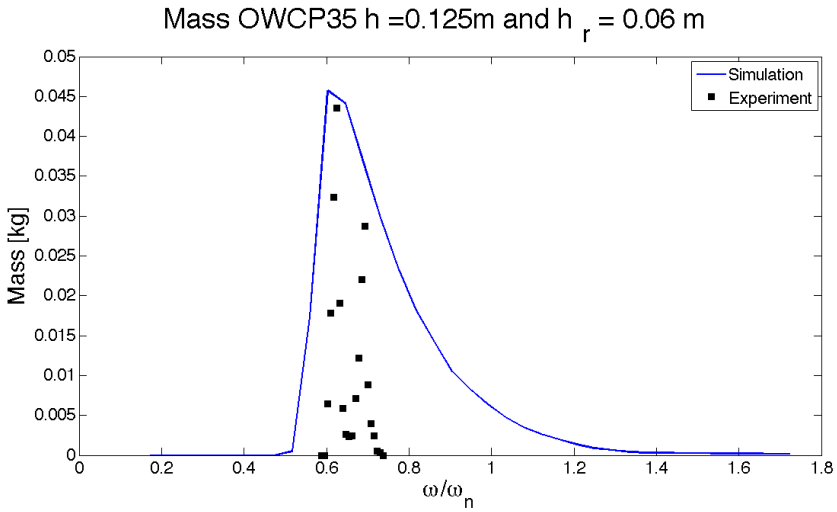

Figure 6.31: Comaprison of water remoaval tests with mathematical simulation for the OWCP35 model. The blue line presents the results obtained from the non-linear mathematical simulations.

simulations.

6.6 Effects of h_r on the Performances of the OWCP

In section 4.4 experimental results on the performances of the OWCP models were presented. It was shown that the values of η_{max} varies between 8 and 12% according to the configuration investigated. The experimental results, however, do not allow to evaluate the ideal configuration that would maximise the delivery of water or the efficiency in conversion of the incoming wave power. For this purpose, the numerical models validated in section 6.5 could be employed to determine the ideal configuration that enhances the performances of the device. For this purpose a parametric study aimed at identifying the role of h_r on η and water delivery was undertaken.

6.6.1 Effects of h_r on water delivery

One of the applications the OWCP has been designed for is the delivery of water. Experimental results showed that h_r affects the mass of water overtopping in the reservoir and could reduce the performances of the device. Numerical simulations based on the results obtained from numerical experiments were run, with h_r varying between 0.035 and 0.08 m, corresponding to real scale values of 1.2 and 3.2 m respectively. Figure 6.34 and Figure 6.35 show the response curve expressed in terms of mass of water delivered from the OWCP25 and OWCP30 device. The simulation was run for regular waves with $H = 0.02\,m$. In both cases, it can be seen that the

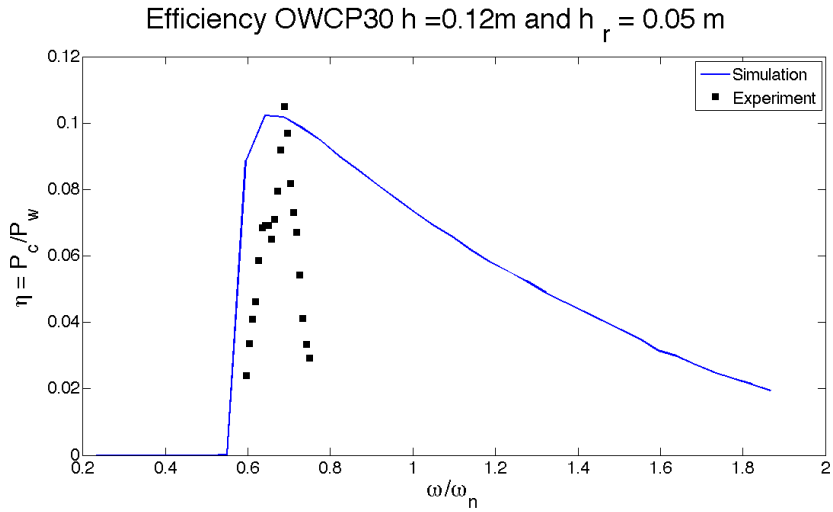

Figure 6.32: Comaprison of efficiency in conversion with mathematical simulation for the OWCP30 model. The blue line presents the results obtained from the non-linear mathematical simulations.

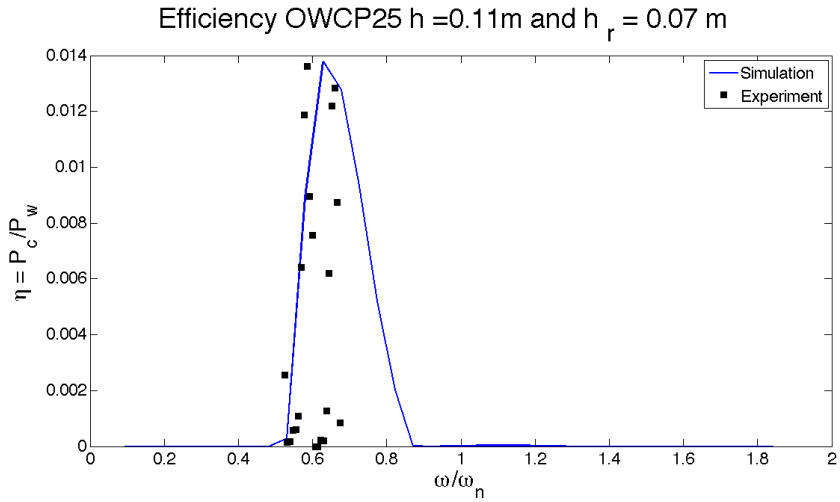

Figure 6.33: Comaprison of efficiency in conversion with mathematical simulation for the OWCP25 model. The blue line presents the results obtained from the non-linear mathematical simulations.

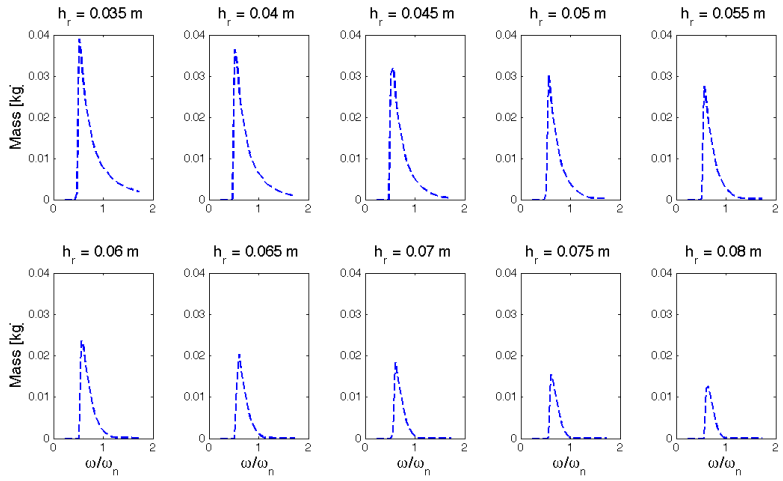

Figure 6.34: Water delivery for the OWCP25 for $0.035 < h_r < 0.08\,m$ with $h = 0.125\,m$. It can be seen the the amount of water delivered decreases as h_r increases

mass of water delivered decreases as h_r increases. The effects of h_r on the total mass delivered by the OWCP25, OWCP30 and OWCP35 devices is presented in Figure6.36.

From Figure6.36 it can be seen that the rate of decrease in mass delivered is also affected by the configuration of the device with steeper decrease rate for higher α.

6.6.2 Effects of h_r on OWCP efficiency

In section 6.6.1 it was shown that the amount of water delivered from the OWCP decreased significantly at the increase of h_r. h_r may have a different effect on the efficiency of the OWCP as seen in equation 6.10. Numerical simulations were run with $0.035 < h_r < 0.08\,m$ for the different OWCP configurations. Figure 6.37and Figure 6.38 present the efficiency curves for the OWCP25 and the OWCP35 model respectively with $h = 0.11\,m$ and $H = 0.02\,m$. In both cases it can be noticed that there is a value of h_r which maximises the efficiency in power conversion of the OWCP.

Figure 6.39 shows the effects of h_r on η_{max} for the different OWCP configurations. Contrary to the behaviour of the mass delivered, it can be seen that increasing h_r does not generate a decrease of η. For each OWCP configuration an ideal value of h_r that maximise the efficiency in conversion of the OWCP can be found. For the scenarios presented maximum efficiency is obtained when $h_r = 0.065$ for the OWCP25, $h_r = 0.065$ for the OWCP30 and $h_r = 0.040$ for the OWCP35 devices.

h_r has different effect on the performances of the OWCP depending on the application the

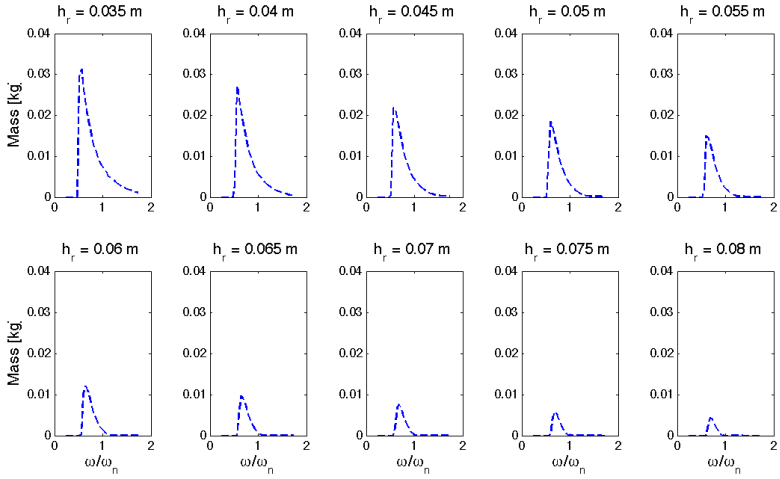

Figure 6.35: Water delivery for the OWCP25 for $0.035 < h_r < 0.08\,m$ with $h = 0.125\,m$. It can be seen the the amount of water delivered decreases as h_r increases

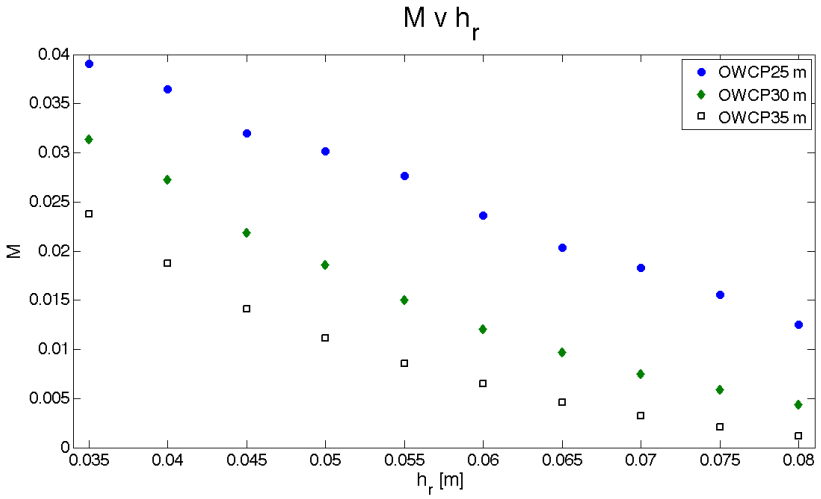

Figure 6.36: Water delivery vs h_r for different OWCP configurations.

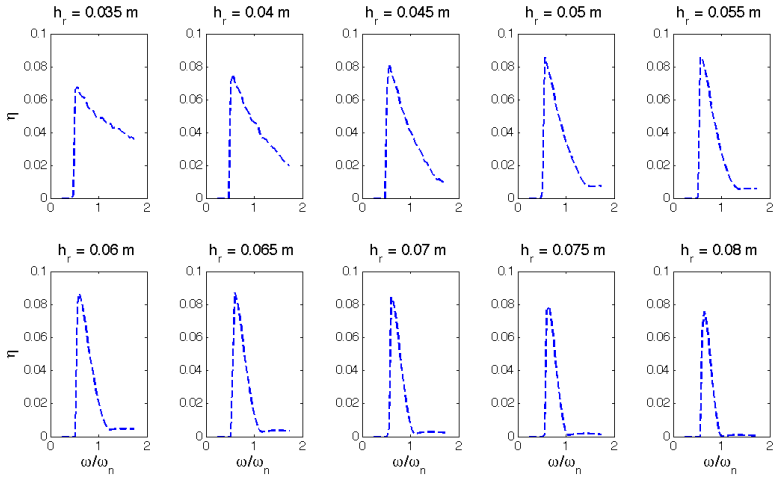

Figure 6.37: Efficiency of the OWCP25 for $0.035 < h_r < 0.08\,m$ with $h = 0.11\,m$. It can be seen that the efficiency curves present a broader response and a higher η_{max} when $h_r = 0.65$.

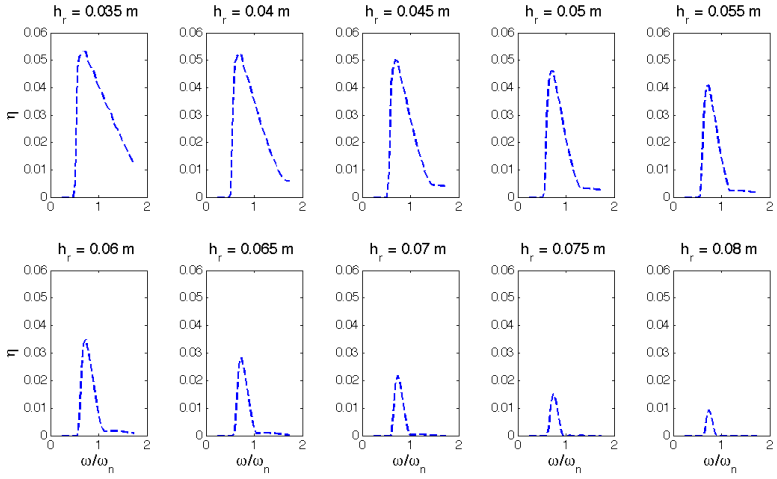

Figure 6.38: Efficiency of the OWCP35 for $0.035 < h_r < 0.08\,m$ with $h = 0.11\,m$. It can be seen that the efficiency curves present a broader response and a higher η_{max} when $h_r = 0.45$. The

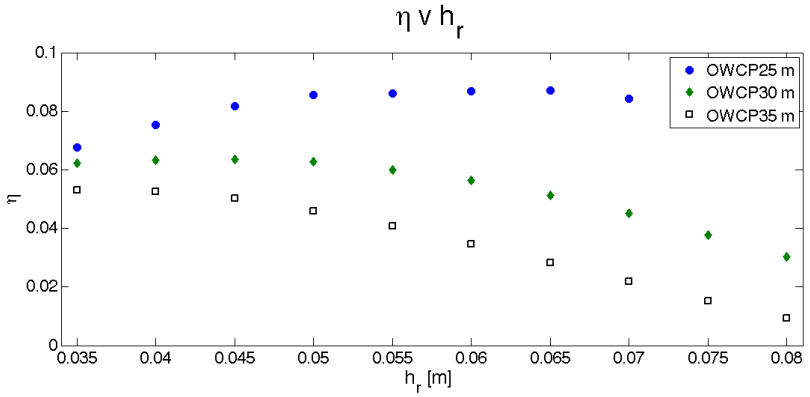

Figure 6.39: Efficiecy vs h_r for different OWCP configurations.

device is employed for. If the OWCP is to be employed for water delivery purposes a low value of h_r should be employed. This configuration will allow for water delivery to be maximised. On the other, if the main aim is to maximise energy conversion of the OWCP a higher value of h_r could be set.

6.7 Discussion

So far, research on the use of an OWC as a device implemented for overtopping has been limited and falls short in terms efficiencies and performances. Knott and Flower (1979) proposed an overtopping OWC and carried out mathematical simulations of a vertical OWC for water removal, however no physical tests were undertaken to determine the validity of their hypothesis.

This chapter showed results obtained from the experimental testing of the proposed OWCP in order to evaluate the response and performances of the device. Investigations were carried out by using different configurations of the OWCP and different experimental setups. The experimental investigation were carried out in order to:

- Determine the hydrodynamic coefficients of radiation damping and added mass for validation of the numerical models
- Evaluate the response of the OWCP when no PTO was installed
- Assess the performances of the OWCP when water was removed from the device.

6.7.1 Hydrodynamic coefficients

The effects of the water depth on the damping, affecting the motions of the water column within the output duct, were determined. The damping ratio increases with the the increase in water depth. The water depth also affects the inertia mass of the water column, shifting to lower values the natural frequency of oscillation of the device ω_n. The determination of the damping ratio and added mass allowed the implementation of the mathematical models describing the response of the OWCP.

6.7.2 Response of the OWCP

The response of the OWCP to incident waves was evaluated when the PTO was not active. In this case the OWCP behaves like a standard OWC device with no turbine installed. The RAO

tests showed that for conditions close to resonance, the response of the device is affected by non-linearities. It was shown that the RAO varied with the variation of the incident wave height H, as showed by Lopes et al. (2009) for tests of a generic type of OWCP. The presence of non-linearities attributed to vortex formation in front of the input pipe of the OWC was therefore included in the mathematical models implemented for the description of the OWCP.

The values of RAO obtained, expressed in terms of vertical displacement of the water column, are comparable with those obtained by Evans (1978), who showed magnification of up to 5 times the incoming wave amplitude. Response amplitude tests showed that a value of the amplification of the wave amplitude in the output duct of the OWCP model up to 5.9 can be achieved. The maximum RAO was achieved at frequencies 20-30% below the natural frequency of the model tests, while a shift of 10% between ω and ω_n was recorded in the mathematical simulations presented by Knott and Flower (1979). This is consistent with the higher values of damping ratio ξ_r obtained during the force oscillation tests compared to the one employed by Knott and Flower (1979).

The RAO tests provided an insight on the behaviour of the device under the influence of monochromatic waves. It was noticed that for low wave frequencies, cnoidal waves were generated within the 2D Narrow Flume affecting the response of the OWCP. The cnoidal waves forced the OWCP to respond to a nearly pulsating impulse, thus allowing for a double motion of the water column during a wave period.

From the RAO tests it was possible to notice how the inclination α affects the performances of the devices and to assess the vertical displacement for the device tested. The RAO tests provided useful information with regards to which models could be employed for the delivery of water above a fixed freeboard h_r. Of the 5 models tested, the OWCP25, OWCP30 and OWCP35 were employed in tests to assess the removal of water and the performances of the device.

6.7.3 Efficiency of the OWCP

The determination of the efficiency of removal of the OWCP was carried with the device installed within a rubble-mound structure to replicate the proposed installation of the OWCP on an existing breakwater. Efficiencies up to 14% in the removal of water were recorded for the OWCP25 and OWCP30 with experimental freeboard heights of 0.05 and 0.06 m. This corresponds to the generation of a hydraulic head of 2-2.5 m of height above at full scale for wave heights, as indicated in the objectives of the research. Higher hydraulic heads would affect the

overall performance of the device.

In particular it was found that the removal efficiency was subject to the interaction between different parameters: h, h_r, K_r, H and on the incoming wave frequency f. Non-linearities affected the removal of water from the OWCP confirming the initial evaluation of Knott and Flower (1979) which suggested a complex mechanism of removal of water from overtopping OWC devices. Moreover the work of Knott and Flower (1979) indicated that the efficiency of removal was not dependent on the wave height and on the removal height.

However, experimental results showed that for $h_r > 0.06\,m$ higher efficiencies are obtained for higher values of H. The effect of H on η was minimal for the cases in which $h_r = 0.05\,m$. The greater mass of water conveyed by the OWCP as a result of higher H was minimised by the higher energetic content of the waves. However, in order to reach higher h_r more energetic waves are needed. Changes in the removal height h_r caused changes in the frequency for which maximum delivery was achieved, as described by Knott and Flower (1979). It is therefore possible to use h_r as a parameter to control resonance and improve the performances of the OWCP for changing wave conditions.

A de-tuning effect and a shift of the maximum η towards lower wave frequencies were noticed for reduced water depth scenarios. A similar effect was reported in the functioning of the SIBEO device by Czitrom et al.,(2000).

Through the analysis of the reflection coefficient, it was shown that delivery is affected from high reflection rates due to the presence of the breakwater. Higher efficiencies are obtained when wave reflection of the structure is limited to $K_r < 0.5$, showing that it is possible to integrate the OWCP as part of an existing coastal structure, without affecting the protective characteristics of the structure.

The work of Knott and Flower (1979) considered a vertical OWC and did not consider the presence of a reservoir, allowing them to predict a wide range of h_r for which high efficiencies can be achieved. The constriction of experimental testings showed that only a few ranges of h_r and d_s are possible given a fixed structure where the device is to be installed.

6.7.4 Mathematical models

In order to develop the mathematical models for this research, it was assumed that the behaviour of the OWCP could be represented with the mechanical comparison to a single-mass harmonic oscillator. With this hypothesis, two models were developed: one assuming that only linear forces

acted on the OWCP, and the other concerning a non-linear model where the non-linear forces were accounted for. Both models used monochromatic sinusoidal waves to force the movement of the OWCP representing the wave generated in the narrow wave flume.

The mathematical models can be used as a tool to assess the removal of water from the OWCP, to determine its efficiency and to identify the values of h_r that optimise the OWCP configuration. Mathematical simulations showed that low values of h_r would assure higher water delivery for each OWCP configuration; whilst a low h_r would not insure that the OWCP is optimised in terms of efficiency. According to the application the OWCP is employed a different value of h_r can be used and its performances maximised.

Discrepancies between the models and experimental results were noticed in terms of response bandwidth, and of Ω for which the maximum RAO, delivery and η are obtained. It was shown, in the case of the RAO comparison, that by including the non-linear terms in the exciting wave it is possible to increase the agreement between the model and experimental results for the lower end of the frequency spectra. The mathematical models could be further improved in order to increase the accuracy of the simulation. This can be achieved through a better estimation of the hydrodynamic coefficients and by accounting for the role of the beach profile on the performances of the device. The mathematical models developed in this work provide a good estimate of the performances of the OWCP in relation to the experiments carried out in the wave flume, thus proving the theoretical description of the OWCP presented in chapter 4.

6.7.5 Summary of findings

The results obtained from the experimental analysis of the various OWCP configurations allow to draw conclusions with regards to the performances of the device both in terms of RAO and efficiency and to contextualise them with existing research.

In particular RAO tests showed that amplification up to 5.9 times the initial wave amplitude were achieved for the OWCP25 and OWCP30 devices, in agreement with the work of Evans (1978). The RAO was maximised for lower values of the incoming wave height H; thus validating the description of the OWCP as a single-mass oscillator presented in Chapter 4. Non-linearities affected the values of RAO for higher wave heights when the device was operating in close to resonance conditions, in agreement with the work of Lopes et al. (2009).

In contrast with the work of Knott and Flower (1979) higher values of the RAO were achieved when the incoming wave frequencies were 20-30% lower compared to the natural frequency of

oscillation of the tested devices.

The response of the device is affected by both water depth and submersion depth, with higher RAO obtained for deeper water conditions and lower submersion. The ideal conditions for 1/40 scale tests were obtained with $h = 0.13\,m$ and $d_s = 0.065\,m$. However, higher RAOs do not correspond directly to higher delivery heights. It was therefore chosen to investigate the delivery of the OWCP25, OWCP30 and OWCP35.

Removal tests were carried out with the OWCP models installed on a low-reflective structure replicating a rubble mound breakwater. Tests showed a predominance of the OWCP25 and OWCP30 model with up to 14% of incident wave energy being converted into useful potential energy.

Water removal was found to be affected by the interaction of different experimental parameters h, d_s, h_r, H, K_r and f. In addiction, non-linearities were found to play a role on the efficiency of the OWCP. A complex interaction mechanisms between the different parameters controls the delivery of water of the OWCP, in agreement with the hypothesis presented by Knott and Flower (1979). This mechanism allows regulating one of more parameters in order to increase the performances of the device either in terms of efficiency or in terms of delivery rate.

In contrast with the work of Knott and Flower (1979) the removal of water was found to be dependent on the incoming wave height, especially for higher values of h_r. The freeboard height h_r plays a fundamental role in the performances of the OWCP by affecting the frequencies at which removal is obtained. This was found to be in agreement with the assumptions that the force associated with the PTO affects the response of the device, as presented in Chapter 4. h_r can therefore be used as a resonance control parameter for the OWCP, thus adjusting the generated response to varying wave conditions. De-tuning of the frequencies for which maximum efficiencies are obtained was observed for reduced water depth scenarios. As a result the performances of the OWCP were sensibly reduced for low water depth, in agreement with the results from testing of SIBEO (Czitrom, Godoy, Prado, Perez and Peralta-Fabi, 2000).

Delivery and performances of the OWCP are affected by freeboard height and submersion depth, with the device able to operate effectively in a limited range of h_r and d_s. h_r as to be minimised if the delivery of water is to main application the OWCP is empolyed for. An ideal value of h_r

should be determined in order for η to be maximised.

The efficiency curves obtained from the experimental testing of the OWCP indicates that the device obtains low conversion efficiency for a very narrow bandwidth. Full scale assessment of the performances of the device are needed to evaluate its possible applications, and to compare it with other wave energy technology.

Chapter 7

Evaluation of the Perfomances of Multiple OWCPs Installed in an Array Configuration

In Chapter 6 the performances of OWCP devices working autonomously were discussed. It was shown that different configurations of the OWCP achieved peak performances at different wave frequencies. The efficiency curves of the OWCP25 and OWCP30 model showed that maximum efficiencyη were achieved for $f = 0.73\,Hz$ and $f = 0.88Hz$ respectively.

In order to maximise the performances of each configuration and to increase the frequency response spectrum, the installation of OWCPs in arrays is hereby investigated.

A proposed installation of three OWCPs working in a "pan-flute" type of array is assessed through a series of experimental tests in the 3D wave basin. Such configuration is aimed to increase delivery rate and at to understand potential inter-device effect that could affect performances.

7.1 Introduction

Array installations of multiple OWCPs are described in this chapter, with the aim to assess and maximise the overall power output, whilst providing an insight of the interaction of multiple OWCPs.

The installation of multiple WECS in arrays and wave farms has aroused the interest in the scientific community, being regarded as a "Key Research Topic" at the 2010 International

Conference on Ocean Energy in Bilbao, Spain (ICOE, 2010) .

The general expectation, as highlighted by Mei (2009) and Babarit (2010), is that by installing multiple WECs in an array configuration, it is possible to generate a positive interaction between devices and generate a higher power output compared to independently working devices. However, the interference between devices and waves could have a negative effect reducing the overall power output.

It is therefore necessary to assess the interaction between single components of the arrays and the waves to insure that the array installation provides a constructive effect on the energy production (Babarit, 2010).

In order to assess the overall output of the array, Babarit (2010) defined the quality factor q as the ratio between the overall power output of the array, P_a, produced by N devices installed in an array to the power generated by N devices working autonomously (P_s) .

$$q = \frac{P_a}{N \times P_s} \tag{7.1}$$

When $q > 1$, positive effects are obtained by the array configuration. One of the determining factors in the evaluation of the q-factor is the separation distance, s_d, between two devices. The practical role of s_d is to influence the interaction between the radiated waves generated by the oscillation of each single device.

The determination of q, thus far, has been predominantly conducted using numerical models; with the experimental testing being limited due to scaling and sizing issues and the lack of appropriate facilities.

The mathematical approach presented by Falcao (2002) and McIver (2002) was based on the assumptions of infinitely long arrays and of linear wave conditions. Whilst providing a good evaluation of the array performances, where higher efficiencies can be obtained (Falcao, 2002), the formulation is based on idealised conditions with limited applicability. However, from the study carried out by Falcao (2002) , it emerged that for OWCs with linear PTO and no resonance control implemented the interferences between the devices are important, with the array efficiency decreasing with the increase of s_d.

Furthermore, the majority of the research is focused around the interaction of point-absorbing WECs and their dynamics. Vicente et al. (2009) assessed the interactions of point-absorbers with inter-body mooring connections, with the use of a BEM solver for a triangular shaped array;

Weller et al. (2009) and Alexandre et al. (2010) studied the interactions and the modification of the wave fields due to linear arrays of heaving wave energy converters. In both cases, experimental testing at the University of Manchester wave basin were used to validate numerical simulations. However the studies did not present any investigation on how to maximise the power output nor suggestions on the role of the separation distance between the devices.

With regards to the installation of OWC devices in arrays, Thiruvenkatasamy and Neelamani (1997) carried experimental testing of caisson breakwaters with integrated OWC systems for the generation of electricity. The work was carried in a 2D wave flume and the device built within a channelling harbour to convey more powerful waves. The performances of the array were simulated by assuming similar behaviour between the OWC, thus neglecting any interferences that can affect the single response of the devices. Thiruvenkatasamy et al. (2005) later showed that the capture width of OWCs arrays within caisson breakwater can be magnified if the diffraction and scattering of the waves is reduced, hence if the separation distance is kept to a minimum. Torre-Enciso et al. (2009) presented the development of the Mutriku wave power plant, comprising of 16 OWC chambers for a total nominal power of 300 kWh. Each chamber has a capture width of 6 m, and the separation distance between devices is of 2m. No particular information was given with regards of the layout chosen, and whether the chosen geometrical design was tested to maximise the power output. However resonance control at the Mutriku Power Plant is designed to operate on 8 turbines at a time, requiring the chambers to be subjected to similar conditions.

From the literature review it appears clearly that the separation distance represents a significant parameter in the determination of the performances of arrays of multiple WECs; however no physical investigations are reported in assessing the effects of s_d.

The objective of this chapter is to quantify the performances of OWCPs closely spaced in an array configuration, to assess the role of s_d on the response of each device in the array, and to determine the overall and single device efficiency of the array configuration.

7.2 Wave Basin Setup

The determination of the best performance layout of an array of 3 OWCP was carried out in the 3D wave basin presented in Chapter 5. The array was installed in the centre of the wave

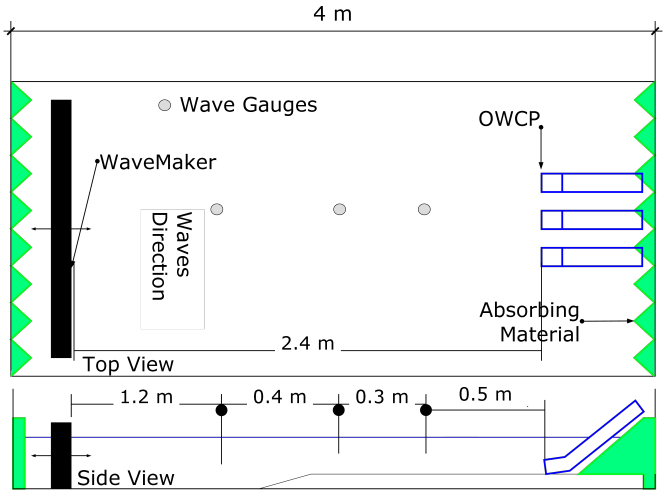

Figure 7.1: Setup of 3D wave basin for the determination of best forming array of 3 OWCPs

Array Name	Model 1 side	Model 2 central	Model 3 side	Sepration distance s_d	Type of investigation
Square 1*	OWCPS1	OWCPS1	OWCPS1	0, 15, 30 mm	RAO, Capture
Square 2*	OWCPS1	OWCPS2	N.A	0 m	RAO, Capture
Square 3*	N.A	OWCPS3	N.A	0 m	RAO, Capture
20-25-30	OWCP20	OWCP25	OWCP30	0, 15, 30 mm	RAO
20-25-30 W +	OWCP20	OWCP25	OWCP30	0, 30, 60 mm	RAO
25-30-35	OWCP25	OWCP30	OWCP35	0, 15, 30 mm	RAO
25-30-35^r	OWCP25	OWCP30	OWCP35	10, 45 mm	REMOVAL

Table 7.1: Configurations of the arrays tested. The superscript *indicates tests carried with similarly tuned device and with the the overall width of the array kept costant by employing OWCPS devices. The superscript + indicates tests where a reflective front wall was installed in front of the array. The superscript ^{r} indicates the array configuration for which the efficiency of the devices and the removal of water was assessed.

basin, within a 1:2.5 gravel beach replicating a breakwater (Figure 7.1). The water depth in the basin was varied between 0.1 to 0.135 m. Waves with a period varying between 0.8 s to 2 s were generated by the linear wave paddle with wave heights varying between 0.01 and 0.05 m; corresponding to real case waves between 0.4 and 2 m wave height with periods between 5 and 13 s.

7.2.1 Models employed and configurations

With regards to the models of the OWCP presented in Chapter 5, different configurations of the array were assessed, as presented in Table 7.1.

7.2.1.1 RAO tests for the arrays

With reference to Table 7.1, RAO tests of the array are carried out in order to asses the role of s_d on the response of each device. These tests are carried out for both differently tuned devices (configurations 20-25-30 and 25-30-35) and for similarly tuned ones (configuration Square1).

7.2.1.2 Capture width tests for the arrays

Capture width tests present a different approach to the analysis of the response of the OWCP. In this case, the overall capture width of the array is kept constant at 60 mm, and similarly tuned devices are employed. Different OWCPS models are employed to assess the role of different sized caissons for OWCs installed together. The configurations employed for these tests, presented in Table 7.1, are Square 1, Square 2 and Square 3.

7.2.1.3 Removal and efficiency tests for arrays

As indicated in Table 7.1 the array configuration 25-30-35^r is assessed when water is removed from each OWCP component of the array. This allows the comparison with the removal and efficiency tests carried out for the OWCP25, OWCP30 and OWCP35, as presented in Chapter 6.

7.3 RAO Tests: Results

The response of each device installed in the different array configuration is determined for the varied s_d and h. The RAO is determined by considering the displacement of the water column within each OWCP when no PTO is applied.

The aim of these tests is to asses the possibility of implementing a pan-flute type of array of the OWCP with differently tuned devices in order to increase the overall frequency response and to maximise the RAO.

Figure 7.2 presents the frequency response of the array configuration 20-25-30 with $s_d = 0$, for driving wave frequencies between 0.6 to 1.2 Hz.

It can be seen that the array arrangements allow an overall RAO of the array with peaks above 4 for a wider range of frequencies, with each device achieving its maximum at different frequencies.

This validates the chosen arrangement, since increased RAO and different peak frequency for each component of the array means that delivery of water can be obtained regardless the

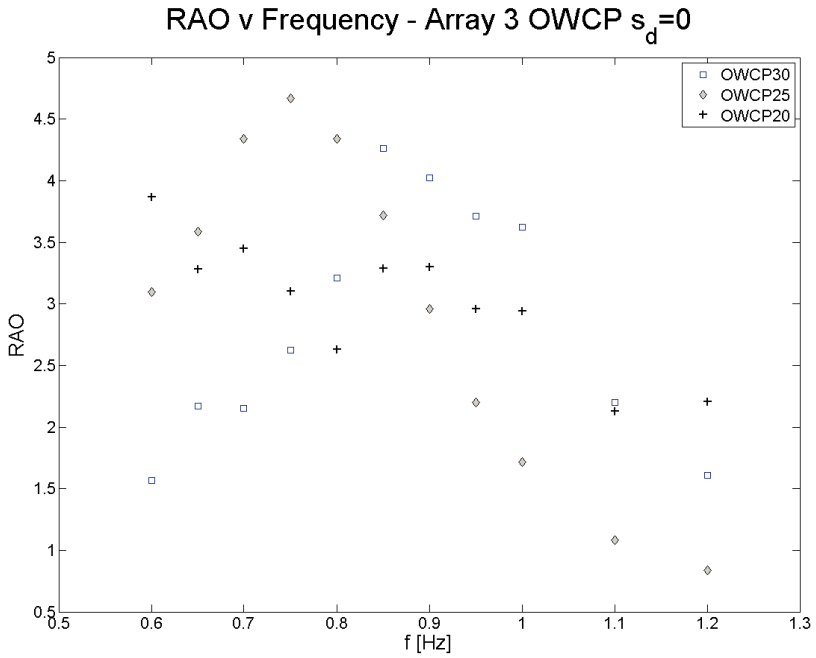

Figure 7.2: Frequency Response for the array configuration 20-25-30 of 3 differently tuned OWCPs. OWCP25 was located at the centre of the array. Separating distance between the devices was of 0 mm.

incoming waves conditions.

The effects of s_d on the RAO of the single components of the array are presented in Figure 7.3 and Figure 7.4. Both figures refer to the array configuration 20-25-30 with the OWCP25 model installed at the centre of the array.

In Figure 7.3 the RAO of the OWCP30 model is assessed to show the influences of s_d on the response of the device. It can be seen that the response of the device when installed within the array is reduced compared to the model working autonomously. Moreover it is possible to verify that the maximum response of the OWCP30 working within the array is achieved when $s_d = 0$. The array installation shifts the value of f for which the maximum RAO is obtained, towards higher values.

Similar behaviour is shown by the central device OWCP25 for the same array configuration. It can be seen from Figure 7.4 that the maximum RAO is obtained once again for $s_d = 0\,mm$. It is also evident that by increasing s_d a contemporaneous decrease in the maximum value of RAO is obtained. As for the OWCP30 device, it was found that the response of the OWCP25 installed within the array is lower compared to the device working autonomously. Furthermore it can be seen that the value of f for which the maximum RAO is obtained is about 15% higher

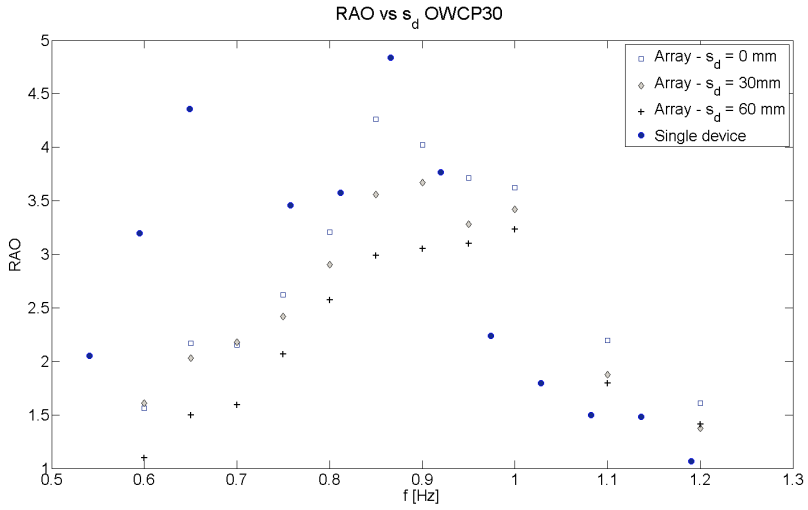

Figure 7.3: Changes in the RAO for the OWCP30 configuration based on the separating distance among the devices. The device was located on the side of the array. RAO is reduced with the increase of the separating distance.

in the array compared to single device case.

Changes in the RAO of each device are observed when a reflective wall is installed in front of the array. The presence of the reflective walls increased the wave height in front of the array due to a superposition of the reflected wave with the incoming wave. This provides a further increase in the RAO for the central device (OWCP25) and generates smoothing effects on the side devices OWCP20 and OWCP30, as shown in Figure 7.5. The responses of the OWCP20 and OWCP30 in the presence of the wall appeared to be independent of the driving frequency f, and related to the higher wave heights generated by the wave reflection.

In each tested configuration, higher RAOs were experienced for the model located at the centre of the array. This occurred even when 3 similarly tuned devices, OWCPS1, were tested.

Figure 7.6 shows the RAO for the OWCPS1 devices installed in the array configuration Square 1. The central device presents a higher RAO compared to those installed on the side of the array. The maximum RAO obtained is of 2.95 for the central device respect to the maximum of 2.37 achieved in the side models.

The overall RAOs obtained by the similarly tuned devices were lower than those obtained for the devices operating at different tuning frequencies. The downward motion of the water column of each device in the case of differently tuned models is phased differently reducing the effect of the radiation damping. In the case of the Square 1 array, the downward motions are synchronous and higher radiation forces are expected to act on the system.

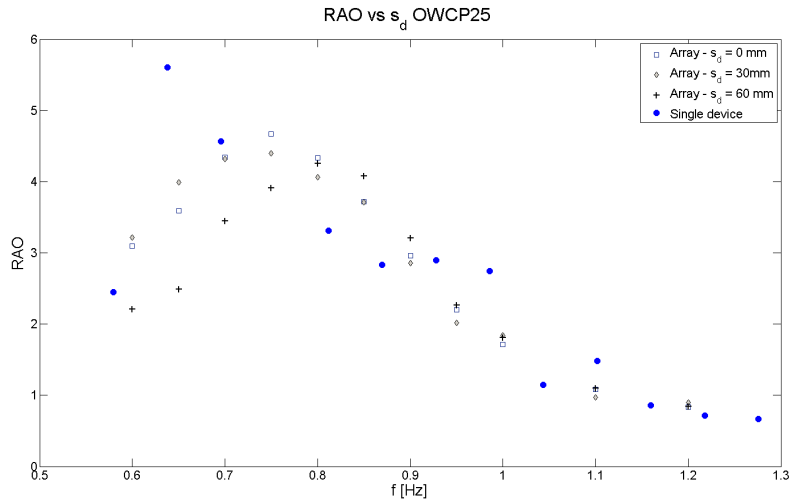

Figure 7.4: Changes in the RAO for the OWCP25 configuration based on the separating distance among the devices. The device was located on the side of the array. RAO is reduced with the increase of the separating distance.

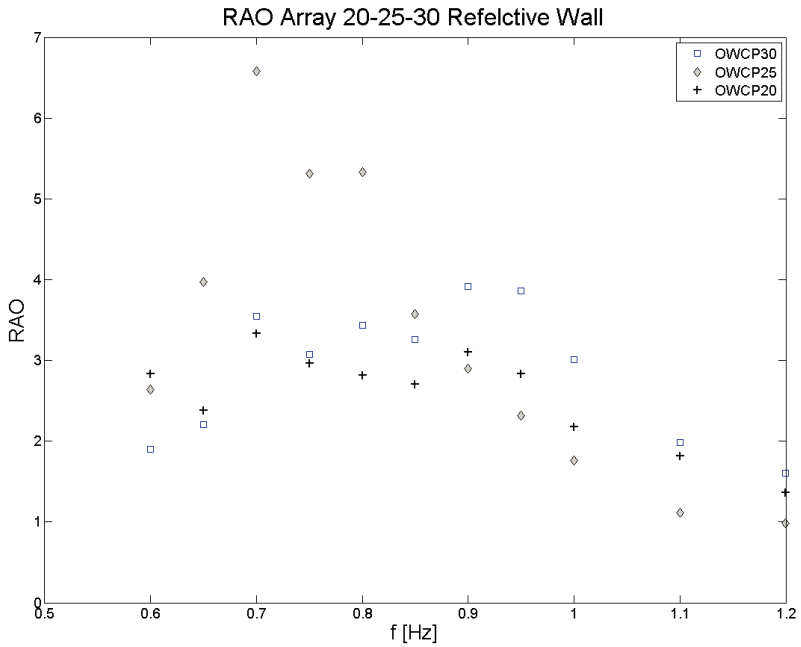

Figure 7.5: Frequency Response for the array 20-25-30 W^+ configuration with a 50 mm reflective wall installed in front of the array. The separation distance between the devices was of 30 mm.

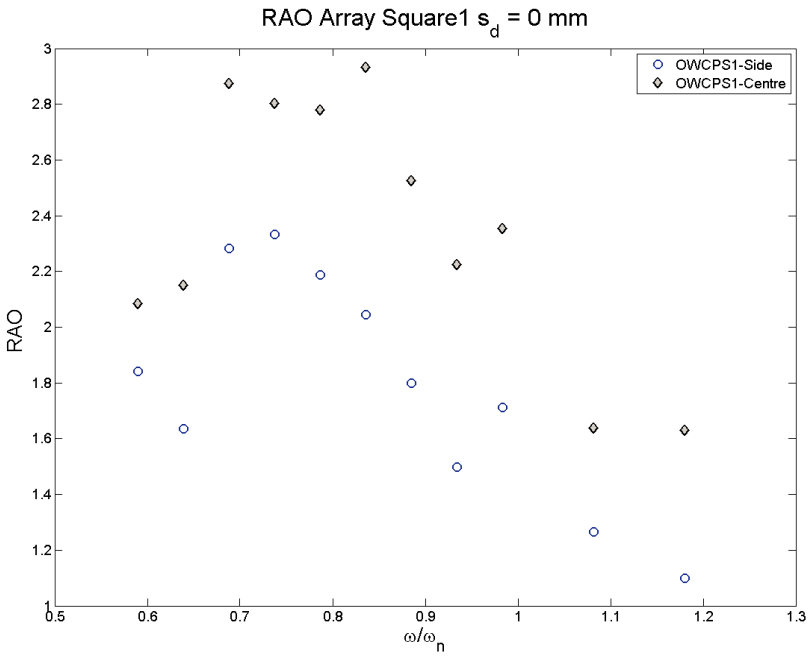

Figure 7.6: Frequency Response for an array of 3 OWCPS1. The comparison is made between the central pipe and the side pipes.

Figure 7.7 and Figure 7.8 present the frequency analysis for the components of the array 20-25-30 and array 25-30-35 configuration when $s_d = 0$. In both cases it can be seen that for the main driving frequency (indicated by the dashed line) the phase of response between the devices is different, suggesting that whilst the wave forces the movement of the devices simultaneously, their response is phased differently.

In Figure 7.9, the frequency analysis and phase response for the Square1 array configuration is shown. The phase of response for the installed devices is identical for the driving frequency.

As suggested by Murphy (1996) the greater is the phase difference between the phase of the OWCP and the phase of the waves, the greater is the response of the device.

7.3.1 Effects of s_d on the RAO

The results obtained from the RAO showed that the response of each component of the array is lower than when each model is working autonomously. However from the tests it resulted that a positive array effect was noticed on the response of the device located at the centre of the configuration. The RAO of each component decreased by increasing s_d. The effects of s_d on the response of each device are presented for the 20-25-30, 25-30-35 and Square1 configuration.

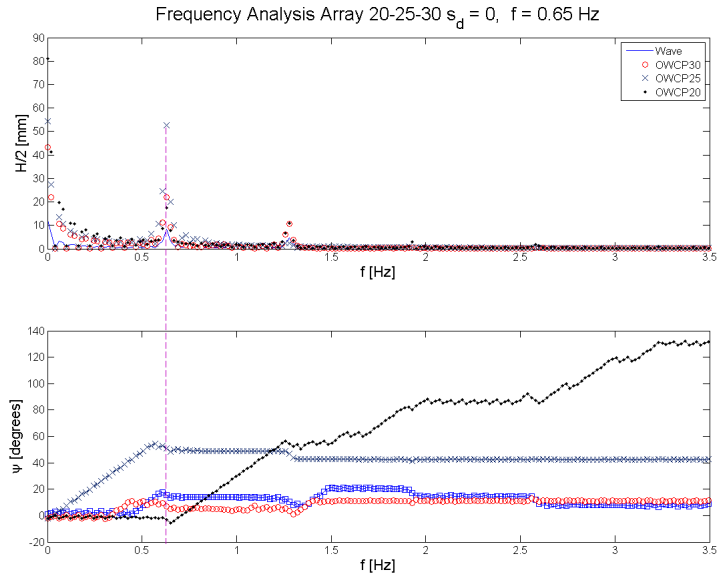

Figure 7.7: Frequency analysis and phase response for the 20-25-30 array configuration, with driving frequency $f = 0.65\,Hz$.

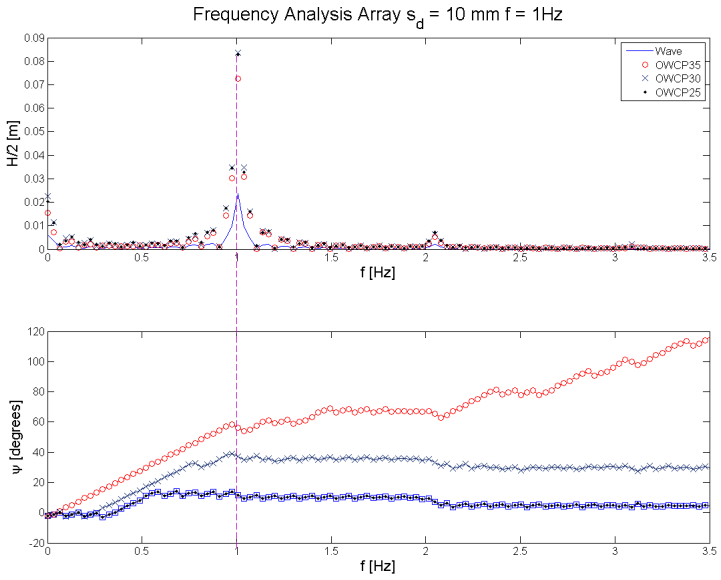

Figure 7.8: Frequency analysis and phase response for the 25-30-35 array configuration, with driving frequency $f = 1.0\,Hz$.

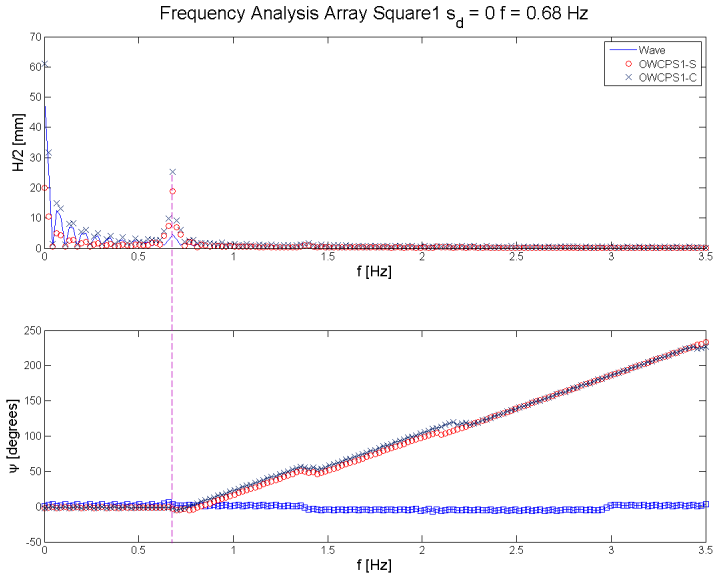

Figure 7.9: Frequency analysis and phase response for the Square1 array configuration, with driving frequency $f = 0.68\,Hz$.

These are expressed in terms of maximum RAO, and assessed through the variation in s_d and in Ω for the different configurations.

Figures 7.10, 7.11, 7.12 show the changes in the RAO for the different separating distances evaluated. The trend shows a decay of the RAO with the increase of s_d, suggesting that better performances of the device can be obtained when the distance is minimised. To assess the role of the separating distance on each device, it is necessary to see how the natural frequency of oscillation is affected by the increased spacing between the devices.

Figures 7.13, 7.14 and 7.15 show how the RAO and the Ω ratio is affected by increased values of s_d. It can be seen that Ω increases with s_d, showing that the devices become independent and autonomous with increased distances.

The influence of the the layout on the device can be seen in Figure 7.16 for the 20-25-30 array configuration. The graph shows the RAO for the central device (OWCP25) compared to the performances of the OWCP30 side device for increased s_d over Ω by varying the wave steepness. It can be seen that higher RAOs are obtained for the central device and for lower s_d.

The differences in response between the central and side device in an array situation is presented in Figure 7.17. The graph shows the response of the devices in the Square1 array configuration for $s_d = 0$ and 30 mm. It can be seen that the response of the two devices is similar (identical tuning frequency), however the central device presents a broader response

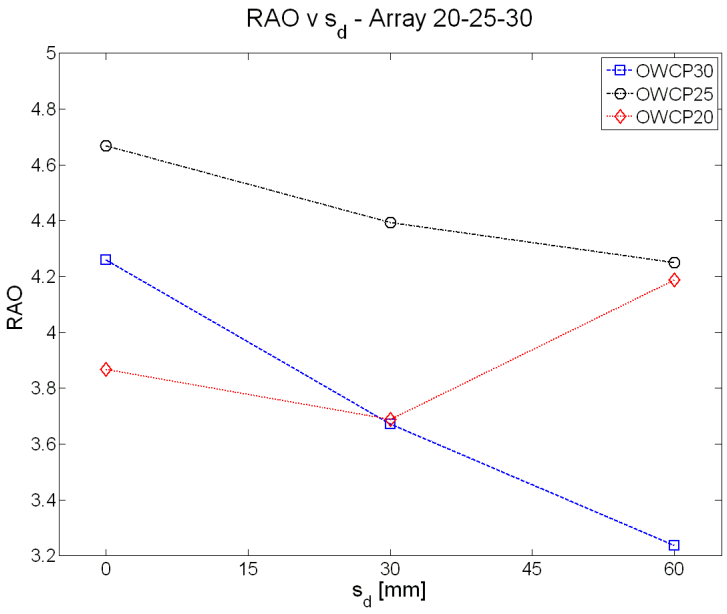

Figure 7.10: Changes in the RAO of each component of the 20-25-30 array configuration versus s_d for water depth $h = 140\,mm$ and $d_s = 100$mm. A steady decrease in the RAO is noted for the OWCP25 and OWCP30 with increased s_d.

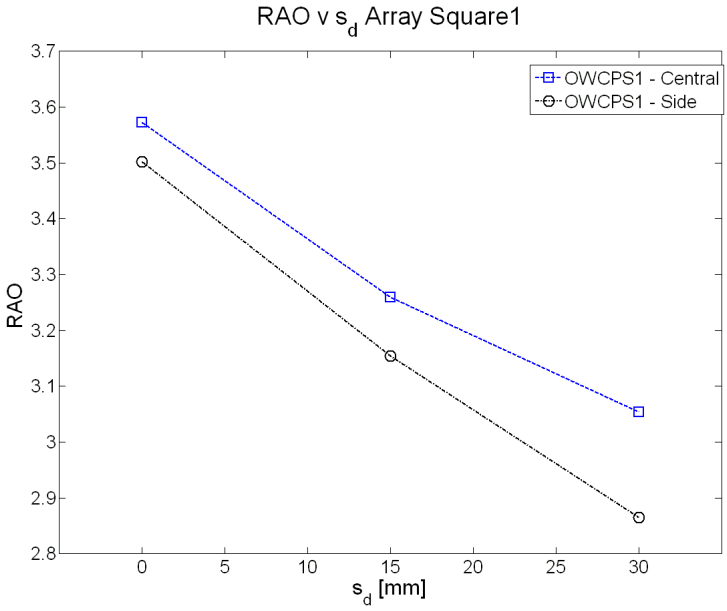

Figure 7.11: Changes in the RAO of each component of the Square1 array configuration versus s_d for water depth $h = 140\,mm$ and $d_s = 100$mm. A steady decrease in the RAO is noted for both the central device (OWCPS1 - central) and the side devices (OWCPS1 - side) with increased s_d.

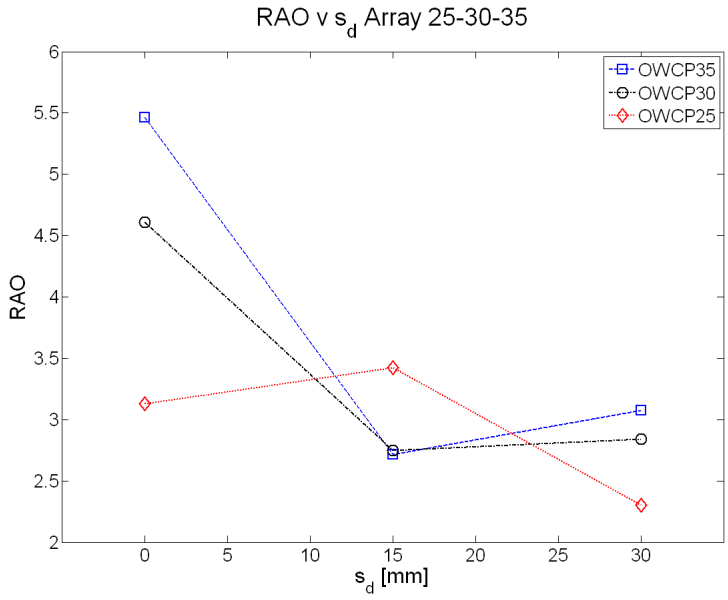

Figure 7.12: Changes in the RAO of each component of the 25-30-35 array configuration versus s_d for water depth $h = 140\,mm$ and $d_s = 80$mm.

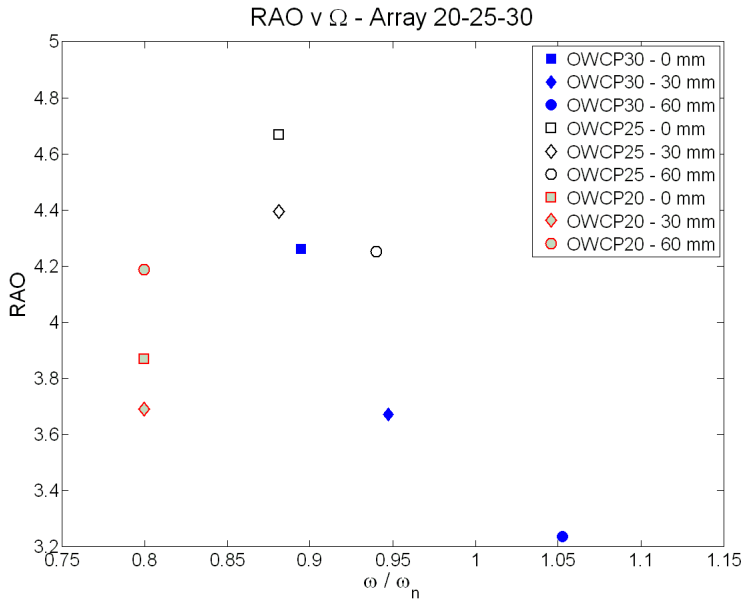

Figure 7.13: Changes in the RAO and Ω each component of the 20-25-30 array configuration for different s_d for water depth $h = 140\,mm$ and $d_s = 100$mm. An increase in the ratio ω/ω_n can be seen with the increase of s_d.

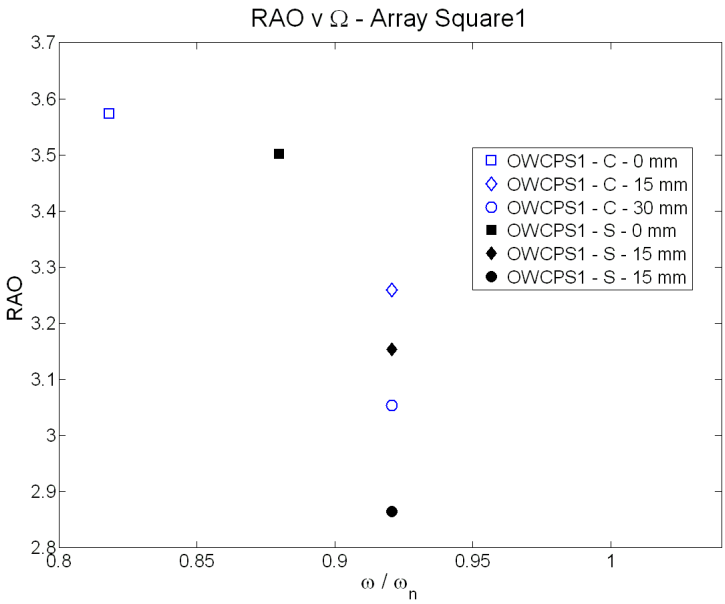

Figure 7.14: Changes in the RAO and Ω each component of the Square1 array configuration for different s_d for water depth $h = 140\,mm$ and $d_s = 100$mm. An increase in the ratio ω/ω_n can be seen with the increase of s_d.

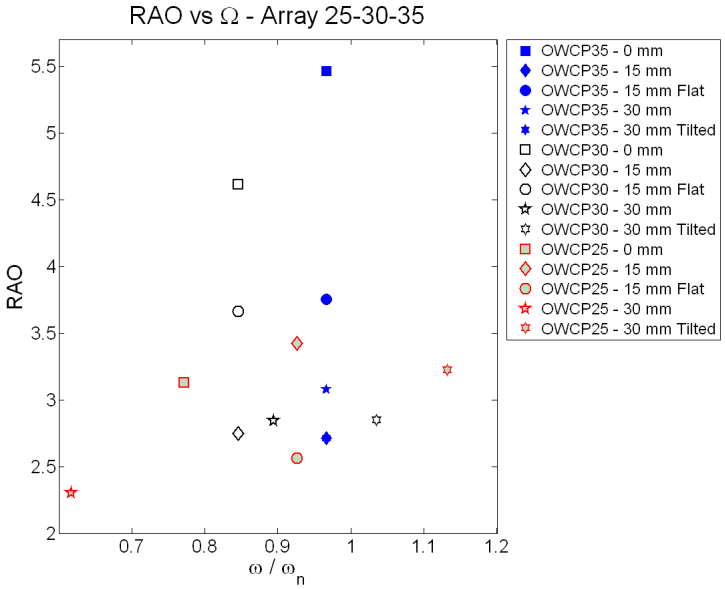

Figure 7.15: Changes in the RAO and Ω each component of the 25-30-35 array configuration for different s_d for water depth $h = 140\,mm$ and $d_s = 80$mm. The configurations marked with the term flat, consisted of the three devices presenting the input pipe located at the same d_s and flush with each other. The configurations marked with the term tilted consisted of the central device being channeled between the two side devices of 40 mm.

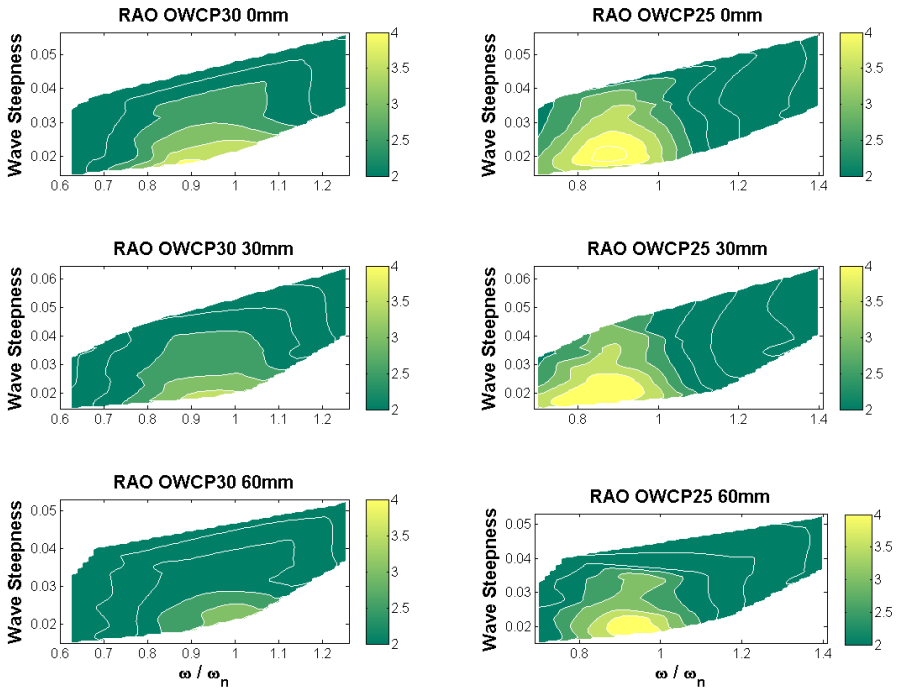

Figure 7.16: RAO for the OWCP25 and OWCP30 components of the 20-25-30 array configuration for different s_d for water depth $h = 140\,mm$ and $d_s = 100$mm. Focus is given at the behaviour of the side device (OWCP30, left) compared to the central device (OWCP25, right) at different conditions of wave steepness (H/L) and for different s_d.

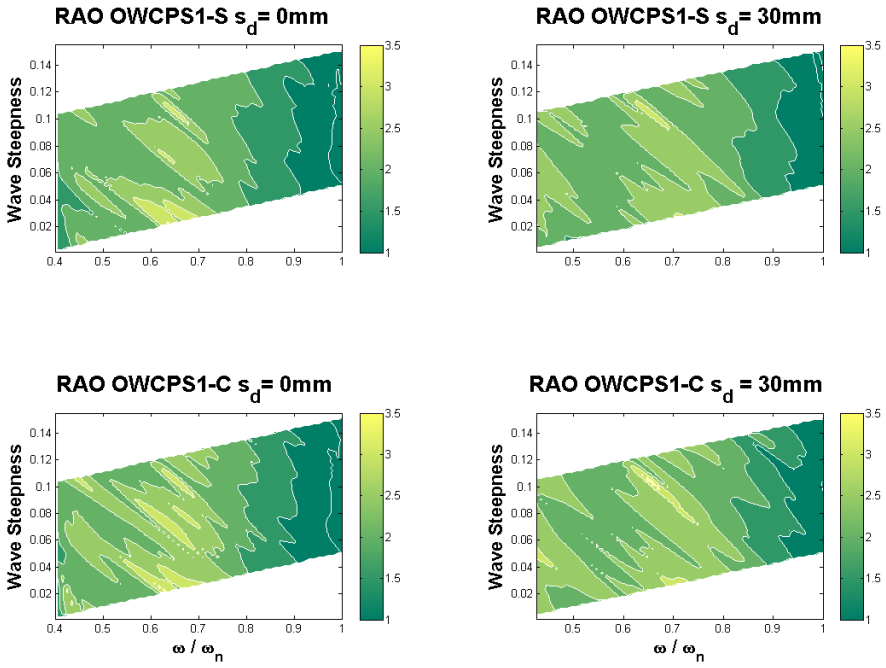

Figure 7.17: RAO for the OWCPS1-S (Side, top) and OWCPS1-C (Central, bottom) components of the Square1 array configuration for different s_d for water depth $h = 140\,mm$ and $d_s = 100$mm.

bandwidth area respect to the side OWCPS.

In both Figure 7.16 and Figure 7.17 it is possible to notice how the bandwidth for higher RAOs achieved is reduced by increasing the separating distance.

As a results of the RAO tests for the array configuration, it was chosen to assess the removal of water from the $25 - 30 - 35$ array configuration for $0 \leq s_d \leq 60\,mm$.

7.4 Capture width analysis

The analysis of the capture width was intended to determine the effects of the width of the devices in the array on the response of the device. As presented in Table 7.1 the Square1, Square2 and Square3 array configuration were built and tested by maintaining the overall width of the array constant to a value of 60 mm and by varying the components of the array as shown in Figure 5.6.

The RAO for an array of three OWCPS1 was presented in Figure 7.6, showing that the central device was the predominant device in the array with maximum RAO achieved of 3.8.

The RAOs for the Square2 and Square3 configurations are presented in Figure 7.18 and Figure 7.19.

In Figure 7.18 the RAOs for the components of the Square2 Array are shown. It can be

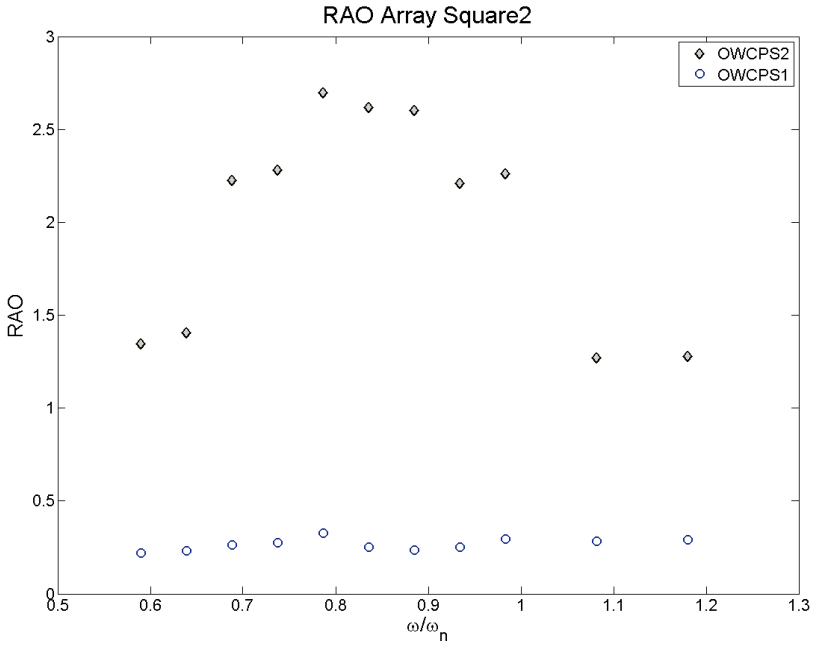

Figure 7.18: Frequency Response for an array of one OWCPS1 coupled with one OWCPS2 device.

seen how this combination generates a negative effect on the delivery within the model compared to Figure 7.6. The maximum RAO achieved is of 2.8 for the OWCPS2 device. OWCPS1 are negatively affected by the presence of a double width device installed in close proximity.

Figure 7.19 shows the response of the Square 3 array configuration. In this case, the OWCPS3 device is installed alone with the total width of 60 mm. It can be seen that the RAO obtained is significantly higher compared to the Square2 configuration (maximum of 2.8) and Square1 configuration (maximum of 3.8), with maximum values for the RAO obtained of 5.5.

Furthermore the RAO of the OWCPS3 is not affected by the presence of the other devices and due to an increase in the cross-sectional area of the duct, the effects of the device wall is minimised in front of the model, with also local losses due to friction playing a smaller role.

In all the configurations tested, the maximum RAO is obtained when the ratio ω/ω_n is between 08-0.9, with a secondary pick for $\Omega = 1$.

7.5 Removal of Water from the Array

The results presented in sections 7.3 and 7.4 have shown the effects of the array layout, separating distance and width on the performances of each component of the arrays, in terms of RAO.

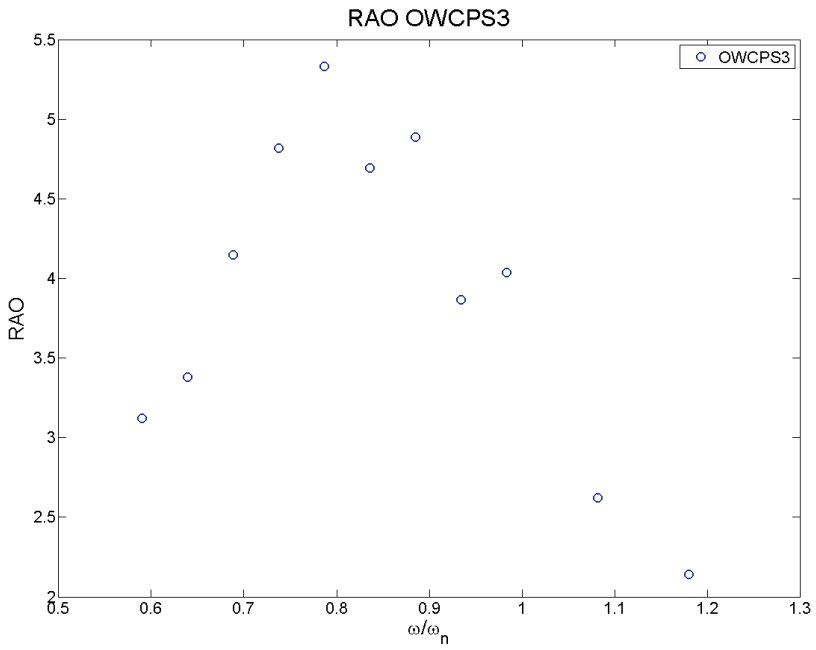

Figure 7.19: Frequency Response for the OWCPS3 configuration. Peak delivery is obtained for a ratio ω/ω_n of 0.8.

Physical investigations showed that the central component of the array is positively affected by the layout and that with an increased separation distance between the devices a decrease in RAO is expected with each component working more independently.

As seen in chapter 6, the RAO analysis provides an indication on the behaviour of the OWCP; which is partly related to the removal of water from the OWCP.

The non linear effects due to the PTO can only be assessed when water is removed from the array. The role of the PTO is accounted in the 25-30-35^r array configuration where water removal is implemented for each device.

7.5.1 Wave basin setup

Tests were carried out in the 3D wave basin, with the array installed within the absorbing beach at the far end of the tank, as showed in Figure 7.20 and Figure 7.21. Water is collected for a set of 25 waves, and the potential energy generated is assessed through the determination of the mass removed as explained in section 6.4 for each device. The devices were installed with a submersion depth $d_s = 80$ mm, with the removal height $y_r = 175$ mm for the 3 devices.

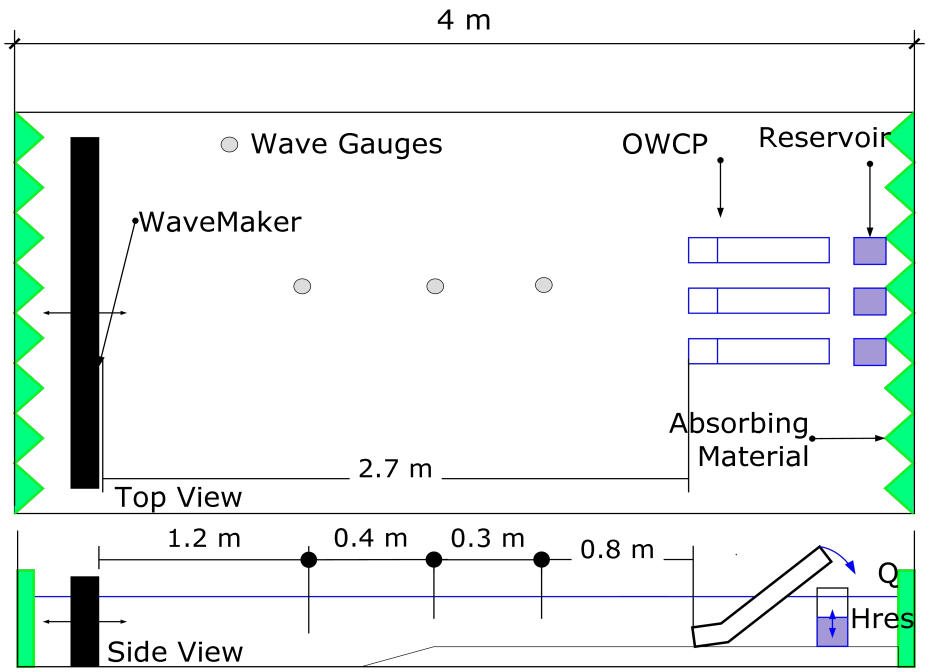

Figure 7.20: Setup ofthe 3D wave basin for array removal tests for the 25-30-35^r array configuration. A reservoir for each OWCP model is implemented, with the array being installed with a 1:2.5 absorbing gravel beach.

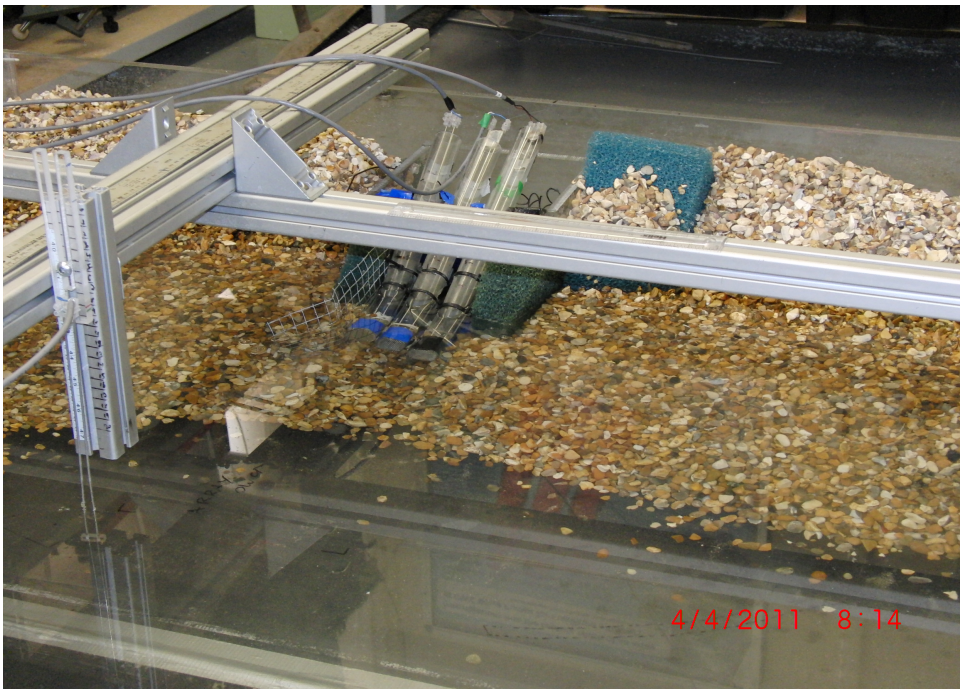

Figure 7.21: Installation of the 25-30-35^r array configuration within the 3D wave basin with $s_d = 10$ mm.

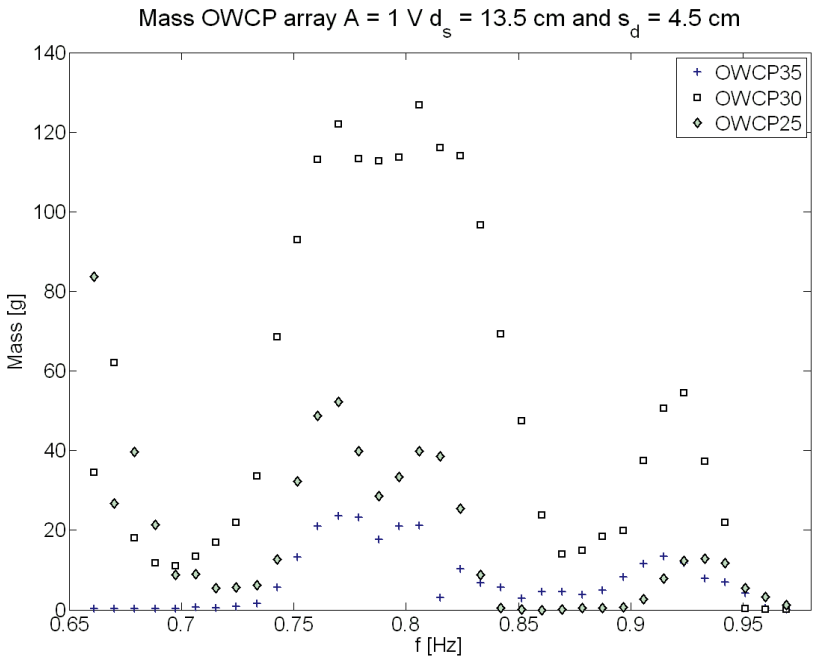

Figure 7.22: Mass of water removed from the 25-30-35^r array configuration within with $s_d = 45$ mm, $h = 135$ mm .

7.5.2 Mass of water removed

The assessment of the water removed from the array is not fundamental in the assessment of the efficiency of the array, however its analysis allows an evaluation of the dynamics of the array when the PTO is active.

Figure 7.22 shows the mass removed from the 25-30-35^r array configuration as a function of the wave frequency f. It can be seen that the removal of the mass is directly dependent on the incoming wave frequency; with higher mass removal for frequencies between 0.75 snd 0.85 Hz and between 0.9 and 0.95 Hz.

The behaviour of the devices in the array with an active PTO is different from the ones assessed in section 7.3. It is evident that when the water is removed from the array the OWCPs behave and respond to the wave frequency in a similar way even though the tuning frequency is different for each device. The three devices present a double peak of mass removed between 0.75 and 0.85 Hz, and a similar behaviour between the devices is then achieved when $0.9 < f < 0.95\,Hz$.

As indicated from the assessment of the RAOs, the central model (OWCP30), outperforms the other devices with higher masses of water removed throughout the frequencies tested compared

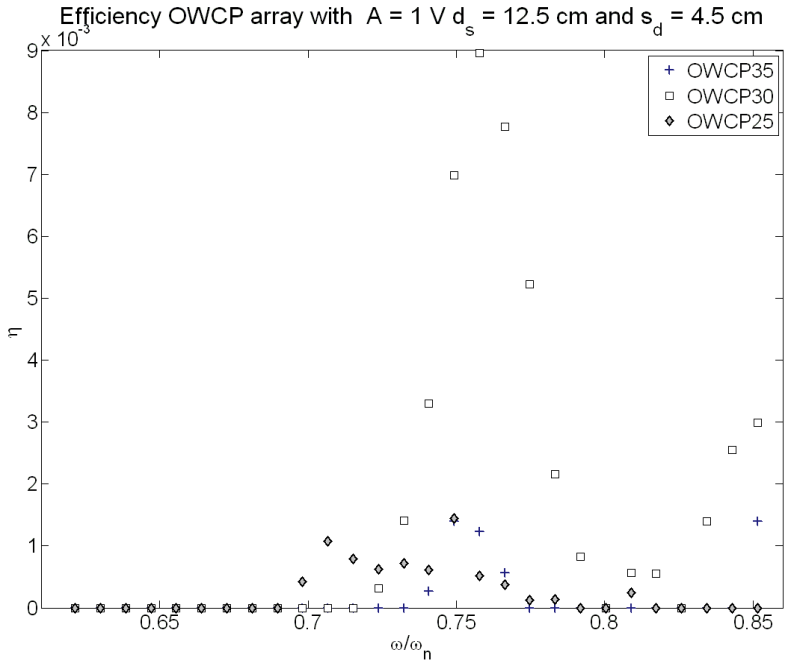

Figure 7.23: Efficiency of each component of the 25-30-35^r array configuration with $h = 125$ mm, $s_d = 45$ mm and $A = 1.V$. A maximum efficiency of ˜1% for the OWCP30 is achieved.. This is significantly lower compared to η obtained for similar configurations in 2D tests.

to the side devices.

7.5.3 Efficiency of the array

The efficiency of the array is assessed through the determination of the efficiency of each single device; expressed in terms of potential energy removed from each OWCP as a function of the energy carried by the incoming waves.

The removal efficiencies obtained from the array tests are significantly smaller to those obtained from the device working alone in the 2D wave flume. It was shown by Margheritini et al. (2008) that when moving from 2D to 3D tests a decrease in efficiency is to be expected due to basin effects .

Reduction of more than 50% from peak efficiency are registered for the side devices, with η dropping to less than 1% in the case of a higher freeboard ($d_s = 125\,mm$ and $y_r = 175\,mm$, Figure 7.23 and Figure 7.24). This shows a significant reduction of the efficiency of the devices compared to the 2D tests presented in Chapter 6. The performance of each single device and of the array are hampered by the particular array layout; nullifying the expected improvements of an array installation. The values of efficiency obtained from the side devices are significantly low

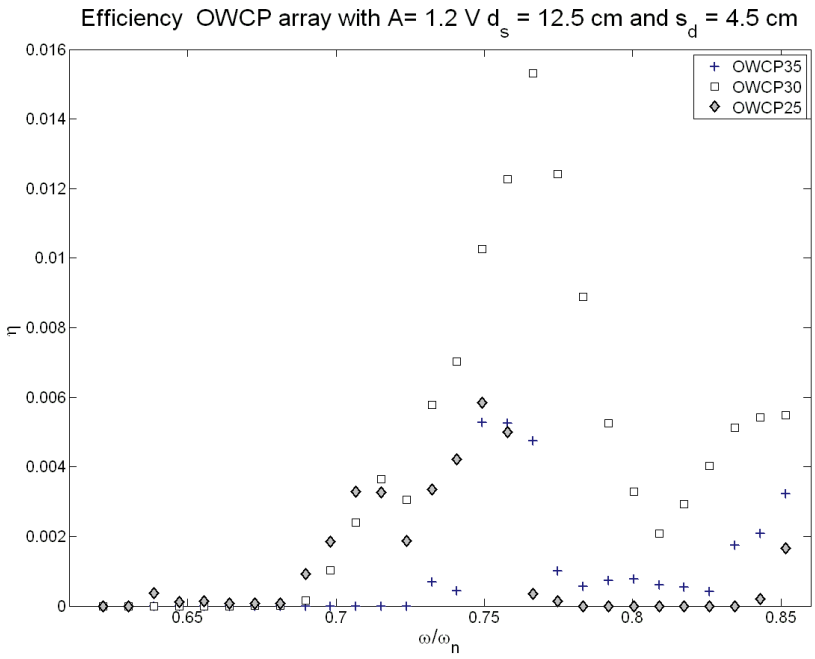

Figure 7.24: Efficiency of each component of the 25-30-35^r array configuration with $h = 125$ mm $s_d = 45$ mm, and $A = 1.2$V. A maximum efficiency of 0.0157 for the OWCP30 is achieved.

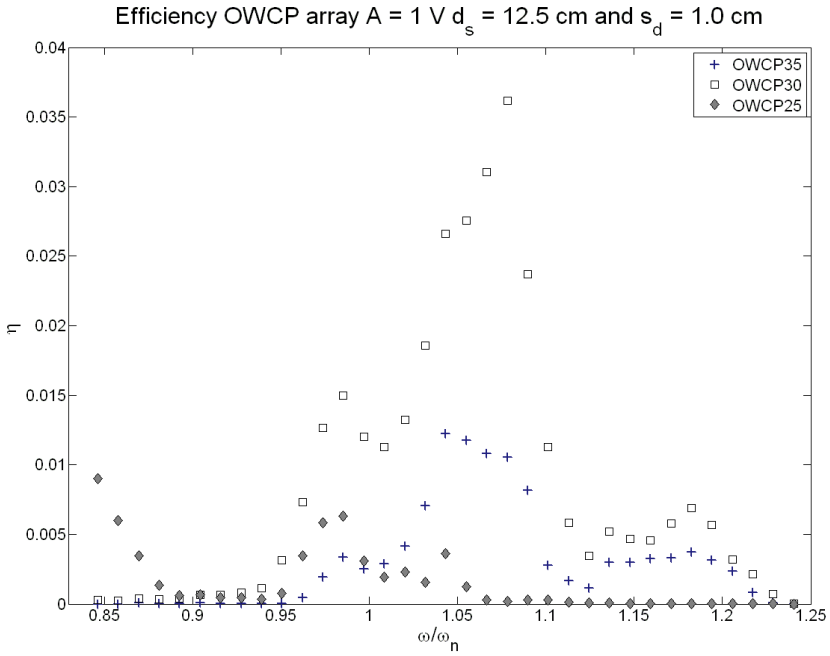

Figure 7.25: Efficiency of each component of the 25-30-35^r array configuration with $h = 125$ mm, $s_d = 45$ mm and $A = 1V$. A maximum efficiency of 0.038 for the OWCP30 is achieved.

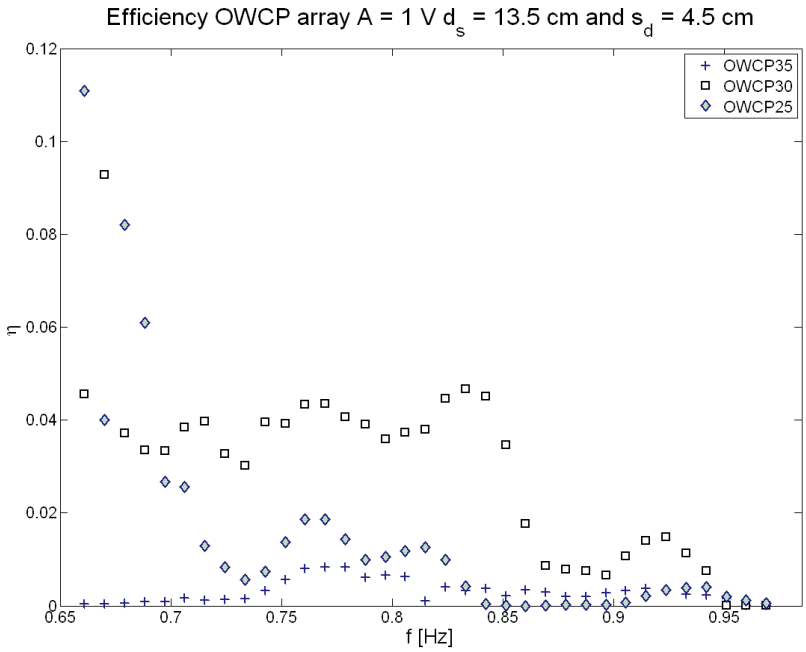

Figure 7.26: Efficiency of each component of the 25-30-35^r array configuration with $h = 135$ mm, $s_d = 45$ mm and $A = 1V$. A maximum efficiency of 0.09 for the OWCP30 is achieved and $\eta = 0.12$ for the OWCP25 is achieved.

indicating that the current layout is not advantageous and that single device installation could be more effective. Values of $\eta = 1\%$ significantly limit the application of the OWCP.

As expected when the freeboard is reduced to 4 cm ($d_s = 135\,mm$ and $y_r = 175\,mm$) η increases (Figure 7.26) with peak values of 0.12 for the OWCP25 and 0.09 for the OWCP30. These values compared to those obtained in 2D tests with similar freeboard and submersion depth conditions. It has to be noted that the maximum efficiency obtained for OWCP30 is of 15.7 when $d_s = 135\,mm$ and $y_r = 175\,mm$ and $s_d = 45mm$. This represents an increase in η for the device indicating reflecting in an increase of water delivery for the given array configuration.

The overall efficiency is given by the sum of the efficiency obtained from each device, since the water removed could be accumulated in a common reservoir. Figure 7.27 shows the cumulative efficiencies for the array 25-30-35^r array configuration for different values of s_d and h. It can be seen that the when $s_d = 45\,mm$ and $f < 0.75$ the array achieves the highest efficiency due to the contemporaneous delivery due to the OWCP25 and OWCP30 models; with peak efficiency reaching 16%. The overall array efficiency stabilises to values between 7% and 8% for $0.85 < f < 0.95$, indicating steady delivery of water in the reservoir for a larger frequency range. This validates the proposed array installation which aimed to increase frequency spectrum and

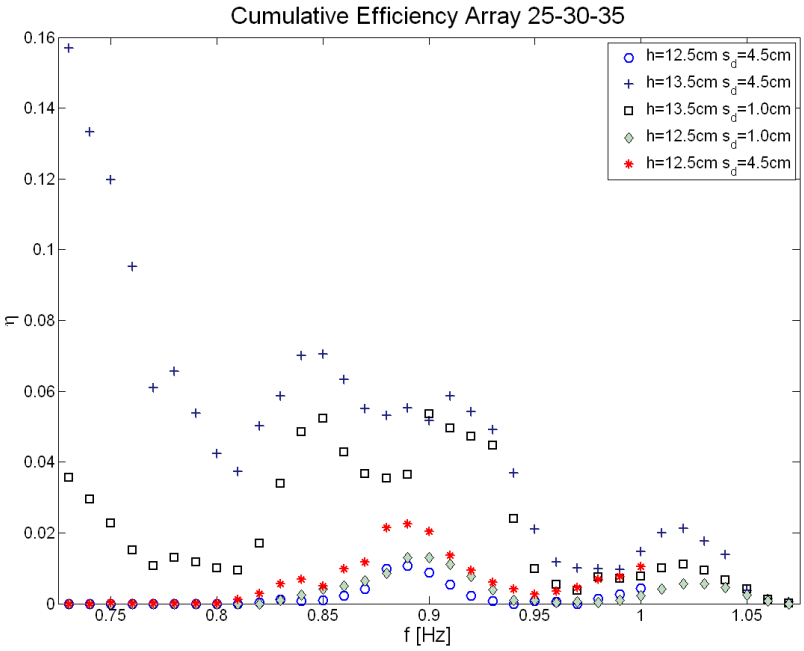

Figure 7.27: Overall efficiency for the 25-30-35^r array configuration for different values of h and s_d. Maximum efficiencies are obtained for $h = 135\,mm$ and $h_r = 40\,mm$.

delivery of water in the reservoir.

7.5.4 Determination of the q factor

A tool for the evaluation of the performances of the array was introduced in section 7.1, where the q factor was presented. Babarit (2010) defined the q factor in terms of the power output that can be obtained by the array compared to the sum of the power generated by each device when working independently.

For an array of OWCP under investigation in this work, the q factor can be rearranged and expressed in terms of mass removed from each device as follows:

$$q = \frac{h_{r,a} \times (m_{25,a} + m_{30,a} + m_{35,a})}{h_{r,i} \times (m_{25,i} + m_{30,i} + m_{35,i})} \tag{7.2}$$

where the subscripts 25,30 and 35 refer respectively to the OWCP25 OWCP30 and OWCP35 models, and the subscripts a, i refer to the device working in the array configuration(a) and independetly (i). The expression of q in terms of mass removed is obtained by rearranging the power generated by each OWCP from equation 4.46.

Once defined q it is possible to determine it for the different configurations examined during

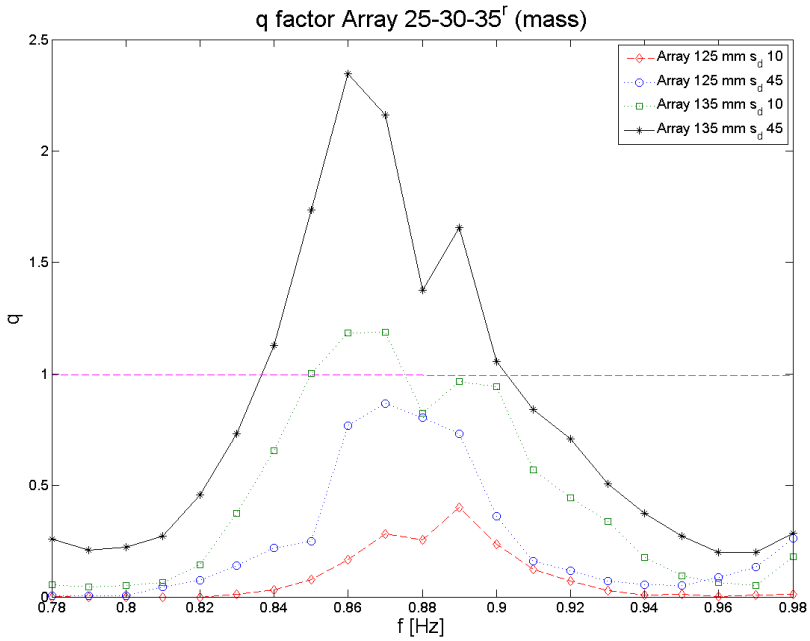

Figure 7.28: q factor deterimined for the for the array configuration 25-30-35^r for different s_d. It can be seen that values of q higher than one are achieved for $s_d = 45\,mm$

the experimental investigations. The values of q expressed in terms of mass removed are presented in Figure 7.28.

Figure 7.28 shows that both the water depth and the separation distance play a significant role in the performances of the array. The role of the water depth h on the η of the OWCP when working independently was discussed Chapter 6. Through the determination of q it can be seen that the array performs better when $s_d = 45\,mm$. Values of $q > 1$ are obtained when $0.83 \leq f \leq 0.9$ indicating that a positive array effect is achieved by the proposed array configuration.

Expressing q in terms of mass removed as presented in equation 7.2 is not sufficient in expressing the interaction between the device as it does not consider the energy carried by the incident waves. A new q factor is hereby proposed and expressed in terms of efficiency of removal as follows:

$$q_e = \frac{\eta_{25,a} + \eta_{30,a} + \eta_{35,a}}{\eta_{25,i} + \eta_{30,i} + \eta_{35,i}} \tag{7.3}$$

where the subscripts 25,30 and 35 refer respectively to the OWCP25 OWCP30 and OWCP35 models, and the subscripts a, i refer to the device working in the array configuration(a) and independetly (i).

By expressing q in terms of q_e, the amount of incident energy absorbed by each device

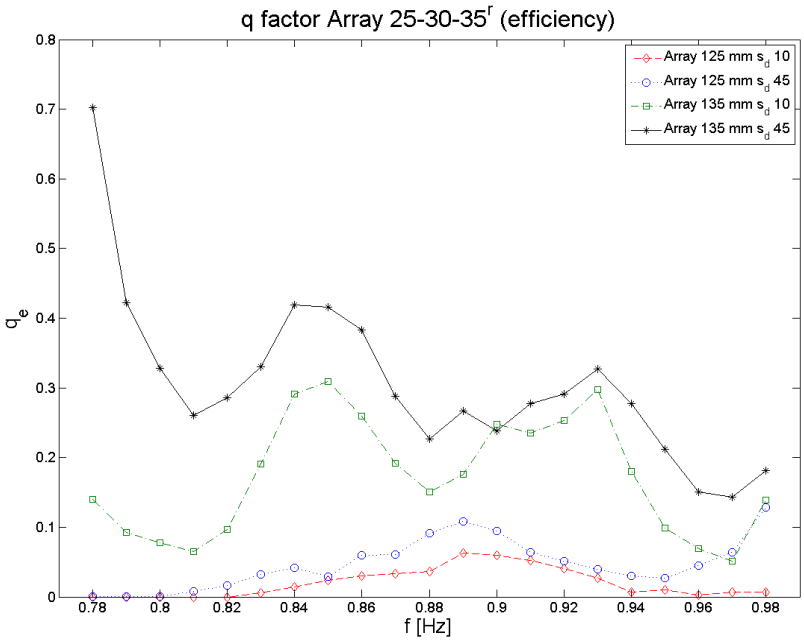

Figure 7.29: q_e factor deterimined for the for the array configuration 25-30-35^r for different s_d. It can be seen that values of q higher than one are achieved for $s_d = 45\,mm$

is considered. In this case it can be seen that if $q_e > 0.3$ more than one OWCP model are operating simultaneously and positive array effects are achieved. Figure 7.29 presents the q_e factor determined for the cases investigated.

Figure 7.29 shows that for $s_d = 45\,mm$ positive effects of the array are achieved for a wide range of frequencies. This shows that the components are positively affected by the layout. Furthermore the presence of positive effects validate the proposed layout of the array of differently tuned devices. The proposed configuration allows to obtain the delivery of water and the generation of the hydraulic head with changing wave conditions without the need of a resonance control system.

7.6 Discussion

From the literature review it has emerged that there is an increasing interest in evaluating the performances of multiple wave energy converters installed in array configuration in order to improve the power output that can be generated. Whilst studies on the subject are still at an initial stage, it appears clearly that one of the determining factors in the performances of arrays is the separation distance s_d between each device installed. So far, however, investigations

of the role of s_d were mainly conducted through the use of mathematical models and limited experimental investigations have been carried out to assess the effects of the separation distance. In this work array configurations of differently tuned OWCPs was proposed in order to increase water delivery into the reservoir. The use of differently tuned devices allowed to generate an array where each device would respond to a selected wave frequency without the need of implementing a resonance control system.

In order to determine the performances of an array of OWCPs, experimental tests were employed to assess the response and the efficiency of multiple models working together. Different configurations of the array were investigated. The experimental investigation were carried out in order to:

- Determine the response each component of the array and investigate the role of s_d on the response of each OWCP model
- Assess the performances of similarly tuned devices
- Determine the efficiency in removal of an array of three differently tuned OWCP models and evaluate the q factor of the proposed array.

7.6.1 Array Response and s_d effects

RAO tests were employed to validate the proposed array installation with differently tuned devices. Two main configurations comprising the OWCP20, OWCP25, OWCP30 and OWCP35 were considered. RAO tests of the array configuration showed that it was possible to achieve a high response from the array at different wave frequencies, thus validating the proposed installation. Through a spectral analysis it was found that the phase at which each component of the array responded to the incoming waves was different, hence the radiation component of the array was phased-out providing a reduced destructive effect to the incident wave field.

The analysis of the RAO of each component showed that for both the 20-25-30 and 25-30-35 configurations the central device was achieving higher RAOs compared to the side models, thus showing positive interactions towards the centre of the array.

By comparing the RAO of each component against the RAO of the same model working autonomously, a shift towards higher frequency, for which the maximum RAO was achieved, was found.

The analysis of the role of the s_d on the response of the array showed that at the increase of the separation distances between the models, the response of each component decreased. In particular, results show better performances for the cases when $s_d = 0\,mm$. The maximum values of the RAO varied accordingly with the type of array configuration with RAO = 5.46 for the 25-30-35 configuration, 4.669 for the 20-25-30 array. Reductions in RAO of 14% can be expected by increasing the separation distance of 15 mm, the decrease being dependent on the array configuration.

The decrease in RAO varied between 30% for the 25-30-35 array to 6% for the 20-25-30 for a 30 mm increase in the separation distance. As a results of the RAO tests it was chosen to investigate the removal of water from the 25-30-35 array configuration with separation distance $s_d = 10\,mm$ and $s_d = 45\,mm$.

7.6.2 RAO of similarly tuned devices

Similarly tuned devices were tested in an array configuration to provide comparison with the results obtained from the RAO tests of differently tuned devices. Tests showed that by employing similarly tuned devices in array configuration negative effects are found to affect the overall array performance, with a RAO reduced of the 20% compared to those obtained by array configurations of differently tuned OWCPS. The maximum RAO obtained in the Square1 array configuration was of 3.573.

From the spectral analysis of the components of the Sqaure1 array it was seen that the phase of response of each component to the incoming wave was identical, hence a higher radiation effect is expected when similar device are employed in close proximity.

By changing the cross-sectional area of the OWCP it can be seen how the different components of the array interacted with each other. Negative interferences are noted in the RAO when devices with similar tuning frequency but different cross-sectional area were coupled together, reducing the overall array performance. Using an OWCP with a wider cross-sectional area provides a higher response, but it is limited to lower wave frequencies, since the mass moved by the waves increases.

7.6.3 Efficiency and q factor

The array configuration 25-30-35^r was tested in order to determine the efficiency in removal of the array for different values of s_d.

Falcao (2002) suggested that for OWC devices installed in array configurations with a standard PTO and no resonance control, the interference between the devices is relatively unimportant, however removal tests for the array showed that the central OWCP is positively affected by the layout of the installation, with the OWCP30 device outperforming those installed on the side in every configuration tested. An overall negative effects was found to affect the devices on the side of the array where η achieved significantly lower values than those achieved by the device working autonomously. Similar attenuation effects were found by Weller et al. (2009) for an array of 4×3 heaving bodies WECs.

An overall maximum efficiency of 21% was achieved for the 25-30-35^r array configuration when $h = 135\,mm$, $y_r = 175\,mm$, and $s_d = 45\,mm$.

The determination of the q factor with the method presented by Babarit (2010), indicated that positive array interaction can be generated in order to maximise the power output that can be obtained from the array. Babarit (2010) reported values of $q > 1$ obtained from the simulation for closely spaced devices with the values of q being dependent on the incoming wave frequency. For the separation distances investigated it was seen that when $s_d = 45\,mm$ the q factor was higher than the cases where $s_d = 0\,mm$. The values of q were found to be dependent on the incident wave frequency, however it was seen that for the conditions close to resonance, with $0.83 \leq f \leq 0.9$ the separation distance between the devices was the predominant factor in the performances of the array.

In order to consider the role of the incident waves in the performances of the array, a quality factor expressed in terms of efficiency was presented. It was shown by Weller et al. (2009) that the interaction between devices vary accordingly to the position of the devices and to the incident waves, with both constructive and destructive interferences taking place. The determination of q_e showed the quality factor to oscillate for different wave frequencies with values of $q_e > 0.3$ indicating than more than an OWCP was delivering water for the given incident frequency when $s_d = 45\,mm$. As determined by Weller et al. (2009) higher values of q_e were found for lower wave frequencies.

The use of physical tests allowed the consideration of a finite-length array installed on an absorbing beach, compared to simulations where infinite-length arrays were considered in literature as presented by Falcao (2002), or the case where infinite separation distances are considered as presented by Babarit (2010).

The removal tests for the array validated the initial hypotesis of employing differently tuned

OWCPs simultaneously to generate a costant flow of water without the need of employing a resonance control. However, as seen in Falcao (2002), the total output of the array could be increased if a control system is implemented for each device.

7.6.4 Summary of findings

The installation of multiple OWCPs was evaluated with the aim to increase the performances of each single device and the overall delivery of water. Experimental testing was undertaken investigating the performances of three differently tuned OWCPs for different values of the separation distancess_d.

It was found that the RAO of the models is dependent on the separation distance, with maximum response obtained when$s_d = 0\,mm$. Reductions of up to 14% in the RAO are expected with an increasing s_d of 15 mm, further decreases in RAO will take place when $s_d = 30\,mm$. Lower values of RAO were obtained for array installation compared to the scenario where the same device would operate independently. Array configurations allowed for the devices to respond to a wider range of incoming wave frequencies without requiring the installation of a resonance control system. It was determined that each device respond to the incoming waves with a different phase, effectively reducing the radiated wave generated by the downward motion of the water exiting each OWCP. The performance of the central OWCP are positively affected compared to side devices, both in terms of RAO and efficiency.

The efficiencies of removal of the 25-30-35^r array configuration were determined for $s_d = 10\,mm$ and $s_d = 45\,mm$. Significant interferences take place between the devices forsmall separation distances; resulting in a positive effect on the performances of the central device, OWCP30. In agreement with the experimental findings presented by Weller et al. (2009) for a 4×3 array of heaving WECs, it was found that the efficiencies of the outer devices of the array was reduced compared to stand-alone operation.

Positive array effects were evaluated through the determination of the q factor. Literature shows that values of $q > 1$ are possible for closely spaced heaving and surging devices, with the quality factor being dependent on the wave frequency (Babarit, 2010). Tests showed that values of $q > 1$ were achieved when $s_d = 45\,mm$ and $0.83 \leq f \leq 0.9$. In agreement with the work carried by Weller et al. (2009), it was found that higher q_e values were obtained when $s_d = 45\,mm$ for low wave frequencies. q_e represented the quality factor expressed in terms of efficiency, therefore accounting the role of the incoming waves on the performances of the array.

Positive effects between array components can be genereated through the optimization of thes_d between the devices. This was achived when $s_d = 0.045\,m$, resulting in an overall array efficiency of up to 16% for lower wave frequencies.

It is therefore possible to employ multiple OWCPs in order to increase water delivery through the installation of differently tuned devices in an array configuration. Through the implementation of a resonance control system it will be possible to further increase the array output generated, as indicated by Falcao (2002).

Chapter 8

Full Scale Performances of the OWCP

Chapter 6 presented results of testing of the OWCP expressed in terms of RAO, η and mass delivered by the device; allowing for the validation of mathematical models describing the response of the device. These models can be employed to assess the performances of the OWCP at full scale, and to determine the yearly amount of water delivered from a full scale device.

The values of damping coefficients and angle bends coefficient have been scaled up using the laws presented in section 5.3. These could lead to conservative estimate of the full scale performances of the OWCP. However no significant differences were notice in the response of the OWCP25 when tested at two different scale of $\lambda = 40$ (chapter 6) and $\lambda = 20$ (A.1). The values of the angle bend coefficients k_b for full scale simulations, have been extracted from Figure 4.5.

In this Chapter, a full scale installation of the OWCP is considered in order to evaluate its performances under the influence of irregular wave conditions, for an OWCP device with $\alpha = 25^{\text{o}}$ and $\alpha = 30^{\text{o}}$ installed in a typical North Sea location. Details of the OWCP configurations chosen are presented in Table 8.1. Such installation was chosen as it allows for comparison of of the OWCP with other overtopping devices such as the Wave Dragon and the SSG. Wave conditions in the North Sea, measured at Ekofisk, are presented in Table 8.2(Rugbierg and Nielsen, 1999). It can be seen that the total frequency of occurence of the 5 sea states is of 87.7%; with wave heights below $0.5\,m$ for the remaining 12.3% of the year.

A JONSWAP spectrum is generated for each of the wave conditions presented in Table 8.2. Irregular wave series are generated from the superposition of 89 components of regular waves with frequency from 0.0556 to $4.944\,Hz$ with a step of $0.0556\,Hz$. The amplitude of the wave components are obtained from the spectrum, whilst their phase is random. Figure 8.1 shows an examples of irregular wave series generated for the full scale simulation of the OWCP. Simula-

Parameter/Configuration	OWCP30	OWCP25
Inclination α	30°	25°
Input Duct l_1	1.8 m	2 m
Submersion Depth d_s	3.2 m	3.2 m
Water Depth h	4.8 m	4.8 m
Removal Height h_r	1.4 - 2.4 m	1.4 - 2.4 m
Diameter OWCP d_{OWCP}	1 m	1 m

Table 8.1: Configurations of the OWCP models for full scale evaulation

H_s [m]	T_P [s]	Incident Wave Power P_w [kW/m]	Frequency of Occurence %
1	5.6	2.5	46.8%
2	7	12.4	22.6%
3	8.4	33.5	10.8
4	9.8	69.6	5.1%
5	11.2	124.2	2.4%

Table 8.2: North Sea wave conditions, measured at Ekofisk. The significant wave height H_s, peak period T_P , wave power and probability of occurence for each sea state are presented.

tions were run for a total time of 1800 s. The simulations did not take into account any wave transformation that can take places in the near shore are as they aimed to provide an indication of the mass that could be delivered by the OWCP under the influence of irregular waves.

Figure 8.2 shows the mass of water delivered over a year for each sea state of Table 8.2. It can be seen that largest component of the mass is delivered for stronger sea states, with the stronger contribution obtained for $H_S = 4\,m$ and $T_P = 9.8\,s$ despite a probability of occurrence of 5.1% a year. The amount of mass delivered is affected by the h_r, as previously shown in chapter 6. The annual prediction of water delivered for each OWCP configuration is presented in Figure 8.3. A yearly estimate of 9×10^9 kg of water could be delivered by the OWCP25 with $d_{OWCP} = 1\,m$ and $h_r = 1.4\,m$. The amount of mass delivered decreases with both h_r and α.

The simulations allow to estimate the efficiency of the device under the influence of irregular waves. Figure 8.4 shows the efficiency achieved by the OWCP25 device for each sea state evaluated for different values of h_r. It can be seen that values of η above 16% can be obtained by the device when $H_s \geqslant 4\,m$; indicating that through a different design it would be possible to increase the efficiency in conversion of the OWCP for lower values of H_s.

Figure 8.5 shows the efficiency of the OWCP25 and OWCP30 configuration under investigation. installed in the North Sea. It can be seen that a maximum efficiency of about 2.45% is expected for the OWCP25 when $h_r = 1.4\,m$, indicating a reduction of four time compared to the

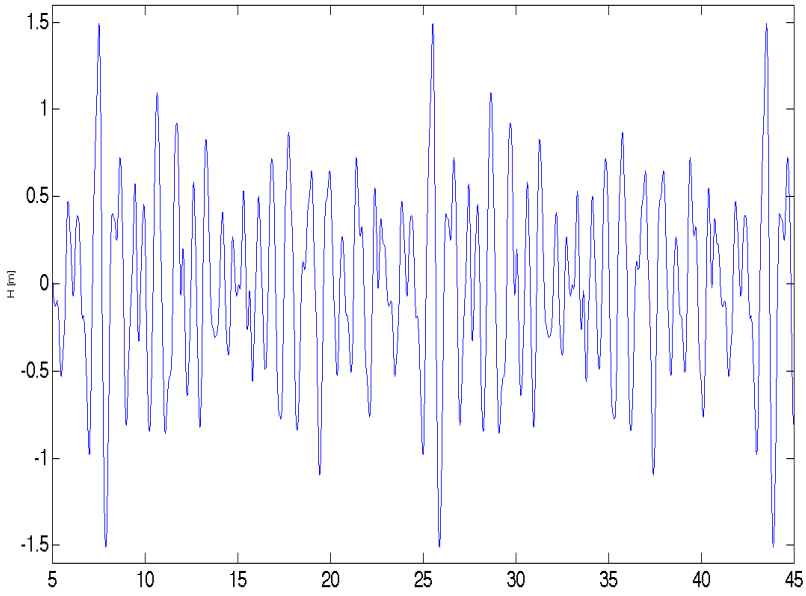

Figure 8.1: Time series generated for full scale simulation of the OWCP with $H_s = 2\,m$ and $T_P = 7\,s$

values of efficiency obtained for the OWCP25 during experimental testing under the influence of regular waves.

8.1 Comparison with other WECs

The performances of the device in regard to efficiency of conversion are significantly lower compared to other WECs developed and tested under North Sea wave conditions. A maximum efficiency of 14% and a narrow bandwidth was recorded for the OWCP device under regular waves (shown in chapter 6), with η dropping to 2.45% for irregular sea states. The efficiency of overtopping devices such as the Wave Dragon was found to be of $\eta = 18\%$ (Kofoed et al., 2006), whilst the SSG device could achieve $\eta = 10 - 25\%$ under the influence of multi-directional waves(Margheritini et al., 2008). The efficiency values obtained for the Wave Dragon and for the SSG refer to total output of the devices in terms of kW of electricity generated; whilst the values obtained from the OWCP refer to hydraulic efficiency. It is expected that the efficiency of the OWCP will be further reduced if the device is employed for the generation of electricity. The low values of conversion efficiency for the OWCP indicate that the device should not be employed for the generation of electricity but as a low cost system to pump water into enclosed

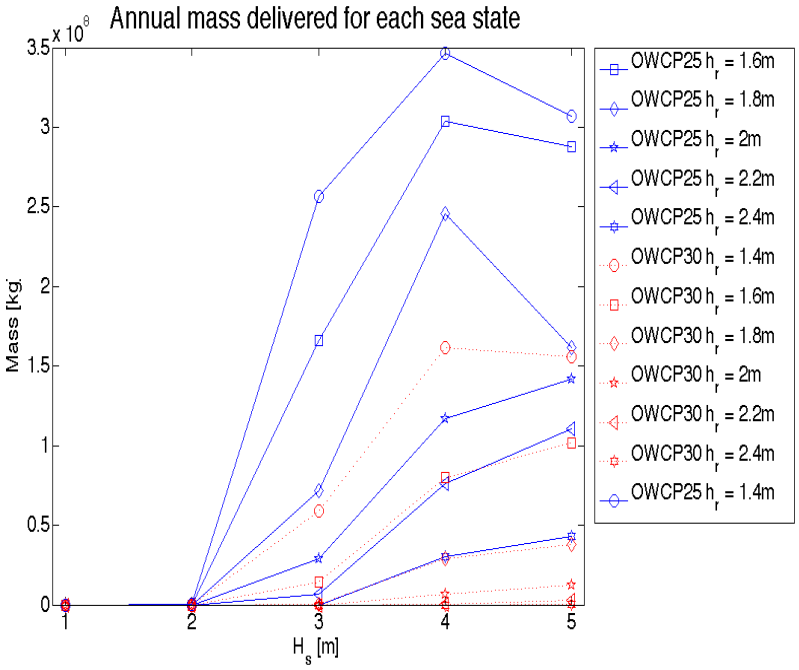

Figure 8.2: Mass of water delivered from the OWCP25 and OWCP30 for different values of h_r

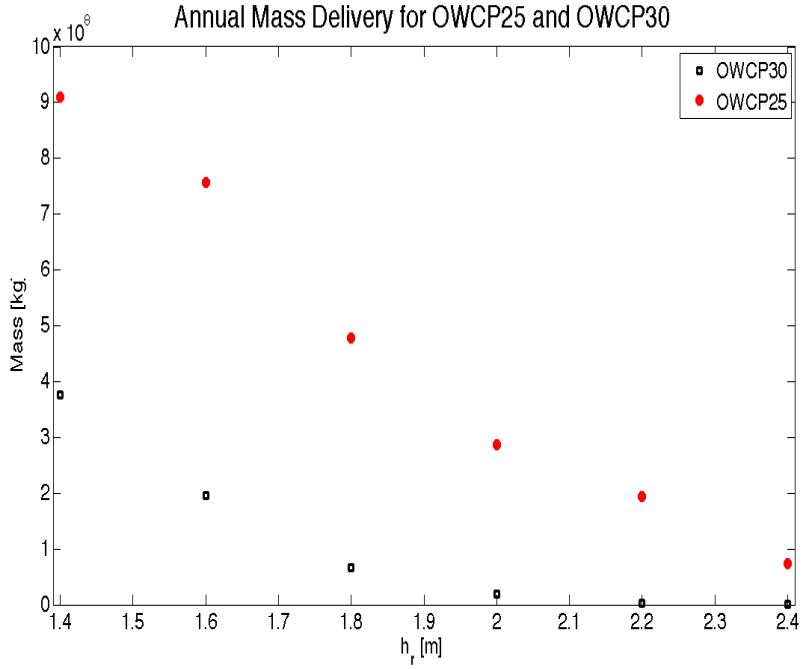

Figure 8.3: Annual prediction of mass of water delivered for the OWCP25 and OWCP30 configurations for different values of h_r.

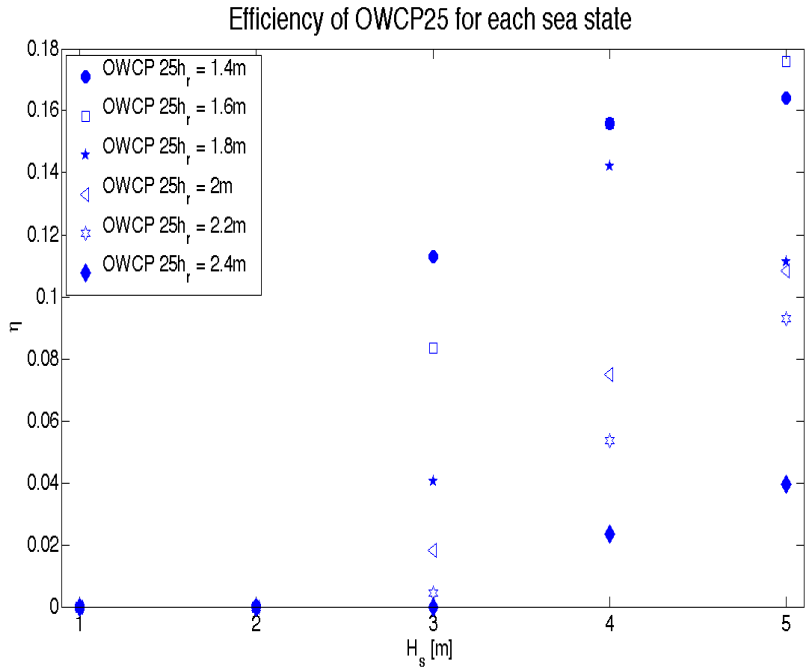

Figure 8.4: Efficiency of the OWCP25 a for given sea states

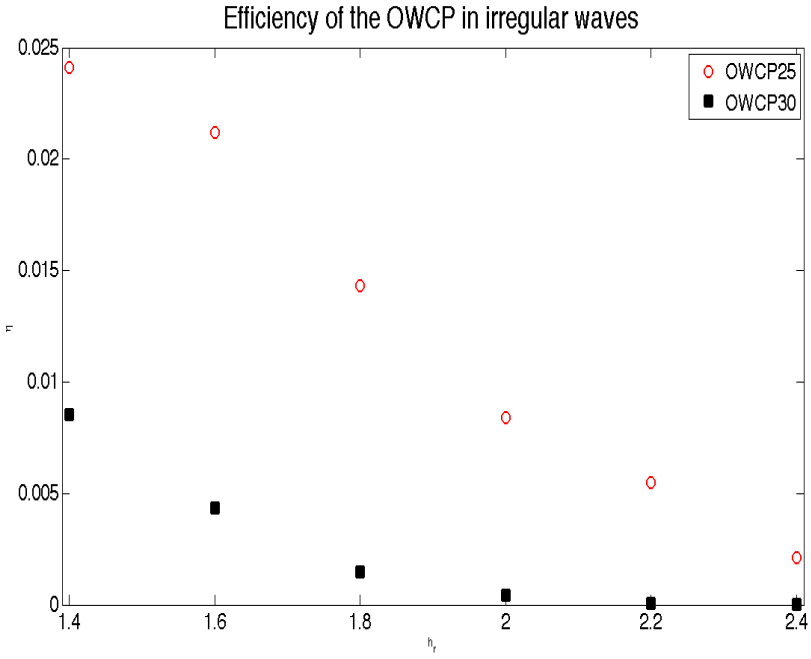

Figure 8.5: Efficiency of the OWCP25 and OWCP30 for irregular sea conditions.

areas facilitating the circulation of water; such as marinas.

In terms of water delivery, an OWCP with $d_{OWCP} = 1\,m$ could deliver up to $9 \times 10^6\,m^3$ of water year compared to the $6.3 \times 10^6\,m^3$of water a year ($200\,l/s$) that a SIBEO with $1.4\,m$ diamater could achieve. The OWCP could therefore provide a cheap and reliable alternative for the flushing of enclosed harbours.

Chapter 9

Discussion and Conclusions

9.1 Introduction

The overall objective of this thesis was to develop a suitable wave energy converter aimed to supply water delivery. The OWCP was developed on the basis of the existing technology identified in the OWC. The OWC was chosen through a review of the current state of the art technology, as a suitable WEC to be modified and adapted for water delivery.

The chosen design of the OWCP consisted in two cylindrical ducts joint together at a fixed angle. Investigation of the performances involved analysis of the response of the device to sinusoidal waves to determine which device could be employed for water delivery. Efficiency tests were carried on the selected devices, and their performances were ultimately evaluated in array configuration. Linear and non-linear mathematical models were developed to predict the behaviour of the OWCP on the basis of the results obtained from physical tests.

The work involved is discussed in this chapter. The most relevant conclusions presented are recalled.

9.2 Discussion and Conclusions

9.2.1 Literature review

The state of the art review presented in section 3.1 showed a variety of wave energy converters which have been developed over the past 5 decades. The WECs were analysed on the basis of their interactions with the waves, and on their applications. As a result of the analysis of the current state of the technology, it was chosen to investigate the possibility of adapting the

OWC device to a resonating-type wave energy converter. The OWC technology has already been adapted for marina flushing through the successful implementation of the SIBEO device presented by Czitrom (1997).

In section 3.2 the design characteristics of the OWC were presented from the initial development to the main theoretical aspects. It was shown how the waves-OWC interactions have often been modelled through the use of mechanical similarities as a damped linear oscillator when no power take-off was installed, or as a double-mass damped oscillator when the turbine was considered.

To properly model the OWC, BEM codes have been employed in order to determine the hydrodynamics coefficients of radiation damping and added mass which affect the response of the water column. The use of linear models has been preferred to non-linear models to predict the performances of the OWC and to optimise the device itself as shown in the work of Brito-Melo (2000) and Delaure (2001) due to faster computational time.

An attempt to develop an overtopping OWC was presented by Knott and Flower (1979), who considered the possibility of generating potential energy. Their work was left incomplete with no physical investigation carried out. Knott and Flower (1979), however, showed that water delivery from the OWC was possible even though limited to low wave frequencies.

The review literature showed the limitations that affect experimental testing of the OWC, due to the presence of the air-water interface when the PTO is installed. This affected the comparison with mathematical results and limited the use of physical tests to structural analysis and investigations into the formation of vortexes in front of the device.

As a result a working plan was devised for the investigation of the OWCP:

1. Implementation of a theory for the OWCP based on the damped-oscillator system to determine the response of the device to linear waves. This included the assessments of non-linear forces that affect the movement of the water column. The objective was to develop a linear and a non-linear mathematical model to assess the performances of the OWCP.

2. An experimental plan was outlined in order to assess the performances of the OWCP under wave induced oscillation. The objective was to determine the response of the device, and

its efficiency when water is removed from the device. The data collected were used to provide validation to the mathematical model presented.

9.2.2 Theoretical approach

The response of the OWCP has been represented through the mechanical similarities with a single mass, damped oscillator. This allowed to determine the response of the OWCP to linear incident waves.

The first task consisted of developing a model of the OWCP when no PTO was installed. This allowed to determine the RAO for different configurations of the the OWCP, by changing the values of h, d_s, ξ_r, and α. The values of ξ_r where obtained from the early work carried out by Knott and Flower (1979). The RAO obtained from linear simulations were similar to those obtained by Evans (1978), with values up to 4 compared to the incoming wave amplitude.

From the determination of the RAO, it was possible to determine the displacement of the water column within the device and implement a model of the OWCP to account for the role of the PTO and to assess the effects of water removal.

The second task consisted of including the PTO force in the theoretical formulation of the OWCP. The PTO force was found to be non-linear due to its dependence on the lift height within the OWCP, and to affect the restoring force when water was removed. The influence of non-linear forces acting on the OWCP such as, friction, drag and bend losses has been determinted allowing the implementation of a non-linear mathematical model.

Comparison between the linear mathematical model and the non-linear one showed that the non-linearities affect the RAO and delivery of the water of the OWCP by shifting the response bandwidth to lower peak frequencies.

9.2.3 Experimental results

In section 5.1 the importance of physical models for the evaluation of the performances of WECs was highlighted through a review of the most updated guidelines available in literature. Experimental tests of OWC device were found to be affected by scaling issues of the air/water interface reducing the effectiveness of the investigations, as presented in section 3.2.4. With regards to overtopping OWC device no physical investigation of the performances of such WEC were carried out following the mathematical work of Knott and Flower (1979). Holmes (2003) emphasised the role of experimental testing of WECs from the early stage in order to successfully develop a

valid device. In order to validate the proposed OWCP presented in this research extensive series of physical tests were carried out for scaled models of the OWCP for varying water depths and wave conditions.

9.2.3.1 Performance of a single OWCP

RAO tests of the OWCP models showed that an amplification up to 5.9 times of the initial wave amplitude can be achieved for the OWCP25 and OWCP30 device. Higher RAOs were obtained for those tests where the incoming wave height H was lower, thus confirming the mathematical description of the OWCP as a single-mass oscillator as assumed in Chapter 4. Non-linearities were found to affect the RAO of the OWCP for higher wave heights due to vortex formation for conditions close to resonance. Similar effects were found in the tests carried out by Lopes et al. (2009) for an OWC chamber without PTO. The values of RAO obtained for the OWCP are comparable with those obtained by Evans (1978) in absence of the PTO.

The maximum RAOs obtained for the OWCP were achieved at frequencies 20-30% lower than the natural frequency of the tested models, with a further low shift in frequency compared to the work carried out by Knott and Flower (1979).

It was found that the response of the device is affected by both water depth and submersion depth, with higher RAO obtained for deeper water conditions and lower submersion. The ideal conditions for 1/40 scale tests were obtained with $h = 0.13\,m$ and $d_s = 0.065\,m$. Through the analysis of the the motion of the water column OWCP it was possible to see that high RAOs do not correspond directly to higher delivery heights. It was therefore chosen to investigate the delivery of the OWCP25, OWCP30 and OWCP35.

The removal of water was carried out for the aforementioned devices. The models were installed on a low-reflective structure replicating a rubble mound breakwater. Different freeboard heights were considered. Removal tests showed a predominance of the OWCP25 and OWCP30 model with up to 14% of incident wave energy being converted into useful potential energy.

Water removal was achieved for $h_r = 0.05\,m$ and $h_r = 0.06\,m$, corresponding respectively to freeboards height of $h_r = 2\,m$ and $h_r = 2.4\,m$ at full scale, as declared in the objectives of this research.

The removal of water was found to be be dependent on the interaction of different experimental parameters h, d_s, h_r, H, K_r and f. Non-linearities were found to affect the efficiency

of the OWCP, confirming the hypothesis of Knott and Flower (1979) of a complex mechanism involved in the water removal for overtopping OWC devices.

In particular, in contrast with the work of Knott and Flower (1979) the removal of water was found to be dependent on the incoming wave height, especially when h_r was increased. As a result, h_r plays a fundamental role in the performances of the OWCP, affecting the frequencies at which removal is obtained; confirming the assumptions presented in Chapter 4 that the force associated with the PTO affects the response of the OWCP. It is therefore possible to use h_r as a resonance control parameter of the OWCP, to generate response for varying wave conditions. Reduced water depths were seen to play a de-tuning effect on the frequencies for which maximum efficiencies were obtained, with the performances of the OWCP being sensibly reduced for lower water depths, as in the case of the SIBEO (Czitrom et al.,2000).

With regards to the theoretical work of Knott and Flower (1979), it was found that the OWCP works effectively in a limited ranges of h_r and d_s when installed within a fixed structure and couple with a reservoir for collection of the removed mass. However, the presence of the OWCP on an coastal defence structure was found to further reduce the energy impacting the structure due to absorption and conversion of part of the incident energy.The efficiency values of the OWCPs are small compared to those obtained from other WECs convertes, indicating that the device may found its applications for water delivery purposes. Experimental results obtained from the testing of the OWCP led to the validation of the mathematical models developed; allowing for full scale prediction of the performances of the OWCP.

9.2.3.2 Array installation of the OWCP

In order to increase the performances of the OWCP and the delivery of water into the reservoir the installation of multiple OWCPs in array configurations was considered. From the literature review it was found that the separation distance s_d is a fundamental factor in the determination of the performances of the array, however till now its role has been mainly assessed through mathematical simulations. In our experiments, array performances for configurations of three differently tuned OWCPs were investigated for different values of s_d.

The response of the OWCP models was found to be related to the separation distance with higher RAOs obtained for lower separation distances. It was seen that the response was maximum when $s_d = 0\,mm$. RAOs decrease up to 14% are expected by increasing the s_d of 15 mm, with a further reduction when $s_d = 30\,mm$. The RAO of each component of the array was lower

than in the case of the same model working independently. It was seen that using differently tuned devices allow the array to respond to a wider range of wave frequencies without the need of implementing a resonance control system. From a spectral analysis it was determined that the devices respond to the incoming wave with a different phase; reducing the destructive effect generated by the radiated wave generated by the downward motion of the water exiting each model. The performances of the central device in the array are favourably affected both in terms of RAO and in terms of efficiency compared to the OWCP models installed on the side.

The efficiencies of removal of the 25-30-35^r array configuration were determined for $s_d = 10\,mm$ and $s_d = 45\,mm$. Tests showed significant interferences between the devices for small separation distances with the central device, OWCP30, being positively affected and outperforming the side devices. Lower efficiencies for outer components of the array agreed with the experimental findings presented by Weller et al. (2009) for a 4×3 array of heaving WECs.

Through the determination of the q factor it was possible to identify if positive effects on the performances of the array took place for the geometrical layout investigated. The results presented by Babarit (2010) showed that values of $q > 1$ were possible for closely spaced heaving and surging devices., with the quality factor being dependent on the wave frequency.

Results showed that for $0.83 \leq f \leq 0.9$ values of $q > 1$ were achieved by the array when $s_d = 45\,mm$. The quality factor was modified to include the role of the incident waves and expressed in terms of efficiency.

It was found that higher q_e were obtained for $s_d = 45\,mm$ for lower wave frequencies, in agreement with the work carried by Weller et al. (2009).

The possibility of generating positive effects from an array of differently tuned devices proved that it is possible to employ multiple OWCPs simultaneously to increase delivery of water without the need of a resonance control system. However, as the showed by Falcao (2002), by implementing a resonance control system it will be possible to further increase the output generated by the array.

The array tests showed that a positive effect between each array component can be achieved if the s_d between the devices is optimised. For the cases under investigation this was found to be $s_d = 0.045\,m$ with an overall array efficiency reaching a maximum of 16% at lower frequencies. The layout of the array could hampered the performances of each single device with values of efficiency dropping to 1% and below.

In conclusion it can be said that the overall array performance could be improved by the

chosen layout and that careful investigations are need to optimise the geometrical layout of the array.

9.2.4 Mathematical modelling

Two mathematical models have been implemented to describe and predict the behaviour of the OWCP. The models used the data obtained from the forced oscillation tests to include the radiation damping and added mass term in their formulation, allowing for the models to be validated against experimental results.

Good agreement was observed between experimental data when compared with simulation results from the non-linear model. It was found that the response of the OWCP was affected by non-linear forces and their inclusion in the mathematical model improved the accuracy obtained.

The simulations provided an indication of the RAO expected for the case tested, thus showing a larger a bandwidth response compared to our experimental results. The decrease in the RAO noticed in the experimental tests was not matched by the numerical simulation, indicating an under-estimation of the damping coefficients. Through a spectral analysis of the experimental tests, it was noticed that non-linear effects took place in the wave flume and affected the response of the device; particularly for low wave frequencies generated in the 2D Narrow Wave Flume.

Mathematical simulations of the behaviour of the OWCP expressed with regards to the mass removed from the OWCP and conversion efficiency showed good agreement with experimental data; albeit presenting a larger bandwidth compared to physical testing results. The non-linear model was found to forecast with good accuracy the efficiency of the device for the different configurations and to provide an good estimate of the mass of water that could be removed from the OWCP.

The non-linear model was employed to assess the influence of parameters such as the removal height on the performances of the devices. In section 6.6 it was shown that a low value of h_r would assure a higher water delivery; but would not assure that the device is performing at peak efficiency. The good agreement found between mathematical simulation and experimental results allowed evaluation of the performances of the OWCP at full scale.

The numerical models developed in this work could be further implemented to increase the accuracy of the simulations. In section 6.5 it was shown that including non-linear wave terms in the model increased the agreement with experimental data. It is therefore necessary to include reflection terms generate by the rubble mound and assess the non-linear development of waves in

the proximity of the OWCP. Further improvements to the numerical models could be obtained by addressing variations of damping coefficients due to different incoming wave frequencies.

9.2.5 Full scale performances of the OWCP

The non-linear mathematical model developed in chapter 4 and validated in section 6.5 was employed to assess the performances of the OWCP at full scale. The performances of the OWCP were simulated for a device installed at a location in the North Sea under the influence of irregular waves. In chapter 8 an estimate of $9 \times 10^9\, kg$ of water delivered per year by the OWCP25 was estimated for $h_r = 1.4\, m$ and $d_{OWCP} = 1\, m$. The corresponding efficiency obtained for the OWCP25 was of 2.45%, despite the device obtaining efficiencies of over 16% for given sea states. conditions. The design of the OWCP could be altered in order for the device to respond to different sea states and enhance both water delivery and efficiency.

The performances of the OWCP are significantly lower compared to other WECs such as the Wave Dragon ($\eta = 18\%$) and the SSG ($\eta = 10 - 25\%$); suggesting that the device should be employed for the delivery of water to enclosed area such as marina to facilitate water circulation.

9.2.6 Applications of the OWCP

9.2.6.1 Marina flushing

The OWCP is designed to deliver water and to be installed over existing coastal defence structures such as rubble mound breakwater. These structures are often found in the proximity of enclosed harbours where water circulation is minimised. In such enclosed spaces, the quality of water could be reduced due to the increase of pollutants and engineering methods such as flushing culverts. These factors have already been assessed to reduce cleaning time of harbours and reduce the concentrations of pollutants. The possibility of delivering water into enclosed area, represents a possible application of the OWCP to exploit wave energy and to reduce the concentration of contaminants in harbours and marinas.

As seen in chapter 8 a single OWCP with $d_{OWCP} = 1\, m$ could deliver up to $9 \times 10^6\, m^3$ of water in the reservoir, increasing the supply of water in the enclosed basin. The yearly estimate delivery of mass of a full scale OWCP is in the same order of magnitude of the one obtained for the SIBEO device ($6 \times 10^3\, m^3/year$), whilst providing a simpler system as presented in section 4.1

9.2.6.2 Wave driven desalination

The possibility of employing the OWCP for wave driven desalination has been evaluated. A high pressure pump was developed in order to collect the water delivered from the OWCP, and exploit the potential energy to generate the pressure required to drive a reverse osmosis membrane. An initial feasibility study, shown in Appendix D, was carried out highlighting the low-cost and advantages of such a system for the developing communities near the coasts. Such a system could be employed in areas where generating desalted water is of primary importance and the efficiency of conversion of the OWCP does not constitute a limiting factor.

9.3 Concluding Remarks

With reference to the the Aims and the Objectives presented in sections 1.3 and 1.4, the followings can be stated:

- A suitable Wave Energy Converter was identified in the Oscillating Water Column device to be implemented for water delivery. The Oscillating Water Column Wave Pump was therefore developed and its performances investigated.
- Experimental tests showed that the OWCP can be employed as a WEC for the delivery of water for the generation of more than a 2 m of hydraulic head through the conversion of the energy contained within incident wave fields.
- The efficiency of removal of the OWCP is dependent on the freeboard height h_r and on the type of coastal structure upon which it is installed.
- According to the configuration of the OWCP and to the freeboard height, efficiency in conversion of up to 14% can be achieved under the influence of regular waves conditions. This could be further improved through optimisation of the design of the OWCP.
- The employment of physical tests allowed for the inclusion of beach-effects on the performances of the device, and broadened the possibility of employment of small-scale tests for array installation.
- The interactions of multiple OWCP installed in array configuration generated positive effects on the response of the device. Similar effects are expected when standard OWC devices are installed with a low separation distance between the devices.

- The assessment of the performances of the OWCP at full scale indicates that, despite low efficiency in conversion for irregular wave conditions (2.45%), the device should be employed for water delivery purposes.
- The estimate yearly amount of water delivered from the OWCP ($9 \times 10^9\, kg$) indicate that the OWCP could find its application for the flushing of enclosed areas.

9.4 Recommendations for Further Research

- The experimental program was aimed to assess the validity of the OWCP concept and to evaluate the removal of water from the device. Further experiments are required in order to maximise the installation configuration of the OWCP in terms of submersion depth, freeboard height and slope of the rubble mound. Ideally this should provide the possibility of further enhancing the performances of the devices. The application of the aforementioned tests at a higher scale will allow the use of load cells for the monitoring of the removal ratio and provide the response of the device for each incident wave.
- In order to optimise the mathematical model of the OWCP, the use of BEM tests for the determination of the hydrodynamic coefficients of the OWCP is recommended. This should allow to consider the changes of the radiation damping and added mass with the incoming wave frequency and provide higher accuracy in the simulation.
- Additional optimisation of the OWCP design could be obtained by modifying the shape of the input duct of the device in order to reduce vortex formation and drag forces in front of the device. A 7^{o} degree funnel-shaped input duct is suggested following review of existing studies.
- To better quantify and assess the interaction between the different devices installed in the array configuration, the use of surface Particle Imaging Velocimetry (PIV) is recommended. This should show the modification of the wave field in front of the array and between the models. The use of a 1:20 scale is recommended for PIV tests.
- Evaluation of the possible applications of the OWCP through a thorough analysis of the flowrate of delivery under regular and irregular seastates, is required to further implement the assessment of the performances of the OWCP.

References

Airy, G. (1845). On the laws of the tides on the coasts of ireland, as inferred from an extensive series of observations made in connexion with the ordnance survey of ireland, *Philosophical Transactions of the Royal Society of London* **1**: 124.

Alexandre, A., Stallard, T. and Stansby, P. (2010). Wave field modification due to a wec array., *Coastlab - Third International Conference on the Application of Physical Modelling to Port and Coastal Protection, Barcelona, Spain*.

ASCE (1990). *Charts for the Hydraulic Design of Channels and Pipes*, American Society of Civil Engineers.

Babarit, A. (2010). Impact of long separating distances on the energy production of two interacting wave energy converters, *Ocean Engineering* **In Press, Corrected Proof**: –.
URL: *http://www.sciencedirect.com/science/article/B6V4F-4YC1KCF-1/2/5767f93fd49491ebe5f577f9cf463fc1*

Babarit, A. and Clement, A. H. (2006). Optimal latching control of a wave energy device in regular and irregular waves, *Applied Ocean Research* **28**(2): 77–91. doi: DOI: 10.1016/j.apor.2006.05.002.

Battjes, T. (1974). Surf similarity, *Proceedings of 14th Coastal Engineering Conference, Copenhagen, Denmark, American Society of Civil Engineers, New York*.

Bjarte-Larsson, T. and Falnes, J. (2006). Laboratory experiment on heaving body with hydraulic power take-off and latching control, *Ocean Engineering* **33**(7): 847–877. doi: DOI: 10.1016/j.oceaneng.2005.07.007.

Boccotti, P. (2004). A method to obtain the directional wave spectrum, *Ocean Engineering* **31**(5-6): 539–545. doi: DOI: 10.1016/j.oceaneng.2003.10.002.

Boccotti, P. (2007). Caisson breakwaters embodying an owc with a small opening–part i: Theory, *Ocean Engineering* **34**(5-6): 806–819. doi: DOI: 10.1016/j.oceaneng.2006.04.006.

Boccotti, P., Filianoti, P., Fiamma, V. and Arena, F. (2007). *Ocean Engineering* **34**(5-6): 820–841. doi: DOI: 10.1016/j.oceaneng.2006.04.016.

Brendmo, A., Falnes, J. and Lillebekken, P. M. (1996). Liner modelling of oscillating water columns including viscous loss, *Applied Ocean Research* **18**(2-3): 65–75. doi: DOI: 10.1016/0141-1187(96)00011-9.

Brito-Melo, A. (2000). *Modelação e Pré-dimensionamento de Centrais de Coluna de Água Oscilante:Aplicação à Central de Energia das Ondas do Pico, Açores. (Modelling and Design of Oscillating Water Column Devices: Application to the Wave Power Plant, at Pico, Azores.)*, PhD thesis, Universidad Tecnica de Lisboa, Instituto Superior Tecnico.

Brito-Melo, A., Castro, R. A. and Sarmento, A. (2003). The estimation of the diffraction flow from sea trials measurements in owc plants, *in* P. o. t. t. E. W. E. Conf. (ed.), *5th European Wave Energy Conference*, Cork ,Ireland.

Brito-Melo, A., Sarmento, A., Clement, A. and Delhommeau, G. (1999). A 3d boundary element code for the analysis of owc wave-power plans, *in* P. I. S. O. Engineering and Polar (eds), *ISOPE '99*.

Brooke, J. (2003). *Wave Energy Conversion*, Vol. 6 of *Elsevier Ocean engineering Book Series*.

Bruun, P. M. and Viggosson, G. (1977). The wave pump: Conversion of wave energy to current energy, *Journal of the Waterway, Port, Coastal and Ocean Division, Proceedings of the American Society of Civil Engineers* **103**(4): 449–469. Compilation and indexing terms, Copyright 2008 Elsevier Inc.77120006400WAVE ENERGYENERGY CONVERSIONWAVE PUMPSWAVE PROPAGATION.

Budar, K. and Falnes, J. (1975). A resonant point absorber of ocean-wave power, *Nature* **256**(5517): 478–479. 10.1038/256478a0.

Callaghan, D. P., Nielsen, P., Cartwright, N., Gourlay, M. R. and Baldock, T. E. (2006). Atoll lagoon flushing forced by waves, *Coastal Engineering* **53**(8): 691–704.

Chadwick, A. and Morfett, J. (1998). *Hydraulics in Civil and Environmental Engineering*, E&FN Spon.

Chaplin, J., Farley, F., Prentice, M., Rainey, R., Rimmer, S. and Roach, A. (2007). Development of the anaconda all-rubber wec, *in* P. of the 7th European Wave and L. Tidal Energy Conference (eds), *European Wave and Tidal Energy Conference, Lisbon*, Lisbon, Portugal.

Chung, D. H. (2008). Water oscillation in an open tube, *ISB Journal of Physics* **2**(1).

Clerc, C. and Clerc, P. (2003). *Physisque Mécanique MPSI - Course Méthodes et Exercises Résolus*, Breal.

Count, B. M. (1978). On the dynamics of wave-power devices, *Proceedings of the Royal Society of London. A. Mathematical and Physical Sciences* **363**(1715): 559–579.

Cruz, J. (2008a). Numerical and experimental modelling of wecs, *in* J. Cruz (ed.), *Ocean Wave Energy*, Springer, New Yourk.

Cruz, J. (2008b). *Ocean Wave Energy. Current Status and Future Prespectives*, Green Energy and Technology.

Cruz, J. and Salter, S. (2006). Numerical and experimental modelling of a modified version of the edinburgh duck wave energy device, *Proceedings of the Institution of Mechanical Engineers, Part M: Journal of Engineering for the Maritime Environment* **220**(3): 129–147. 10.1243/14750902JEME53.

Curran, R. and Folley, M. (2008). *Air Turbine Design for the OWC in "Ocean Wave Energy: current status and future perspectives"*, Springer, chapter 6, pp. 189–219.

Czitrom, S. P., Coronado, C. and Nunez, I. (2006). Flushing of the port of ensenada using a sibeo wave-driven seawater, *9th Pan American Congress of Applied Mechanics (PACAM 9)*, Mathematical Science Publ, Merida, MEXICO, pp. 1459–1469. ISI Document Delivery No.: 308RDTimes Cited: 0Cited Reference Count: 29Peter Czitrom, Steven Coronado, Cesar Nunez, Ismael.

Czitrom, S. P. R. (1997). Wave energy-driven resonant sea-water pump, *Journal of Offshore Mechanics and Arctic Engineering* **119**(3): 191–195.

Czitrom, S. P. R., Godoy, R., Prado, E., Olvera, A. and Stern, C. (2000). Hydrodynamics of an oscillating water column seawater pump. part ii: tuning to monochromatic waves, *Ocean Engineering* **27**(11): 1199–1219.

Czitrom, S. P. R., Godoy, R., Prado, E., Perez, P. and Peralta-Fabi, R. (2000). Hydrodynamics of an oscillating water column seawater pump: Part i: theoretical aspects, *Ocean Engineering* **27**(11): 1181–1198.

Davies, P. A. (2005). Wave-powered desalination: resource assessment and review of technology, *Desalination* **186**(1-3): 97–109.

Dean, R. G. and Dalrymple, R. (1990). *Water Wave Mechanics for engineers and scientists*, Vol. 2 of *Advanced Series on Ocean Engineering*, World Scientific, New York.

Delaure, Y. (2001). *A hydrodynamic investigation of Oscillating Water Column Wave Energy Converters*, PhD thesis, Hydraulics and Maritime Research Centre, Depeartment of Civil Engineering, University College Cork.

Delaure, Y. M. C. and Lewis, A. (2003). 3d hydrodynamic modelling of fixed oscillating water column wave power plant by a boundary element methods, *Ocean Engineering* **30**(3): 309–330.

Dhinakaran, G., Sundar, V., Sundaravadivelu, R. and Graw, K. U. (2002). Dynamic pressures and forces exerted on impermeable and seaside perforated semicircular breakwaters due to regular waves, *Ocean Engineering* **29**(15): 1981–2004. Compilation and indexing terms, Copyright 2008 Elsevier Inc.02327047115Wave energyWater depth.

El Marjani, A., Castro Ruiz, F., Rodriguez, M. A. and Parra Santos, M. T. (2008). Numerical modelling in wave energy conversion systems, *Energy* **33**(8): 1246–1253. doi: DOI: 10.1016/j.energy.2008.02.018.

EMEC (2009). Tank testing of wave energy conversion systems, *Technical report*, EMEC.

Evans, D. V. (1976). A theory for wave-power absorption by oscillating bodies, *Journal of Fluid Mechanics Digital Archive* **77**(01): 1–25.

Evans, D. V. (1978). Oscillating water column wave-energy device, *Journal of the Institute of Mathematics and Its Applications* **22**(4): 423–433.

Evans, D. V. (1981). Power from water waves, *Annual review of fluid mechanics. Vol.13*, Annual Reviews Inc, Palo Alto, CA, USA, pp. 157–87. Copyright 1982, IEE1825120water waveshydrodynamic propertiesidealized devicesirregular wavesenergy-absorbing structuresclassical linearized water-wave theorylinear body dynamicsbody boundary conditionslinearized equationsnonlinear power take-off systemwave power extraction.

Evans, D. V. (1982). Wave-power absorption by systems of oscillating surface pressure distributions, *Journal of Fluid Mechanics Digital Archive* **114**(-1): 481–499.

Evans, D. V. and Porter, R. (1995). Hydrodynamic characteristics of an oscillating water column device, *Applied Ocean Research* **17**(3): 155–164.

Evans, D. V. and Porter, R. (1997). Efficient calculation of hydrodynamic properties of owc-type devices, *Journal of Offshore Mechanics and Arctic Engineering* **119**(4): 210–218.

Falcao, A. F. (2002). Wave-power absorption by a periodic linear array of oscillating water columns, *Ocean Engineering* **29**(10): 1163–1186. doi: DOI: 10.1016/S0029-8018(01)00076-2.

Falcao, A. F. d. O. (2008). The development of wave energy utilisation, *Technical report*, International Energy Agency - Ocean Energy Systems.

Falnes, J. (1993). Optimum control of oscillation of wav-energy converters, *Technical report*, European Union.

Falnes, J. (2003). *Ocean waves and Oscillating systems*, Cambridge University Press, 40 West 20th Street, New York, New York 1011-4211, U.S.A. doi: DOI: 10.1016/S0029-8018(02)00070-7.

Faltinsen, O. (1990). *Sea Loads on Ships and Offshore Structures*, Cambridge Ocean Technology Series.

Filianoti, P. and Camporeale, S. M. (2008). A linearized model for estimating the performance of submerged resonant wave energy converters, *Renewable Energy* **33**(4): 631–641. doi: DOI: 10.1016/j.renene.2007.03.018.

Finavera (2010). Acquabuoy wave energy technology, online.
URL: *http://finavera.com/en/wavetech/*

Flocard, F. and Finnigan, T. (2010). Laboratory experiments on the power capture of pitching vertical cylinders in waves, *Ocean Engineering* **37**: 989.

Folley, M. (2008). Alternative applications: Desalination, *in* J. Cruz (ed.), *Ocean Wave Energy. Current status and future prespectives*, Green energy and technology, Springer, Berlin.

Folley, M., Penate Suarez, B. and Whittaker, T. (2008). An autonomous wave-powered desalination system, *Desalination* **220**(1-3): 412–421. doi: DOI: 10.1016/j.desal.2007.01.044.

Folley, M. and Whittaker, T. (2009). The cost of water from an autonomous wave-powered desalination plant, *Renewable Energy* **34**(1): 75–81. doi: DOI: 10.1016/j.renene.2008.03.009.

Forestier, J., Holmes, B., Barret, S. and Lewis, A. (2007). Value and validation of small scale physical model test of floating wave energy converters.

Franco, L. (1996). Ancient mediterranean harbours: a heritage to preserve, *Ocean & Coastal Management* **30**(2-3): 115–151.

Frigaard, P. and Brorsen, M. (1995). A time-domain method for separating incident and reflected irregular waves, *Coastal Engineering* **24**(3-4): 205 – 215.
URL: *http://www.sciencedirect.com/science/article/B6VCX-3YCN1HJ-2/2/1f5c21a458d04168f4f6bad129b7d05d*

Godoy-Diana, R. and Czitrom, S. P. R. (2007). On the tuning of a wave-energy driven oscillating-water-column seawater pump to polychromatic waves, *Ocean Engineering* **34**(17-18): 2374–2384.

Graw, K. U. (1996). Wave energy breakwaters - a device comparison, *CONFERENCE IN OCEAN ENGINEERING - COE'96*, Madras, INDIA.

Hagerman, G. (2002). Wave energy systems for recharging auv energy supplies, *Autonomous Underwater Vehicles, 2002. Proceedings of the 2002 Workshop on*, pp. 75–84.

Hamill, L. (2001). *Understanding Hydraulics*, Palgrave.

Heath, T. (2008). *Ocean Wave Energy: Current status and future perspective*, Spri, chapter 7. Full Scale - Limpet, pp. 287–295.

Hedges, T. (1989). Wave breaking and reflection.

Hicks, D. C., Mitcheson, G. R., Pleass, C. M. and Salevan, J. F. (1989). Delbouy: Ocean wave-powered seawater reverse osmosis desalination systems, *Desalination* **73**: 81–94. doi: DOI: 10.1016/0011-9164(89)87006-7.

Holmes, B. (2003). Ocean wave energy: Development and evaluation protocol, part 1: Wave power, *Technical report*, HMRC.

Hotta, H., Washio, Y., Yokozawa, H. and Miyazaki, T. (1996). R&d on wave power device mighty whale, *Renewable Energy* **9**(1-4): 1223 – 1226. World Renewable Energy Congress

Renewable Energy, Energy Efficiency and the Environment.
URL: *http://www.sciencedirect.com/science/article/B6V4S-3VTSS54-9D/2/76d864f1cf9d8b352a6d499c52e5c7ff*

Houghtalen, R., Hwang, N. and Akan, A. (1996). *Fundamentals of Hydraulic Engineering Systems*, Prentice Hall.

Hughes, S. (1993). *Physical models and laboratory techniques in coastal engineering*, Vol. 7 of *Advanced series on coastal engineering*, World Scientific, New York.

ICOE (2010). Official programme of icoe 2010 bilbao, http://www.icoe2010bilbao.com/ing/programa.aspx.
URL: *http://www.icoe2010bilbao.com/ing/programa.aspx*

Isaacs, J. and Schimtt, W. (1980). Ocean energy: forms and prospects, *Science* **207**: 265–273.

Josset, C., Babarit, A. and Clement, A. (2006). A wave-to-wire model of the searev wave energy converter, *Proceedings of the Institution of Mechanical Engineers Part M Journal of Engineering for the Maritime Environment* **221, 2**: 81–93.

Josset, C. and Clement, A. (2007). A time-domain numerical simulator for oscillating water column wave power plants, *Renewable Energy* **32**: 1379.

Knott, G. F. and Flower, J. (1979). Simulation studies of the basic non-linear effects of wave-energy conversion by an overtopping water-column, *Energy Conversion and Management* **19**(1): 11.

Knott, G. F. and Flower, J. (1980). Measurement of energy losses in oscillatory flow through a pipe exit, *Applied Ocean Research* **2**: 155–164.

Kofoed, J. (2002). *Wave Overtopping of Marine Structures Utilization of Wave Energy*, PhD thesis, Hydraulics Coastal Engineering Laboratory, Department of Civil Engineering, Aalborg University, Denmark.

Kofoed, J. P., Frigaard, P., Friis-Madsen, E. and SÃ¸rensen, H. C. (2006). Prototype testing of the wave energy converter wave dragon, *Renewable Energy* **31**(2): 181–189. doi: DOI: 10.1016/j.renene.2005.09.005.

Koo, W. and Kim, M. (2010). Nonlinear time-domain simulation of a land-based oscillating water column, *Journal of Waterway, Port, Coastal, and Ocean Engineering* **136**: 276–284.

Koola, P. M., Ravindran, M. and Narayana, P. A. A. (1995). Model studies of oscillating water column wave-energy device, *Journal of Energy Engineering-Asce* **121**(1): 14–27.

Lee, C., J.N., N. and F.G., N. (1996). 'wave interactions with an oscillating water column", *Proceedings International Offshores and Polar Engineering Conference.*

Lighthill, M. J. (1979). Two-dimensional analysis related to wave-energy conversion by submerged resonant ducts, *Journal of Fluid Mechanics* **91**: 253.

Liu, Y. and Bergdahl, L. (1999). Motion of an owc in the time domain. Private Communication between Delaure, Y. and Liu Y. and Bergdahl, L. at Chalmers University of Techonology, Sweden.

Lopes, M. F. P., Hals, J., Gomes, R. P. F., Moan, T., Gato, L. M. C. and Falcao, A. F. d. O. (2009). Experimental and numerical investigation of non-predictive phase-control strategies for a point-absorbing wave energy converter, *Ocean Engineering* **36**(5): 386–402. doi: DOI: 10.1016/j.oceaneng.2009.01.015.

Maciel, J. (2009). Implementation of a breakwater integrated owc power plant in portugal, *Technical report*, EDP.

Margheritini, L., Vicinanza, D. and Frigaard, P. (2008). Sea slote cone generator overtopping performace in 3d conditions., *International Offshore and Polar Engineering Conference, ISOPE, number 18, ISSN 1098-6189, Vancouver, Canada.*

Margheritini, L., Vicinanza, D. and Frigaard, P. (2009). Ssg wave energy converter: Design, reliability and hydraulic performance of an innovative overtopping device, *Renewable Energy* **34**(5): 1371 – 1380.
URL: *http://www.sciencedirect.com/science/article/B6V4S-4TTNCB6-2/2/7f87d456690c101551b61b86023ee036*

Masuda, Y., Kuboki, T., Ravindrum, M., Pathak, A. G., Jayashankar, V. and Xianguang, L. (1986). Development of backward bent duct buoy (bbdb), *in* I. S. of Offshore and P. Engineers (eds), *Ninth (1999) international offshore and polar engineering conference*, Brest (France).

McCabe, A. (2004). An appraisal of a range of fluid modelling software, *Technical report*, Supergen Marine Workpackage 2.
URL: *http://www.supergen-marine.org.uk/drupal/files/reports/McCabe2004.pdf*

McConnel, K. (1998). *Revetment systems against wave attack - A design Manual*, Thomas Telford.

McCormick, M. E. (1981). *Ocean Wave Energy Conversion*, 2 edn, Wiley, New York.

McIver, P. (2002). Wave interaction with arrays of structures, *Applied Ocean Research* **24**(3): 121–126. doi: DOI: 10.1016/S0141-1187(02)00034-2.

Mehlum, E. (1986). *Hydrodynamics of Ocean Wave Energy Utilization*, Springer, chapter Tapchan, pp. 51–55.

Mei, C. (1976). Power extraction from water waves, *Journale of Ship Research* **20(2)**: 63–66.

Mei, C. (1989). *The applied dynamics of ocean surface waves*, World Scientific.

Mei, C. (2009). Comparison of wave power extraction by a compact array of small buoys and by a large buoy, *in* EWTEC (ed.), *European Wave and Tidal Energy Conference, Uppsala, Sweden.*

Morris-Thomas, M. T., Irvin, R. J. and Thiagarajan, K. P. (2007). An investigation into the hydrodynamic efficiency of an oscillating water column, *Journal of Offshore Mechanics and Arctic Engineering* **129**(4): 273–278.

Murphy, B. (1996). Report on proceeding of ocean wave energy colloquim held at trinity college dublin held on 30 september 1996. Private Communication.

Neumann, F., Brito-Melo, A., Didier, E. and Sarmento, A. (2007). Pico owc recovery project: Recent actvities and performance data, *in* EWTEC (ed.), *European Wave and Tidal Energy Conference*, EWTEC, Porto, Portugal.

Newman, J. (1992). Panel methods in marine hydrodynamics, *Proc. 11th Australasian Fluid Mechanics Conference, Hobart, Australia.*

Newman, J. N. (1974). Interaction of water waves with two closely spaced vertical obstacles, *Journal of Fluid Mechanics Digital Archive* **66**(01): 97–106.

Newman, J. N. (1977). *Marine Hydrodynamics*, MIT press.

Olvera, A., Prado, E. and Czitrom, S. (2007). Parametric resonance in an oscillating water column, *Journal of Engineering Mathematics* **57**(1): 1–21.

OPT (2010). Autonomous power system - power buoy.
URL: *http://www.oceanpowertechnologies.com/power.htm*

Payne, G. (2006). *Numerical modelling of a sloped wave energy device*, PhD thesis, University of Edinburgh.

Perdigao, J. and Sarmento, A. (2003). Overall-efficiency optimisation in owc devices, *Applied Ocean Research* **25**(3): 157–166.

Previsic, M., Bedard, R. and Hagerman, G. (2004). Offshore wave energy conversion devices., *Technical report*, Electric Power Research Institute (EPRI).

Reitan, A. (1991). Wave-power absorption by an oscillating water column, *Physica Scripta* (1): 60.

Rugbierg, M. and Nielsen, K. (1999). Mapping of wave energy conditions in the danish scetor of the north sea, *Technical report*, Danish Energy Agency.

Salter, S. (1974). Wave power, *Nature* **249**.

Sharmila, N., Jalihal, P., Swamy, A. K. and Ravindran, M. (2004). Wave powered desalination system, *Energy* **29**(11): 1659–1672.

SPPL (2010). The ceto wave energy device, www.carnegiewave.com. last accessed 01-02-2010.

Stagonas, D. (2010). Wave loadings on coastal structures. Lecture notes for the course "Coastal and Maritime Engineering and Energy".

Svendsen, I. A. (2006). *Introduction to nearshore hydrodynamics*, Vol. 24 of *Advanced Series on Ocean Engineering*, Hackensack, Singapore.

Sykes, R., Lewis, A. and Thomas, G. (2007). A physical and numerical study of a fixed cylindrical owc of finite wall thickness, *in* EWTEC (ed.), *7th European Wave and Tidal Energy Conference*, EWTEC, Porto.

Tedd, J., Kofoed, J., Jasinski, M., Morris, A., Friis-Madsen, E., Wisniewski, R. and Bendtsen, J. (2006). Advanced control techniques for wec wave dragon, *Technical report*, Aalborg University.

Thiruvenkatasamy, K. and Neelamani, S. (1997). On the efficiency of wave energy caissons in array, *Applied Ocean Research* **19**(1): 61 – 72.
URL: *http://www.sciencedirect.com/science/article/B6V1V-3SN64T1-6/2/ba4f99ac91ba537eb78ffad12f58e806*

Thiruvenkatasamy, K., Neelamani, S. and Sato, M. (2005). Nonbreaking wave forces on multiresonant oscillating water column wave power caisson breakwater, *Journal of Waterway, Port, Coastal, and Ocean Engineering* **131**(2): 77–84.

Tjugen, K. J. (1995). Tapchan ocean wave energy project at java - updated project status, *in* L. Proceedings of the Second European Wave Energy Conference (ed.), *Second European Wave Energy Conference*, Lisbon, Portugal.

Torre-Enciso, Y., Ortubia, I., López de Aguileta, L. and Marqués, J. (2009). Mutriku wave power plant: from the thinking out to the reality, *in* EWTEC (ed.), *European Wave and Tidal Energy Conference, Uppsala, Sweden*.

U.S.D.E (2009). Marine and hydrokinetic technology database.
URL: *http://www1.eere.energy.gov/windandhydro/hydrokinetic/default.aspx*

Vennard, J. K. (1940). *Elementary Fluid Mechanics*, Braunworth & Co. Inc.

Verhulst, F. (2005). *Methods and Applications of Singular Perturbations: Boundary Layers and Multiple Timescale Dynamics.*, Springer.

Vicente, P., Falcao, A., Gato, L. M. C. and Justino, P. (2009). Dynamics of arrays of floating point-absorber wave energy converters with inter-body and bottom slack-mooring connections, *Applied Ocean Research* **31**: 267.

Vicinanza, D. and Frigaard, P. (2008). Wave pressure acting on a seawave slot-cone generator, *Coastal Engineering* **55**(6): 553 – 568.
URL: *http://www.sciencedirect.com/science/article/B6VCX-4S9RDGB-1/2/a0f87e8368df6bba5d76655ec5b83ae2*

Wamit, I. (2006). *Wamit User Manual*, versions 6.4, 6.4pc, 6.3s, 6.3s-pc edn. Copyright c 1998-2006 WAMIT, Incorporated and Massachusetts Institute of Technology. No part of the WAMIT software or documentation may be reproduced, translated, or transmitted in any form without the express written permission of WAMIT, Inc.

Wang, D. J., Katory, M. and Li, Y. S. (2002). Analytical and experimental investigation on the hydrodynamic performance of onshore wave-power devices, *Ocean Engineering* **29**(8): 871–885. doi: DOI: 10.1016/S0029-8018(01)00058-0.

WavePlane, I. (retrieved on 15 May 2009). www.waveplane.com.

Webber, J., Mouwer, F., Parish, A. and Robertson, D. (2009). Wavebob. research and development network and tools in the context of systsems engineering, *in* EWTEC (ed.), *European Wave and Tidal Energy Conference*.

Weber, J. and Thomas, G. (2001). An investigation into the importance o f the air chamber design of an oscillating water column wave energy device, *Proceedings o f the Eleventh (2001) International Offshore and Polar Engineering Conference, Stavanger, Norway, June 17-22, 2001*, The International Society o f Offshore and Polar Engineers.

Weller, S., Stallard, T. and Stansby, P. (2009). Experimental measurements of irregular wave interaction factors in closely spaced arrays, *Proceeding of the 8th European Wave and Tidal Energy Conference, EWTEC, Uppsala, Sweden*.

Whittaker, T. and Folley, M. (2007). The oyster wave energy converter., *in* Ewtec (ed.), *Seventh European wave and tidal energy conference*, 7.

www.guardian.co.uk (retrieved on May 6 2009). Anaconda wave-power generator snakes into next stage of production.

Yemm, R., Henderson, R. and Taylor, C. (2000). The pwp pelamis wec: Current status and on-ward programme., *Proc 4th European Wave Energy Conference.*, Aalborg, Denmark.

Young, I. (1999). *Wind generated ocean waves*, Vol. 2 of *Elsevier Ocean Engineering Series*, Elsevier, New York.

Appendix A

Additional Results

In this chapter additional results obtained from the experimental tests of the OWCP models are presented in the chapter.

A.1 OWCP25B

The following graphs refer to the tests carried in the Large Wave Flume with $\lambda = 20$. Figure A.1 and Figure A.2 present the RAO obtained from the testing of the OWCP25B. The maximum RAO is obtained for the shallow water case of testing with RAO =5.837 when $d_s = 0.14m$. The response bandwidth of the OWCP25B are presented in Figure A.3 and Figure A.4. It can be seen from Figure A.3 that the device persents two frequency/energy areas for which maximum RAO is achived. Both the shallow and deep water tests of the OWCP25B show that the device responds to higher frequency compared to the OWCP25 model tested in the narrow wave flume, indicating that the effects of viscous forces and angle bend are reduced at a bigger scale.

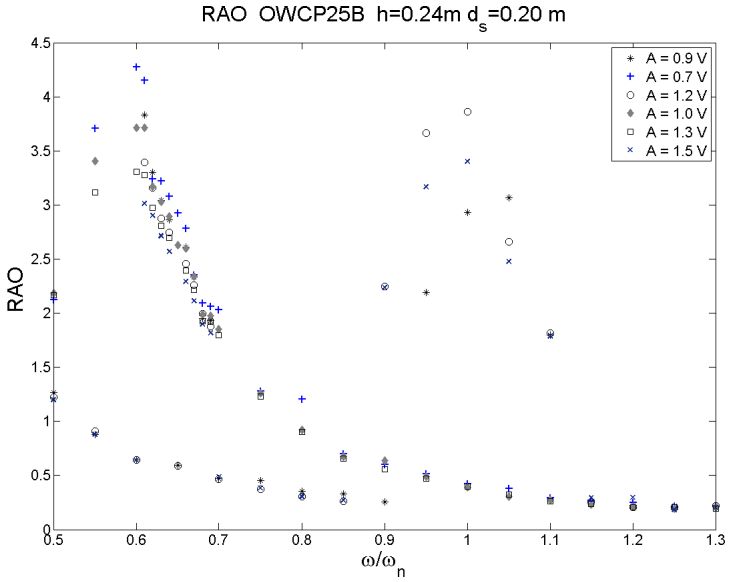

Figure A.1: RAO for the OWCP25B model with $h = 0.24$m and $d_s = 0.20m$. The RAOis presented for different amplitudes A of the wave paddle. It is possible to notice that the highest RAO obtained is of 4.273 for $\Omega = 0.6$. The device, shows a strong secondary pick for $\Omega = 1$ with $RAO = 3.86$

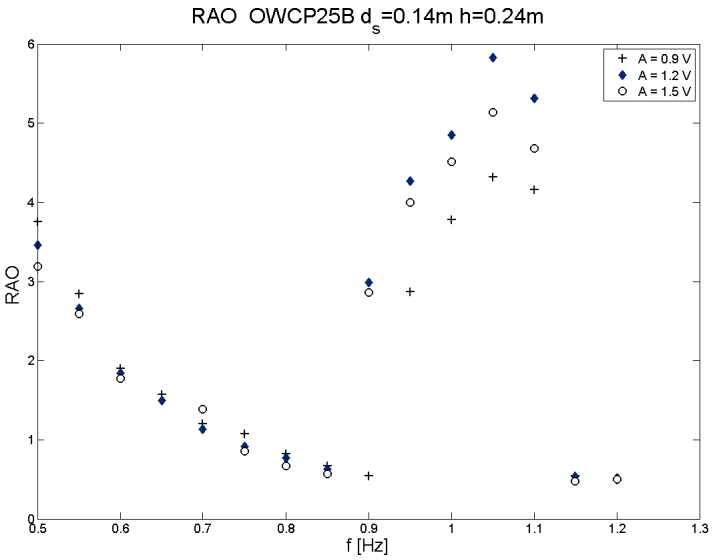

Figure A.2: RAO for the OWCP25B model with $h = 0.24$m and $d_s = 0.14m$. The RAOis presented for different amplitudes A of the wave paddle. It is possible to notice that the highest RAO obtained is of 5.827 for $f = 1.05$. Discontinuties in the RAO are noted for$f < 0.9$.

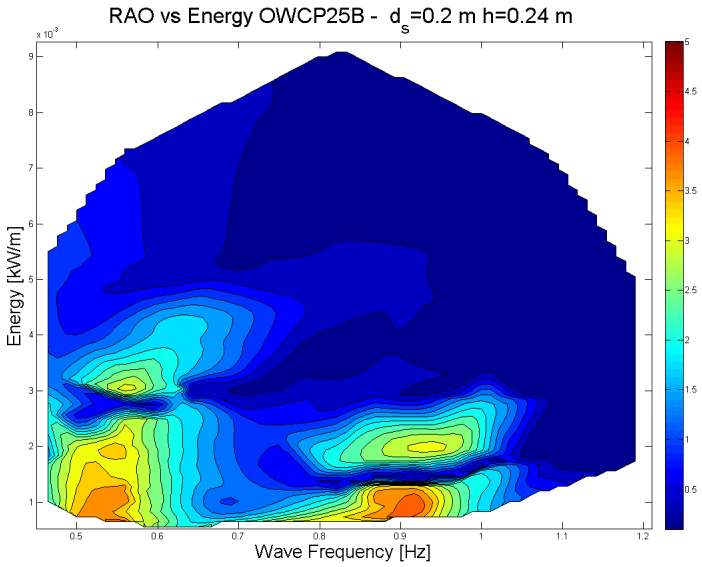

Figure A.3: . Response bandwitdh OWCP25B. The maximum response of the device is obtained for $0.5 < f < 0.6$ and for $0.85 \leq f \leq 0.95$.

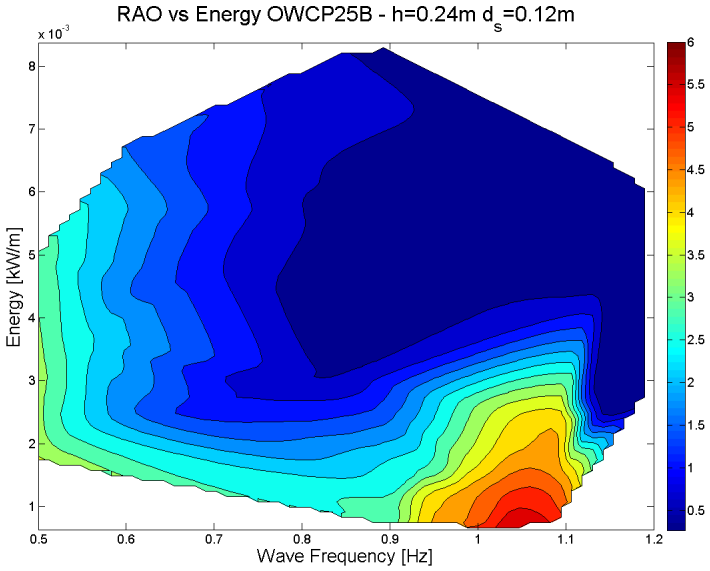

Figure A.4: . Response bandwitdh OWCP25B. The maximum response of the device is obtained for $1 < f < 1.1$.

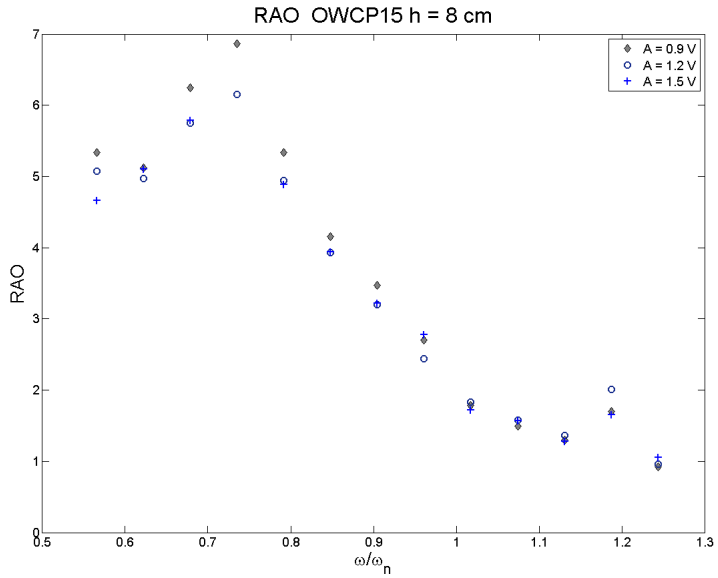

Figure A.5: RAO for the OWCP15 model with $h = 0.08$m and $d_s = 0.068m$. The RAO is presented for different amplitudes A of the wave paddle. It is possible to notice that the highest RAO obtained is of 6.863 for $\Omega = 0.735$. Tests carried in 3D wave basin.

A.2 OWCP15

In this section the RAO tests carried for the OWCP15 model are presented. The maximum RAO obtained for the device is 11.57 with the following installation conditions $h = 0.13\,m$, $d_s = 0.065\,m$ for $\Omega = 0.6135$ (Figure A.7).

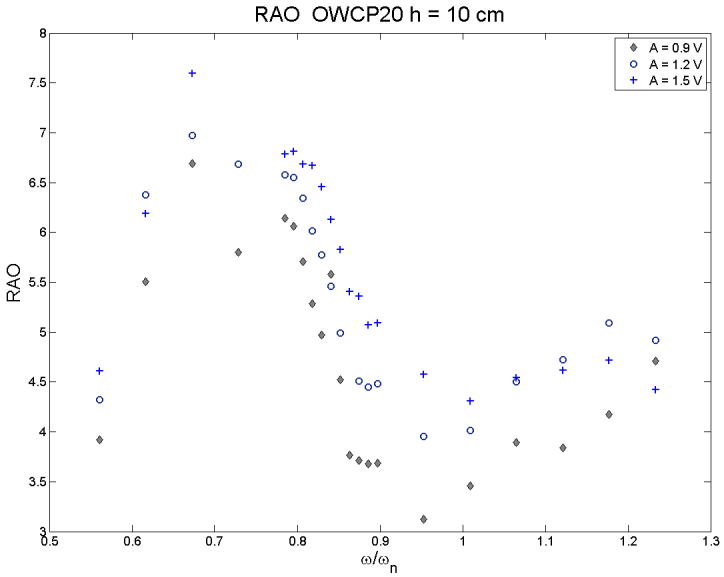

Figure A.6: RAO for the OWCP15 model with $h = 0.10$m and $d_s = 0.088m$. The RAO is presented for different amplitudes A of the wave paddle. It is possible to notice that the highest RAO obtained is of 1.697 for $\Omega = 0.7565$. Tests carried in 3D wave basin.

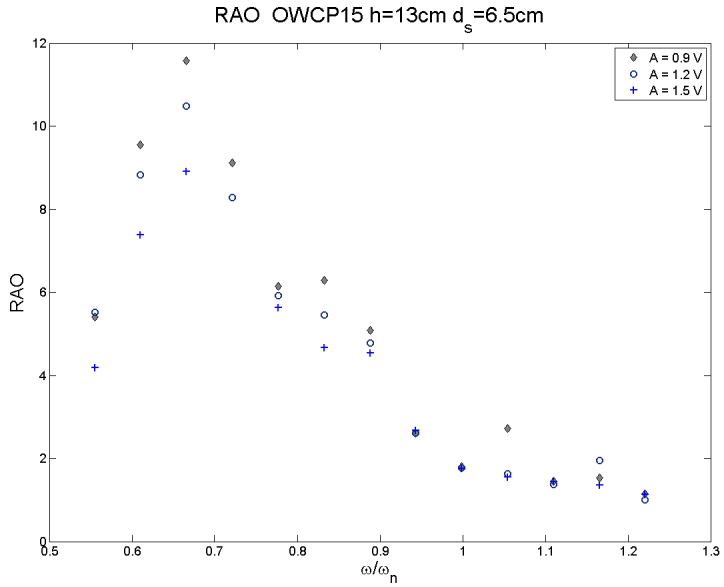

Figure A.7: RAO for the OWCP15 model with $h = 0.13$m and $d_s = 0.065m$. The RAO is presented for different amplitudes A of the wave paddle. It is possible to notice that the highest RAO obtained is of 11.57 for $\Omega = 0.666$. Tests carried in 3D wave basin.

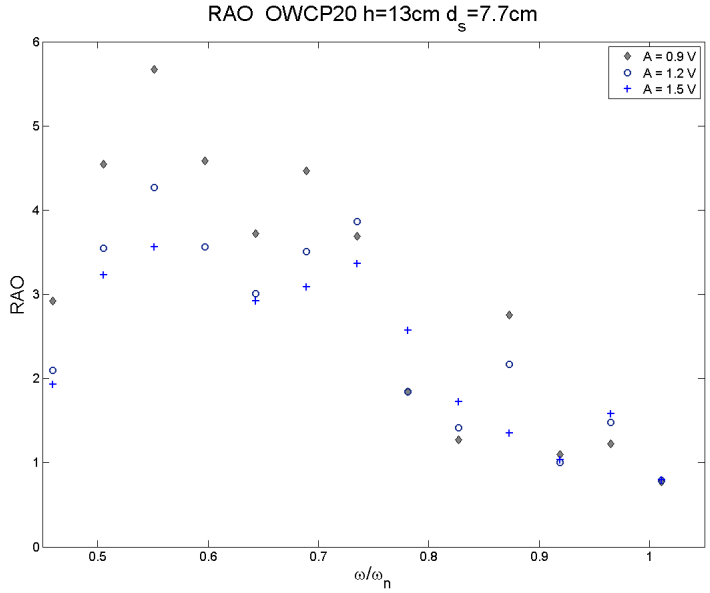

Figure A.8: RAO for the OWCP15 model with $h = 0.13$m and $d_s = 0.077m$. The RAO is presented for different amplitudes A of the wave paddle. It is possible to notice that the highest RAO obtained is of 8.863 for $\Omega = 0.613$. Tests carried in 3D wave basin.

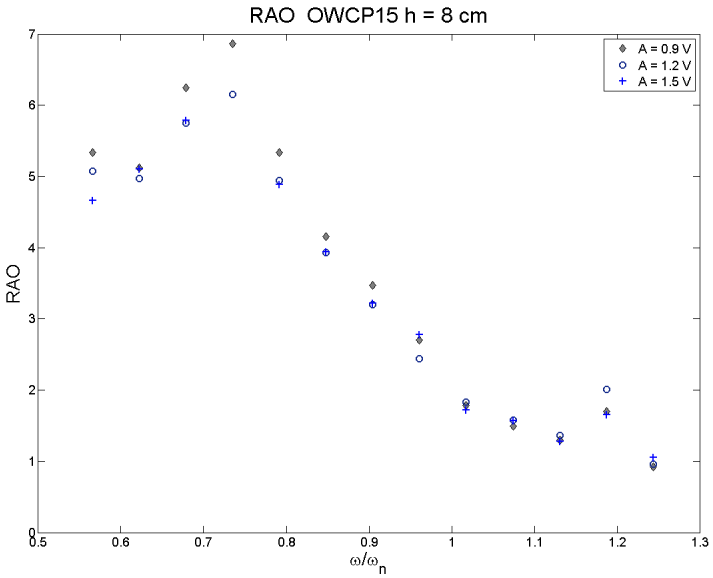

Figure A.9: RAO for the OWCP20 model with $h = 0.08$m and $d_s = 0.068m$. The RAO is presented for different amplitudes A of the wave paddle. It is possible to notice that the highest RAO obtained is of 4.728 for $\Omega = 0.6569$. Tests carried in 3D wave basin.

A.3 OWCP20

In this section the RAO tests carried for the OWCP20 model are presented. The maximum RAO obtained for the device is 9.52 with the following installation conditions $h = 0.13\,m$, $d_s = 0.065\,m$ for $\Omega = 0.5462$ (Figure A.11).

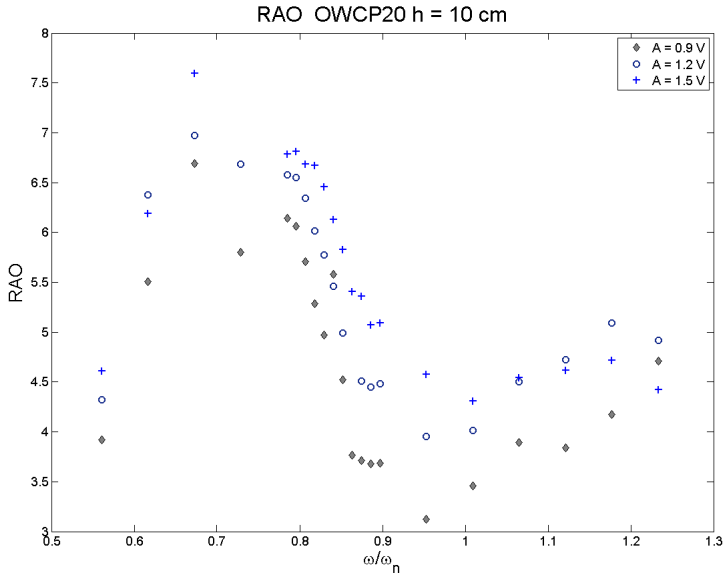

Figure A.10: RAO for the OWCP20 model with $h = 0.10$m and $d_s = 0.088m$. The RAO is presented for different amplitudes A of the wave paddle. It is possible to notice that the highest RAO obtained is of 7.595 for $\Omega = 0.6726$. Tests carried in 3D wave basin.

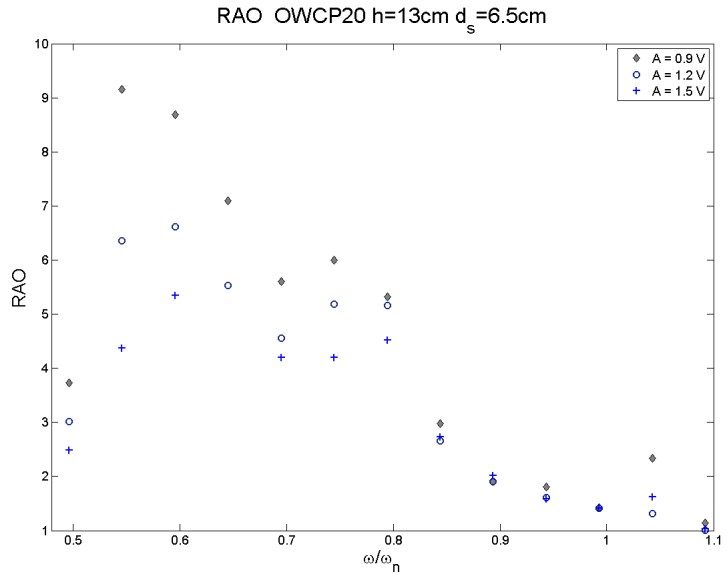

Figure A.11: RAO for the OWCP20 model with $h = 0.13$m and $d_s = 0.065m$. The RAO is presented for different amplitudes A of the wave paddle. It is possible to notice that the highest RAO obtained is of 9.52 for $\Omega = 0.5462$. Tests carried in 3D wave basin.

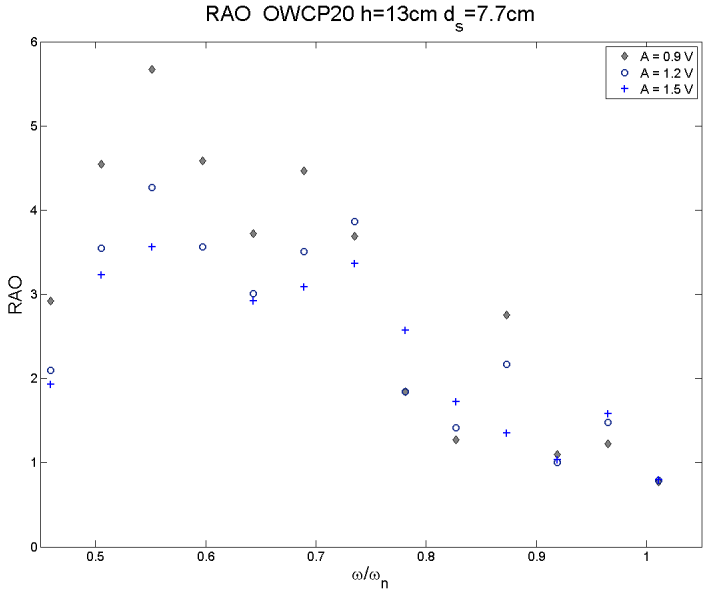

Figure A.12: RAO for the OWCP20 model with $h = 0.13$m and $d_s = 0.077m$. The RAO is presented for different amplitudes A of the wave paddle. It is possible to notice that the highest RAO obtained is of 5.667 for $\Omega = 0.551$. Tests carried in 3D wave basin.

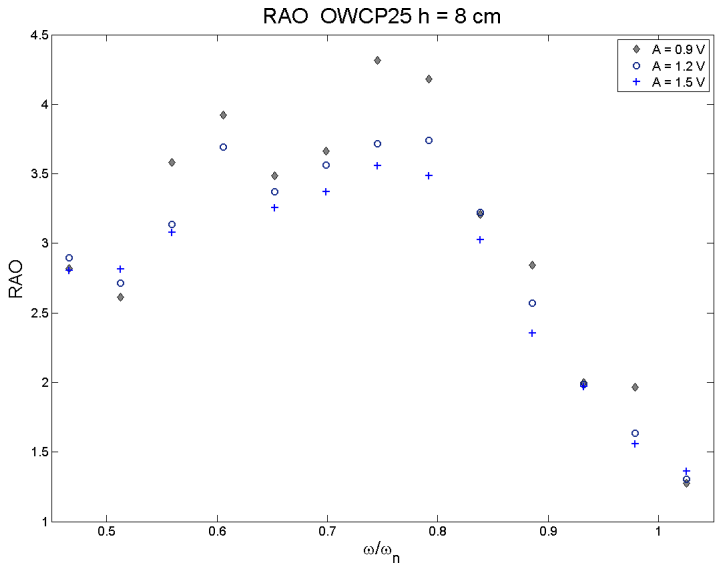

Figure A.13: RAO for the OWCP25 model with $h = 0.08$m and $d_s = 0.068m$. The RAO is presented for different amplitudes A of the wave paddle. It is possible to notice that the highest RAO obtained is of 4.315 for $\Omega = 0.7457$. Tests carried in 3D wave basin.

A.4 OWCP25

In this section the RAO tests carried for the OWCP25 model are presented. The maximum RAO obtained for the device is 14.12 with the following installation conditions $h = 0.13\,m$, $d_s = 0.065\,m$ for $\Omega = 0.733$ (Figure A.16)

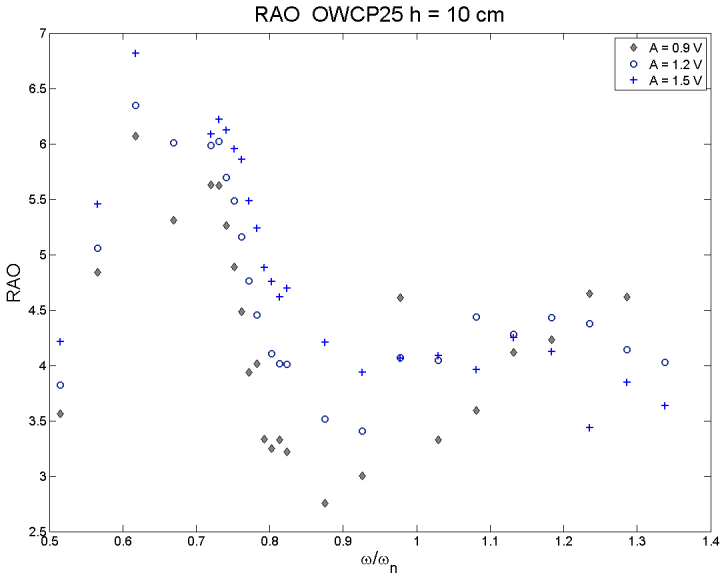

Figure A.14: RAO for the OWCP25 model with $h = 0.10$m and $d_s = 0.088m$. The RAO is presented for different amplitudes A of the wave paddle. It is possible to notice that the highest RAO obtained is of 6.816 for $\Omega = 0.6175$. Tests carried in 3D wave basin.

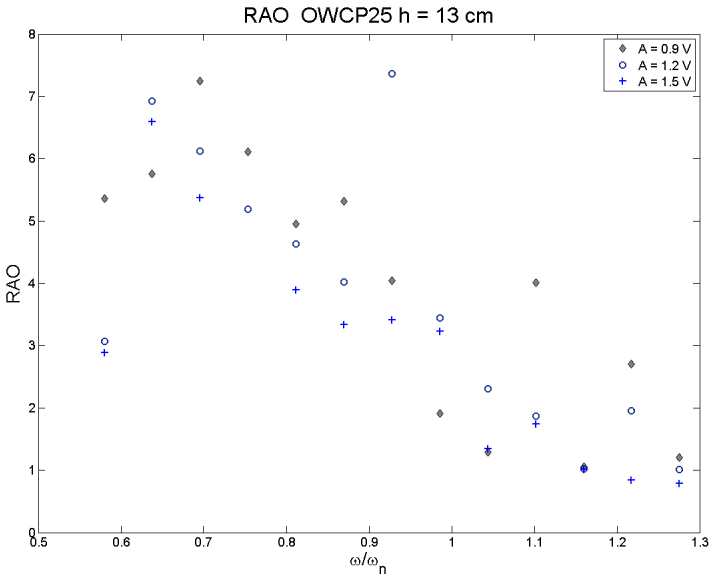

Figure A.15: RAO for the OWCP25 model with $h = 0.08$m and $d_s = 0.1188m$. The RAO is presented for different amplitudes A of the wave paddle. It is possible to notice that the highest RAO obtained is of 7.248 for $\Omega = 0.6958$. Tests carried in 3D wave basin.

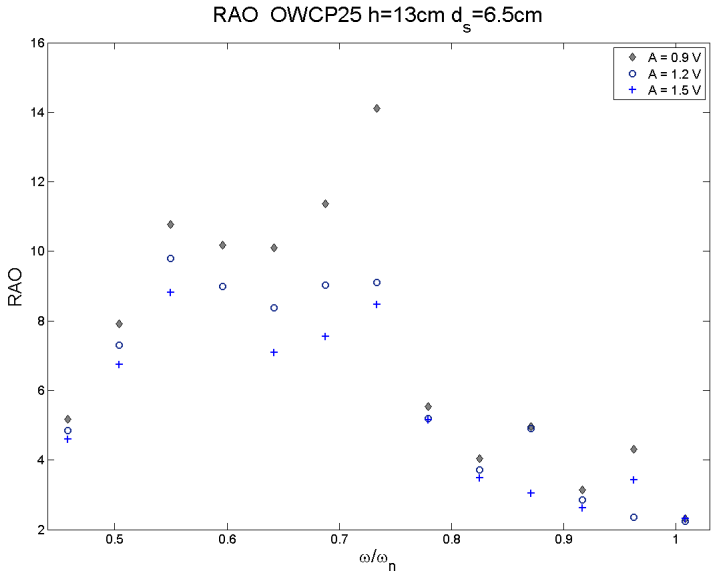

Figure A.16: RAO for the OWCP25 model with $h = 0.13$m and $d_s = 0.065m$. The RAO is presented for different amplitudes A of the wave paddle. It is possible to notice that the highest RAO obtained is of 14.12 for $\Omega = 0.7333$. Tests carried in 3D wave basin.

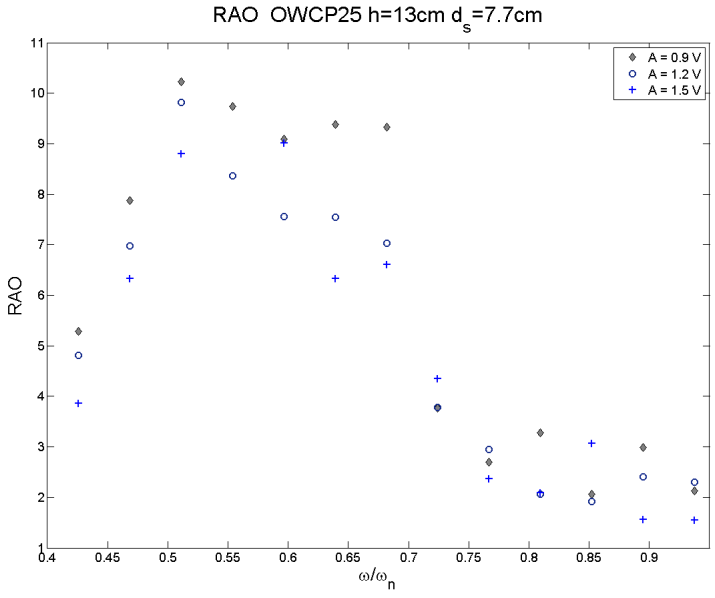

Figure A.17: RAO for the OWCP25 model with $h = 0.13$m and $d_s = 0.77m$. The RAO is presented for different amplitudes A of the wave paddle. It is possible to notice that the highest RAO obtained is of 10.22 for $\Omega = 0.5112$. Tests carried in 3D wave basin.

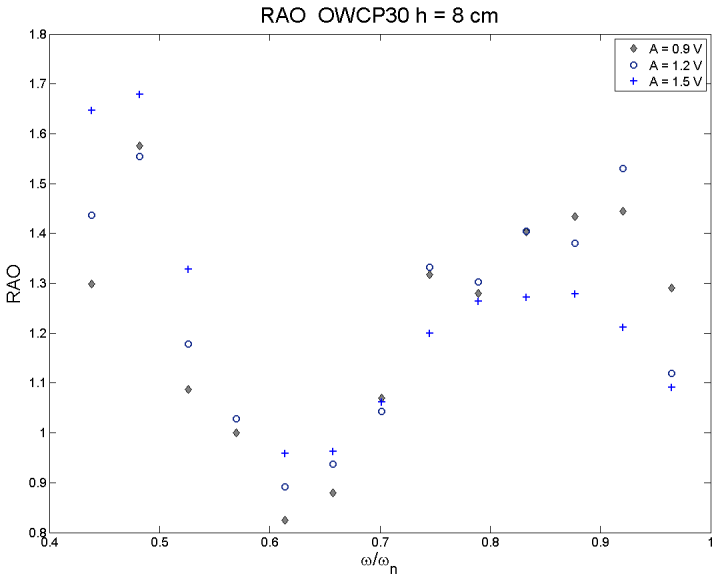

Figure A.18: RAO for the OWCP30 model with $h = 0.08$m and $d_s = 0.068m$. The RAO is presented for different amplitudes A of the wave paddle. It is possible to notice that the highest RAO obtained is of 1.679 for $\Omega = 0.4822$. Tests carried in 3D wave basin.

A.5 OWCP30

In this section the RAO tests carried for the OWCP25 model are presented. The maximum RAO obtained for the device is 10.31 with the following installation conditions $h = 0.13\,m$, $d_s = 0.065\,m$ for $\Omega = 0.693$ (Figure A.21)

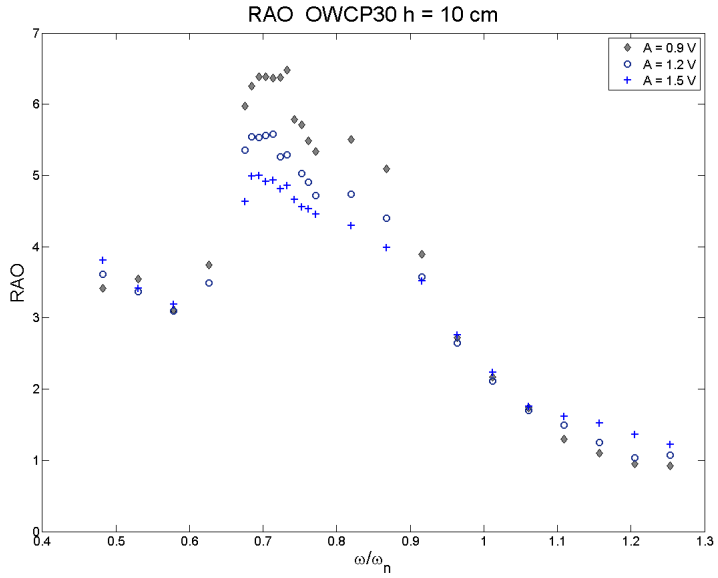

Figure A.19: RAO for the OWCP30 model with $h = 0.10$m and $d_s = 0.088m$. The RAO is presented for different amplitudes A of the wave paddle. It is possible to notice that the highest RAO obtained is of 6.483 for $\Omega = 0.7328$. Tests carried in 3D wave basin.

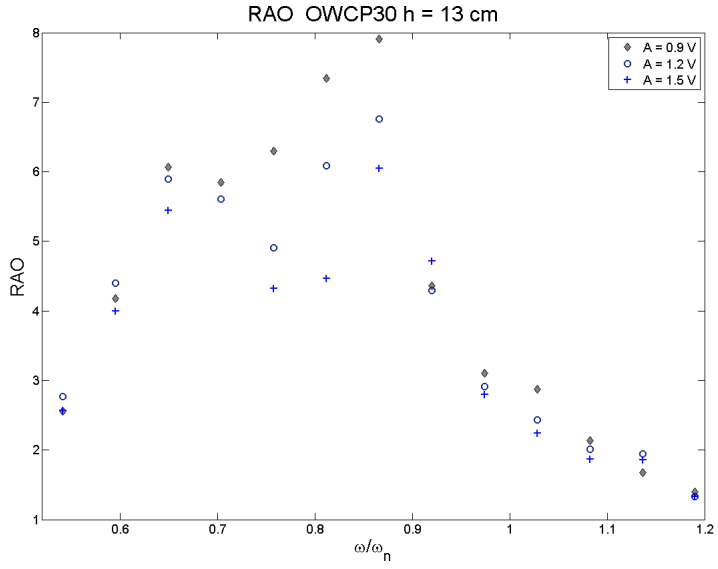

Figure A.20: RAO for the OWCP30 model with $h = 0.13$m and $d_s = 0.118m$. The RAO is presented for different amplitudes A of the wave paddle. It is possible to notice that the highest RAO obtained is of 7.904 for $\Omega = 0.8657$. Tests carried in 3D wave basin.

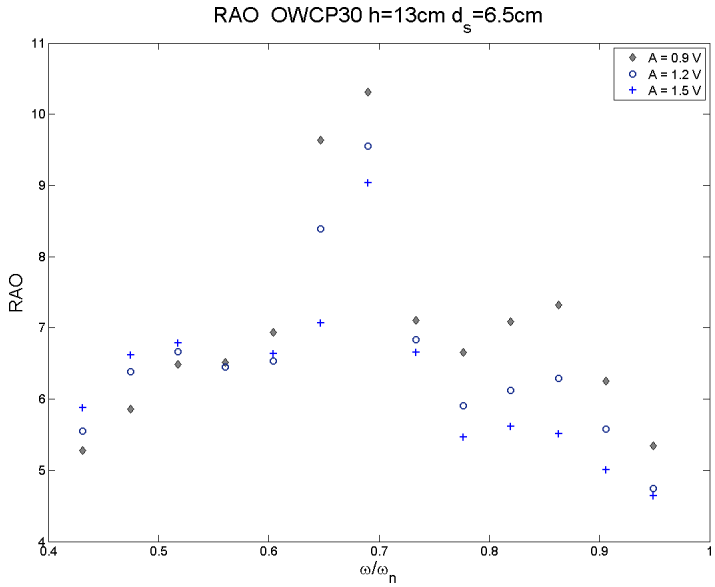

Figure A.21: RAO for the OWCP25 model with $h = 0.13$m and $d_s = 0.065m$. The RAO is presented for different amplitudes A of the wave paddle. It is possible to notice that the highest RAO obtained is of 10.31 for $\Omega = 0.6903$. Tests carried in 3D wave basin.

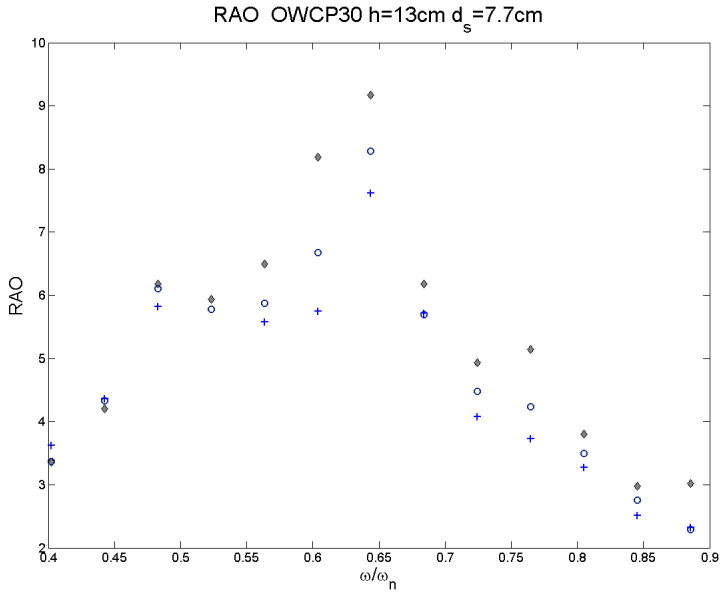

Figure A.22: RAO for the OWCP30 model with $h = 0.13$m and $d_s = 0.077m$. The RAO is presented for different amplitudes A of the wave paddle. It is possible to notice that the highest RAO obtained is of 9.168 for $\Omega = 0.6439$. Tests carried in 3D wave basin.

Appendix B

Matlab Codes

The matlab codes used to solve the linear and non-linear model of the OWCP are presented in this Chapter

B.1 RAO Overall Solver

The RAO overall solver consider linear and non-linear terms and calls the phase shift between waves and model as assessed from experimental tests.

```
%% determine the rao of the owcp

%% starting Parameters
hov= 0.05; %overptopping height
g= 9.81; % gravitational constant
ro= 1000; % water density
alpha=25*pi()/180; % angle inclination
ds=0.06; %submersion depth
l1=0.045; %input length
h=0.11; %waterdepth
xsi=0.7;
diam=0.024;
Area=0.24^2*pi()/4;
a=0.02; %amplitude of the wave 1/2 wave height
f=0.5:0.02:1.28; %wave frequency
w=2*pi()*f;
%% length pipe
```

```
L=l1+ds/sin(alpha);
wn=sqrt(g/L);
%% omegazero,Ce,Ci
W=w./wn;
Cr=2*ro*sqrt(g*L)*xsi;
maxRAO=zeros(length(w),3);
kb=0.05; %bend angle loss

%% the phase angle file is required from tests
fs=load('batchremoval.csv');

[phase3,phase5] = anglefrequency(fs);



%%non-linear solver
for k=1:1
    Crk=Cr(k);
    for j=1:length(w)
        wu=w(j);
        phasea=phase5(j);
        Ce=-(3.8772*(wu/wn)^3+13.808*(wu/wn)^2+17.9211*(wu/wn)-5.5203);
        Ci=1.9003*(wu/wn)^3+6.7679*(wu/wn)^2-8.7851*(wu/wn)+4.2731;
        [t,y]=ode45(@(t,s) OWCPsolverNL(t,s,a,wu,wn,ro,g,L,Ce,Ci,phasea,Crk,kb), [0 55], [0 0]);
%         figure
%         plot (t,y(:,1))
        ymin=min(find(t>45 & t<50));
        ymax=max(find(t>45 & t<50));
        maxRAO(j,k)= (max(y(ymin:ymax,1)))/a;
    end
end

%%linear solver
for k=1:1
    Crk=Cr(k);
    for j=1:length(w)
        wu=w(j);
        phasea=phase5(j);
        Cex=3.873*(wu/wn)^3+13.808*(wu/wn)^2+17.9211*(wu/wn)+5.5203;
        [t,y]=ode45(@(t,s) OWCPsolverL(t,s,a,wu,wn,ro,g,L,phasea,Crk), [0 55], [0 0]);
```

```
%          figure
%          plot (t,y(:,1))
         ymin=min(find(t>45 & t<50));
         ymax=max(find(t>45 & t<50));
         maxRAO2(j,k)= (max(y(ymin:ymax,1)))/a;
    end
end

%% plots
     batch =load('batchremoval.csv');
results = load('results.dat');
data = [batch results];
freq= data(:,1);
freqn=2*pi()*freq./wn;


figure1 = figure('Color',[1 1 1]);
axes1 = axes('Parent',figure1,'FontSize',20);
box(axes1,'on');
hold(axes1,'all');
plot(freqn(1:40),data(1:40,8),'LineStyle','none','MarkerFaceColor',[0.800000011920929 0.80000
    'Marker','diamond',...
    'Color',[0 0 0],'DisplayName','Exp,A=0.6 V','MarkerSize',8);
hold on
plot(freqn(41:80),data(41:80,8),'LineStyle','none','Marker','+','Color',[0 0 0],'LineWidth',2
hold on
plot(freqn(81:120),data(81:120,8),'LineStyle','none','Marker','o','Color',[0 0 0],'DisplayNam
hold on
plot(W,maxRAO(:,1),'Marker','.','LineStyle','--','DisplayName','Simulation NL',...
    'Color',[0 0 0])
hold on
plot(W,maxRAO2(:,1),'Marker','x','LineStyle','-.','Color',[1 0 0],...
    'DisplayName','Simulation L')
xlabel('\omega/\omega_n','FontSize',24);
ylabel('RAO ','FontSize',24);
title('RAO  OWCP25 h = 11.5 cm','FontSize',30);
```

B.1.1 Function - Linear Solver

Linear ODE used in RAO Solver

```
function ds = OWCPsolverL(t,s,a,wu,wn,ro,g,L,phasea,Crk)
ds = zeros(2,1);
ds(1) = s(2);
ds(2) = 1/(ro*L*1.5)*(a*ro*sin(wu*t-phasea)*(wu)^2-ro*g*s(1)-Crk*s(2)*(wu/wn)^2);
```

B.1.2 Function - Non Linear Solver

ODE used in RAO Solver including non-linear terms.

```
function ds = OWCPsolverNL(t,s,a,wu,wn,ro,g,L,Ce,Ci,phasea,Crk,kb)
ds = zeros(2,1);
ds(1) = s(2);
ds(2) = 1/(ro*L*1.5)*(a*ro*sin(wu*t-phasea)*(wu)^2-ro*g*s(1)-max(Ce*(s(2)), Ci*(s(2)))*(s(2))...
    -Crk*s(2)*(wu/wn)^2)-0.5*kb*s(2)^2*(pi*0.012^2);
% ds(3:4) = [Ce*abs(s(2)); Ci*abs(s(2))];
```

B.1.3 Function - Non Linear Solver with Removal

ODE used for the determination of the water removal

```
function ds = OWCP_NL_Final(t,s,a,wu,wn,ro,hov,g,L,Ci,Crk,Ce,kb)
ds = zeros(3,1);
ds(1) = s(2);
ds(2) = 1/(ro*L*1.5)*(a*ro*sin(wu*t)*(wu)^2-...
        ro*g*(min(s(1),hov))-pi*0.012^2*ro*g*(max(0,(s(1)-hov)))-...
        (max(Ce*(s(2)), Ci*(s(2))))*(s(2))-Crk*s(2)*(wu/wn)^2)-0.5*kb*s(2)^2*(pi*0.012^2);
ds(3)= max(0,(s(1)-hov));
```

B.1.4 Funcation - Regular Waves Efficiency

Overall Solver used to determine efficiency for OWCP configurations

```
%%% determine the removal power with the method presented by Knott and
%%% Flower
%%% Damping ratio considered of 0.09 0.15 0.25

% Ci= 0.05; %internal damping component
% Ce= 0.95; %external damping component
clear all
close all

hov_arr= [0.035 0.04 0.045 0.05 0.055 0.06 0.065 0.07 0.075 0.08];
xsi_arr= [0.37 0.56 0.75] ;%overptopping height (scale it up?)
alpha_arr=[25 30 35];
alpha_arr=alpha_arr*pi()/180; % angle inclination
kb_arr=[0.06 0.08 0.1];
g= 9.81; % gravitational constant
ro= 1000; % water density
ds=0.08; %submersion depth (scale it up?)
l1=0.045; %input length (scale it up?)
h=0.125; %waterdepth (scale it up?)
diam=0.024; %(scale it up?)
Area=diam^2*pi()/4;

a=0.02; %amplitude of the wave 1/2 wave height (scale)
f=0.2:0.05:2; %wave frequency (scale)
w=2*pi()*f;
t=0:0.01:100; %(scale it up?)



maxRAO=zeros(length(w),length(alpha_arr),length(hov_arr));
Power=zeros(length(w),length(alpha_arr),length(hov_arr));
Mass=zeros(length(w),length(alpha_arr),length(hov_arr));
Efficiency=zeros(length(w),length(alpha_arr),length(hov_arr));
%%calling ode


    for ii=1:length(alpha_arr)
        alpha=alpha_arr(ii);
        kb=kb_arr(ii);
```

```
xsi=xsi_arr(ii);
alphadeg=alpha*180/pi();
L=l1+ds/sin(alpha);
wn=sqrt(g/L);
W=w./wn;
Crk=2*ro*sqrt(g*L)*xsi;
for kk=1:length(hov_arr)
    hov=hov_arr(kk);

    for j=1:length(w)

    wu=w(j);

    Ce=-(3.8772*(wu/wn)^3+13.808*(wu/wn)^2+17.9211*(wu/wn)-5.5203);
    Ci=1.9003*(wu/wn)^3+6.7679*(wu/wn)^2-8.7851*(wu/wn)+4.2731;
    [t,y]=ode45(@(t,s) OWCP_NL_Final(t,s,a,wu,wn,ro,hov,g,L,Ci,Crk,Ce,kb), [0 15], [0 0 0
    yr=zeros(length(t),1);
    maxRAO(j,ii,kk)= (max(y(:,1)))/a; %do i need rao?

        for jj=1:length(t)
            if y(jj,1)>0
            y(jj,1)=y(jj,1);
            end
        end


yrem=y(:,3);
mass=Area*ro*yrem;
Mass(j,ii,kk)=mass(length(t));
Power(j,ii,kk)=g*Mass(j,ii,kk)*hov/(max(t)-min(t));
Efficiency(j,ii,kk)=32*pi()^2*Mass(j,ii,kk)*hov/((max(t)-min(t))*g*4*a^2*((2*pi()/wu)^2))
YMatrix1=[y(:,1) (yr+hov)];


    end

%Graphs

end
```

```
    end
```

B.1.5 Function - JONSWAP Spectrum and Amplitude

Numerical code used to define the JONSWAP Spectrum and amplitude components

```
%This function generates a wave spectrum based on JONSWAP for a given value of Hs and Tp
%It also generates the amplitude of each frequency component for
%superposition

%DEFINE NUMBER OF POINTS
T=30*60; %30 minutes simulation
df=1/T;
n=floor(T/0.1);
f=df:df:(floor(n/2)-1)*df;
% DEFINE WAVE  CLIMATE
Prob_arr=[0.468 0.226 0.108 0.051 0.024];
Hs_arr=[1 2 3 4 5];
Tp_arr=[5.6 7 8.4 9.8 11.2];
w=2*pi()*f;
Spectrum=zeros(length(Hs_arr),length(f));
Amp=zeros(length(Hs_arr),length(f));
Phase=zeros(length(Hs_arr),length(f));

for i=1:length(Hs_arr);

  Hs=Hs_arr(i);
  Tp=Tp_arr(i);


  Aspectrum = 5/16*(Hs)^2/(Tp)^4;
  Bspectrum = 5/4*1/(Tp)^4;
  Spectrum (i,:) = Aspectrum./(f.^5).*exp(-1*Bspectrum./f.^4);
  Amp(i,:) = sqrt(2.*Spectrum(i,:).*df);
  Phase(i,:) = 2*pi*rand(size(f));


end
```

B.1.6 Function - Frequency Analysis Angle

This function is used to dtermine tha phase between the incident waves and the response of the OWCP.

```
fs=load('batchremoval.csv');
fs=fs(1:40,1);


for i=1:40

        fname=strcat('30DR-',num2str(i),'.dat');


    if  exist(fname,'file')~=0;
            ddata=load(fname);

            data3=ddata(1000:6500,3);
            data5=ddata(1000:6500,5);

            Fs=256*fs(i);

            [freq3,y3,a3]=my_ffta(data3,Fs);
            [freq5,y5,a5]=my_ffta(data5,Fs);


%             %% graph
%             % Create figure
%             figure1 = figure('Color',[1 1 1]);
%             subplot1 = subplot(2,1,1,'Parent',figure1);
%             xlim(subplot1,[0 3.5]);
%             box(subplot1,'on');
%             hold(subplot1,'all');
%             plot(freq3,y3,'DisplayName','Wave')
%             hold on
%             stem(freq5,y5,'LineStyle','none','MarkerFaceColor',[1 1 1],'Color',[1 0 0],...
%              'DisplayName','OWCP35');
%
%             xlabel('f [Hz]');
```

```
%             ylabel('H/2 [m]');
%             title(['Frequency Analysis Array h = 125 mm s_d = 10 mm— ',num2str(i),' Test'])
%
%             subplot2 = subplot(2,1,2,'Parent',figure1);
%             xlim(subplot2,[0 3.5]);
%             box(subplot2,'on');
%             hold(subplot2,'all');
%             plot(freq3,a3,'—s','DisplayName','Wave')
%             hold on
%             plot(freq5,a5,'Marker','o','MarkerFaceColor',[1 1 1],'Color',[1 0 0],...
%              'DisplayName','OWCP35');
%                         xlabel('f [Hz]');
%             ylabel('\psi [degrees]');
%             title('phase');
%
%             legend(subplot1,'show');



    end
end
for i=1:length(fs)
    c=fs(i);
    position(i)=min(find(freq3>=c));
    phase3(i)=a3(position(i));
    phase5(i)=a5(position(i));
end
```

B.1.7 Fucntion - my_ffta

Fast Fourier Transform to determine frequency and phase of incident wave and OWCP response.

```
function [freq,Y,ang] = my_fft(data,Fs)
%data = data sample
%Fs = samle rate

%FFT analysis of 'data'
L = length(data);
```

```
% T = 1/Fs; %Sample time
% t = (0:L-1)*T; %Time vector
y = data; %Sample
% subplot(2,1,1); plot(Fs*t,y)
% title('Plot of data in the time domain')
% xlabel('Sample number')
% ylabel('Magnitude')

NFFT = 2^nextpow2(L); %next power of 2 from length of y
Y = fft(y,NFFT)/L;
Y(1) = []; %the first component of Y, Y(1), is simply the sum of the data, and can be removed
freq = Fs/2*linspace(0,1,NFFT/2+1);
ang=unwrap(angle(Y(1:NFFT/2+1)));
Y = 2*abs(Y(1:NFFT/2+1)); % provides single-sided amplitude spectrum
```

B.2 Removal Function

B.3 Reflection Analysis

Routine for the Frigaard and Brorsen (1995) reflection analysis.

```
% Frigaard and Brorsen's method for the seperation of incoming and
% reflected waves using two wave probes(1993)


clear all




% close all

%% Data loading from excel files.
%x1 is timeseries from wave probe 1
%x2 is timeseries from wave probe 2
%x1=xlsread('name1.xls');
%x2=xlsread('name2.xls');
```

```
% File loading from txt files.
% x1=load('test1.txt');
% x2=load('test2.txt');



m=0;
n=0.1;
fs=256;   % above as a function of dt
Dx=0.142;
% ainc=0.015;
% aref=0.015;
% fI=pi;
% fR=pi/2;
% x_1=0;
% x_2=x_1+Dx;
T=1/0.5;
omega=(2*pi)/T;
g=9.81;
h=0.1; % water depth
% t=0:0.005:3;
[kappa,err] = lin_disp(omega,g,h);

dt=1/fs; %sec



% [x1,x2]=signal_2(T,ainc,aref,fI,fR,x_1,Dx);
% n1=ainc*cos(omega*t-kappa*x_1+fI);
% n2=aref*cos(omega*t+kappa*x_1+fR);
% x1=n1+n2;
%
% n1_2= ainc*cos(omega*t-kappa*x_2+fI);
% n2_2=aref*cos(omega*t+kappa*x_2+fR);
% x2=n1_2+n2_2;
%% Cutting off the mirror image for both data series
%  dt is the time difference between each sampling point/interval of
% measurment, dt=1/fs (fs=sampling frequency)
```

```
%% Calculation of amplification factor (C) and phase shift (Fth1 and Fth2)
% input: T:...wave period (sec)
%        g:...gravity accelaration, 9.81 (m/sec2)
%        h:...water depth (m)
%        Dx:...distance between wave gauge 1 and 1 =wg2-wg1
%        m:...(+- 0,1,2..)
%        n:...(+- 0,1,2..)
%        fs:...sampling frequency

for j=1:6;
    fname=strcat('F50_probe',num2str(j),'.dat');
    sep=load(fname);
    clear x1
    clear x2

    x1=sep(:,1);
    x2=sep(:,4);
    xtran=sep(:,3);

nfft1=length(x1);
nfft2=length(x2);
T01=nfft1*dt; % T0 is the signal length (or sampling period)
T02=nfft2*dt;
Df1=1/T01; %Df is the frequency width
Df2=1/T02;
mirror1=nfft1/2;
mirror2=nfft2/2;

%% Run an fft for both timeseries
x1f=fft(x1,nfft1);
x2f=fft(x2,nfft2);

Fth1=kappa*Dx+(pi/2)+m*pi+n*2*pi;
Fth2=-(pi/2)-m*pi+n*2*pi;
C=1/(2*cos(-kappa*Dx-pi/2-m*pi));
Fth3=-pi/2-kappa*Dx;
Fth4=pi/2;
```

```
%% Manipulation of original signals (amplification and phase shift)

x1fa=x1f.*C;
x2fa=x2f.*C;
xref1a=x1f.*C;
xref2a=x2f.*C;
i=sqrt(-1);


x1fas=x1fa.*(exp(i*Fth1));

x2fas=x2fa.*(exp(i*Fth2));

xref1as=xref1a.*(exp(i*Fth3));

xref2as=xref2a.*(exp(i*Fth4));

%% Reverse fft
x3i=ifft(x1fas);
x4i=ifft(x2fas);
xref3=ifft(xref1as);
xref4=ifft(xref2as);
xinc=real(x3i)+real(x4i);
xref=real(xref3)+real(xref4);

% Zero momenent calculation
% fs=256;


m0ref=(std(xref))^2;
m0inc=(std(xinc))^2;
m0tran=(std(xtran))^2;

% Reflection and transimition coeficient

R=sqrt(m0ref/m0inc);

Tr=sqrt(m0tran/m0inc);
% Hrms=2* sqrt2* sqrtm0
```

```
H=2*sqrt(2)*sqrt(m0inc);

Hrms(j)=H;
ref(j)=R;
tran(j)=Tr;

end
ref=ref';
tran=tran';
Hrms=Hrms';
kh=1:6;
kh=kh./kh;
kh=kh.*(kappa*h);
kh=kh';

RTHKh=[ref,tran,Hrms,kh];
% fname=strcat('ref200','.dat');
% save('-ascii',fname,'ref');
% fname=strcat('tran200','.dat');
% save('-ascii',fname,'tran');
% fname=strcat('Hrms200','.dat');
% save('-ascii',fname,'Hrms');

fname=strcat('R_Tr_Hrms_Kh','50','.dat');
save('-ascii',fname,'RTHKh');




%
%
%
% figure('name','fftplots');
% subplot(2,1,1);
% plot(real(x3i));
% hold on
% plot(real(x4i),'r--');
% legend('ifft1','ifft2');
% subplot(2,1,2);
% plot(real(x1fas));
```

```
% hold on
% plot(real(x2fas),'r--');
% legend('phase1','phase2');
%
%
% figure('name','shifted original signals');
% subplot(2,2,1);
% plot(real(x3i));
% hold on
% plot(real(x4i),'r--');
% legend('wp1 shifted','wp2 shifted');
% subplot(2,2,2);
% plot(x1);
% hold on
% plot(x2,'r--');
% legend('wp1','wp2');
% subplot(2,2,3);
% plot(real(x3i));
% hold on
% plot((x1),'r--');
% legend('wp1 shifed','wp1');
% subplot(2,2,4);
% plot(real(x4i));
% hold on
% plot(x2,'c--');
% legend('wp2 shifted','wp2');
%
%

% figure;
% plot(x1);
% hold on
% plot(x2,'r');

%% Plots

%% Plots of the original signals

% Magnitude plots
```

```
% Ts=1/fs; % is the sampling period
% df1=fs/length(x1f) % is the frequency width (1/To)
% df2=fs/length(x2f)
% df3=fs/length(x23f)
% df4=fs/length(xreff);
%
% N1=0:length(x1f)-1; % number of sample points for x1f
% N2=0:length(x2f)-1; % number of sample points for x2f
% N3=0:length(x23f)-1; % number of sample points for x23f
% N4=0:length(xreff)-1; % number of sample points for xreff
%
% figure('Name','Plots of the original signals','NumberTitle','off')
% subplot(3,2,1);
% stem((N1/2)*df1,abs(x1f),'b');
% ylabel('Magnitude');
% xlabel('fr');
% title('Wave probe 1');
%
% subplot(3,2,2);
% stem((N2/2)*df2,abs(x2f),'b');
% ylabel('Magnitude');
% xlabel('fr');
% title('Wave probe 2');

%% Spectral density plot (energy/density*g)
% Sn1=((1/2)*abs(x1f))/df1
% Sn2=((1/2)*abs(x2f))/df2
%
% subplot(3,2,3);
% stem((N1/2)*df1,Sn1,'b');
% ylabel('Spectral density');
% xlabel('fr');
% title('Wave probe 1');
%
% subplot(3,2,4);
% stem((N2/2)*df2,Sn2,'b');
% ylabel('Spectral density');
% xlabel('fr');
% title('Wave probe 2');
```

```
%% Plot for the final, manipulated signal

% Magnitude plot_Incoming

% figure('Name','Plots of the final signal','NumberTitle','off')
% subplot(3,2,1);
% stem((N3/2)*df3,abs(x23f),'b');
% ylabel('Magnitude');
% xlabel('fr');
% title('Wave probe 1 Incoming');
%
% %% Spectral density plot_Incoming (energy/density*g)
%
% Sn3=((1/2)*abs(x23f))/df3
%
% subplot(3,2,2);
% stem((N3/2)*df3,Sn3,'b');
%
% ylabel('Spectral density');
% xlabel('fr');
% title('Wave probe 1 Incoming');

%% Plot for the reflected signal


% Magnitude plot_Reflected
%
% subplot(3,2,3);
% stem((N4/2)*df4,abs(xreff),'b');
% ylabel('Magnitude');
% xlabel('fr');
% title('Wave probe 1 Reflected');

%% Spectral density plot_Reflected (energy/density*g)

% Sn4=((1/2)*abs(xreff))/df4
%
% subplot(3,2,4);
```

```
% stem((N4/2)*df4,Sn4,'b');
% ylabel('Spectral density');
% xlabel('fr');
% title('Wave probe 1 Reflected');

%% Plot in the time domain

% figure('Name','Time domain','NumberTitle','off')
%
% % A=real(x23);
% % B=real(xreftest);
% R=real(xref);
%
% lx23=length(x23);
% % lxreftest=length(B);
% lxref=length(R);
%
% t=0:lx1;
%
% if length(t)==lx1;
%     t=t;
% else
%     t=0:lx1-1;
% end
%
% plot(t,x1);
% hold on
% plot (t,x23,'r');
% % plot (t,B,'g');
% plot (t,R,'c');
% ylabel('Surface elevation');
% xlabel('Time');
% legend('Original signal', 'Incoming wave signal','Reflection wave signal');
%
% %% Wave amplitude calculation
%
% % Incoming wave
%
% d23=abs(t-T);
```

```
% f=find(d23==min(d23));
% S1=f;
% S2=floor(lx23/S1);
% Y=reshape(x23(1:S1*S2),S1,S2);
% ainc=range(Y);
% Haver=mean(range(Y))
%
% % Reflected wave
% dref=abs(t-T);
% fref=find(dref==min(dref));
% S1=fref;
% S2=floor(lxref/S1);
% Yref=reshape(R(1:S1*S2),S1,S2);
% aref=range(Yref);
% Haverref=mean(range(Yref))
```

Appendix C

Theory of the SIBEO Device

This section presents the formulation of the mechanism of the SIBEO device as derived by Czitrom, Godoy, Prado, Perez and Peralta-Fabi (2000), and it is intended for the comparison with the mathematical description of the OWCP presented in section 4.2.

In order to describe the mechanism of the SIBEO seawater pump Czitrom, Godoy, Prado, Perez and Peralta-Fabi (2000) applied the time dependent form of the Bernoulli equation (Equation C.1) to the stream lines $X_1E_1M_1B_1$ and $X_2E_2M_2B_2$ of Figure C.1

$$\int_a^b \frac{\partial V}{\partial t} ds + \frac{V^2}{2} + \frac{P}{\rho} + gX = Const \tag{C.1}$$

giving

$$\left(X_1 + L_1(1+\varepsilon_1) + \frac{T_d}{cos\theta}\right)\ddot{X_1} + \frac{\dot{X_1^2}}{2} + \left(\frac{K_1}{2} + \frac{\frac{L_1+T_d}{cos\theta}}{D_1} f_1 + C_{r1}\right)\dot{X_1}|\dot{X_1}| +$$

$$+ \quad \frac{(P_A - \rho g H)}{\rho}\left[\left(1 - \frac{A_1X_1}{V_0} - \frac{A_cX_2}{V_0}\right)^{-\gamma} - 1\right] \quad + \quad gcos\theta X_1 \qquad = \qquad \frac{W}{\rho} \tag{C.2}$$

for the $X_1E_1M_1B_1$ streamline and

$$\left(X_2 + \frac{A_c}{A_2} L2_1(1+\varepsilon_2) + L_c\right)\ddot{X_2} + \frac{\dot{X_2^2}}{2} + \left(\frac{K_2}{2} + \frac{L_2}{D_2} f_2 + C_{r2}\right)\left(\frac{A_c}{A_2}\right)^2 \dot{X_2}|\dot{X_2}| +$$

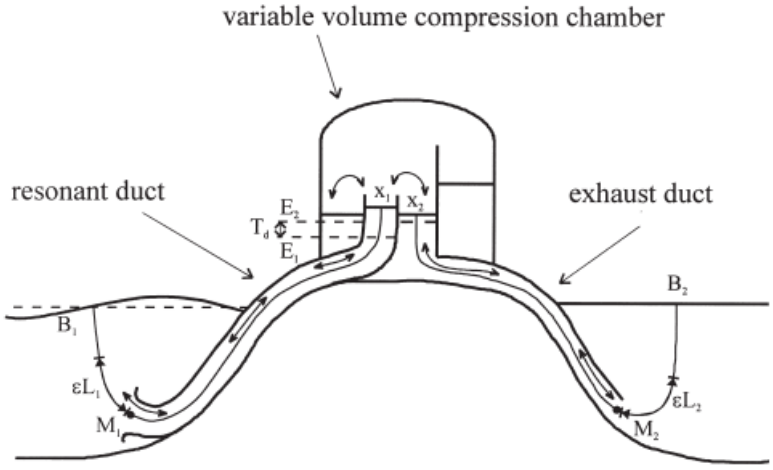

Figure C.1: Schematic diagram of the wave driven resonant seawater pump SIBEO Czitrom, Godoy, Prado, Perez and Peralta-Fabi (2000).

$$+\frac{(P_A - \rho g H)}{\rho}\left[\left(1 - \frac{A_1 X_1}{V_0} - \frac{A_c X_2}{V_0}\right)^{-\gamma} - 1\right] + gX_2 = \frac{W}{\rho} \tag{C.3}$$

for the $X_2E_2M_2B_2$ stream line.

The second and fifth term of equations C.2 and C.3 are derived from Bernoulli's Equation. The two equations are coupled together through the air compression term, which is the fourth term in both equations.

The terms used by Czitrom, Godoy, Prado, Perez and Peralta-Fabi (2000) were:

- Subscripts 1 and 2 were used to identify respectively the resonant (input) duct and the exhaust (output) duct. The subscript c was used to identify term related to the compression chamber.

L_i Length of the i^{th} duct, with L_1 taken at the equilibrium position of the exhaust duct E_2

D_i Diameter of the i^{th} section

A_i Area of the i^{th} section

P_A Atmospheric Pressure $[Pa]$

ρ Seawater density $[kg\,m^{-3}]$

$\gamma = \frac{C_p}{C_v}$ Air compressibility [1.4]

W Wave pressure signal $[Pa]$

T_d Height of sea level above receiving body of water (including tidal signal at E_2) $[m]$

$V = 0$ Compression chamber volume $[m^3]$

H Height of compression chamber equilibrium above the receiving body of water $[m]$

ε Fractional added length due to edge effect at the duct mouth

θ Resonant duct inclination at the compression chamber

f Friction loss coefficient for oscillating flow in pies

K Vortex formation energy loss coefficient

C_r Radiation damping coefficient

Czitrom, Godoy, Prado, Perez and Peralta-Fabi proceeded then to model the behaviour of the SIBEO, neglecting non linear terms and comparing the dynamics of the device to a damped, two-mass, spring oscillator as shown by Figure C.2. Equations C.2 and C.3 were reduced to a set of fourth order differential equations as follows:

$$\frac{d^4 X_i}{dt^4} + a_1 \frac{d^2 X_i}{dt^2} + a_2 X_i = a_{3i} sin(\Omega t) \tag{C.4}$$

where the term $a_{3i} sin(\Omega t)$ represent the incoming wave signal with frequency Ω and amplitude a_3. The values a_1 and a_2 represents the surface wave amplitude of the oscillating water in the ducts.

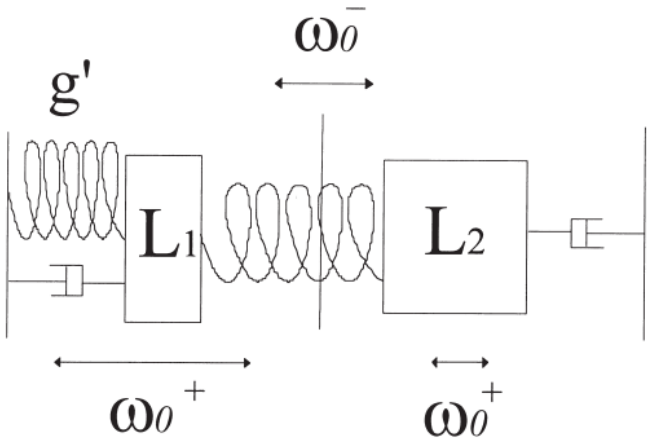

Figure C.2: Representation of the model pump as a damped, two-mass, spring oscillator. Czitrom, Godoy, Prado, Perez and Peralta-Fabi (2000). L_1 and L_2 represent the masses of water in the two ducts, g' is the corrected gravitational force ($g' = gcos\theta$), ω_0^+ the natural frequency of oscillation of the masses, ω_0^- the bodily oscillation of the centre of mass.

Appendix D

Paper Published on Desalination and Water Treatment, 2009

Desalination and Water Treatment 7 (2009) 47–52
www.deswater.com
1944-3994/1944-3986

A wave energy driven RO stand-alone desalination system: initial design and testing

Davide Magagna*, Gerald Muller

Sustainable Energy Research Group, School of Civil Engineering and the Environment, University of Southampton, Highfield, SO17 1BJ, UK
Tel. +44 2380 594656; Fax +44 2380 677519; email: dm7@soton.ac.uk

Received 30 September 2008; Accepted 28 May 2009

ABSTRACT

Traditional desalination systems have high energy requirements which can be considered as the limiting factor for their application. Using renewable energy sources for desalination of seawater and brackish water can help to alleviate water scarcity in those areas with no electricity grid connection or supply shortages. This paper describes the development of a stand-alone, off-grid desalination system powered by wave energy. The device is designed to drive a reverse osmosis (RO) membrane. No electricity is required. The system consists of two main parts; a high pressure pump (WaveCatcher) that allows generation of a high pressure head from low head differences, and a wave driven pump to supply the necessary head to the WaveCatcher. The high pressure pump is designed to produce 6 MPa of pressure which is necessary to drive a RO membrane for desalination of water. A 1:6 scale physical model was built and tested; pressures of 42 m were achieved from an initial pressure head of 0.2 m. Delivery of water to the WaveCatcher is to be achieved through the use of an oscillating water column (OWC) pump. The pump consists of a two-part resonant duct, which allows resonance control by varying the angle of the output duct. Maximum lift heights of five times the wave height were reached. The initial experiments showed that the WaveCatcher can generate the necessary pressure to run the RO membrane for the production of drinking water without the use of electricity.

Keywords: Reverse osmosis; Wave energy conversion; Sustainable development

1. Introduction

The limitations of traditional desalination systems have prompted researchers to focus on alternative energy sources to power desalination plants. Solar, wind, biomass, wave, and hybrid systems have all been implemented and installed worldwide.

While solar and biomass technology have been widely employed , wave energy driven systems were developed mostly in the last 20 years and still have to find wider applications [1]. The development of wave energy driven desalination has been inhibited by the difficulties of harnessing wave energy in an efficient way. Solving the issue related to wave energy will aid the development of wave driven desalination.

Furthermore, for all renewable energy driven desalination systems, the technical knowledge and complexity of the system always lead to restrictions in the use of clean desalination technologies for supplying water in poor or

*Corresponding author.

Presented at EuroMed 2008, Desalination for Clean Water and Energy Cooperation among Mediterranean Countries of Europe and the MENA Region, 9–13 November 2008, King Hussein Bin Talal Convention Center, Dead Sea, Jordan.

undeveloped areas [2]. In order to provide clean water for rural areas, a different approach for desalination technologies is needed, aiming at reducing the cost of the technology, hence making desalination widespread [3].

Two main features of the system can be defined:

- ease of use, in order to reduce the technical knowledge needed for operational management;
- low cost technology, simple to build and maintain.

Although efficiency in traditional desalination systems is fundamental for reducing running costs of the system, it cannot be used as a limiting factor when the production of clean water is aimed at satisfying primary needs.

This paper describes the development of a simple off-grid wave energy driven desalination system. The system presented here was designed to drive a reverse osmosis (RO) membrane by using wave energy, thus requiring no electricity. The main requirements for the system is the conversion of wave energy into a pressure head, and the provision of the very high pressure needed for the RO cell of 6 MPa or 600 m water column (w.c.) from the low head difference generated by wave action. The system consists of two main parts: (1) a high pressure pump (WaveCatcher) for the generation of a high pressure head from low head differences, and (2) a wave driven pump to supply the necessary amount of water to run the WaveCatcher.

2. The WaveCatcher system

The WaveCatcher system has been designed in order to drive a RO desalination membrane without the generation of electricity. The energy needed to pressurize the feed water will is generated from the high pressure pump, trough conversion of the energy content of the incoming waves.

The key points upon which the design of the WaveCatcher was based were:

- installation in rural areas, requiring ease of use of the system, and therefore minimum maintenance
- installation of the device nearby the sea or ocean in order to exploit energy from wave action [4]
- structure of the WaveCatcher capable of resisting harsh environmental conditions such as wave impact and corrosion.

On this basis a design of the system was developed: initially the WaveCatcher was designed to achieve at full capacity the generation of high pressure head (6 MPa or 600 w.c.) from a low head difference (0.02–0.03 MPa) corresponding to a mean wave height ranging between 2–3 m.

The working principle of the WaveCatcher is based upon the accumulation of water from wave action to cyclically drive a piston: water is collected in a tank; the weight of the water then activates a piston system which generates high pressures.

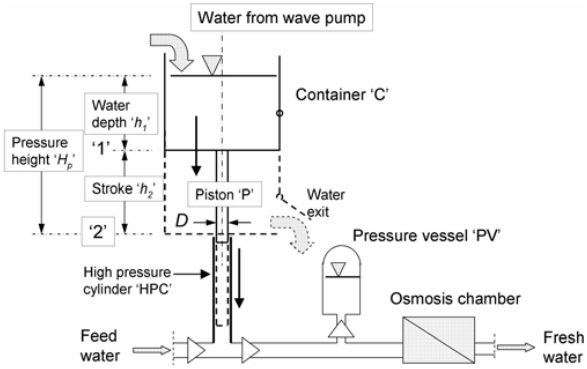

Fig. 1. Scheme of the working principle of the WaveCatcher. The water collected in container C of depth h_1 and area A, drives the piston P of stroke h_2 and diameter D. The feed water is pressurized and sent to the RO chamber. The pressure vessel (PV) is used to avoid pressure surges on the membrane. The system works if the weight of the water in the container generates a pressure of more than 60 MPa (600 m w.c.).

In Fig. 1 a sketch of the installation of the WaveCatcher describing the main components of the system is presented. A series of pressure vessels, valves and a storage tank are installed at the output of the WaveCatcher pump. This allows for the pressurized water to be stored without pressure losses. The use of the storage tank is necessary in order for the WaveCatcher to maintain the required pressure on the RO membrane [5].

$$\frac{\rho g A h_1}{(D^2/4)\pi} \geq 6\,\mathrm{MPa} \tag{1}$$

An initial analysis was conducted to determine the efficiency of the system with regards to the location of the installation, considering the WaveCatcher as a simple potential machine. The overall efficiency of the system depends on two main design parameters: the depth of the collection tank h_1 and the length of the piston stroke h_2 as reported in Fig. 1. Two types of installations were analyzed theoretically with the piston stroke starting at the mean water level (m.w.l.) and with the stroke starting above m.w.l. (Fig. 2). From testing it has been determined that in order to operate at higher efficiency it is necessary to install the WaveCatcher above the main sea level and to be designed to work at high h_2/h_1 ratios. Fig. 3 illustrates how efficiency is maximized by high h_2/h_1 values, suggesting models with wide collecting area and shallow depth, with the piston above m.w.l.

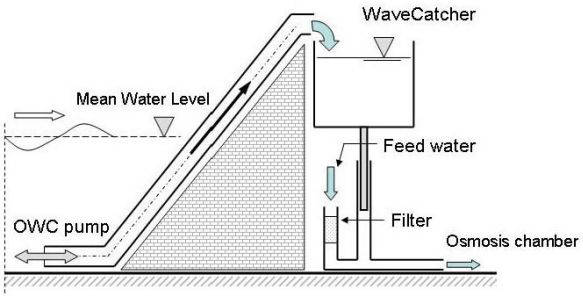

Fig. 2. Proposed installation of the Wavecatcher with OWC pump on an existing breakwater.

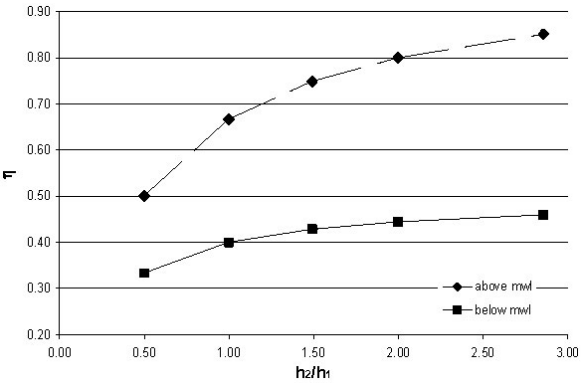

Fig. 3. Efficiency of the WaveCatcher at different configurations.

For this reason, it was determined that the ideal location for the installation of the WaveCatcher would be in the proximity of a steep shore, or on a breakwater. The delivery of water to the WaveCatcher is then of primary importance for the functioning of the system.

The WaveCatcher needs to be supplied with incoming water from wave action in order to generate the required pressure to drive a RO unit. Feed water is to be supplied to the WaveCatcher by an oscillating water column (OWC) water pump. The pump acts as an energy converter exploiting the continuity of the momentum of the incoming wave to amplify the wave height and lift the water conveyed in the ducts to a required level.

3. Methodology

The research project here presented is composed of different phases, each aimed at the development and study of every component of the system. The first phase of the project was aimed at the design, development and testing of the WaveCatcher high pressure pump: the piston pump mechanism was built in different configurations to assure a constant and automatic function of the filling/emptying mechanism of the collection tank. A 1:6 model of the WaveCatcher was built and tested under different conditions in order to determine the maximum pressure achievable. The WaveCatcher was developed to achieve full functionality with a production of 6 MPa of pressure from lift heights of about 1.2 m, i.e. initial pressures of 0.012 MPa. Experiments were conducted to determine the maximum pressure for the scale model. The design characteristics of the scale model used for investigation during the physical testing are given in Table 1. It is important to notice, that according to the required pressure to drive the RO membrane, the dimension of every component of the WaveCatcher can be changed, therefore varying the efficiency of the system and the intensity of the pressure generated

Table 1
Dimensions of the scale model and for the prototype of the WaveCatcher. h_1 and h_2 refer to Fig. 1

Dimensions	Model, mm	Prototype, m
Piston diameter (D)	13 mm	0.078 m
Piston stroke (h_2)	84 mm	0.504 m
Collection tank height (h_1)	200 mm	1.20 m
Collection tank width	200 mm	1.20 m
Collection tank breadth	200 mm	1.20 m

A second phase consisted of theoretical studies and physical testing of an efficient way to convey water to the WaveCatcher. As previously stated, in order for the WaveCatcher to generate the required pressure and achieve full functionality, it is necessary to supply the collection tank with incoming water from wave action. For this purpose two wave energy converters were initially evaluated: an overtopping ramp and an OWC pump. Both convert the kinetic energy of the incoming wave into potential energy to lift the water.

Limitations to the overtopping system were soon noticed; therefore, studies on the delivery system were mostly focused on the functioning of the OWC pump. The pump was developed on the basis of the device presented [6,7], with a different resonance control system, and it is used to convert the kinetic energy of the waves in to potential energy to drive the WaveCatcher.

The proposed OWC pump is composed of a two-part resonant duct connected by a flexible joint, allowing resonance control by varying the angle of the output duct. A sketch of the OWC pump can be seen in Fig. 4. OWC pump tests have been carried out in a 4 m long, 0.2 m wide and 0.2 m deep wave tank. The water depth during testing was of 84 mm. The internal diameter of the pump was of 15 mm, and the horizontal section had a length of l_1 = 45 mm with an inclination angle $\alpha = 30^\circ$ for the lifting section. Tank wave periods ranged between 0.5–1 s with wavelength of testing waves ranging between 0.39 to

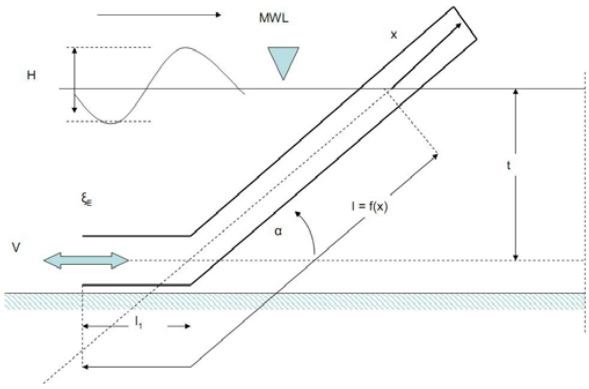

Fig. 4. Diagram of the OWC pump where l_i is the length of the input duct, l length of the input and output duct, t water depth and α angle to horizontal.

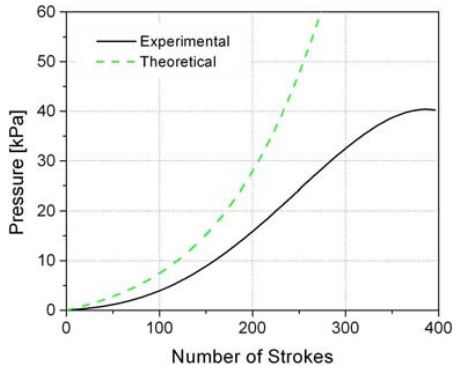

Fig. 5. Pressure build-up vs number of strokes compared with theoretical calculations.

1.56 m. This is translated in real scale to waves with period of about 3.5 to 7 s. Analysis of the volume of water delivered per incoming wave is presented, along with studies of how removal of water affects resonance control.

4. WaveCatcher: pressure testing results

The scale model of the WaveCatcher was tested in order to determine the maximum pressure achievable, and the increase of pressure generated by each stroke of the piston. It was estimated by theoretical calculations that the maximum pressure achievable by the model was 0.48 MPa when considering the losses due to friction between the material and the limitations due to the dimensions of the parts. Friction losses are expected to reduce tenfold when at full scale; however, a precise estimation is not possible at the moment.

In order to determine the maximum pressure achievable, a 2l PET bottle was attached as a load, and water was supplied to the WaveCatcher at constant intervals. At each stroke the change in pressure was determined; the water collected in the tank released and the tank was driven back to the starting position with the use of a 3 kg counterweight. The continuous repetition of the procedure generates the build-up of pressure in the pressure vessel.

A decrease in the ratio of build-up in the storage tank was noticed, with the pressure reaching a stationary level after more than 300 strokes. This is explained by the fact that the pressure in the vessel had to be built up from zero; once the maximum pressure was reached the system losses could be estimated. After 350 strokes the pressure in the vessel stabilized at the maximum value of 0.42 MPa, achieving 85% of the theoretical pressure that could possibly be generated by the model. A plot of the increase of pressure in the pressure vessel can be found in Fig. 5.

5. OWC pump: testing and results

The correct functioning of the OWC pump is critical for the positive outcome of this research. Theoretical studies were therefore conducted before physical testing started. In particular, studies were conducted to determine the resonant frequency, and the effect of the output angle on resonance, and the overall delivery efficiency of the pump. The output angle of the pump acts as resonance control for the system. Resonance in the pump occurs when the natural frequency of oscillation of the pump ω_s is equal to the frequency of the incoming wave f [Eq. (2)] [8]:

$$\frac{\omega_s}{2\pi} = f \tag{2}$$

where ω_s is given by

$$\omega_s = \sqrt{\frac{g}{l + \frac{t}{\sin\alpha}}} \tag{3}$$

Here g is the gravitational constant, l the length of the input duct, t the water depth and α the angle of inclination of the output duct. When resonance is reached, lift heights considerably exceeding the wave height can be achieved [9].

In Fig. 6 a plot of the relationship between ω_s and the angle α for different input pipe lengths is presented. One can notice how different configurations of the OWC pump can adapt to different wave frequencies, or different wave conditions. The adaptability of the OWC pump to promptly respond to a variation of the wave regime is of high importance allowing the WaveCatcher system to work independently from the variability of the renewable energy source.

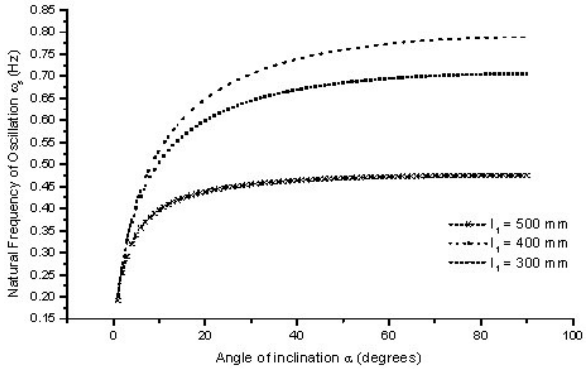

Fig. 6. Plot frequency vs angle for different input pipe lengths.

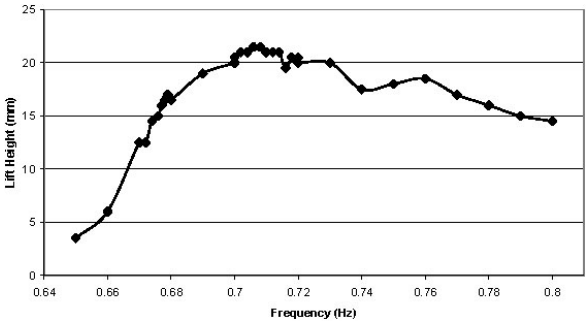

Fig. 7. Plot Lift heights by varying wave frequency near resonance for α = 30°. Resonance is obtained when f = 0.707 Hz.

Physical testing of the OWC pump was conducted in the hydraulic laboratory at University of Southampton, initially at a scale of approximately 1:20. Limitations due to the scaling of the experiments affected the testing by increasing the damping. Damping was determined to reduce the natural frequency of oscillation, as in Eq. (4).

$$\omega_s = \frac{2\pi}{T\sqrt{1-D^2}} \quad (4)$$

The damping coefficient D was estimated to be 0.76, affecting ω_s by increasing it by 54%.

Two types of investigation were carried out: first a series of tests was used to observe the average lift height; the lift height/wave height ratio was then determined. In Table 2 the ratio lift height/wave height for α = 30° is presented.

A second series of tests was conducted with a fixed wave height, while the wave period was varied in order to determine the range of frequencies where lift height and delivery is maximized. Fig. 7 presents the plot of the height achieved by varying wave frequency for α = 30°.

From the physical testing of the OWC it can be noticed that the maximum lift height is approximately 4 to 5 times higher than the height of the incoming wave. This means that a volume of water ranging between 3 and 4×10^{-6} m^3 is conveyed by the pump during the tests, which at full capacity, and assuming a wave height of 1 m, translates to 0.14 m^3 of water being delivered to the WaveCatcher for each incoming wave. The delivery of water can be increased by varying the diameter of the OWC pump, since it does not affect the resonance control.

Table 2
Lift height/wave height ratio determination for testing when α = 30° (average lift height/wave height ratio is 4)

Paddle stroke (mm)	Lift height, h_l (mm)	Wave height, H (mm)	Ratio h_l/H
10.6	0.0	1.8	0.0
13.8	2.0	2.3	0.9
15.8	7.5	2.7	2.8
18.2	14.5	3.1	4.7
23.2	17.0	3.9	4.3
23.6	**20.0**	**4.0**	**5.0**
26.0	**21.5**	**4.4**	**4.9**
30.6	23.5	5.2	4.6
33.8	25.0	5.7	4.4
37.1	26.5	6.3	4.2
41.3	28.0	7.0	4.0
45.9	31.0	7.7	4.0
45.89	31.5	7.7	4.1

6. Discussion and conclusions

This paper presents the first results of the investigation into an off-grid, wave energy driven desalination system. The main emphasis has been placed on the development of a stand-alone system that can be used for primary desalination needs in rural communities. Among the main advantages of the WaveCatcher is the fact that no electricity is required to drive the RO cell; therefore, the system is employable in any location with proximity to a shore or a cliff.

The WaveCatcher has been designed to be user-friendly being a full mechanical system that can be easily maintained without training required.

Tests showed that a 1:6 scale model of the WaveCatcher can generate a maximum pressure of 0.42 MPa from an initial head difference of 2 kPa (or 42 m w.c. from 0.2 m w.c.), translating into a full scale pressure of 2.52 MPa. This pressure can be maximized: with respect to the value reported in Table 1, if the piston diameter D of the prototype is reduced to 8.43 mm, the pressure generated should rise to 0.6 MPa at model and 6 MPa at full scale.

The system also has a number of practical advantages: the driving water does not have to be even cleaned, it can

contain sand or biological components; only the feed water needs filtering. Due to the proximity with the shore, brine can be easily disposed of into the sea, while pressurized water can either be stored or directly used.

The WaveCatcher needs to be supplied with water from wave action in order to function correctly. The necessary amount of water to drive the WaveCatcher is supplied by an OWC water pump.

Studies have shown that an OWC pump, fitted with resonance control can lift the incoming wave of up to five times the initial wave height. The volume of water carried with each wave is then the accumulated in the collection tank of the WaveCatcher.

In order to expand the research presented here further work is required to reduce friction losses in the WaveCatcher mechanism. Studies on a group of OWC pumps working in parallel are underway in order to increase the volume of water delivered to the WaveCatcher and to stabilize the resonance control for random sea conditions. These studies will be carried out at a 1:10 scale in order to be directly comparable with the WaveCatcher needs.

Finally the systems will be coupled with a RO membrane. Pretreatments will be investigated when the OWC pump and WaveCatcher are fully operative.

Acknowledgments

This project could not have been carried out without the help of William Delabre, Pascal Galloway, Robert Hooper and Rob Winkel, who worked with dedication on the design of the WaveCatcher, achieving full functionality of the system.

References

[1] P.A. Davies, Wave-powered desalination: resource assessment and review of technology. Desalination, 186 (2005) 97–109.
[2] E.M. Nfah, J.M. Ngundam, M. Vandenbergh and J. Schmid, Simulation of off-grid generation options for remote villages in Cameroon. Renewable Energy, 33(5) (2008) 1064–1072.
[3] M. Qadir, B.R. Sharma, A. Bruggeman, R. Choukr-Allah and F. Karajeh, Non-conventional water resources and opportunities for water augmentation to achieve food security in water scarce countries. Agricul. Water Manage., 87(1) (2007) 2–22.
[4] E. Fosberry, Z.L. Gunton, G.M.P. Hawkswood and H. Radford, The WaveCatcher: A Micro-Renewable Energy System for the Generation of Fresh Drinking Water, University of Southampton, 2007.
[5] W. Delabre, P.W. Galloway, R. Hooper and R. Winkel, The WaveCatcher — A Wave-Powered Desalination System, University of Southampton, 2008.
[6] S.P.R. Czitrom, R. Godoy, E. Prado, P. Perez and R. Peralta-Fabi, Hydrodynamics of an oscillating water column seawater pump. Part II: tuning to monochromatic waves. Ocean Eng., 27(11) (2000) 1181–1198.
[7] S.P.R. Czitrom, R. Godoy, E. Prado, A. Olvera and C. Stern, Hydrodynamics of an oscillating water column seawater pump: Part I: theoretical aspects. Ocean Eng., 27(11) (2000) 1199–1219.
[8] D.V. Evans, Power from water waves, in: Annual Review of Fluid Mechanics, Vol. 13, Annual Reviews, Palo Alto, CA, 1981, pp. 157–187.
[9] R. Godoy-Diana and S.P.R. Czitrom, On the tuning of a wave-energy driven oscillating-water-column seawater pump to polychromatic waves. Ocean Eng., 34(17–18) (2007) 2374–2384.

Appendix E

Paper for European Wave and Tidal Energy Conference. Uppsala Sweden, September 2009

Resonating wave energy converter for delivery of water for desalination and energy generation

Davide Magagna[1], Dimitris Stagonas[1]; David Warbrick[1]; Gerald Muller[1]

[1] Sustainable Energy Research Group, School of Civil Engineering and the Environment, University of Southampton, Southampton SO17 1BJ, United Kingdom

Abstract

The supply of clean drinking water is of great concern in many remote coastal areas. One method of providing this clean water is the process of desalination of seawater. This process generally requires either high temperatures (evaporation processes) or very high pressures (6MPa for reverse osmosis processes).

Current research at the University of Southampton focuses on the development of a wave powered stand-alone system for desalination and/or electricity production. A high pressure pump has been developed for pressurization of seawater for direct use in a reverse osmosis desalination process. The high pressure pump is driven by a supply of water, of 2 meter head, delivered by a simple wave energy converter. The proposed system has the benefit of simple technology and possesses significant potential for use in developing countries. This paper focuses on the device which will deliver water to the high pressure pump. The delivery device constitutes a wave energy converter and uses the principles common to most Oscillating Water Column (OWC) systems to pump water.

Keywords: OWC, desalination, energy conversion

Nomenclature

α	=	output duct angle
$\xi_{I,E}$	=	friction losses coefficient at entry
ξ_{Ex}	=	friction losses for outflow of water from OWCP
$\xi_{I,E}$	=	friction losses for inflow of water into OWCP
ξ_R	=	radiation damping
ω_p	=	natural frequency of oscillation pump
A	=	cross sectional area of the pipe
d	=	water depth at rest
D	=	damping coefficient
g	=	gravitational constant
H	=	incoming wave height
H_p	=	pumping height
l_1	=	length of input duct
l_2	=	length of output duct
l	=	total length of pipe representing mass of water at rest
l_a	=	added length of water in the pipe following a wave surge
L_F	=	length of fluid existing the output duct
MWL	=	Mean Water Level
OWC	=	Oscillating Water Column
$OWCP$	=	Oscillating Water Column Pump
RO	=	Reverse Osmosis
T	=	Wave Period experimental setup
T_{max}	=	Maximum T_w to give significant amplification
T_{min}	=	Minimum T_w to give significant amplification
T_n	=	Natural period of oscillation pump
T_{peak}	=	T_w at which amplification was maximum
T_w	=	incoming wave period
V_p	=	pumped volume
x	=	vertical displacement
xH	=	Amplification factor of H

1 Introduction

Most existing desalination systems present limitations, such as high costs and energy requirements, which have prompted researchers to explore alternative energy sources to power desalination plants. Solar, wind, biomass, wave, and hybrid systems have all been implemented worldwide.

Whereas solar and biomass technology have been widely employed, wave energy driven systems have only seen significant development over the last 20 years and have still to find wider applications [1] .

The development of wave energy driven desalination has been inhibited by the difficulties of harnessing wave energy in an efficient way. Solving the issue related to wave energy will aid the development of wave driven desalination.

The practical application of most of the existing renewable energy driven desalination systems is limited by the high level of technical knowledge required by the operators and the complexity of the systems. This has inhibited the installation of desalination technologies for supplying clean water in poor and undeveloped areas; areas where this technology could be of greatest benefit [2] .

In these rural areas a different approach to the design of desalination technologies is needed to reduce the total costs of installation and operation and hence enable the wider use of this technology [3].

It is therefore important to define the main features that need to be taken into account in the

implementation of a renewable energy driven system for supplying fresh water in rural areas. In particular the following two points must be satisfied for successful implementation:

- ease of use; in order to reduce the technical knowledge needed for operational management
- low cost technology; robust and simple to build and maintain .

A wave energy driven desalination system has been developed and it is characterized by being designed as a stand alone system – not requiring connection to an electricity grid - and not requiring electricity or supervision during normal operation. The system comprises of two main units: the WaveCatcher, a pressure intensifier, and a delivery pump, OWCP; which effectively uses the momentum contained in the incoming waves together with resonance principles to lift water to the WaveCatcher. (Figure 1)

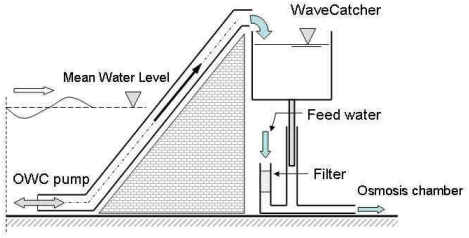

Figure 1: Proposed installation of the OWC wave Pump with WaveCatcher.

The WaveCatcher, a high pressure pump, was developed in order to pressurize seawater, which is then fed directly into a RO membrane for desalination. It comprises a large container, into which the wave pump empties the water, a small diameter high pressure piston onto which the full weight of the container acts thus generating a very high pressure, and an RO membrane, Figure 1. The design characteristics of the WaveCatcher allow for generation of at least 6 MPa of pressure (RO requirements) from low head pressure differences [4].

Whilst the high pressure pump can operate continuously to generate and maintain the required osmotic pressure, it is necessary to maintain a continuous supply of water, of 1-2 m head, from wave action. The delivery of water to the High pressure pump is achieved by an Oscillating Water Colum wave Pump (OWCP).

The OWCP consists of a pipe with a horizontal underwater section and an inclined pumping section, which extends above MWL (Figure 2). As waves pass, the pipe acts as a resonator with a natural period of oscillation, T_N. To maximize water delivery, the pump must be tuned to the incident wave period.

This paper discusses the use of the OWCP as an active wave energy converter for the delivery of water at 1 – 2 m head and presents recent developments in this field. It has to be noted that although the water for the high pressure pump is lifted above the structure, the OWCP does not constitute a classical overtopping device, such as the Tapchan or the WaveDragon. It is a resonator which shows a dynamic response to the incoming wave and uses this effect to transport water above crest height of the incoming waves.

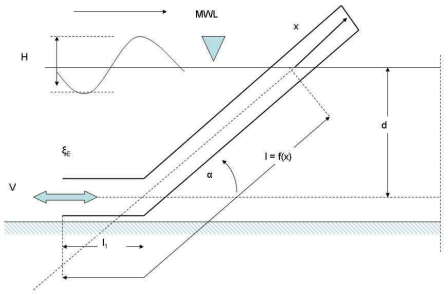

Figure 2: OWC Wave Pump - Theoretical variables l_1 the length of the input duct, d the water depth, H the incident wave height, l the total length of the column of water contained in the pipe and α the angle of inclination of the output duct.

2 Resonating wave energy converter

The OWCP proposed here is based on a principle first presented by Evans [5] and a somewhat similar but significantly more complex device previously developed by Czitrom et al., [6, 7]. The new OWC pump system is composed of a two part resonant duct connected with a flexible joint, allowing resonance control by varying the angle of the output duct (Figure 2). The OWC pump works effectively as an energy converter, changing the kinetic energy of the incoming wave into potential energy to lift the water inside the tubes. The difference to Czitrom's SIBEO device is the way in which resonance control is achieved, describing the pump as a damped oscillator.

In the original design [6] resonant conditions were maintained through control of the air compression chamber; adjustment of the volume of air contained in the chamber to modify the stiffness of the air spring [8]. In order to modify the air spring and the volume of air contained within the chamber, the SIBEO was equipped with a microchip that sampled the wave conditions and varied the volume of air in the chamber accordingly [9]. The system proposed by the authors for maintaining resonant conditions, by varying the angle of the output duct, is a simplification of the OWC pump aimed at reducing costs and increasing ease of use; both of which have been identified as essential for the application of this technology in rural areas and developing nations.

Mechanical similitude of the OWC wave pump

Research into the performance of OWC devices has been conducted since the 1970s [5], followed by a detailed mathematical description of the forces acting on such systems [10, 11]. More details can be found in

Chung's review of the oscillatory motion of water in an open pipe [12]. In the literature, the OWC wave pump was characterized as a damped oscillator. The OWC effectively acts as a resonator, described by its natural frequency of oscillation ω_s determined as shown in equation (1)

$$\omega_s = \sqrt{\frac{g}{l}} \tag{1}$$

Where l represents the total mass of water contained in the pipe and depends on the angle of inclination α as described by equation (2)

$$l = l_1 + \frac{d}{\sin\alpha} \tag{2}$$

Alternatively the OWCP is described by it natural period of oscillation. Whilst T_N can generally be expressed as$T_N = 2\,\pi / \omega_s$ it is important to include the effect of damping (D) on the natural period of oscillation as shown in equation (3)

$$T_N = \frac{2\pi}{\sqrt{(g/l)(1-D^2)}} \tag{3}$$

To reach resonance, it is necessary that the pump is tuned with the wave climate, hence that $T_N = T_w$. When, resonance conditions are reached, lift heights considerably exceeding the wave height can be achieved. Damping effects are due to friction inside the pipe and turbulence at the entry ($\xi_{I,E}$) and to radiation of waves outside the OWCP (ξ_R). The overall effect D is given by

$$D = \xi_{I,E} + \xi_R \tag{4}$$

It can now be observed that the angle α effectively acts as a resonance control; when the angle of inclination is changed the natural frequency of oscillation ω_s varies accordingly as shown in

Figure **3**, widening the ranges of frequencies that amplify the lift height achievable to a maximum.

Previous work showed that alterations of a single parameter of the system can cause changes in the resonance control of the OWC pump [13].

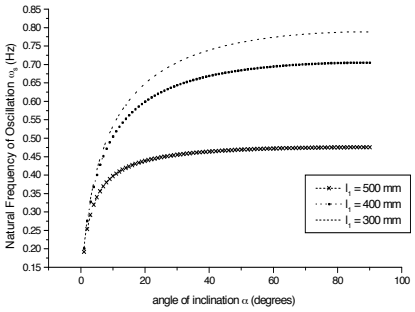

Figure 3: Frequency vs. angle, for different input pipe length

The theory behind the OWC pump has so far proven that a device like the one presented here can act as a wave energy convertor (WEC) for delivery of water and can easily be tuned to different wave conditions. Physical testing is, however, required to determine the capability of the OWCP to deliver water to a fixed position.

Consequently, laboratory studies were conducted along with theoretical analysis with the aim of facilitating the implementation of the OWCP at full scale.

3 Methodology

The performance characteristics of the OWCP will be determined using a combination of physical model tests and theoretical modelling. A 1:40 model of the OWCP was built and tested in a wave flume at the University of Southampton, UK, in order to determine the performance under varying incident wave conditions and to evaluate the maximum lift heights achievable. For simplicity, a range of different configurations of the OWCP were used - rather than the proposed flexible joint - for analysis of the resonance control. Implementation and testing of the flexible joint will be carried out at later stage.

The physical model testing allowed for the determination of the relationship between the wave regime (wave height and period) and the lift height achievable.

Different configurations of the OWC pumps and wave flume conditions were taken into account in order to produce the highest possible number of scenarios. The main parameters varied during the experimental procedure are given in Table 1.

Different pump diameters were used to reduce the effect of friction losses (larger diameters yields a smaller friction effect) and to identify damping and scale effects due to the testing conditions.

Parameters	Range of values	Increase Step
Angle of inclination	15 º -30 º	5 º
Internal diameter	15-25 mm	10 mm
Water Depth inside tank	80-105 mm	5 mm
Angle of incoming wave	0 º-15 º	5 º(*)
Type of Slope	1:20 – 1:8	
Location of OWC Pump	Bottom/ half d	

Table 1: Parameters varied during the physical model testing of the OWC PUMP. For each run a parameter was changed, generating 768 possible testing configurations. (*) A programme of testing in a 5m by 2m wave basin is planned to assess 3D effects.

Wave flume test setup

Wave flume tests were conducted in a 6 m long, 0.2 m wide and 0.2 m deep, clear acrylic sided, table top wave flume. A piston type wave paddle was used to generate small, monochromatic waves with heights

ranging between 1 to 5 cm. Wave periods also ranged between 0.5 - 1 s within the flume, corresponding to prototype scale waves of approximately 4.9 to 9.9 seconds wave period using Froude's scaling. Three resistance type wave gauges were used to monitor the wave conditions. In this first testing phase only monochromatic waves have been used.

A Styrofoam ball was placed in the centre of each pump, on a specially designed rail to follow the movement of the water surface. The ball displacement was recorded by a digital camera (60fps) and subsequent image analysis revealed the lift heights achieved (Figure 4).

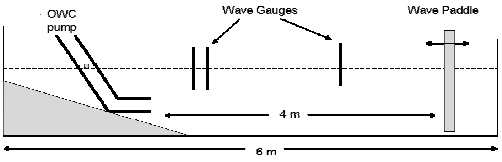

Figure 4 Setup for wave tank physical experiment.

Field tests

In order to verify the response of the OWC pump to real seas and random waves and to test the survivability of the pump under adverse weather conditions, sea testing was started.

A first phase of sea testing started in February 2009 at Milford on Sea (50.71227 N, -1.61415 E) on the South Coast of England.

The location was chosen due the availability of accurate sea state data allowing the rapid mobilization of the equipment in response to favorable conditions.

Wave data, including dominant and peak, deep water wave height, wave period and direction were provided by wave rider buoy located in the English Channel in close proximity to the testing site. The wave data was provided by the Channel Coastal Observatory, UK (CCO).

The wave data was supplemented with local shallow water measurement of incident wave conditions made from the shore during testing of the OWCP. Nearshore measurements consisted of shallow water wave height, wave period and direction, and the vertical lift height achieved by the OWC.

For the sea tests, a pipe with 110 mm diameter was used. The length of the input duct (l_1) was of 1m, while the length of the exit duct was of 5m (l_2). The pipe was positioned at a water depth of 0.9 m, and was attached to a groyne for stability.

For the preliminary testing, an opaque pipe was used; hence, it was necessary to devise a method of extracting the water level within the pipe. To do this, holes of 5mm diameter were drilled at a spacing of every 100mm along the exit duct. The lift height was estimated with the use of a videocamera; using the highest hole where water was seen to escape as a guide to the water level within the duct. The dimension of the holes was such to have negligible effect on the water level achieved within the OWCP, however the spacing of the holes is considered likely to result in a slight underestimation of the lift height achieved, of the order of 100mm. A second phase of testing is underway at the time of writing. This phase of testing has been broadened in order to measure the volume of water delivered to a fixed height for each incoming wave using an array of pipes each tuned to a particular wave frequency. This is because, as seen in the laboratory results and in the literature[7], each configuration of the OWC pipe responds monochromatically to a polychromatic input. Full results of real sea testing of the OWC pump are expected by June-August 2009.

Mathematical Model for the OWCP

A simple linear mathematical model was initially developed. Comparison with experimental results however indicated that a linear model was not suitable. The model was therefore expanded to include two non-linear terms:

1. The mass contained in the tube; $m = \rho\ (l + l_a + x / \sin\alpha)$ whereby x is the vertical displacement

2. The damping: turbulent damping at the entry/exit is considered to be dominating; this is however a function of $(dx/dt)^2$ with different loss factors for inflow ($\xi_I = 1.0$) and exit ($\xi_E = 0.5$).

The model is needed to validate the data obtained from physical testing and better evaluate parameters such as friction and damping. The model, once validated will be used to forecast real sea applications.

The numerical scheme used takes into consideration the wave conditions generated in the physical modeling and computes the movement of the mass of water inside the OWCP at the passing of each wave. Each incoming wave exerts a force $F(t)$ acting on the input pipe of the OWC pump and at any time can be expressed by equation (5)

$$\rho\left(l + l_a + \frac{x}{\sin\alpha}\right)\frac{d^2x}{dt^2} + \rho g x \sin\alpha + \operatorname{sgn}\left(\frac{dx}{dt}\right)(\xi_{I,E} + \xi_R)\frac{\rho}{2}\left(\frac{dx}{dt}\right)^2 = F(t) \tag{5}$$

The first part of equation (5) includes terms for the mass acceleration inside the pump; the losses due to friction and the action of the restoring gravitational force. In the numerical solution, the $(dx/dt)^2$ damping term is multiplied with $\operatorname{sgn}(dx/dt)$ in order to maintain energy extraction from the system. The mathematical model has also been implemented for the determination of the volume of water that can be pumped for a given pump height H_P. The pumped volume V_P is given by equation (6)

$$Vp = (x - H_p) \times A \tag{6}$$

The pumped volume corresponds to the amount of water that can be delivered to the High Pressure desalination pump and the influence of the cycle time of the WaveCatcher. The pumping action was implemented into the numerical model, and the pumped

volume per wave can then be expressed as the length of fluid L_F which exits the pump at the prescribed pumping height H_P. Both values are non-dimensionalised by dividing them by the wave height H. **Figure 5** shows the normalized pumping volume L_F /H as a function of the ratio of wave period and natural period of the pump for relative pump heights H_P /H ranging from 2 to 4.

The removal of mass and energy from the system increases the system bandwidth as expected; the more energy that is extracted, the wider the response curve becomes.

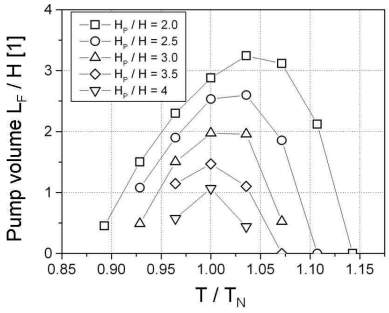

Figure 5: Pumping volume as function of pump height, wave height and period

4 Results and discussions

Video analysis was used to determine the lift height achieved at various stages of the process, for both resonant and non resonant conditions. From image analysis it was possible to determine the wave height of the incoming wave, the maximum height of wave on the column and the maximum lift height inside the pump.

Analysis of the data obtained from physical testing of the OWCP have shown that the maximum lift height for a 30º angle pump with 95 mm water depth was 45 mm (taken at the level of Styrofoam) for 20 mm incident deepwater wave height, giving an amplification factor of 2.25H. The maximum lift height achieved for the same test, taken as the maximum height a particle of water can achieve is of 60 mm, 3 times H.

and Figure 7 present frameshots highlighting the effect of the incoming wave period on the maximum lift height that is achievable for two different wave conditions for the same pipe configuration (30º angle at 95 mm water depth).

For each of the OWCP model presented in Table 1, the natural period of oscillation was determined along with the range of periods that produced remarkable amplification of the incoming wave height. These are reported in Table 2 along with the average amplification factor determined for the case study presented.

Angle	T_{min}	T_{max}	T_{Peak}	xH
15 º	1.12	1.53	1.25	1.9
20 º	1.11	1.42	1.17	2.0
25 º	0.83	1.05	1.00	2.2
30 º	0.76	0.95	0.85	2.25

Table 2 Natural Period of oscillation for specified configuration of the OWC tested with 95 mm water depth

Damping, friction and scale effects

Strong damping effects were observed in all the physical model tests.

For the 30º angle at 95 mm water depth a theoretical value of the natural period of oscillation was determined as 0.98 s; damping and friction effects shifted the observed value to 1.41 s. The fact that damping increases the natural period of the system means that it can be employed to tune the pump to the prevailing wave period.

Furthermore the use of dye allowed the observation of the friction and reflection effects that occurred at the mouth of the input duct of the pipe as well as the visualization of the behaviour of the mass of water contained in the OWCP. (Figure 8): dye was inserted when maximum amplification was achieved within the pipe. The use of dye was considered suitable since the interest focused on the visualization of the mass of water and its dispersion while exiting the mouth of the input duct.

Figure 6 Frameshots of incoming wave exerting force on the pump at non resonant conditions. (a) Incoming Wave and measurement of wave height on the slope; (b) maximum wave height achieved and (c) maximum lift height.

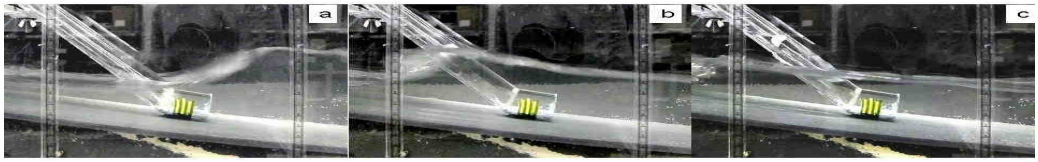

Figure 7 Frameshots of incoming wave exerting force on the pump at close to resonant conditions. (a) Incoming Wave and measurement of wave height on the slope; (b) maximum wave height achieved and (c) maximum lift height

In order to quantify the losses at lip (entrance) of the OWCP pump the us of Particle Image Velocimetry (PIV) is preferred [14].

PIV experiments for the determination of losses around the OWCP are planned at a later stage of the present research. Reduction of these losses will be beneficial to the implementation of the OWCP in future.

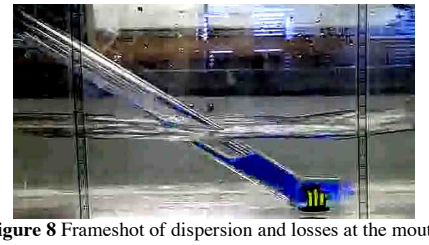

Figure 8 Frameshot of dispersion and losses at the mouth of the OWCP. It is possible to notice that the dye is dispersing while exiting the OWCP.

Comparison with mathematical model

The mathematical model was developed to replicate the laboratory experimental. At the present time, only a few simulations have been run to validate the numerical model against laboratory tests.

A more thorough validation of the numerical model against a broader range of laboratory tests is planned and will enable determination of the value of the ξ_E , ξ_I, ξ_R coefficients.

However, it was possible to compare the data obtained from experiments with the data obtained from the numerical model for some particular cases. Figure 9 presents the comparison of the data obtained from the simulation model and those obtained in the lab for the 30° angle, 85 mm water depth, 15 mm diameter test.

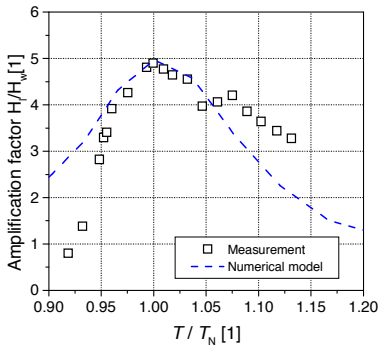

Figure 9 Comparison of the lift height amplification factor (H_l/H_w) between simulation and experiment.

The correlation obtained between simulation data and experimental data is good for values close to the natural period of oscillation; however when moving away from resonant conditions, experimental and theoretical values are found to disagree somewhat although the trends are similar (graph is skewed towards higher ration T / T_N). It is believed that pipe wall effect has a strong influence in reducing the amplification factor at low frequencies, while it amplifies the wave signal at frequencies higher than resonant. The non-linear equation does however provide a significant improvement over the hitherto employed linear models which utilized empirical 'added mass' factors to match experimental results.

5 Conclusion and further work

In this paper the use of an OWC wave pump, as an energy converter for the delivery of water to be coupled with desalination devices, was presented.

The OWC wave pump is an affordable alternative energy source that, when coupled with the WaveCatcher can be used for the supply of clean water in remote areas without the high costs of conventional desalination technology.

Experiments showed that the OWCP, fitted with resonance control is able to amplify the incoming wave signal by up to 5 times the incident wave height, with an average value of the amplification factor ranging between 2.25 and 4 time the incident deep water wave height.

With the physical model test it could be demonstrated that for each configuration the OWCP achieves it maximum delivery with waves of a period close to the natural period of the OWCP. These results show that it is possible to tune a particular type of OWC wave pump according to the dominant wave periods present in a defined area.

The research presented here provided encouraging results for the future application of the OWCP wave pump. Further work is required to more fully assess the use of the OWCP as a water delivery device. The device may also have further potential as a system for increasing water exchange between the ocean and enclosed basins for the improvement of water quality and hence amenity value.

In particular current and further work is focused on the development of a Pan-flute array of pumps each tuned to a different incident wave period; making the OWCP independent of seasonal changes of wave climate and 3D wave flume test to analyze arrays effects and determine how different angles of incoming waves affect the delivery.

The simplicity of design of the OWC pump prototype allows for efficient testing of the device at sea utilizing the availability of local wave climate data. In future work, for both sea and laboratory testing, the maximum volume of water delivered will be measured. Particle tracking software will be used to determine, with higher accuracy, the maximum achievable lift heights. Focus will also be given to analyze the changes in the resonance properties due to the removal of water

from the OWCP and into the correct estimation of the values of the friction $\xi_{I,E}$, and damping ξ_R coefficients.

6 Acknowledgements

This work has been funded by the School of Civil Engineering and the Environment of the University of Southampton.

References

[1]. Davies, P.A., *Wave-powered desalination: resource assessment and review of technology*. Desalination, 2005. **186**(1-3): p. 97-109.

[2]. Nfah, E.M., et al., *Simulation of off-grid generation options for remote villages in Cameroon*. Renewable Energy, 2008. **33**(5): p. 1064-1072.

[3]. Qadir, M., Sharma, B. R. , Bruggeman, A. Choukr-Allah, R. , Karajeh, F., *Non-conventional water resources and opportunities for water augmentation to achieve food security in water scarce countries*. Agricultural Water Management, 2007. **87**(1): p. 2-22.

[4]. Magagna, D. and G. Muller, *A wave energy driven RO stand-alone desalination system: initial design and testing*, in *Desalination Cooperation among Mediterranean Countries of Europe and the MENA Region*, E.E. Society, Editor. 2008: Dead Sea, Jordan. p. 6.

[5]. Evans, D.V., *Oscillating Water Column Wave-Energy Device*. Journal of the Institute of Mathematics and Its Applications, 1978. **22**(4): p. 423-433.

[6]. Czitrom, S.P.R., Godoy, R. , Prado, E. , Perez, P. , Peralta-Fabi, R., *Hydrodynamics of an oscillating water column seawater pump: Part I: theoretical aspects*. Ocean Engineering, 2000. **27**(11): p. 1181-1198.

[7]. Czitrom, S.P.R., Godoy, R. , Prado, E. , Olvera, A. , Stern, C., *Hydrodynamics of an oscillating water column seawater pump. Part II: tuning to monochromatic waves*. Ocean Engineering, 2000. **27**(11): p. 1199-1219.

[8]. Czitrom, S.P.R., *Wave Energy-Driven Resonant Sea-Water Pump*. Journal of Offshore Mechanics and Arctic Engineering, 1997. **119**(3): p. 191-195.

[9]. Czitrom, S.P., C. Coronado, and I. Nunez. *Flushing of the port of Ensenada using a SIBEO wave-driven seawater*. in *9th Pan American Congress of Applied Mechanics (PACAM 9)*. 2006. Merida, MEXICO: Mathematical Science Publ.

[10]. Evans, D.V., *Power from water waves*, in *Annual review of fluid mechanics. Vol.13*. 1981, Annual Reviews Inc: Palo Alto, CA, USA. p. 157-87.

[11]. Brendmo, A., J. Falnes, and P.M. Lillebekken, *Lineår modelling of oscillating water columns including viscous loss*. Applied Ocean Research, 1996. **18**(2-3): p. 65-75.

[12]. Chung, D.H., *Water Oscillation in an Open Tube* ISB Journal of Physics, 2008. **2**(1).

[13]. Godoy-Diana, R. and S.P.R. Czitrom, *On the tuning of a wave-energy driven oscillating-water-column seawater pump to polychromatic waves*. Ocean Engineering, 2007. **34**(17-18): p. 2374-2384.

[14]. Muller, G. and T.J.T. Whittaker, *Visualization of flow conditions inside a shoreline wave power-station*. Ocean Engineering, 1995. **22**(6): p. 629-641.

Appendix F

Paper for Third International Conference on the Application of Physical Modelling to Port and Coastal Protection. Barcelona, Spain, September 2010

USING SMALL-SCALE HYDRAULIC MODELS FOR THE PRELIMINARY DEVELOPMENT AND INVESTIGATION OF NEAR-SHORE WAVE ENERGY CONVERTERS

DAVIDE MAGAGNA (1), DIMITRIS STAGONAS (2) and GERALD MULLER (3)

(1) Mr., Sustainable Energy Research Group, University of Southampton, Southampton, SO17 3TG, United Kingdom.
d.magagna@soton.ac.uk
(2) *Dr., Sustainable Energy Research Group, University of Southampton, Southampton, SO17 3TG, United Kingdom.*
d.stagonas@soton.ac.uk
(3)Dr*., Sustainable Energy Research Group, University of Southampton, Southampton, SO17 3TG, United Kingdom.*
g.muller@soton.ac.uk

Due to ease of installation and operational management; installations of onshore Wave Energy Converters are strongly favoured. The successful implementation of WECs is dependent on the correct analysis of the devices' response to wave climate and waves modification. Due to limitations in applying mathematical models for nearshore devices due to the hydrodynamics processes taking places, strong non linearities and wave breaking. Physical models experiments are therefore essential to the development of wave energy converters. The use of physical tests is limited by time and financial constraints, and low costs solutions to evaluate and implement devices in the early stages of development are essential. Accordingly the present work explores the potentials of using physical models with scales smaller than e.g. 1:30, which can be facilitated in table-top wave basins and flumes, for the preliminary development and investigation of near-shore Wave Energy Converters (WEC). The small-scale models (i.e. 1:50) of two novel energy converters are briefly described here and their validity and robustness is assessed through the comparison with larger scale physical models (i.e. 1:23) and theoretical analysis.

Keywords: Wave Energy Converters ; Near-Shore Energy Processes; Small Scale Models; Physical Models.

1. Introduction

Wave energy generation at the shoreline is attractive from the point of view of access and ease of construction. Generation is limited by the fact that the available wave energy reduces with decreasing water depth and by the exposure to the extreme conditions created by breaking waves.

Recent studies showed that only a minimal part of the energy is lost when energy conversion is taking place near shore. Folley (2007) determined that effectively only a 10% reduction in the usable energy is to be taken into account when moving from offshore to near-shore energy conversion; thus allowing for a re-evaluation of on shore Wave Energy Converters (WEC). The performances of near-shore WECs are influenced by the changes in the hydrodynamics processes of the wave travelling, and are better assessed through the use of physical models from the initial stages of the device's development.

Mathematical models have been predominantly employed in the initial assessment of WECs (Cruz, 2008), however, in order to fully assess the processes taking place in the coastal environment physical models are more suited. Numerical Models in fact allow for a quick and fast prediction of the conversion capabilities of a wave energy converter, but only the correct assessment of the behaviour of the device through physical tests can drive the final implementation and commercialization.

Physical models, in opposition to numerical models, involve most if not all the necessary processes found in the coastal environment. However, as in the case of the Wave Dragon (Kofoed et al., 2006) large scale hydraulic facilities are associated with large expenditure, requiring a high level of preparation, while at the same time access, to them is restricted for the majority of researchers and engineers.

In 2009, (EMEC, 2009) drafted guidelines for the physical testing of WECs, including the suggested testing periods, scaling a costing for models from 1:100 scale to prototype testing (Table 1) .

Table 1. Caption heading for a table should be placed at the top of the table and within table width.

	Phase 1	Phase 2	Phase 3
SCALE	1:25 - 1:100	1:10 - 25	1:3 – 1:10
TANK	2D/3D	3D	Site
DURATION	1 w/9 m	6-12 m	6-18 m
BUDGET	5 to 50 k€	50-250 k€	1-2.5 M€

The EMEC guidelines provide an indication of the path towards the optimization and the design of a successful device, and highlight the importance of physical testing for the development of WEC. However, the costs involved with the use of these facilities are elevated and a high level of preparation is required. Furthermore access to them is restricted or limited for the majority of researchers and engineers.

The present work explores the potentials of using physical models with scales smaller than e.g. 1:30, which can be facilitated in table-top wave basins and flumes, for the preliminary development and investigation of near-shore WECs.

This paper describes small-scale tests of three novel wave energy converters. The validity and robustness of the models is assessed with comparison with larger scales models and theoretical analysis.

2. Overview of the devices and facilities

Three novel WECs are currently under development at University of Southampton. Each device exploits different ways to absorb and convert the energy carried by the incoming wave trains. The conversion efficiency for an onshore overtopping device (Composite Sea-Wall, Figure 1), a non-resonant buoyant body device (Buoyant Body, Figure 3) and a resonant overtopping device (OWCP, Figure 5) is determined.

Physical model tests are employed from the initial stage of development for each device in order to assess conversion performance, allow immediate improvements and provide a data for comparison with theory.

For each device the conversion efficiency are evaluated in different testing facilities. Physical model tests are carried using a 3×1.5×0.3m wave basin and a 6×0.2×0.3 (50^{th} scale) wave flume (small flume). A 12×0.46×0.46m wave flume (large flume) is employed to facilitate comparison of the performance at different scale (1:23 scale). Regular waves are employed in all the tests, with wave heights ranging from 1 to 5 cm in the 1:50 scale, and from 2 to 11 cm in the 1:23 scale experiments

3. Composite Sea-Wall

The composite sea-wall consists of an onshore overtopping wave energy device. Onshore overtopping devices are attractive due to their simplicity, ease of construction and operation. Onshore Overtopping devices are independent from the wave period and, to a lesser extent, from wave direction. Composite Sea-walls have recently been built and with the purposes of reducing wave loads and overtopping of existing sea-walls.

The composite sea-wall here presented combines the same principle of energy conversion employed by the Wave Dragon (Kofoed et al., 2006) with the wave absorbing characteristic of a standard composite sea-walls. Composite sea-walls, like the one installed in Japan (Mori et al., 2008), consist of slit wall (or energy absorbing screen) in front of an impermeable wall. Compared with the composite-sea wall of Mori, the slit wall is replaced by a ramp which favours overtopping of water. The presence of the basin between the ramp and the wall reduces impact pressures and scouring effects at the bottom of the wall.

The concept of the composite sea-wall for wave energy conversion is presented in Figure 1. Provided that the lower part of the seaward screen is impermeable, with an upper crest at a distance R_c above mean water level (MWL), wave run-up will transport water into the basin between screen and sea wall. (Stagonas et al., 2010a)

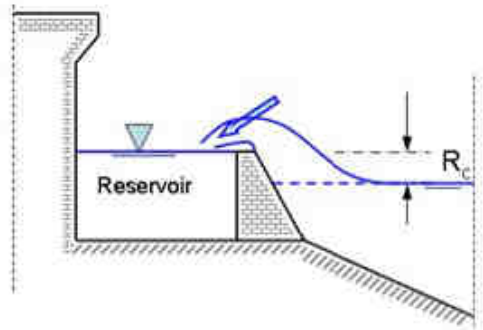

Figure 1 Schematic of the energy capturing composite sea wall

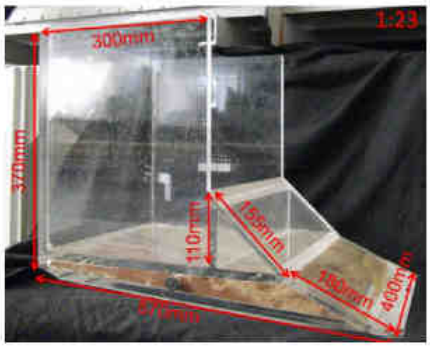

Figure 2 The 1:23 composite sea wall model

The head difference generated will probably be very small. Thus the exploitation of wave energy is realized with a novel and cost-effective hydropower converter for very low head differences which developed in the University of Southampton; the converted has a maximum efficiency of 66%. (Muller et al., 2009)

Experimental tests for the composite sea-wall were aimed at both establishing the conversion efficiency of the device, and in establishing the role of the structure in reducing pressure impacts. Overtopping volume in the basin was measured in the first case while pressure transducers were used to measure pressure impacts on the bottom of the basin and on the wall. Tests for the composite sea-walls were carried in the small and in the big wave flume, with a scale of 1:50 and 1:23 respectively. Both models were built using transparent acrylic (Figure 2)

Overtopping was measured for two different freeboard heights, corresponding to prototype values of R_c =1 m and R_c =1.5 m, and a slope of 1:10. For the test series in the smaller wave tank, regular waves of heights from 20 mm to 50 mm and periods between 0.5 sec and 1.4sec were generated at a water depth of 11.7 cm by a piston type wave paddle; the same, scaled-up, wave conditions were employed in the larger tank as well. Regular waves were considered appropriate since no resonance effects were employed. The average wave height during operational conditions is

considered with no interest in extreme events. For each experiment a wave train of six waves was generated and the volume of water collected in the reservoir was.

Video frames were used in order to observe and analyses the behaviour of the converters, and to provide further information on the conversion mechanism of the device. In particular video stills for the composite sea wall were employed to determine the location of the wave impact on the structure.

2.2 Buoyant Body

The second WEC under investigation at Southampton University is the Buoyant Body wave energy converter presented in Figure 3. The converter consists of a vertically moving uplift body, and a substructure which rests on the seabed. The body, which has positive uplift, is held in its vertical position as the wave crest approaches. Once a given uplift force is exceeded, the body moves upwards and pumps water into a pressure vessel. The converter is therefore only controlled by the incident wave height.

The Buoyant Body here presented differs from common buoyant WECs which are designed to exploit resonance effects to increase energy absorption. The use of resonance effects on the one side maximizes power capture, but on the other hand it requires very large masses and a complex control system to achieve it (Bruce, 2009). For these reasons, a non-resonant buoyant type WEC has been developed at University of Southampton.

A static theory was developed to describe the device, taking into account the buoyancy force F acting on the device and the uplifting effects of the incoming waves. The buoyancy force acting on the main body is given by equation (1).

$$F = \rho g b d \tag{1},$$

Where, with reference to Figure 4 , b represents the breadth of the buoyant body, d the submergence, ρ the water density and g the gravitational constant. When the waves approach the body is lifted of the distance $w = H - d$, where H represents the incoming wave height, generating a work W as follows

$$W = F \times w = \rho g b d (H - d) \tag{2}$$

By differentiating W with respect to d, the maximum power P_{max} can be determined,

$$P_{\max} = \rho g b \frac{H^2}{4} \tag{3}$$

By considering the power per unit width carried by a regular wave, given by P_w

$$P_w = \rho g L \frac{H^2}{8} \tag{4}$$

The efficiency of conversion η becomes function of b and of the wavelength L as reported in equation (5)

$$\eta = \frac{2b}{L} \tag{5}$$

Physical model tests were employed in order to verify the static theory developed for such device and to determine the conversion efficiency of the device with an hydraulic power take-off (PTO) system installed.(Muller et al., 2010)

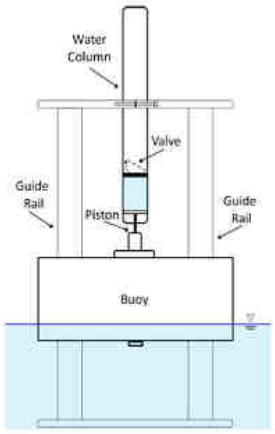

Figure 3 Schematic of the non-resonant, buoyancy type, WEC

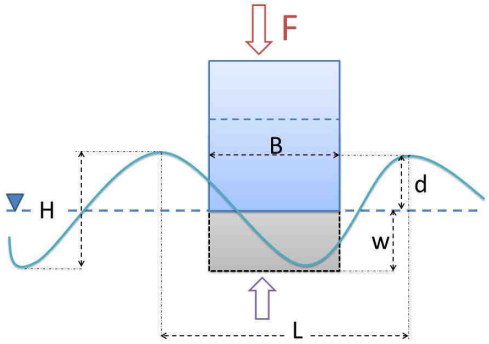

Figure 4 Description of Variables for Buoyant Body WEC

Model tests of the device were conducted in the small wave flume and in the 3D wave basin. Tests in the small flume were aimed at assessing the displacement of the buoy with no PTO installed, whilst 3D test were aimed at determining the conversion efficiency of the WEC. 3D tests were preferred due to the nature of the device that can be considered a point absorber, since the generation of radiated waves in the downward motion of the buoy can affects the behaviour of the device. 2D experiments do not allow for the correct analysis of the radiation component.

The water depth in the basin was kept at 250 mm, waves were generated by a piston-type wave maker with periods from 0.4 to 0.9 seconds, and heights from 7 to 35 mm. The wave energy converter consisted of two 20 mm diameter vertical guiding bars, on which a 0 × 190 mm buoyant body of 60 mm height, made of foam, ran. A 25 mm piston was fitted to the buoyant body or buoy. The power take-off consisted of a vertical riser tube of 25 mm internal diameter, a feeder basin and two valves as shown in Figure 3. During a working stroke, the water level at the float would increase until the buoyancy forces are large enough.

2. 3 Oscillating Water Column Wave Pump

The third type of WEC under investigation at University of Southampton is the Oscillating Water Column Wave Pump (OWCP), a resonant type of wave energy converter aimed at water delivery. The OWCP is a simple overtopping resonant type of wave energy converter based on the more common Oscillating Water Column (OWC).Whilst standard OWC device are aimed at the generation of electricity through the generation of an-air flux from the oscillating movement of water within a resonance chamber; the OWCP is designed to exploit the higher level in the resonance chamber, removing part of the lifted water to store energy in the form of potential energy.

At the passing of waves, when resonant conditions are achieved within the OWCP, the water contained within the OWCP is lifted, removed from the device and collected in a reservoir (Figure 5). The water collected in the reservoir is then used to activate a High Pressure Pump (HPP) designed for direct desalination system. Resonant conditions are achieved when the frequency of the incoming waves matches the natural period of oscillation of the OWCP. Resonance control is achieved through changes in the angle of inclination of the resonant duct of the device (Magagna et al., 2009).

In order to assess the conversion behaviour of the OWCP physical experiments were carried with a 40th scale in the small wave flume and in the wave basin, 1:20 scale in the large wave flume. The aims of these tests were to assess the performance of the OWCP, to validate a mathematical model for the prediction of the delivery rate, and to investigate the behaviour of multiple OWCPs working in an array. In particular, in this paper we highlight the use of physical experiments for an array of three OWCPs. Each pump is designed to operate at a different resonance frequency.

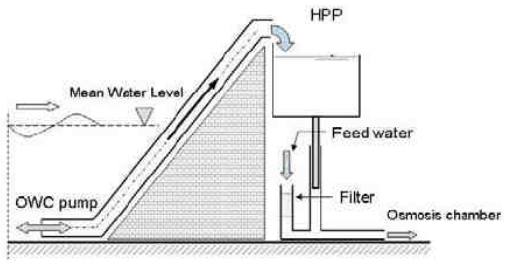

Figure 5 Schematic of an OWCP for water delivery coupled with HPP for water delivery.

Figure 6 1:40 Model of 3 OWCPs organized in a closely spaced array

Three OWCPS were arranged in a pan-flute array (Figure 6). Tests were carried in order to determine the interaction patterns between closely spaced devices and to identify the geometrical configuration which maximizes energy absorption. For this purpose three OWCPs models were built out of transparent Perspex. Each OWCP has a circular section with an internal diameter of 25 mm and an external diameter d of 30 mm. The angle of inclination of the pipes was of respectively 20 °, 25 ° and 30 °. This allowed for a wide range of wave period to be explored within the experimental tests. The water depth in the wave basin was 0.14m, while the array was installed at 0.1 m depth, on the top part of a plateau. Three separating distances (d_s) between the pipes were considered: 0, 30 and 60 mm apart from each other. The tests were complimented with the installation of two reflective walls in front of the array (50 and 100 mm high) to assess whether reflections of waves would increase the delivery of water.

5. Results and Discussions

5. 1 Composite Sea Wall

For the two models tested the hydraulic power was determined. The hydraulic power expresses the amount of kW that can be available in the structure. The hydraulic power is function of the freeboard and the overtopping rate. Figure 7 shows the plots the hydraulic power for the two different freeboard heights over the wave height considering a 50m strip of sea wall. The measured overtopping rates for both physical models are presented in Figure 8.

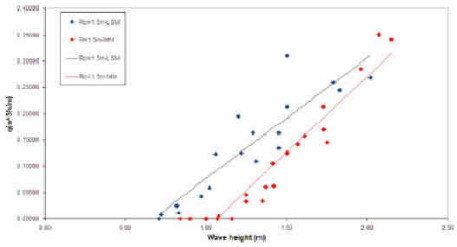

Figure 7 Hydraulic power as a function of H for R_c=1m(red) and R_c=1.5m (blue)

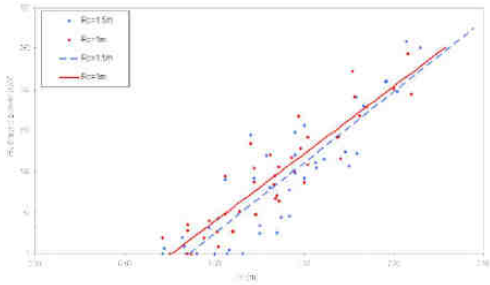

Figure 8 Overtopping rate for R_c=1.5 for different incoming wave heights.

The hydraulic efficiency of the composite sea wall is plotted in

Figure **9** against the dimensionless ratio of the wave height to freeboard ratio. It can be seen that the conversion efficiency increases with the relative wave height, reaching a maximum of 30% for heights between 1 and 1.5 m. The data obtain agree with available literature and with the theoretical predictions.

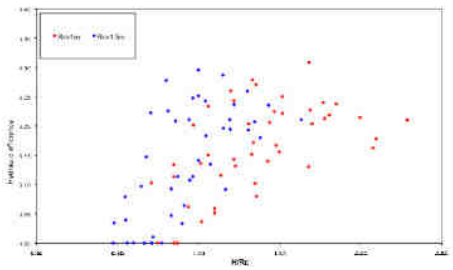

Figure 9 Hydraulic efficiency as a function of the wave height to freeboard ratio; for for R_c=1m(red) and R_c=1.5m (blue).

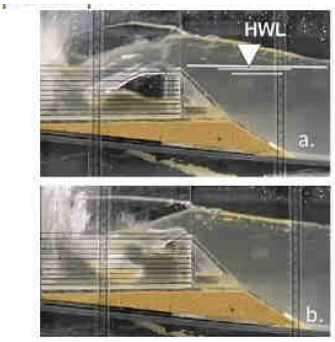

Figure 10 Image sequence (a. to b.) of the initial jet impact and the subsequent impact, up-rush and turbulence.

The defensive role of the Composite sea-wall was also assessed. Preliminary experiments include the comparison between overtopping volumes and wave pressures for/on a vertical seawall and the composite sea wall under investigation. A sensible reduction of the pressure impacts was achieved in presence of the composite sea wall, with energy dispersed by the water hitting the free surface within the basin, and energy dissipation due to turbulence within the basin (Figure 10).

5. 2 Buoyant Body device

The main purpose of the physical model tests of the Buoyant Body WEC was to support the theoretical work from which the device had developed. The efficiency of the device is presented in Figure 11, considered against the column of water contained within the PTO, or ratio of stroke. Figure 12 shows the maximum efficiency against the theoretical efficiency η.

From Figure 11 and Figure 12 it can be seen that the measurement points agree reasonably well with the theory presented, thus validating the theoretical approach. In Figure 12, the encircled group of out of ranges values corresponded with very small displacements and it is assumed that the body tilted slightly from vertical position and got stuck during the tests. The maximum efficiencies obtained were up o 40%, including leakage losses. This appears to be a promising conversion ratio, considering that the device is in first stages of development.

5. 3 OWCPs In array

The tests of the OWCPs in array were carried without any PTO being installed; therefore the measurements were aimed at determining the magnification factor M within each OWCP, e.g. the ratio to the length of water in the resonance tube after excitation (y_p) against the incoming wave height (H); hence $M=y_p/H$ (Magagna et al., 2010).

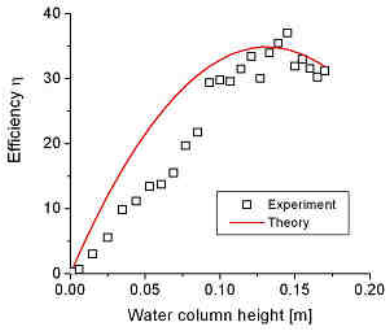

Figure 11Measured and theoretical efficiencies, and effect of applied force (T = 0.435 sec., H=14mm).

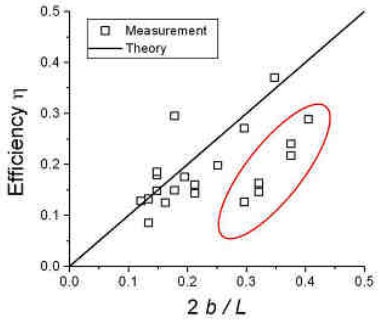

Figure 12 Maximum theoretical and experimental efficiency.

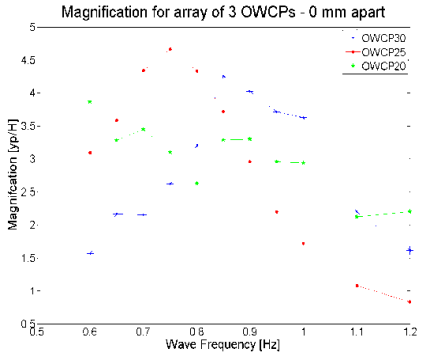

Figure 13 Frequency Response for an array of 3 differently tuned OWCPs. OWCP25 (red) was located at the centre of the array. Separating distance between the devices was of 0 mm.

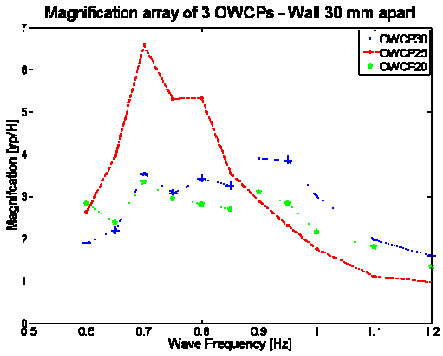

Figure 14 Frequency Response for an array of 3 differently tuned OWCPs with a 50 mm reflective wall installed in front of the array. OWCP25 (red) was placed centrally within array.

Figure 13 and Figure 14 show the changes in the Magnification factor for 3 differently tuned OWCPs with a separating distance of 0mm. In both cases it can be noted that the central device shows a higher magnification that the devices installed on the sides. The magnification factors for OWCP25 and OWCP30against the non dimensional frequency (ω_D/ω_N) for different d_s are presented respectively in Figure 15 and Figure 16.

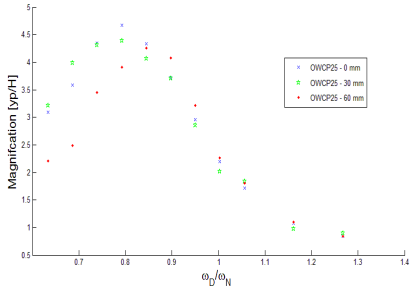

Figure 15 Magnification Factor M for the OWCP25against the non dimensional frequency. Maximum values of M are obtain when d_s = 0 mm (blue).

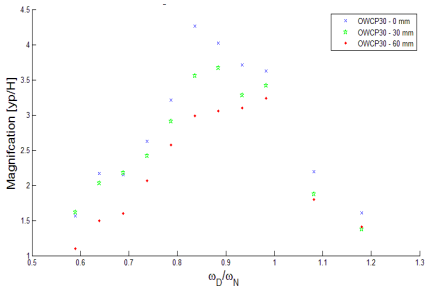

Figure 16 Magnification Factor M for the OWCP30 against the non dimensional frequency. Maximum values of M are obtain when d_s = 0 mm (blue).

From Figure 15 and Figure 16it can be see that the maximum magnification is achieved when the separation distance between the devices is of 0 mm, and that the performances of the devices decrease steadily when d_s increases. In both cases, there is a shift of the non-dimensional frequency to values towards 1, when the incoming wave frequency ω_D matches the natural frequency of oscillation ω_N. The use of small scale physical test for the OWCPs allowed for an intensive investigation into the behaviour of multiple devices deployed in arrays configurations. Due to the size of devices, investigations into the performances of arrays of WECs are normally carried through the use of mathematical models and CFD.

6. Scale effects

The importance of small scale physical tests in the development of wave energy converters has thus far been demonstrated for three devices. Whilst the results so far presented are encouraging, it is important to bear in mind that all of the test are affected by scale effects, particularly at these scales. In order to identify how scale effects play a role on the conversion efficiency of the devices, two approaches have been undertaken:

- Larger Scale Experiments: Comparisons of the test results obtain a 1:40 scale with tests results for test in the big wave flume at half the scale. These tests have, thus far, been run mostly for the Composite Sea Wall and for the OWCP device. The evaluation of tests at double the scale allows for the assessment of the friction losses within the device, and describes the wave processes in the near shore with higher similarity. This allows for the determination of the friction and damping coefficients that can be used later for the validation of numerical models (Figure 17).

- Reduced viscosity tests: Another approach towards the assessment of scale effects is suggested by Stagonas et al. (2010b), who considered the use of an Iso-Propynol Alcohol (IPA) solution instead of freshwater to generate waves within the wave flume. A 10% IPA distilled water solution, reduces the surface tension of the flume from the value of σ_{Water}=0.073N/m for freshwater to the value of σ_{IPA}=0.022N/m for the IPA solution, reducing the formation of capillary waves. Figure 18 present the values of the overtopping rate for the composite seawall, comparing results from freshwater and IPA solution at 50th scale and freshwater at 1:23 scale. It can be seen that overtopping rates are increased for the IPA solution compared to freshwater tests. The reduction in σ of the liquid, reduces the internal bonding forces of the water molecules, replicating the mechanics of full scales waves.

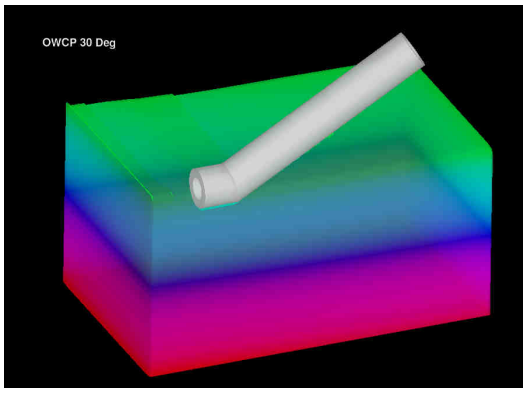

Figure 17 Simulation of Single OWCP device in CFD code Flow 3D. The data obtained by physical tests are used to validate the numerical model.

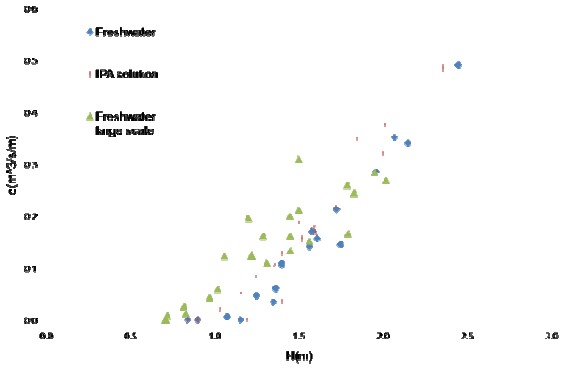

Figure 18 Overtopping rate for the Composite Seawall WEC, for 3 diffirent case studies: 1:50 scale (Blue), 1:50 scale with IPA solution (red) and 1:23 scale (green). It can be seen that the the overtopping rate increases moving from 1:50 to 1:23.

7. Conclusions

The findings presented in this work show that:

- Small-scale hydraulic models can be used for the initial development and investigation of near-shore WEC,
- Overtopping rates are smaller in the smaller model and are subject to surface tension effects.
- With a hydraulic power of 1.5KW per m length of composite sea-wall, for H=1m, and 14KW per m length of the buoyant WEC, for H=1.2m, the initial power generation results look promising and further research is suggested.
- The use of small scale models could provide a viable solution for the assessment of multiple devices operating in array configuration. Providing an indication of the best layout of operation.
- Small hydraulic models allow for a cost-effective development of WECs, allowing for a quick development and evaluation of the devices, providing to researchers the opportunity to adjust and improve the device's characteristic whilst testing.

8. Acknowledgment

The research leading to these results has received funding from the European Community's Seventh Framework Programme (FP7/2007-2013) under grant agreement n°212423.

9. References

Bruce, B., 2009. Investigation into the conversion efficiency of a buoyant type wave energy converter using laboratory experiments., University of Southampton, Southampton.

Cruz, J., 2008. Ocean Wave Energy. Current Status and Future Prespectives Green Energy and Technology, 431 pp.

EMEC, 2009. Tank testing of Wave Energy Conversion Systems, EMEC, Orkney.

Folley, M., Whittaker, T.J.T. and Henry, A., 2007. The effect of water depth on the performance of a small surging wave energy converter. Ocean Engineering, 34(8-9): 1265-1274.

Kofoed, J.P., Frigaard, P., Friis-Madsen, E. and Sørensen, H.C., 2006. Prototype testing of the wave energy converter wave dragon. Renewable Energy, 31(2): 181-189.

Magagna, D., Stagonas, D., Warbrick, D. and Muller, G., 2009. Resonating wave energy converter for delivery of water for desalination and energy generation. In: EWTEC (Editor), European Wave and Tidal Energy Conference. EWTEC, Uppsala, Sweden.

Magagna, D., Stagonas, D., Warbrick, D. and Muller, G., 2010. Physical investigations into the capture width of an array of OWC Wave Pumps for maximum efficiency. In: ICOE (Editor), 3rd International Conference on Ocean Energy. ICOE Bilbao, Spain.

Mori, M., Yamamot, Y. and Kimura, K., 2008. Wave force and stability of upright section of high mound composite seawall. In: ICCE (Editor), ICCE 2008. World Scientific, Hamburg, Germany, pp. 3157-3163.

Muller, G., Bruce, B., Magagna, D. and Jenkins, R., 2010. A non-resonant, buoyancy-type, wave energy converter. In: ICOE (Editor), 3rd International Conference on Ocean Energy. ICOE, Bilbao, Spain.

Muller, G., Maravelakis, N., Stagonas, D., Magagna, D. and Warbrick, D., 2009. Composite Seawalls for Wave Energy Conversion. In: ICE (Editor), Coasts, Marine Structures and Breakwaters 2009 ICE, Edinburgh, Scotland, United Kingdom.

Stagonas, D., Muller, G., Maravelakis, N., Magagna, D. and Warbrick, D., 2010a. Composite seawalls for wave energy conversion: 2D experimental results. In: ICOE (Editor), 3rd International Conference on Ocean Energy. ICOE, Bilbao, Spain.

Stagonas, D., Muller, G., Warbrick, D. and Magagna, D., 2010b. Surface tension effects in small-scale laboratory breaking waves. . In: G. Pacifico (Editor), Coastlab10 - Application of Physical Modelling to Port and Coastal Protection. Grupo Pacifico, Barcelona, Spain.

Appendix G

Paper for 3rd International Conference on Ocean Energy. Bilbao, Spain, October 2010

Physical investigations into the capture width of an array of OWC Wave Pumps for maximum efficiency

D. Magagna[1], D. Stagonas[1], D. Warbrick[1] and G. Müller[1]

[1] Sustainable Energy Research Group
School of Civil Engineering and the Environment
University of Southampton
Southampton, SO17 1BJ, United Kingdom
E-mail: d.magagna@soton.ac.uk

Abstract

The present paper presents experimental results for work carried out on an array of OWCPs and its wider application to OWC arrays installed onshore.

The aim of the present paper is to investigate the interaction between different elements in an array of multiple wave energy converters. For this purpose, physical experiments on a simple wave energy converter were carried. These allowed for the evaluation of the mutual interaction between the devices and for a wider analysis of the effect of the chamber width.

The proposed concept offers the possibility to evaluate the employment of differently tuned devices and reduce the need of optimum resonant and damping control to improve performance in the absorption and conversion of wave energy.

Experimental results showed how installing differently tuned devices in array widens the wave period range for which higher efficiency can be reached and reduces the need for resonance control within the system. The influence of the geometrical layout is assessed for an array of 3 closely spaced onshore wave energy converters. Positive effects are found in the disposition of the device, suggesting improvements can be achieved for onshore devices.

Keywords: Array, Oscillating Water Column, onshore, WEC

1. Introduction

The installation of Wave Energy Converters (WEC) in arrays is considered an essential step towards the commercialization of electricity powered by wave energy sources [1]. The use of series of devices installed together is considered important in order to assure a higher output feed to the electric grid. Each device installed in the array interacts with others by modifying the incoming wave field [2]. Early studies on the interaction of n devices installed in an array showed that the power generated by the array can be greater than the power of the n devices installed singularly [3].

The effect of array interaction is quantified with the factor q, and values of $q>1$ indicate a positive effect of the array on the energy production compared to the N single installations. However, the interaction of the devices and their geometric layout can lead to values of $q<1$; therefore reducing the power output of the array installation. It is therefore important to find a layout of the array to reduce the destructive interactions between components. Different approaches have been attempted over the years in order to identify the interaction between devices, with a predominance of work carried at theoretical level with simplifying assumption to ease the mathematical solution. Only a limited amount of work has been conducted on the interactions between devices through physical experiments. Examples can be found in [4, 5]. Both works highlight how theoretical studies on array interferences are affected by approximation and linearization of wave theory. Other work is focussed on array of point absorbers, which are a class of offshore WECs with their main dimension notably smaller than the predominant wavelength at site of installation.

At the present time installation of multiple devices in arrays can be found in the form of Multi Oscillating Water Column (MOWC) installed on breakwaters as presented in [4, 6, 7]. To the authors knowledge the first array installation for point absorbers is aimed for summer 2011 within the Wavehub project [8].

Of particular interests is the recent deployment of the Mutriku Wave Energy Power plant, where 16 OWC chambers were built with a nominal power of 300 kWh

and a capture width of 100 m (Figure 1). This installation is taken as main reference for the installation of a series of Oscillating Water Column Pump (OWCP) on an existing Breakwater. The aim of this paper is to quantify the interference of closely spaced device on a breakwater aimed at the maximization of the power output. This is achieved through a series of experimental tests intended for the identification of the ideal layout of the array.

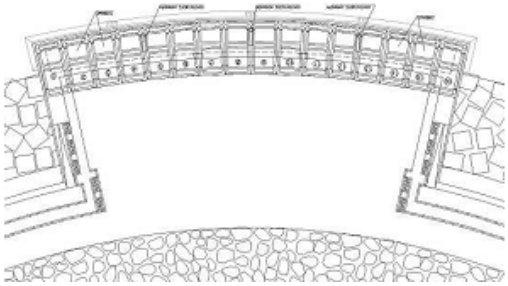

Figure 1: Schematic of the Mutriku OWC Plant

2. The device

The OWCP is a simple overtopping resonant type of wave energy converter based on the more common Oscillating Water Column (OWC) device. The OWCP represents a simplified version of the OWC. At the passing of waves the water contained within the device oscillates and moves within the column. If resonant conditions are achieved within the OWCP, a significant amplification of the wave height can be obtained. The OWCP is designed to lift water out of the pump when conditions close to resonance are achieved. The device is aimed at a delivery of 2-5 m high from 0.5-1 m high waves. This allows for energy to be collected in the form of gravitational potential energy in a reservoir. The OWCP is designed for coupling with a High Pressure Pump (HPP) for desalination purposes (Figure 1) [9] . Resonance control is achieved by varying the inclination of the output duct, thus varying the mass of water contained in each pump.

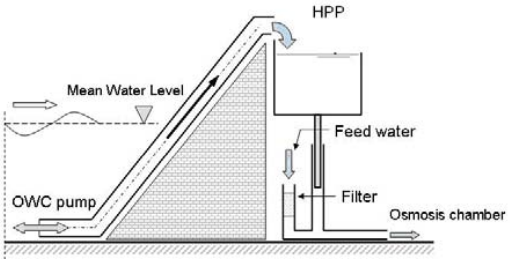

Figure 2: Schematic of the OWCP coupled with HPP

Initial work carried on the OWCP showed that amplification up to 5 times the incoming wave can be achieved [10]. Work was conducted on fixed configurations of the OWCP as reported in Table 1. It can be seen that working with three differently tuned OWCPs allows for a wide range of wave periods T to be covered at full scale.

In order to keep the system as simple and remove the issue of resonance control and wave climate forecasting, a "Pan Flute" arrangement of the OWCPs is currently under investigations. The aim is the identification of positive interaction between the devices and an assessment of the range of wave period *T* at which delivery can be assured.

Angle	T_{min}	TPeak	T Max	M
20 º	1.11 s	1.17 s	1.42 s	2.7
25 º	0.83 s	1 s	1.05 s	4
30 º	0.76 s	0.85 s	0.95 s	4.8

Table 1: Magnification factor (M) for different OWCPs, and identification of the range of wave periods (Tmin – TMax) at which significant amplification is achieved, with TPeak the wave period at which maximum amplification is obtained. Test carried with wave height of 5 mm and water depth of 80mm.

The purpose of the present work is to examine the changes in performance of an array of OWCP and determine the case for positive interaction between the devices.

3. Methodology

In order to assess the behaviour of a "Pan Flute" arrangement tests were carried in a 4 m long, 1.7 m wide end 0.4 m deep wave basin under the influence of monochromatic wave trains. Froude Scaling was used, with a scale factor Λ=40.

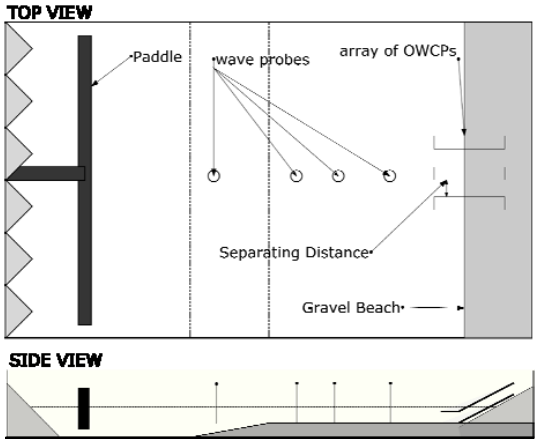

Figure 3: Physical Test Setup

Two types of investigation were carried out:

1. Identification of the interaction patterns between closely spaced devices and changes observed in the maximum delivery height.
2. Determination of the geometric configuration that maximizes capture width.

To do this, devices with same natural frequency but increased area of the opening are tested in a wave basin. The different configurations are tested singularly and in an array, whilst maintaining a constant overall array width.

3.1 Array of differently tuned OWCPs

The first series of investigation was aimed at assessing the effect of differently tuned OWCPs disposed in array of three devices. For this purpose three OWCPs models were built out of transparent Perspex. Each OWCP has a circular section with an internal diameter of 25 mm and an external diameter *d* of 30 mm. The angle of inclination of the pipes was of respectively 20 º, 25 º and 30 º. This allowed for a wide range of wave period to be explored within the experimental tests.

The water depth in the wave basin was 0.14m, while the array was installed at 0.1 m depth, on the top part of a plateau (Figure 3). Three separating distances (*ds)* between the pipes were considered: 0, 30 and 60 mm apart from each other. The tests were complimented with the installation of two reflective walls in front of the array (50 and 100 mm high) to assess whether reflections of waves would increase the delivery of water (Figure 4).

Each OWCPs configuration was equipped with calibrated capacitance probes to monitor the changes in the level of water under the effect of wave acting on the device.

Each OWCP was tested individually to assess the array and distance effects on its performance. The OWCP25 configuration was installed ate the centre of the array for this series of tests.

Figure 4: View of the 3 OWCPs array equipped with front reflective wall.

3.2 Capture width Array

The second series of test was aimed at the analysis of the capture width of identically tuned OWCPs.

For this purpose, three configurations of the OWCPs were built with transparent 3 mm thick Perspex. The input duct for each configuration was 0.04 m long, with the output duct 0.4 m long. The OWCPs had a rectangular section and with a fixed height of 24 mm. The width of the each device was varied as reported in Table 2. This allowed for the assessment of different combinations of a closely spaced array. The total capture with of the array was kept to 60 mm, and different combinations of the array were tested, as shown in Figure 5.

The array was installed with a submersion depth of 0.09-0.13 m, with linear waves used for testing with height between 0.01-0.04 m and period between 0.6-1.6 s.

Configuration	Width
OWCPS1	20 mm
OWCPS2	40 mm
OWCPS3	60 mm

Table 2: Configurations of the OWCP for capture width analysis

Each OWCPS configuration was equipped with resistance probes to measure the rise of the water column with the pipe.

The various configurations of the of the array were varied according to Table 3 to assure a broad analysis of each array configuration and assess the generated interferences

3.3 Magnification factor

In each series of test the wave conditions in the wave basin were assessed with through the use of 3 determination of the incident and reflected wave height.

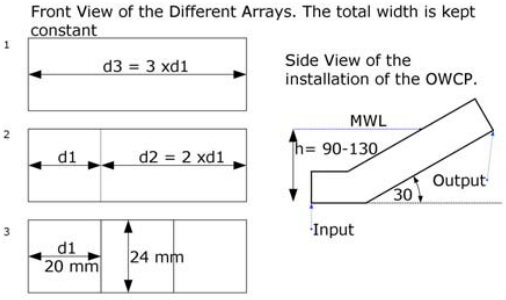

Figure 5: Different layout of the array examined for capture width analysis**.**

Combination	Type
OWCPS1	1 OWCPS1 alone
OWCPS2	1 OWCPS2 alone
OWCPS3	1 OWCPS2 alone
3□OWCPS1a	3 OWCPS1 aligned
OWCPS 2+1	1 OWCPS1 +1 OWCPS2
3□OWCPS1b	3 OWCPS1 with central pipe offset back of 0.04m

Table 3: Combinations of the OWCPS for capture width analysis, and definitions of tests.

This is compared with the delivery height of water *yp* inside the OWCP to determine the magnification factor *M* of each pump, defined as:

$$M = \frac{y_p}{H} \quad (1)$$

Where *H* represents the incident wave height.

4. Results

4.1 Array of differently tuned OWCPs

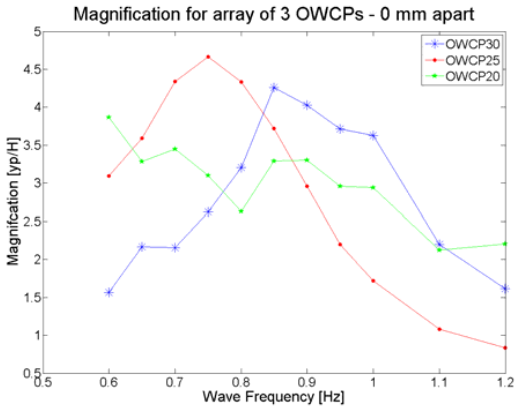

.

Figure 6: Frequency Response for an array of 3 differently tuned OWCPs. OWCP25 was located at the centre of the array. Separating distance between the devices was of 0 mm.

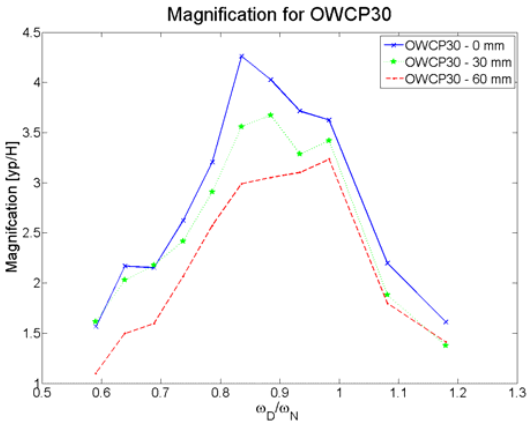

Figure 7: Changes in the magnification for the OWCP30 configuration based on the separating distance from the other devices. The device was located on the side of the array. Magnification is reduced at the increase of the separating. distance

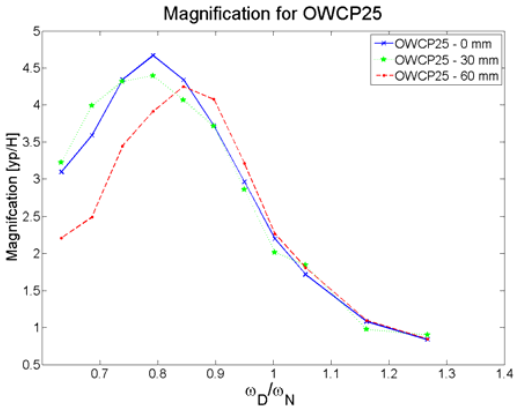

Figure 8: Changes in the magnification of OWCP25 configuration based on the separating distance from the other devices. The device was located at the centre of the array

The data obtained from the experimental investigation on an array of differently tuned devices confirmed that using differently tuned devices in an array widens the response bandwidth of the array. As it can be seen in Figure 6 using three differently tuned OWCPs allows for magnification factor of about 4 times H in the range between 0.6 to 1.05 Hz, translating to real scale for to a range of wave periods between 5.3 and 10.5 seconds. Furthermore it can be noticed that the OWCP20 pipe achieves resonant conditions for a lower wave frequency, hence broadening the response of the array to longer and more powerful wave periods.

The disposition of the array shows that the central OWCP, OWCP25 is positively influenced by the modified wave field in front of the array.

From Figure 7 and Figure 8 it is possible to notice that for increasing the separating distances between the devices the magnification within the pump decreases. Furthermore one can notice how the devices tend to work autonomously when the distance between devices is of the order of $2d$. In this situation, the peak performance is achieved when the wave frequency ω_d matches the natural frequency of oscillation of the device ω_n. It can be seen that M decreases with ds increasing; while the ratio ω_d/ω_n tends towards 1with ds increasing.

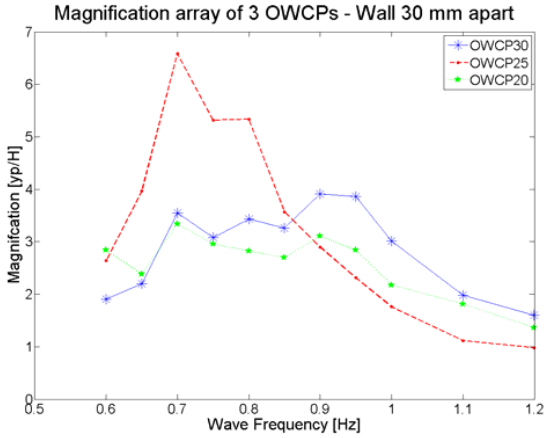

Figure 9: Frequency Response for an array of 3 differently tuned OWCPs with a 50 mm reflective wall installed in front of the array. OWCP25 was placed centrally within array.

The close deployment of the devices increases the mass of water that is moved in front of the array increasing delivery thus shifting. This can be noticed also when a reflective wall is installed in front of the array. It can be seen from Figure 9 that the wall enhances the performances of the OWCP25 pump, while it affects the performance of the devices on the side of the array, which become more selective.

4.2 Capture width analysis

The responses of different configurations of a fixed width array are presented in Figure 10, Figure 11 and Figure 12. In Figure 10 the response for an array of 3 OWCPS1 pumps is presented. It can be noticed how the behaviour of the central device is still favoured compared to the devices located on the side of array. Figure 11 shows the response of an array

combined between one OWCPS1 device and one OWCPS2 device. It can be noticed how this combination generates a negative effect on the delivery compared to Figure 10.

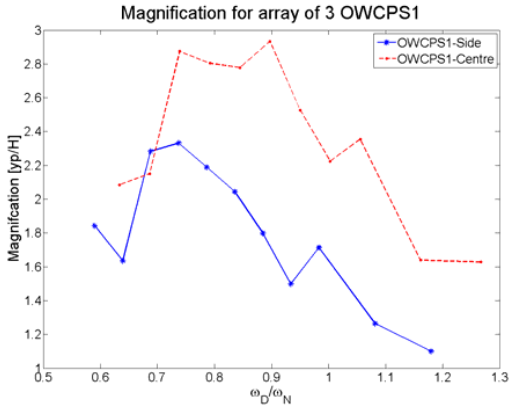

Figure 10: Frequency Response for an array of 3 OWCPS1. The comparison is made between the central pipe and the side pipes.

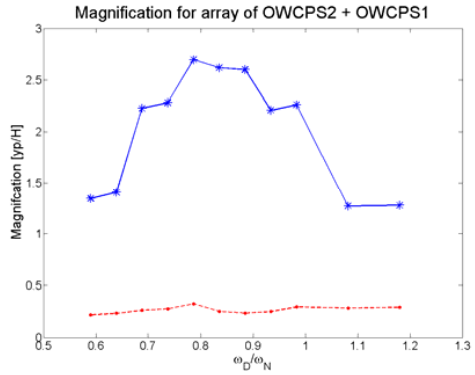

Figure 11: Frequency Response for an array of 1 OWCPS1 coupled with a 1 OWCPS2 device.

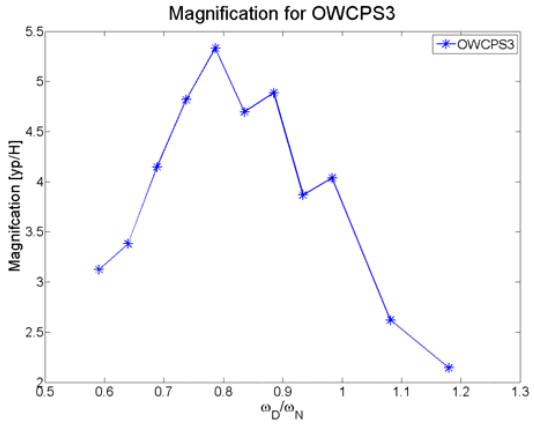

Figure 12: Frequency Response for the OWCPS3 configuration. Peak delivery is obtained for a ratio ω_d/ω_n of 0.8.

Figure 12 shows the response for a single OWCPS3 device. It can be seen that the maximum magnification factor obtained is of about 5.5, compared to a *M* of 2.9 in Figure 10, and of 2.7 Figure 11. In all 3 cases, the maximum magnification is obtained when the ratio ω_d/ω_n is between 08-0.9, with a smaller peak for values of the ω_d/ω_n ratio close to 1

5. Discussion

Experimental work carried out for a series of differently tuned devices showed that a mixed installation allows for the array to provide a broader response bandwidth compared to an array of identically tuned devices. Test showed that a limited separating distance between the devices provide a positive effects in the performance of the device located at the centre of the array. For separating distance of the device higher than *2d* the devices tend to behave autonomously reducing the overall positive effect of the array.

The employment of similarly tuned devices, however, generates a negative effect on the overall array performance. By changing the opening of the OWCP in contact with the wave action it can be seen that the different devices interact within each other. Negative array interference is noted when devices with a different contact area are coupled together, which reduces the overall performance. Using a wider contact area provides a higher response, but is limited to lower ranges of wave periods.

In both cases it can be seen that a close-type of array, with small separating distances, causes resonant type behaviour between the devices, shifting the ω_d/ω_n ratio to lower values but increasing *M*. This is related to the mass of water moved in front of the array, which affects every component of the array. In general positive effects are noticed for the central device in the array.

6. Conclusions

Little experimental work on the assessment of the performance of arrays of onshore wave energy converters is reported in the literature. This is probably due to the impossibility of carrying such experiments in a standard laboratory facility. This paper presents results of a series of tests aimed at assessing the behaviour of a series of simple wave energy devices installed in the near shore area. Array configurations of up to three devices are taken into account. In all tests it was noticed that positive performance effects were obtained in the central device of the array.

The assessment of the capture width confirmed earlier theoretical work on the oscillating water column presented by Evans [11]. The closer the width of the devices get to the ratio $2\pi/L$ the higher its response becomes.

The results presented in this paper show that it is possible to evaluate the use of a "pan flute" arrangement of OWCPs, and in a broader sense OWCPs, to reduce the need of resonant control. Furthermore the devices can be tuned in order to obtain the maximum performance without affecting the performance of the neighbouring converters.

It is possible to assess the geometric dispositions of the array by using similarly tuned devices and investigations showed that the overall performance can be increased in order to obtain a capture factor q >1.

The present paper shows that it is possible to evaluate the performance of an array of devices by carrying the work experimentally with the use of simple techniques. The work will be expanded in order to evaluate different geometrical conditions and provide an indication on how the array disposition for a group of onshore wave energy converters can assure higher efficiency in the performance of each single component.

Acknowledgements

The research leading to these results has received funding from the European Community's Seventh Framework Programme (FP7/2007-2013) under grant agreement n°212423.

.

References

[1] 1.Cruz J., S.R., Siddorn P., Eatock Taylor, R. *Wave farm design: preliminary studies on the influences of wave climate, array layout and farm control.* . in *Proceedings of the 8th European Wave and Tidal Energy Conference*. 2009. Uppsala, Sweden.

[2] Babarit, A., *Impact of long separating distances on the energy production of two interacting wave energy converters.* Ocean Engineering. **In Press, Corrected Proof**.

[3] Falnes, J., *Radiation impedance matrix and optimum power absorption for interacting oscillators in surface waves.* Applied Ocean Research, 1980. **2**(2): p. 75-80.

[4] Thiruvenkatasamy, K. and S. Neelamani, *On the efficiency of wave energy caissons in array.* Applied Ocean Research, 1997. **19**(1): p. 61-72.

[5] Weller S., S., T., Stansby, P.K., *Experimental measurements of irregular wave interaction factors in closely spaced arrays.* , in *Proceedings of the 8th European Wave and Tidal Energy Conference*, EWTEC, Editor. 2009: Uppsala, Sweden. p. pp 952-960.

[6] Torre-Enciso, Y., Ortubia, I., Lopez de Aguileta, L.I., Marques, J. *Mutriku Wave Power Plant: from the thinking out to the reality*. in *Proceedings of the 8th European Wave and Tidal Energy Conference*. 2009. Uppsala, Sweden.

[7] Graw, K.U. *Wave energy breakwaters - a device comparison*. in *Conference in Ocean Engineering - COE '96*. 1996. Madras, India.

[8] Agency, S.W.R.D., *Wave Hub construction underway*. 2009`.

[9] Magagna, D. and G. Muller, *A wave energy driven RO stand-alone desalination system: initial design and testing*, in *Desalination Cooperation among Mediterranean Countries of Europe and the MENA Region*, E.E. Society, Editor. 2008: Dead Sea, Jordan. p. 6.

[10] Magagna, D., et al. *Experimental study to determine flow characteristic effects on marine current turbine behaviour*. in *European Wave and Tidal Energy Conference*. 2009. Uppsala, Sweden: EWTEC.

[11] Evans, D.V. and R. Porter, *Hydrodynamic characteristics of an oscillating water column device.* Applied Ocean Research, 1995. **17**(3): p. 155-164.